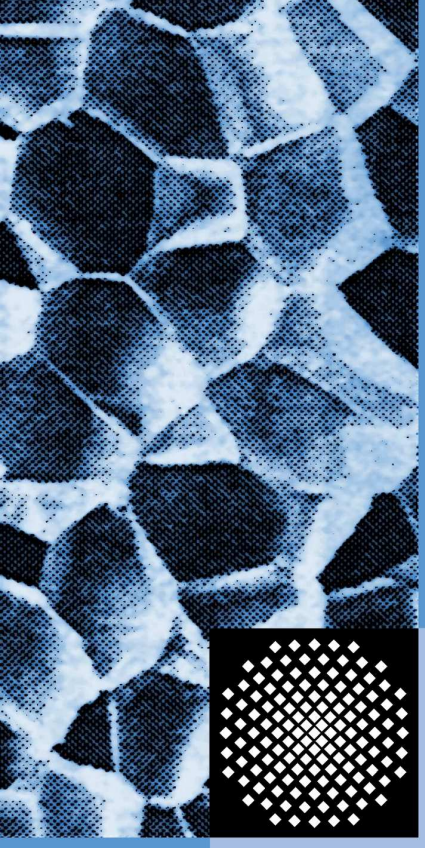

Universität Stuttgart
Germany

Institut für Mechanik (Bauwesen)
Lehrstuhl II, Prof. Dr.-Ing. W. Ehlers

Porous Media Viscoelasticity with Application to Polymeric Foams

Bernd Markert

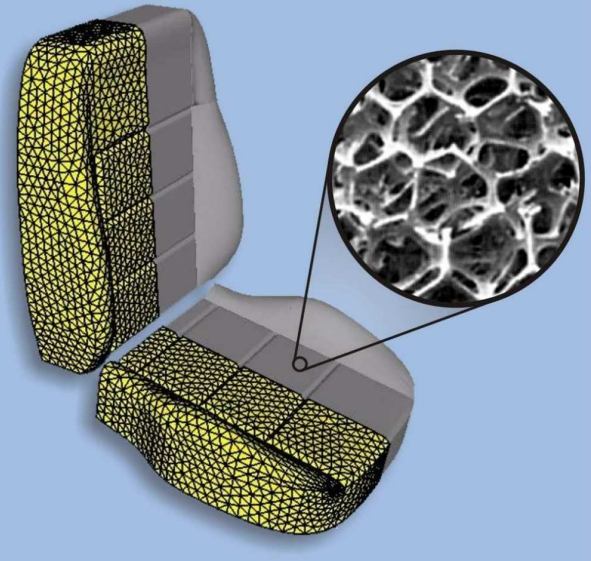

Second Revised Edition

Report No.: II-12 (2005)

Porous Media Viscoelasticity with Application to Polymeric Foams

Von der Fakultät Bau- und Umweltingenieurwissenschaften
der Universität Stuttgart zur Erlangung der Würde
eines Doktor-Ingenieurs (Dr.-Ing.)
genehmigte Abhandlung

vorgelegt von

Dipl.-Ing. Bernd Markert

aus
Mayen/Eifel

Hauptberichter: Prof. Dr.-Ing. Wolfgang Ehlers
Mitberichter: Prof. Dr. techn. Gerhard A. Holzapfel

Tag der mündlichen Prüfung: 14. Juli 2005

Institut für Mechanik (Bauwesen) der Universität Stuttgart
Lehrstuhl II (Kontinuumsmechanik)
Prof. Dr.-Ing. W. Ehlers
2005

Report No. II-12
Institut für Mechanik (Bauwesen)
Lehrstuhl II (Kontinuumsmechanik)
Universität Stuttgart, Germany, 2005

Second Revised Edition 2010

Editor:
Prof. Dr.-Ing. W. Ehlers

Institut für Mechanik (Bauwesen)
Lehrstuhl II (Kontinuumsmechanik)
Universität Stuttgart
Pfaffenwaldring 7
70569 Stuttgart, Germany

ISBN 3–937399–12–7
(D 93 – Dissertation, Universität Stuttgart)

PREFACE

The work described in this doctoral dissertation was carried out between the years 1998 and 2005 at the Institute of Applied Mechanics (Civil Engineering), Chair II (Continuum Mechanics), of the University of Stuttgart. During this period of my scientific development, I started as Ph. D. student, continued as a research associate, then became assistant lecturer, and finally tenure lecturer. This allowed me to gain profound knowledge in the fields of continuum and computational mechanics and guided the success of the presented thesis. However, during the years numerous people contributed in many ways to the realization of this work – all their support is most gratefully acknowledged.

First of all, I particularly want to thank my supervisor, Professor Wolfgang Ehlers, for giving me the opportunity to prepare the thesis in the institute and for granting me all the scientific freedom to make this work possible. He supported me in an open-minded and unreserved fashion, which led to many valuable and fruitful discussions. Besides the scientific support, I also thank him for the friendly and familiar atmosphere at the institute as well as the companionable relationship that grew over the years.

I am also very grateful to Professor Gerhard Holzapfel from the Royal Institute of Technology (KTH), Department of Mechanics in Stockholm, Sweden, for taking the co-chair in my promotion procedure and for carefully reading the manuscript.

Moreover, I want to thank all of my colleagues, who always shared their experience and knowledge with me, especially, my long-lasting colleague Martin Ammann, who often helped me with the programming in PANDAS, Oliver Klar, who partly carried out the uniaxial tests, and our laboratory technician Ralf Plonus, who designed and constructed the required experimental devices.

Also the effort of my student assistants, diploma, and master students is hereby acknowledged with thanks, as they allowed me to follow new ideas and to carry out time-consuming experiments and simulations besides the daily university business. In this regard, special thanks to Axel Nödling, who did the permeability experiments, Joachim Bossert with whom I performed the microstructure simulations, and Andrei Danilov, who helped me with the geometry model of the car seat cushion. Particularly, I have to thank my master student Julie Paterson, who as a native Canadian did most part of the proof reading of the manuscript and untiringly improved my English language.

Finally, I like to deeply thank my wife Agnieszka, who really had a hard time during the writing process of my dissertation and often had to share me with the computer at evenings and weekends. Nevertheless, she always supported and motivated me despite her own exhaustive job as a hospital physician.

Stuttgart, July 19, 2005 Bernd Markert

I hear and I forget. I see and I remember. I do and I understand.
Confucius (551 – 479 BCE)

Contents

List of Figures

Deutsche Zusammenfassung

Es ist das Ziel der vorliegenden Arbeit, die Fortschritte in den Theorien zu porösen Medien mit dem aktuellen Stand der Forschung zur Beschreibung finiter Viskoelastizität von Einphasenmaterialien in einem gesamtheitlichen Modell zu kombinieren. Hierzu wird eine thermodynamisch konsistente Formulierung vorgestellt, wobei auf der Basis des Konzepts interner Variablen ein Viskoelatizitätsgesetz vom *Ogden*-Typ in die makroskopische Theorie Poröser Medien (TPM) integriert wird. Ausgehend von einem unmischbaren, zweiphasigen Festkörper-Fluid-Aggregat werden alle wesentlichen physikalischen Eigenschaften in der Formulierung berücksichtigt, die aus der porösen Mikrostruktur, dem sich bewegenden und interagierenden viskosen Porenfluid (kompressibel oder inkompressibel) und der überlagerten intrinsischen Viskoelastizität des Festkörperskeletts resultieren. Das entwickelte kontinuumsmechanische Zweiphasenmodell ist somit in der Lage, alle für das makroskopische Materialverhalten relevanten Nichtlinearitäten des stark gekoppelten Problems abzubilden. Um die praktische Anwendbarkeit des Modells unter Beweis zu stellen, wird eine Anpassung an reale Versuchsdaten eines offenzelligen Polymerschaumstoffs vorgenommen, da diese Materialien unter finiten viskoelastischen Deformationen alle nichtlinearen Effekte aufweisen. Nach der numerischen Behandlung und Umsetzung der Modellgleichungen im Rahmen der gemischten Finite-Elemente-Methode (FEM) werden zwei illustrative, dreidimensionale (3-d) Simulationen vorgestellt, die die prinzipiellen Fähigkeiten der makroskopischen Formulierung und die Effizienz ihrer numerischen Implementierung verdeutlichen.

Motivation

Es ist offensichtlich, daß die volumetrische Deformation eines permeablen, fluidgesättigten porösen Festkörpermaterials immer eine viskose Porenströmung hervorruft, die unter drainierten Bedingungen zu dem aus der Geotechnik bekannten Konsolidationsprozeß führt (Terzaghi & Jelinek [175]). Dieser zeitabhängige Prozeß wird durch einen weiteren dissipativen Effekt überlagert, sofern das Festkörperskelett selbst ein Relaxations- bzw. Kriechverhalten aufweist, d. h. sich viskoelastisch verhält. Im allgemeinen sind die von der Fluidbewegung abhängigen und unabhängigen (intrinsischen) viskosen Eigenschaften stark miteinander gekoppelt und müssen somit im Rahmen der nichtlinearen Thermodynamik von Mehrphasenmaterialien behandelt werden. In diesem Zusammenhang ist es erforderlich, alle Untersuchungen für den Bereich sehr großer Dehnungen durchzuführen, da die Klasse der betrachteten Materialien, wie z. B. hydratisierte Gele und Gewebe oder Polymerschaumstoffe, in ihrer praktischen Anwendung finiten viskoelastischen Deformationen unterworfen sind. Betrachtet man diese Materialien auf der Mikroskale, so finden sich eine Vielzahl poröser Strukturen von viskoelastischen, molekularen Netzwerken mit interstitieller Flüssigkeit in den Zwischenräumen bis hin zu eher skelettartigen oder zellularen Strukturen, die aus einer Kombination von offenen und/oder geschlossenen, fluidgefüllten Zellen aufgebaut sind. Gerade diese Mikrostrukturen unterliegen komple-

xen Deformationsmechanismen unter äußerer Belastung, was zu einem oftmals hochgradig nichtlinearen Spannungs-Dehnungs-Verhalten des makroskopischen Materials führt.

Moderne Bildgebungsverfahren, wie z. B. die Mikro-Computertomographie (Mikro-CT) oder die Magnetresonanztomographie (MRT), erlauben die 3-d Rekonstruktion diverser poröser Mikrostrukturen bis zu einer Auflösung von wenigen Mikrometern (siehe Abbildung 1.1). Allerdings ist trotz der gestiegenen Leistung moderner EDV-Anlagen die Berechnung realer Problemstellungen auf der Basis mikroskopisch rekonstruierter Geometriemodelle nicht sinnvoll. Alternativ können anstelle der realen Porengeometrie idealisierte Geometriemodelle basierend auf diskreten Partikeln, Balken- oder Schalenelementen verwendet werden. Doch selbst dann sind die benötigten Computerressourcen unverhältnismäßig hoch. Problematisch gestaltet sich zudem die Beschreibung eines sich frei bewegenden Porenfluids und der resultierenden Fluid-Struktur-Interaktion sowie die Behandlung des Kontaktproblems in kollabierenden Poren. Eine weitere Möglichkeit, die Spannungsantwort poröser Materialien zu analysieren, ist durch die Anwendung von Homogenisierungstechniken auf idealisierte Modelle der Mikrostruktur gegeben. Im Fall von Schaumstoffen kann eine Durchschnittspore z. B. durch ein einfaches Balken- oder Schalenmodell eines volumenausfüllenden Polyeders approximiert werden, wobei die effektiven (makroskopischen) Materialparameter mittels geeigneter Skalierungsgesetze bestimmt werden können (Gibson & Ashby [72]). Dies liefert eine gute Beschreibung von Materialien mit einer mehr oder weniger wohl definierten Porenstruktur, wie z. B. in Wabenstrukturen oder zellularen Schaumstoffen. Jedoch ist es auch in diesen Modellen schwierig, den Einfluß einer interagierenden Fluidphase in geeigneter Weise zu erfassen.

Hieraus kann schließlich gefolgert werden, daß für den Fall praxisrelevanter Probleme mit porösen Medien, bei denen die Porenfluidströmung einen signifikanten Einfluß auf das Verhalten des Gesamtmaterials haben kann, nur eine makroskopische Herangehensweise basierend auf einem Mischungsansatz eine geeignete Lösungsstrategie darstellt. Damit ist es auf einfache Weise möglich, eine unabhängige Fluidphase zu berücksichtigen, selbst wenn keine Detailinformationen über die poröse Mikrostruktur vorliegen. Aus diesem Grund wird in dieser Arbeit ein statistisches Mehrphasenkontinuumsmodell verwendet, um das mechanische Verhalten viskoelastischer, fluidgesättigter, poröser Materialien erfolgreich beschreiben zu können.

Zielsetzung und Vorgehensweise

In der vorliegenden Arbeit wird die makroskopische Beschreibung viskoelastischer, fluidgesättigter, poröser Festkörper im Rahmen der Theorie Poröser Medien (TPM) betrachtet. Die TPM als Kontinuumstheorie für Mehrphasenmaterialien vereint die Theorie der Mischungen (TM) mit dem Konzept der Volumenanteile und bildet somit eine ausgezeichnete Basis zur makroskopischen Beschreibung allgemeiner unmischbarer Festkörper-Fluid-Aggregate (siehe z. B. de Boer [19], Bowen [22], Ehlers [54]). Der Inhalt dieser Arbeit konzentriert sich hierbei auf die Anwendung eines standardmäßigen TPM-Ansatzes zur Beschreibung eines porösen Zweiphasenmaterials, in dem ein materiell inkompressibles Festkörperskelett mit einem einzigen Porenfluid gesättigt ist. Thermische Effekte sowie

Massenaustauschprozesse bleiben dabei unberücksichtigt. Basierend auf dem Prinzip der effektiven Spannungen (Bishop [13], de Boer & Ehlers [20], Skempton [167]) ist es dennoch möglich, eine Vielzahl relevanter Ingenieurprobleme zu behandeln, da beliebige thermodynamisch konsistente Konstitutivgleichungen für die effektive Festkörperspannung sowie die effektive Impulsproduktion in die makroskopische Formulierung integriert werden können. Die traditionelle Anwendung der TPM, wie auch anderer Mischungstheorien, auf geomechanische Probleme hat vorwiegend zur Entwicklung elastoplastischer und elastoviskoplastischer Konstitutivmodelle geführt, um Lokalisierungsphänomene in gesättigten und ungesättigten Böden zu beschreiben (Diebels *et al.* [46], Ehlers [50, 51], Ehlers & Müllerschön [62]). Erst neuere Arbeiten zur finiten Elastizität in porösen Medien (Ehlers & Eipper [55], Eipper [64]) führten zu Weiterentwicklungen der elastoplastischen Modelle auf geometrische Nichtlinearitäten und wurden in der Folge unter Verwendung einfacher Neo-*Hooke*scher Elastizitätsformulierungen zur Beschreibung harter Polymer- und Metallschäume angewendet (Droste [47], Mahnkopf [118]).

Im Rahmen dieser Arbeit wird ein geeignetes finites Viskoelastizitätsgesetz entwickelt, das ein stark nichtlineares Verhalten der porösen Feststoffmatrix beschreiben kann und sich in konsistenter Weise in die Zweiphasenformulierung integrieren läßt. Die Idee, eine Theorie zur Beschreibung poröser Medien mit viskoelastischen Konstitutivgleichungen für das Festkörperskelett zu kombinieren, ist hierbei nicht neu (siehe z. B. Biot [11], Mak [119]). Insbesondere die geometrisch lineare, zweiphasige, poroviskoelastische BPVE-Theorie von Mak, die das lineare, integrale Viskoelastizitätsgesetz von Fung [70] verwendet, hat sich zur Beschreibung von Knorpelgewebe etabliert (Setton *et al.* [160]). Die numerische Behandlung derartiger integraler Viskoelastizitätsformulierungen mit kontinuierlichem Relaxationsspektrum, in der die externen Zustandsvariablen als Funktionale der Prozeßgeschichte ausgedrückt werden (vgl. Coleman [33], Coleman & Noll [35, 36], Gurtin & Sternberg [78]), erweist sich aufgrund des hohen Rechenaufwands für die Zeitintegration der enthaltenen Faltungsintegrale als eher ineffizient (Suh & Bai [171]). Eine insbesondere aus numerischen Gesichtspunkten vorteilhaftere Beschreibungsweise viskoelastischer Festkörper ist durch die Modellrheologie in Verbindung mit der Thermodynamik mit internen Zustandsvariablen gegeben (Coleman & Gurtin [34], Lubliner [115], Valanis [184]). Ausgehend von einem rheologischen Modell, das eine viskoelastische Materialantwort durch eine geeignete Anordnung elastischer Feder- und viskoser Dämpferelemente nachbildet (vgl. Tschoegl [183]), wie z. B. das generalisierte *Maxwell*-Modell (siehe Abbildung 1.2), können dehnungsäquivalente interne Variablen eingeführt werden, die direkt als Deformationen der Dämpferelemente interpretiert werden können. Diese phänomenologische Herangehensweise führt auf eine differentielle Darstellung der Viskoelastizität, wobei ein diskretes Relaxationsspektrum eine effiziente numerische Behandlung gestattet. Die internen Variablen können dann im Sinne von Geschichtsvariablen in Abhängigkeit der gewählten Zeitdiskretisierung der inelastischen Entwicklungsgleichungen unabhängig voneinander berechnet werden.

Beim Übergang auf finite Deformationen ist die Einführung interner Variablen und die Wahl geeigneter Evolutionsgesetze jedoch weder offensichtlich noch eindeutig möglich. Im vorliegenden Fall kann hierbei auf aktuelle Methoden zur Modellierung finiter Viskoelastizität von Einphasenmaterialien zurückgegriffen werden, die allerdings hinsichtlich einer

Anwendung auf poröse Medien zu erweitern sind. Folgt man den relevanten Arbeiten von le Tallec *et al.* [173], Lion [111], Reese & Govindjee [151] oder Huber & Tsakmakis [95], so ist es vorteilhaft, basierend auf einer multiplikativen Zerlegung des Deformationsgradienten in elastische und inelastische Anteile (vgl. Lee [108], Sidoroff [162]), das bereits zuvor erwähnte Konzept durch Einführung dehnungsäquivalenter interner Variablen beizubehalten. Hinsichtlich der konstitutiven Beziehungen, die zur Spannungsberechnung in der finiten Viskoelastizität von Einphasenmaterialien eingesetzt werden, kommen meist isotrope Verzerrungsenergiefunktionen zur Beschreibung von dichten gummiartigen oder polymeren Werkstoffen zur Anwendung. Um das nichtlineare Spannungs-Dehnungs-Verhalten dieser quasi-inkompressiblen Materialien abbilden zu können, haben sich, vor allem wegen ihrer mathematischen Gültigkeit (Ball [5], Ciarlet [32], Ogden [137]) und ihrer guten Anpassungsfähigkeit an experimentelle Daten, Formulierungen vom *Ogden*-Typ (Ogden [136, 138, 139]) etabliert. Wegen der Inkompressibilität der betrachteten Werkstoffe sind die verwendeten Formulierungen jedoch im allgemeinen auf isochore Deformationen beschränkt. Im Gegensatz dazu sind im Fall viskoelastischer poröser Medien Formulierungen zur Beschreibung stark kompressibler Materialien erforderlich, da infolge möglicher Porenraumdeformationen und Porenfluidaustritte das makroskopische Material volumetrisch deformierbar ist, auch wenn das Festkörpermaterial und das Porenfluid selbst materiell inkompressibel sind. Folglich müssen spezielle volumetrische Antwortfunktionen entwickelt werden, die das volumetrische Versteifen des porösen Mediums bei Annäherung an den Kompressionspunkt (Eipper [64]), d. h. den Deformationszustand, bei dem alle Poren geschlossen sind und sich das makroskopische Material wie ein inkompressibles Einphasenmaterial verhält, garantieren.

Bei der Beschreibung des Porenfluids ist die Strömung inkompressibler Flüssigkeiten, kompressibler Gase sowie untrennbarer Mischphasen aus Flüssigkeit und Gas durch gesättigte poröse Medien Gegenstand einer Vielzahl von Publikationen. Diese können prinzipiell in zwei Hauptkategorien untergliedert werden. Einerseits werden deformierbare poröse Materialien untersucht, wobei Kontinuumstheorien wie die TPM zur Anwendung kommen, um in erster Linie das makroskopische Deformationsverhalten zu beschreiben. Die hierbei verwendeten Strömungsgesetze basieren jedoch meist auf einem einfachen linearen Ansatz für die effektive Fluidimpulsproduktion, der im quasi-statischen Fall auf ein *Darcy*sches Filtergesetz führt (vgl. Crochet & Naghdi [39], Ehlers [54]). Diese lineare Beziehung zwischen Filtergeschwindigkeit und hydraulischem Gefälle zur Beschreibung schleichender Sickerströmungen ist jedoch in realen Anwendungen nicht immer zutreffend. Um den Einfluß der Festkörperdeformation auf den Strömungsprozeß zu erfassen, stellen einige Autoren die Permeabilität als Funktion des Deformationszustands dar, z. B. in Abhängigkeit der Volumendehnung (Mow *et al.* [128]) oder der Porosität (Eipper [64]). Andererseits gehen die Arbeiten aus den Bereichen der Chemie, der Umweltingenieurwissenschaften, der Gas- und Erdölfördertechnik sowie der Hydrologie in der Regel von undeformierbaren porösen Medien aus, da hier die genaue Beschreibung des Filtrationsprozesses durch ein starres Festkörperskelett im Vordergrund steht (siehe z. B. Bear [7], Dullien [48]). In diesem Zusammenhang werden Turbulenz- und Trägheitseffekte als maßgebliche Faktoren für die Abweichungen von einer laminaren *Darcy*-Strömung experimentell und theoretisch untersucht, wobei auf der Basis empirischer Beobachtungen vor allem unterschiedliche Variationen und Weiterentwicklungen des klassischen eindimensionalen *Forchhei-*

mer-Filtergesetzes (Forchheimer [69]) diskutiert werden. Die Zielsetzung der vorliegenden Arbeit erfordert jedoch die kombinierte Betrachtung beider Aspekte, d. h. einer finiten Festkörperdeformation und einer 3-d nichtlinearen Porenfluidströmung, wobei deformationsabhängige und anisotrope Permeabilitätseigenschaften zu berücksichtigen sind.

Hinsichtlich der numerischen Behandlung gekoppelter Festkörper-Fluid-Probleme bietet die Finite-Elemente-Methode (FEM) eine effiziente Möglichkeit zur Lösung beliebiger Anfangs-Randwertprobleme (vgl. Lewis & Schrefler [109]). Soweit dem Autor bekannt ist, wurden die ersten Resultate aus FE-Simulationen eines flüssigkeitsgesättigten, deformierbaren porösen Mediums von Sandhu & Wilson [156] veröffentlicht. Hierbei ist bemerkenswert, daß ihr grundlegender Ansatz, die Festkörperverschiebungen und den Porenfluiddruck als Primärvariablen zu wählen und über quadratische und lineare Ansatzfunktionen in einer gemischten Elementformulierung zu approximieren, bis heute als Standard bei der FE-Diskretisierung poröser Medien verwendet wird. Daher erfolgt auch in dieser Arbeit die numerische Umsetzung des viskoelastischen TPM-Modells im Rahmen der Finite-Elemente-Methode, wobei von einer Verschiebungs-Druck-Formulierung der beschreibenden Gleichungen ausgegangen wird. Unter der Annahme materieller Inkompressibilität und/oder einer quasi-statischen Betrachtung führt die räumliche Semi-Diskretisierung mit stabilen Finiten Elementen (Arnold [2], Brezzi & Fortin [27]) auf ein System differentialalgebraischer Gleichungen (DAE) in der Zeit. Die numerische Integration dieses semi-diskreten Systems kann durch geeignete Zeitverlaufsverfahren, wie z. B. diagonal implizite *Runge-Kutta*-Verfahren (DIRK), auf effiziente Weise erfolgen, wobei eine adaptive Zeitschrittweitensteuerung einfach integriert werden kann (Ellsiepen [65]). Zudem können diese leistungsfähigen, primär für das globale DAE-System konzipierten Zeitintegrationsverfahren auch erfolgreich für die lokale Zeitdiskretisierung der inelastischen Entwicklungsgleichungen eingesetzt werden (vgl. Diebels *et al.* [46]).

Für die praktische Anwendung muß das mathematische Modell an reales Materialverhalten angepaßt werden, d. h. die konstitutiv eingeführten Materialparameter müssen bestimmt werden. Aufgrund der Komplexität der makroskopischen Materialgleichungen kann jedoch nicht jedem Parameter eine direkte physikalische Bedeutung beigemessen werden. Außerdem erweist es sich versuchstechnisch als schwierig, die überlagerten dissipativen Effekte, die aus der finiten viskoelastischen Festkörperdeformation und der nichtlinearen viskosen Porenfluidströmung resultieren, getrennt voneinander zu erfassen. Ausgehend von wohl definierten Experimenten, die durch entsprechende FE-Simulationen nachgerechnet werden können, ist somit die Anwendung eines numerischen Optimierungsverfahrens zur Parameteridentifikation unumgänglich. Die prinzipielle Aufgabe besteht darin, einen Satz zulässiger Materialparameter zu finden, so daß die Funktion der quadrierten Abweichungen aus Simulations- und Versuchsergebnissen minimal wird. Zu diesem Zweck muß eine restringierte Minimierungsstrategie verwendet werden, die über Ungleichheitsnebenbedingungen die Berücksichtigung von Restriktionen an die Parameter ermöglicht. Basierend auf den Arbeiten von Powell [143, 144] wird hierzu ein gradientenfreier, direkter Suchalgorithmus für die Minimierung des Fehlerquadratfunktionals eingesetzt, wobei eine hierarchische Simulationsstrategie den Rechenaufwand in einem vertretbaren Rahmen hält. Im Detail wird mit Hilfe von Powells *Constrained-Optimization-by-Linear-Approximation*-Algorithmus COBYLA das viskoelastische Zweiphasenmodell an experi-

mentelle Daten eines hochporösen Polyurethanschaumstoffs angepaßt und im Anschluß zur Berechnung von zwei praxisrelevanten Anfangs-Randwertproblemen verwendet.

Zusammenfassend bleibt festzuhalten, daß zur Erreichung der Ziele in der vorliegenden Arbeit eine interagierende, zweiphasige Festkörper-Fluid-Mischung im Rahmen der Theorie Poröser Medien betrachtet werden muß. Zur Vereinfachung wird die Darstellung auf isotherme Bedingungen eingeschränkt und Massenaustauschprozesse zwischen den Konstituierenden, z. B. aufgrund von Phasenübergängen oder chemischen Reaktionen, werden ausgeschlossen. Das makroskopische Verhalten des als materiell inkompressibel und isotrop angenommenen viskoelastischen Festkörperskeletts wird, ausgehend von einem multiplikativen geometrischen Konzept, durch eine finite Viskoelastizitätsformulierung beschrieben, die auf einer auf poröse Medien erweiterten *Ogden*-Verzerrungsenergie basiert. Die Interaktion mit einem materiell kompressiblen oder inkompressiblen Porenfluid wird über eine nichtlineare, viskose Schleppkraft berücksichtigt, die über ein 3-d *Forchheimer*-Filtergesetz mit deformationsabhängigen Permeabilitätskoeffizienten beschrieben wird. Darüber hinaus werden anfängliche und deformationsinduzierte anisotrope Permeabilitätseffekte in der makroskopischen Formulierung berücksichtigt. Alle Untersuchungen werden im Rahmen einer thermodynamisch konsistenten Theorie durchgeführt, in der die Zulässigkeit der eingeführten Konstitutivgleichungen über das Entropieprinzip garantiert wird. Die numerische Behandlung erfolgt mit Hilfe der FEM, in dem die Festkörperverschiebung und der Porenfluiddruck als Primärvariablen durch stabile gemischte Elementformulierungen approximiert werden. Die Verwendung von *Runge-Kutta*-Zeitintegrationsverfahren für die globale sowie die lokale Zeitdiskretisierung ermöglicht eine effiziente zeitadaptive Berechnung großer, gekoppelter, viskoelastischer Probleme. Schließlich werden die Anwendbarkeit und die praktische Bedeutung der vorgestellten makroskopischen Formulierung gezeigt, in dem das Modell numerisch an das mechanische Verhalten eines weichen, zellularen Polymerschaumstoffs angepaßt und auf zwei illustrative numerische Beispiele angewendet wird. Damit liefert die vorliegende Arbeit einige neue Aspekte zur Theorie Poröser Medien hinsichtlich der konsistenten Modellierung, der effizienten numerischen Umsetzung und der erfolgreichen Parameteranpassung, wobei das gesamtheitliche Modell den derzeitigen Stand der Technik im Bereich der Viskoelastizität poröser Medien definiert.

Gliederung der Arbeit

In *Kapitel 1* wird die Arbeit eingeleitet, und das makroskopische Konzept wird motiviert. Des weiteren wird ein umfangreicher Überblick über den Stand der Forschung hinsichtlich der Beschreibung poröser Materialien, der Modellierung viskoelastischen Festkörperverhaltens sowie der Behandlung nichtlinearer Strömungsprozesse in fluidgesättigten, porösen Medien gegeben.

Die kontinuumsmechanischen Grundlagen der Theorie Poröser Medien (TPM) inklusive der Kinematik, der Bilanzgleichungen und des Entropieprinzips für Mischungen werden in *Kapitel 2* dargestellt. Basierend auf einem multiplikativen geometrischen Konzept wird hierbei besonderer Wert auf eine verständliche Einführung der finiten inelastischen Deformationsgrößen des Festkörperskeletts gelegt, wobei die anschauliche Darstellung mittels

natürlicher Koordinaten erfolgt.

In *Kapitel 3* wird ein geeigneter Satz an Konstitutivgleichungen auf der Basis einer allgemeinen Festkörper-Fluid-Mischung vorgestellt, der die gekoppelten dissipativen Effekte erfaßt, die sich aus der Überlagerung einer viskosen Porenfluidströmung durch ein viskoelastisches Festkörperskelett ergeben. Hierzu wird eine thermodynamisch konsistente Zweiphasen-TPM-Formulierung bereitgestellt, die um speziell entwickelte Stoffgesetze zur Beschreibung der viskoelastischen Feststoffmatrix bei finiten Deformationen und des nichtlinearen Strömungsprozesses eines allgemeinen Porenfluids ergänzt wird.

Die numerische Behandlung des viskoelastischen Zweiphasenmodells im Rahmen der gemischten Finite-Elemente-Methode (FEM) ist Bestandteil von *Kapitel 4*. In diesem Zusammenhang werden die schwache Form der beschreibenden Bilanzgleichungen und deren Linearisierung präsentiert, gefolgt von geeigneten Techniken zur Orts- und Zeitdiskretisierung inklusive einer effizienten Strategie zur Behandlung der inelastischen Evolutionsgleichungen. Des weiteren wird auf den Algorithmus zur Berechnung der viskoelastischen Festkörperextraspannung näher eingegangen.

Kapitel 5 beschäftigt sich mit der praktischen Anwendung des entwickelten Modells. Hierzu wird die viskoelastische Zweiphasenformulierung mittels eines gradientfreien, numerischen Optimierungsverfahrens an experimentelle Daten eines offenzelligen Polyurethanschaumstoffs angepaßt. Danach werden die FE-Simulationen zweier illustrativer Anfangs-Randwertprobleme vorgestellt, um den Einfluß des Porenfluids auf die makroskopische Materialantwort, die Effizienz der numerischen Implementierung und die allgemeine Anwendbarkeit des Modells auf reale Ingenieurprobleme zu verdeutlichen.

Eine abschließende Zusammenfassung und Diskussion wird im *letzten Kapitel* gegeben, wobei mögliche Weiterentwicklungen und das generelle Zukunftspotential des viskoelastischen TPM-Modells in anderen Ingenieurdisziplinen, wie z. B. der Biomechanik, gezielt angesprochen werden.

Nomenclature

As far as possible, the nomenclature in this monograph follows the conventions and symbols that are commonly used in modern tensor calculus, such as in the books by de Boer [17], Papastavridis [141], or Holzapfel [93], ch. 1. Concerning porous media theories, the work adheres to the established notations given by de Boer [19] and Ehlers [54].

Conventions

Index and suffix conventions

$i, j, k, l, \ldots$	indices as sub- or superscripts range from 1 to N; usually $N = 3$ in the 3-d physical space of our experience
$(\bullet)_k\,(\bullet)^k = \sum_k (\bullet)_k\,(\bullet)^k$	*Einstein*'s summation convention, i. e., summation over indices that appear twice unless stated otherwise
$\sum\!\!\!\!\!\!\diagup\, k$	suspend summation convention for the index k
$(\bullet)_S$, $(\bullet)_F$	capital subscripts indicate the belonging of kinematical quantities to a constituent within mixture theories
$(\bullet)^S$, $(\bullet)^F$	capital superscripts indicate the belonging of non-kinematical quantities to a constituent within mixture theories
$(\bullet)_{Se}$, $(\bullet)_{Si}$	special subscripts "Se" and "Si" indicate the elastic and inelastic parts associated with an inelastic solid deformation

Kernel conventions

$(\bullet)$			place holder for kernel quantity
$s, t, \ldots$	or	$\sigma, \tau, \ldots$	scalars (0th-order tensors)
$\mathbf{s}, \mathbf{t}, \ldots$	or	$\boldsymbol{\sigma}, \boldsymbol{\tau}, \ldots$	vectors (1st-order tensors)
$\mathbf{S}, \mathbf{T}, \ldots$	or	$\boldsymbol{\sigma}, \boldsymbol{\tau}, \ldots$	2nd-order tensors
$\overset{n}{\mathbf{S}}, \overset{n}{\mathbf{T}}, \ldots$	or	$\overset{n}{\boldsymbol{\sigma}}, \overset{n}{\boldsymbol{\tau}}, \ldots$	nth- or higher-order tensors, e. g., $\overset{4}{\mathbf{D}}$, $\overset{3}{\mathbf{E}}$, $\overset{2}{\mathbf{F}} = \mathbf{F}$, $\overset{1}{\mathbf{G}} = \mathbf{g}$
$\boldsymbol{s}, \boldsymbol{t}, \ldots$	and	$\boldsymbol{S}, \boldsymbol{T}, \ldots$	general column vectors $(n \times 1)$ and general matrices $(n \times m)$

Selected tensor operations (cf. appendix A)

$(\bullet)^T$	transpose of vectors, tensors or matrices
$(\bullet)^{\overset{kl}{T}}$	special transposition of higher-order tensors by an exchange of the kth and the lth basis system of the tensorial basis
$\overset{n}{\mathbf{S}}\,\overset{s}{\mathbf{T}} = \overset{n-s}{\mathbf{R}}$ with $n \geq s$	contracting (inner) tensor product (linear mapping)
$\overset{n}{\mathbf{S}} \cdot \overset{n}{\mathbf{T}} = r$	scalar (dot) product (special contracting tensor product)
$\overset{n}{\mathbf{S}} \otimes \overset{s}{\mathbf{T}} = \overset{n+s}{\mathbf{R}}$	dyadic (vector space) tensor product

Remark: Specific formulæ and rules of tensor algebra and analysis that are required throughout this work are directly given in the text or in appendix A. ■

Symbols

Symbol	Unit	Description
α		constituent identifier (here: $\alpha = \{S, F\}$)
$\alpha_{0(m)}, \alpha_{n(m)}$	[–]	dimensionless *Ogden* parameters (exponents)
β	[–]	exponent governing the deformation dependency of B^S
γ^{FR}	[N/m^3]	effective fluid weight
γ_0^S, γ_n^S	[–]	parameters governing the volumetric response of φ^S
$\delta_{kl} = \delta^{kl} = \delta_l^k$	[–]	*Kronecker* symbol
$\varepsilon, \varepsilon^\alpha$	[J/kg]	mass-specific internal energy of φ and φ^α
ε_S	[–]	1-d infinitesimal solid strain
$\hat{\varepsilon}^\alpha$	[J/(m^3 s)]	volume-specific direct energy production of φ^α
ϵ_{klm}	[–]	*Levi-Cevita* permutation symbol
ζ_n^S	[N s/m^2]	2nd solid viscosity constant
$\hat{\zeta}^\alpha$	[J/(K m^3 s)]	volume-specific direct entropy production of φ^α
η_n^S	[N s/m^2]	solid shear viscosity constant
η, η^α	[J/(K kg)]	mass-specific entropy of φ and φ^α
$\hat{\eta}, \hat{\eta}^\alpha$	[J/(K m^3 s)]	volume-specific direct entropy production of φ^α
θ^k	[$\cdot$]	general curvilinear coordinate
Θ^α	[K]	absolute *Kelvin*'s temperature of φ^α
κ	[–]	exponent governing the deformation dependency of K^S
$\lambda_{S(k)}$	[–]	eigenvalue of $\mathbf{C}_S$ or $\mathbf{B}_S$ (squared principal stretch)
Λ_0^S, Λ_n^S	[N/m^2]	2nd *Lamé* constants of φ^S
μ_0^S, μ_n^S	[N/m^2]	1st *Lamé* constants (conventional shear moduli) of φ^S
$\mu_{0(m)}^*, \mu_{n(m)}^*$	[–]	dimensionless *Ogden* parameters (polynomial coefficients)
μ^F, μ^{FR}	[N s/m^2]	partial and effective dynamic fluid viscosity
ν^{FR}	[m^2/s]	effective kinematic viscosity
ξ_n^S	[N s/m^2]	solid bulk viscosity constant
Π	[–]	dimensionless number relating friction and interaction force
ρ	[kg/m^3]	mixture density
$\rho^\alpha, \rho^{\alpha R}$	[kg/m^3]	partial and effective (realistic) density of φ^α
$\hat{\rho}^\alpha$	[kg/(m^3 s)]	volume-specific mass production of φ^α

σ_E^S	$[\mathrm{N/m^2}]$	1-d solid extra stress of the linear theory
$\sigma_\eta, \sigma_\eta^\alpha$	$[\mathrm{J/(K\,m^3\,s)}]$	volume-specific external entropy supply of φ and φ^α
$\tau_n^S, \overline{\tau}_n^S$	$[\mathrm{s}]$	solid relaxation and retardation time constant
φ, φ^α		entire mixture and constituent α
ψ^α	$[\mathrm{J/kg}]$	mass-specific constituent *Helmholtz* free energy
a_{kl}, a^{kl}	$[\,\cdot\,]$	co- and contravariant actual metric coefficient
B^S	$[\mathrm{m}]$	intrinsic deformation-dependent tortuosity[1]
$\mathcal{B}, \mathcal{B}^\alpha$		mixture body and partial body
D_n^S	$[\mathrm{N\,s/m^2}]$	solid viscosity parameter
$\mathcal{D}_{\mathrm{int}}$	$[\mathrm{J/(m^3\,s)}]$	entire volume-specific internal dissipation
e_{VS}	$[-]$	finite solid volume dilatation
$\hat{e}^\alpha$	$[\mathrm{J/(kg\,s)}]$	volume-specific total energy production of φ^α
E_0^S, E_n^S	$[\mathrm{N/m^2}]$	solid elasticity constants (*Young*'s moduli)
g	$[\mathrm{m/s^2}]$	scalar gravitational acceleration
g_{kl}, g^{kl}	$[\,\cdot\,]$	general co- and contravariant metric coefficient
$\mathcal{G}^S$	$[\mathrm{N/m^2}]$	solid relaxation function
h_{kl}, h^{kl}	$[\,\cdot\,]$	co- and contravariant reference metric coefficient
I_S, II_S, III_S	$[-]$	three principal invariants of $\mathbf{C}_S$ and $\mathbf{B}_S$
J_α	$[-]$	*Jacobi*an determinant of φ^α
$\mathcal{J}^S$	$[\mathrm{m^2/N}]$	solid creep or retardation function
k_0^S, k_n^S	$[\mathrm{N/m^2}]$	solid bulk moduli
K^S	$[\mathrm{m^2}]$	intrinsic deformation-dependent permeability[1]
L	$[\mathrm{m}]$	characteristic length
M_m^F	$[\mathrm{kg/mol}]$	molar mass of the compressible fluid constituent
n^α	$[-]$	volume fraction of φ^α
$p = p^{FR}$	$[\mathrm{N/m^2}]$	excess pore-fluid pressure
$\mathcal{P}$	$[\mathrm{N/m^2}]$	*Lagrange*an multiplier (here: identified as the fluid pressure)
P	$[\mathrm{N/m^2}]$	characteristic pressure
$\mathcal{P}^\alpha$		material point of φ^α
$\overline{q}$	$[\mathrm{kg/(m^2\,s)}]$	area-specific mass efflux
r, r^α	$[\mathrm{J/(kg\,s)}]$	mass-specific external heat supply of φ and φ^α
R	$[\mathrm{J/(K\,mol)}]$	universal gas constant
Re	$[-]$	*Reynolds* number
$\mathcal{S}, \mathcal{S}^\alpha$		mixture surface of $\mathcal{B}$ and partial surface of $\mathcal{B}^\alpha$

[1] A summary of further permeability and tortuosity measures is given in box (3.158) on page 85.

t	[s]	time
$\mathcal{U}^S$	[J/m^3]	volumetric part of the solid strain energy $\mathcal{W}^S$
$\overline{v}$	[m/s]	area-specific volume efflux
$\mathcal{V}^{FR}$	[m^3/kg]	effective specific fluid volume
V	[m/s]	characteristic velocity
V, V^α	[m^3]	mixture volume of $\mathcal{B}$ and partial volume of $\mathcal{B}^\alpha$
$\mathcal{V}^3$		proper *Euclid*ean vector space
w_F	[m/s]	1-d fluid filter velocity
$\mathcal{W}^S$	[J/m^3]	volume-specific solid strain-energy function
$\widehat{z}_{kl}, \widehat{z}^{kl}$	[•]	co- and contravariant intermediate metric coefficient
$\boldsymbol{\phi}_\eta, \boldsymbol{\phi}_\eta^\alpha$	[J/(K m^2 s)]	entropy efflux vector of φ and φ^α
$\boldsymbol{\chi}_\alpha, \boldsymbol{\chi}_\alpha^{-1}$	[m]	motion and inverse motion function of φ^α
$\mathbf{a}_k, \mathbf{a}^k$	[•]	co- and contravariant actual basis vector
$\mathbf{b}, \mathbf{b}^\alpha$	[m/s^2]	mass-specific body force vector acting on $\mathcal{B}$ and $\mathcal{B}^\alpha$
$\mathbf{d}_\alpha$	[m/s]	diffusion velocity vector
$\mathbf{e}_k$	[–]	orthonormal (rectangular *Cartesi*an) basis vector
$\mathbf{f}, \mathbf{f}^\alpha$	[N]	resultant force vector acting on $\mathcal{B}$ and $\mathcal{B}^\alpha$
$\mathbf{g}_k, \mathbf{g}^k$	[•]	general co- and contravariant basis vector
$\mathbf{h}_k, \mathbf{h}^k$	[•]	co- and contravariant reference basis vector
$\hat{\mathbf{h}}^\alpha$	[N/m^2]	volume-specific total angular momentum production of φ^α
$\mathbf{i}$	[–]	hydraulic gradient
$\mathbf{m}_{S(k)}$	[–]	eigenvector of $\mathbf{C}_S$ related to the reference configuration
$\hat{\mathbf{m}}^\alpha$	[N/m^2]	volume-specific direct angular momentum production of φ^α
$\mathbf{n}$	[–]	outward oriented unit surface normal vector
$\mathbf{n}_{S(k)}$	[–]	eigenvector of $\mathbf{B}_S$ related to the actual configuration
$\hat{\mathbf{p}}^\alpha, \hat{\mathbf{p}}_E^\alpha$	[N/m^3]	volume-specific direct and extra momentum production of φ^α
$\mathbf{q}, \mathbf{q}^\alpha$	[J/(m^2 s)]	heat influx vector of φ and φ^α
$\boldsymbol{q}$	[•]	column vector of all internal integration point variables[2]
$\hat{\mathbf{s}}^\alpha$	[N/m^3]	volume-specific total momentum production of φ^α
$\mathbf{t}, \mathbf{t}^\alpha$	[N/m^2]	surface traction vector acting on $\mathcal{S}$ and $\mathcal{S}^\alpha$
$\overline{\mathbf{t}}$	[N/m^2]	area-specific external load vector (traction force)
$\mathbf{t}_E^F$	[N/m^3]	volume-specific fluid friction force
$\mathbf{u}_S$	[m]	solid displacement vector
$\boldsymbol{u}$	[•]	column vector of all FEM degrees of freedom[2]

[2] Further symbols associated with the numerical treatment are given in chapter 4.

$\mathbf{w}_F, \mathbf{w}_{FR}$	$[\mathrm{m/s}]$	fluid filter and seepage velocity vector
$\dot{\mathbf{x}}$	$[\mathrm{m/s}]$	mixture velocity vector
$\overset{\prime}{\mathbf{x}}_\alpha = \mathbf{v}_\alpha$	$[\mathrm{m/s}]$	constituent velocity vector
$\mathbf{X}_\alpha = \mathbf{x}_{0\alpha}$	$[\mathrm{m}]$	reference position vector of $\mathcal{P}^\alpha$
$\mathbf{x}$	$[\mathrm{m}]$	actual position vector
$\widehat{\mathbf{x}}_{Si}$	$[\mathrm{m}]$	(fictitious) position vector of the intermediate configuration
$\ddot{\mathbf{x}}$	$[\mathrm{m/s^2}]$	mixture acceleration vector
$\overset{\prime\prime}{\mathbf{x}}_\alpha$	$[\mathrm{m/s^2}]$	constituent acceleration vector
$\widehat{\mathbf{z}}_k, \widehat{\mathbf{z}}^k$	$[\,\cdot\,]$	co- and contravariant intermediate basis vector
$\widehat{\boldsymbol{\Gamma}}_S$	$[-]$	contravariant intermediate solid strain tensor
$\boldsymbol{\varepsilon}_S$	$[-]$	infinitesimal solid strain tensor
$\boldsymbol{\sigma}_E^S$	$[\mathrm{N/m^2}]$	solid extra stress tensor of the linear theory
$\boldsymbol{\tau}^S$	$[\mathrm{N/m^2}]$	*Kirchhoff* solid stress tensor
$\widehat{\boldsymbol{\tau}}^S$	$[\mathrm{N/m^2}]$	intermediate solid stress tensor
$\overset{4}{\boldsymbol{\tau}}{}_n^S$	$[\mathrm{s}]$	4th-order relaxation tensor
$\boldsymbol{\Omega}_S$	$[1/\mathrm{s}]$	solid gyration tensor
$\mathbf{A}_S$	$[-]$	contravariant *Almansi*an solid strain tensor
$\mathbf{B}_S$	$[-]$	left *Cauchy-Green* solid deformation tensor
$\overset{4}{\mathbf{B}}{}_0^S, \overset{4}{\mathbf{B}}{}_n^S$	$[\mathrm{N/m^2}]$	4th-order elasticity tensors of the reference configuration
$\mathbf{C}_S$	$[-]$	right *Cauchy-Green* solid deformation tensor
$\overset{4}{\mathbf{C}}{}_0^S, \overset{4}{\mathbf{C}}{}_n^S$	$[\mathrm{N/m^2}]$	4th-order elasticity tensors of the actual configuration
$\mathbf{D}_\alpha$	$[1/\mathrm{s}]$	stretching or deformation rate tensor of φ^α
$\overset{4}{\mathbf{D}}{}_n^S$	$[\mathrm{N\,s/m^2}]$	4th-order viscosity tensor of the linear theory
$\mathbf{E}_S$	$[-]$	contravariant *Green-Lagrange*an solid strain tensor
$\overset{3}{\mathbf{E}}$	$[-]$	*Ricci* permutation tensor (3rd-order fundamental tensor)
$\overset{4}{\mathbf{E}}{}_0^S, \overset{4}{\mathbf{E}}{}_n^S$	$[\mathrm{N/m^2}]$	4th-order elasticity tensors of the linear theory
$\mathbf{F}_\alpha$	$[-]$	material deformation gradient tensor of φ^α
$\boldsymbol{\mathcal{H}}^S$	$[-]$	hydraulic structural tensor of the permeable solid constituent
$\mathbf{I}$	$[-]$	identity tensor (2nd-order fundamental tensor)
$\overset{4}{\mathbf{I}}, \overset{4}{\mathbf{I}}_T, \overset{4}{\mathbf{I}}_{\mathrm{tr}}$	$[-]$	4th-order fundamental tensors
$\mathbf{K}_S$	$[-]$	covariant actual *Karni-Reiner* solid strain tensor
$\overset{\mathrm{R}}{\mathbf{K}}_S$	$[-]$	covariant referential *Karni-Reiner* solid strain tensor
$\widehat{\mathbf{K}}_S$	$[-]$	covariant intermediate *Karni-Reiner* solid strain tensor
$\mathbf{K}^F$	$[\mathrm{m^4/(N\,s)}]$	permeability tensor

$\boldsymbol{\mathcal{K}}^S$	[–]	deformation-dependent part of $\boldsymbol{\mathcal{H}}^S$
$\mathbf{L}_\alpha$	[1/s]	spatial velocity gradient tensor of φ^α
$\mathbf{M}_{S(k)}$	[–]	eigentensor of $\mathbf{C}_S$ related to the reference configuration
$\boldsymbol{\mathcal{M}}^S$	[–]	solid structural tensor
$\mathbf{N}_{S(k)}$	[–]	eigentensor of $\mathbf{B}_S$ related to the actual configuration
$\mathbf{P}^S$	[N/m^2]	1st *Piola-Kirchhoff* solid stress tensor
$\mathbf{Q}_S, \widehat{\mathbf{Q}}_S$	[–]	proper orthogonal tensors
$\boldsymbol{\mathcal{Q}}^S$	[$\cdot$]	general tensor-valued internal variable related to φ^S
$\mathbf{R}_S$	[–]	solid rotation tensor of the polar decomposition of $\mathbf{F}_S$
$\mathbf{S}^S$	[N/m^2]	2nd *Piola-Kirchhoff* solid stress tensor
$\mathbf{T}$	[N/m^2]	total *Cauchy* stress tensor of φ
$\mathbf{T}^\alpha, \mathbf{T}^\alpha_E$	[N/m^2]	partial and partial extra *Cauchy* stress tensor
$\mathbf{U}_S$	[–]	right solid stretch tensor of the polar decomposition of $\mathbf{F}_S$
$\mathbf{V}_S$	[–]	left solid stretch tensor of the polar decomposition of $\mathbf{F}_S$
$\mathbf{W}_\alpha$	[1/s]	spin or vorticity tensor of φ^α

1 Introduction

The goal of this contribution is to merge the advances in porous media theories and the state of the art in single-phase finite viscoelasticity within a well-founded thermodynamical framework. In particular, a thermodynamically consistent constitutive setting is presented where, based on the internal variable concept, an extended *Ogden*-type viscoelasticity formulation is embedded into the macroscopic Theory of Porous Media (TPM). By focusing on immiscible binary solid-fluid aggregates, essential nonlinearities of the strongly coupled problem are included in the formulation. Thus, the developed biphasic continuum mechanical model accounts for the relevant physical properties stemming from the porous microstructure, the moving and interacting viscous pore fluid (compressible or incompressible), and the directly coupled intrinsic viscoelasticity of the skeleton material itself. In order to demonstrate its suitability, the presented model is especially adapted to the behavior of open-celled polymer foams, as these materials combine all nonlinearities under absolute finite viscoelastic deformations. Finally, after the numerical treatment of the governing model equations through the mixed finite element method (FEM), large strain 3-d simulations reveal the capabilities of the proposed macroscopic formulation and the efficiency of its numerical implementation.

1.1 Motivation

It is quite obvious that the volumetric deformation of a permeable fluid-saturated porous solid will always cause viscous pore-fluid motion thereby initiating the well-known consolidation process under drained conditions (Terzaghi & Jelinek [175]). This time-dependent effect is overlaid by another dissipative phenomenon if the porous solid skeleton itself exhibits relaxation and creep behavior, i. e., behaves viscoelastic. In general, the flow-dependent and the flow-independent (intrinsic) viscoelastic properties are strongly coupled and must be treated within the framework of the nonlinear thermodynamics of multi-phase materials. In this context, all investigations must be carried out in the large strain regime since the materials of interest, such as hydrated tissues and gels or foamed polymers, are generally intended to undergo finite viscoelastic deformations during their practical application. Focusing on the microscale of these materials, a variety of different porous structures can be found ranging from viscoelastic molecular chain meshworks with interstitial fluid filling the gaps to more skeletal or cellular viscoelastic structures built by a combination of open and/or closed fluid-filled cells. In particular, these microstructures undergo complex deformation mechanisms under external loads often resulting in a highly nonlinear stress-strain response of the macroscopic material.

Nowadays, sophisticated imaging techniques, e. g., the Micro Computer Tomography (Micro CT) or the Magnetic Resonance Imaging (MRI), allow the 3-d reconstruction of many porous microstructures with resolutions up to a few microns (figure 1.1). However, even through increased computer power, the numerical simulation of real applications on the

microscale using reconstructed models is currently not reasonable. Alternatively, the microstructure can be idealized by discrete particles, beam, or shell elements, instead of dealing with the real pore geometry. Even then, the computer resources required to solve problems of practical relevance are out of scale. Furthermore, in these discrete approaches, the description of a free-moving pore fluid and, as a consequence, the frictional drag on the microstructural skeleton, as well as the inner contact in collapsing pores, are more than problematic.

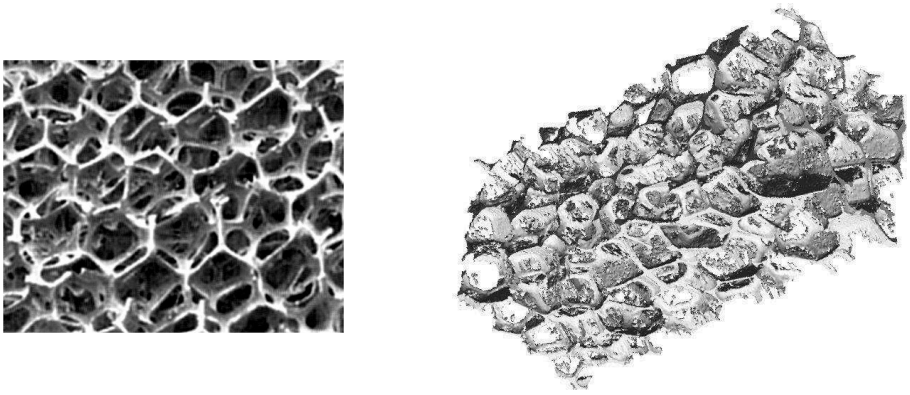

Figure 1.1: *Microscopic photograph of an open-celled PUR foam and 3-d reconstruction of a PUR foam microstructure from Micro-CT scans (courtesy of RJL Micro & Analytic)*

A further possibility to analyze the stress response of porous materials is to apply homogenization techniques to idealized models of the microstructure. In the case of foamed solids, an average pore can be approximated by a simple beam or shell model of a volume filling polyhedron, where the effective (macroscopic) material parameters can be determined from scaling laws (Gibson & Ashby [72]). This leads to a good description concerning materials with a more or less well-defined pore structure, such as honeycombs and cellular foams. However, these models usually reach their limits in describing the coupled influence of an interacting pore fluid properly.

Thus, it can be concluded that in the case of real-scale porous media problems, where the pore-fluid flow can have a distinct influence on the transient response of the entire material, a macroscopic mixture approach provides the convenient solution strategy. Following this, an independent fluid constituent can be easily included, even if there is no detailed information about the porous microstructure. As a consequence, a statistical, multiphasic continuum mechanical model will be used to successfully represent the fully coupled behavior of viscoelastic fluid-saturated porous materials under external loads.

1.2 State of the Art

In the present contribution, the macroscopic description of viscoelastic fluid-saturated porous solids is considered in the framework of the well-founded Theory of Porous Media (TPM). The TPM as a multiphasic continuum theory combines the Theory of Mixtures (TM) with the concept of volume fractions yielding an excellent tool for the macroscopic

description of general immiscible solid-fluid aggregates. In particular, according to the TM, all constituents are assumed to be statistically distributed over the regarded domain in the sense of superimposed and interacting continua, where the microstructural information is only considered by local volumetric ratios, the so-called volume fractions, following the corresponding concept. For a more detailed discussion of the general frame of the TPM, its extensions, e. g., to micropolar (*Cosserat*) continua (Cosserat & Cosserat [37]), and its historical development, the interested reader is referred to the works of Bowen [22, 23], de Boer [18, 19], and Ehlers [50, 54], as well as to the quotations therein. Moreover, additional information on porous media theories, particularly following the ideas of Biot [10], can be found in the textbooks by Coussy [38] and Lewis & Schrefler [109].

Here, focusing on the applicability of the standard TPM approach to biphasic porous materials excluding thermal effects and any mass exchanges where one solid skeleton is saturated by a single pore fluid, a broad field of engineering problems can still be addressed. This is because arbitrary, thermodynamically admissible constitutive relations for the effective solid stress and the effective fluid momentum production can be consistently added to the macroscopic formulation according to the effective stress principle (Bishop [13], Skempton [167], de Boer & Ehlers [20]). However, the traditional application of the TPM, as well as any other mixture theory, to geomechanical problems, primarily led to the development of sophisticated elastoplastic and elasto-viscoplastic constitutive models that are capable of describing localization phenomena in saturated and unsaturated soils (Ehlers [50, 51], Ehlers & Müllerschön [62], and Diebels *et al.* [46]). More recently, proceeding from the works of Eipper [64] and Ehlers & Eipper [55] on finite porous media elasticity, the elastoplastic models are extended towards geometrical nonlinearities applying simple neo-*Hooke*an-type elasticity formulations and are adapted for the description of hard polymer and metal foams, which suffer immense plastic deformations (Mahnkopf [118] and Droste [47]).

For the purpose of this work, an appropriate finite viscoelasticity law accounting for a highly nonlinear behavior of the porous solid matrix must be developed and has to be added to the biphasic formulation. Certainly, the combination of porous media theories with viscoelastic constitutive equations for the solid skeleton is not a new idea, see, e. g., Biot [11] and Mak [119]. Particularly, the linear biphasic poroviscoelastic (BPVE) theory proposed by Mak, which applies the linear integral-type viscoelasticity model by Fung [70], has been established for the description of cartilaginous tissues (Setton *et al.* [160]). However, the numerical treatment of such integral-type formulations, where the external state variables expressed as functionals of the process history capture the idea of materials with fading memory by a continuous relaxation spectrum (Coleman & Noll [35, 36], Gurtin & Sternberg [78], Coleman [33]), turns out to be very inefficient because of the intensive computational burden associated with the time integration of the convolution integrals (Suh & Bai [171]).

A more convenient approach to solid viscoelasticity, especially from a numerical point of view, is provided by the model rheology in combination with the thermodynamics with internal state variables (Coleman & Gurtin [34], Lubliner [115], Valanis [184]). Proceeding from a rheological model that covers the response of viscoelastic solids by an appropriate assembly of elastic springs and viscous dashpots (cf. Tschoegl [183]), such as the gener-

alized *Maxwell* model (figure 1.2), strain-equivalent internal variables can be introduced, which can directly be associated with the dashpot deformations. This phenomenological procedure yields a differential representation of viscoelasticity, where a discrete relaxation spectrum allows for an efficient numerical treatment. The internal variables can then be treated as history variables depending on the time discretization of the constitutive differential evolution equations. For the simple geometrically linear case, the discrete spectrum algorithm has already been successfully applied within the TPM for the 3-d simulation of soft hydrated biological tissues (Ehlers & Markert [59, 60]). A general introduction to linear viscoelasticity can be found in the books by Christensen [30], Tschoegl [183], and Wineman & Rajagopal [193] among others.

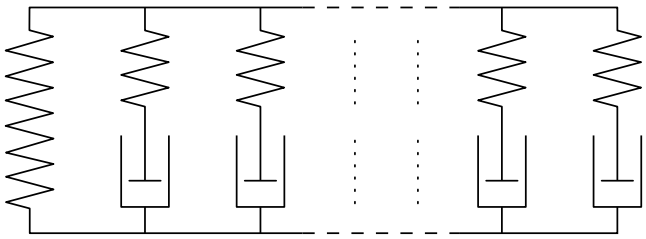

Figure 1.2: *Rheological structure of the generalized Maxwell model, a parallel assembly of one spring and a finite number of Maxwell elements (spring and dashpot in series)*

In terms of finite deformations, where the introduction of internal variables and the choice of evolution laws is not so evident nor unique, one can adopt the state of the art in finite viscoelasticity of non-porous solids and extend it to porous media applications. Following the related literature, e. g., le Tallec *et al.* [173], Lion [111], Reese & Govindjee [151] or Huber & Tsakmakis [95], it is convenient to proceed from the aforementioned internal variable concept, where the phenomenological introduction of strain-equivalent internal variables is accomplished by multiplicative decompositions of the deformation gradient into elastic and inelastic parts, as it is well-established in finite plasticity theories according to Lee [108]. As far as it is known, the multiplicative geometric approach in connection with the notion of an *intermediate state* originates from Kröner [104], § 4 in the context of crystal plasticity. In principle, the formal similarities in multiplicative inelasticity allow the exploitation of the sophisticated solution strategies that were developed over the years in the field of finite elastoplasticity. For further particulars on multiplicative viscoelasticity and possible micromechanical motivations, e. g., based on the transient network theory (Green & Tobolsky [76]), see Sidoroff [162], Lubliner [116], Reese [149], and the references therein.

Alternatively, avoiding the direct application of the multiplicative geometrical concept, Miehe & Keck [124] chose inelastic metric tensors as developing internal variables to characterize the inelastic deformation state, see also Miehe [122, 123]. Moreover, it should be noted that also stress-equivalent internal variables can be introduced representing the rate-dependent overstresses, which relax towards the thermodynamical equilibrium. The current stress state can then be computed from a recursive formula, which is derived from a time discretization of the convolution integrals covering the categorical linear differential evolution equations of the overstresses. Therefore, this procedure can be regarded as

an intermediate approach applying the internal variable concept in combination with an integral-type representation of the evolution equations. For more details, see, e. g., Taylor *et al.* [174], Simo [164], Holzapfel [92], or Kaliske & Rothert [99]. However, the required linearity of the evolution laws actually restricts the theoretical applicability of this procedure to problems with moderate deformation rates. Instead, following the multiplicative concept, consistent evolution equations for the introduced strain-equivalent internal variables can be found by evaluation of the entropy principle without being restricted to small perturbations away from the thermodynamic equilibrium as pointed out by Reese & Govindjee [151].

Regarding the constitutive relations used for the stress and the overstress computation in finite viscoelasticity of single-phase materials, mostly isotropic strain-energy functions are concerned with the description of dense rubber-like or polymeric materials, where also thermoviscoelastic phenomena (see Holzapfel & Simo [94], Lion [111], Reese & Govindjee [150]) and damage mechanisms, such as the *Mullins* effect (Mullins [129]), are considered. In order to reproduce the nonlinear stress-strain behavior of these materials, *Ogden*-type formulations (Ogden [136, 138, 139]) are extensively used because of their mathematical validity (Ball [5], Ciarlet [32], Ogden [137]) and their good, although challenging, adaptability to experimental observations. However, due to the supposed incompressibility of the considered materials, the formulations are usually restricted to isochoric deformations. In contrast, in the case of porous media viscoelasticity, compressible formulations are required, since, due to pore-space deformations and possible pore-fluid outflows, the macroscopic material is volumetrically deformable even if both the skeleton material and the pore fluid itself are materially incompressible. Therefore, special volumetrical extensions must be developed following the ideas of Eipper [64], which guarantee the volumetric stiffening of the porous medium towards the point of compaction, i. e., the deformation state with zero void ratio, where all pores are closed. This concept of the compaction point directly implies the characteristic property of structural densification of porous media under finite compression, which can be very well observed experimentally for foamed solids (Gibson & Ashby [72]). In this context, it is also referred to the constitutive strain energies suggested by Blatz & Ko [14] and Ogden [135] for the description of foam-like elastomers as compressible singlephasic materials.

Now, focusing on the description of the pore-fluid constituent, the flow of incompressible liquids, compressible gases, as well as inseparable mixture phases of liquid and gas, through saturated porous media is a common issue addressed in various publications. However, two main categories can be distinguished. On the one hand, investigating deformable porous materials, continuum theories like the TPM are applied to primarily recover the macroscopic deformation behavior. However, the included flow equations are usually based on a simple, although consistent, linear ansatz for the effective fluid momentum production, i. e., the interaction or drag force in biphasic solid-fluid mixtures, yielding a *Darcy*-type filter law (cf. Ehlers [54] and also Crochet & Naghdi [39]). This linear relation between lingering seepage flow and hydraulic gradient, firstly obtained by Darcy [41], indeed, cannot always be met in real applications. In order to account for flow changes due to skeleton deformations, some authors introduce the permeability as a function of the deformation state, e. g., governed by the volume dilatation using an expo-

nential ansatz (Mow *et al.* [128]) or governed by the current porosity following a power law (Eipper [64]). On the other hand, particularly in the disciplines of chemical, environmental and petroleum engineering, and hydrology, investigators proceed from undeformable porous media and are therefore primarily concerned with the detailed description of the percolation process through the rigid skeleton. In this context, turbulence and inertia effects, apparently responsible for the deviations from a laminar *Darcy* flow, are experimentally and theoretically discussed, where usually empirical observations lead to slight variations of the classical 1-d *Forchheimer* flow rule (Forchheimer [69]). For more details, see, e. g., Bear [7] and Dullien [48]. However, the objective of the present study requires the combination of absolutely finite skeleton deformations with a 3-d non-*Darcy*-type filter law including deformation-dependent permeability parameters. Moreover, initial and deformation-induced anisotropic permeability properties are of practical importance.

Concerning the numerical treatment of coupled solid-fluid problems, the finite element method (FEM) is a convenient technique for the solution of arbitrary initial boundary-value problems (Lewis & Schrefler [109]). For further particulars on the general fundamentals of the FEM, the interested reader is referred to the basic textbooks by Hughes [96] and Zienkiewicz & Taylor [199, 200, 201] among others. As far as the author is aware, the first results of finite element simulations of a fluid-saturated deformable porous medium are published by Sandhu & Wilson [156]. It is noteworthy that their principle approach, particularly the choice of the skeleton displacement and the pore-fluid pressure as primary field variables in combination with the approximation by quadratic and linear interpolations in mixed finite elements, defines the standard of porous media FE discretizations. Alternative approaches, which are especially designed for dynamical porous media problems in the field of geotechnical earthquake engineering, proceed from so-called splitting (operator split) or fractional algorithms, which are adopted from computational fluid dynamics (CFD) (Zienkiewicz *et al.* [196, 198]). These iterative semi-implicit-explicit schemes allow for an equal-order interpolation of the coupled fields without loss of stability (Pastor *et al.* [142], Zienkiewicz & Codina [197]). However, the procedure has other drawbacks, such as the somehow tricky treatment of the boundary conditions. Nevertheless, the growing popularity of the FEM as a solution strategy of coupled consolidation problems is associated with the tremendous increase of available computer power[1], which is displayed in the ongoing progress concerning size and complexity of the solved boundary-value problems. This becomes more clear by a chronological survey of some selected publications, such as Christian & Boehmer (1970) [31], Carter *et al.* (1977) [28], Prevost (1981) [148], Li *et al.* (1990) [110], Ehlers & Volk (1998) [63], Ehlers & Ellsiepen (2001) [57], and Wieners *et al.* (2002) [189]. Following this, the numerical treatment of the presented TPM model is carried out through the finite element method proceeding from a displacement-pressure formulation of the governing field equations with respect to the whole mixture. Due to material incompressibility and/or quasi-static considerations, the spatial semi-discretization by stable mixed finite elements (Arnold [2], Brezzi & Fortin [27]) leads to a system of differential-algebraic equations (DAE) in the time domain. The numerical integration of this semi-discrete system can be efficiently performed by suit-

[1] It can be observed that the ongoing speed-up of processing units follows *Moore's law*, stating that the amount of information storable on a given amount of silicon roughly doubles every year.

able time integration schemes, such as diagonally implicit *Runge-Kutta* (DIRK) methods (Diebels *et al.* [46], Ellsiepen [65]), where an embedded error estimator and a time step control can be added. For details concerning the general treatment of DAE systems, see Brenan *et al.* [25] or Hairer & Wanner [79]. Moreover, Diebels *et al.* [46] successfully used the sophisticated global time integration schemes also for the local time discretization of plastic evolution equations. This idea can directly be adopted for the time integration of viscoelastic evolution laws including an adaptive time step control, which is crucial in the case of creep or relaxation dominated processes. Note in passing that *Runge-Kutta* schemes have already been approved by Hartmann [80] in the frame of finite single-phase viscoelasticity.

For the practical application, the mathematical model has to be adjusted to real material behavior, i. e., the constitutively introduced material parameters have to be determined. Due to the complexity of the macroscopic material formulation, not all of the included material parameters can be associated with a distinct physical meaning. Moreover, the superposed dissipative phenomena of the viscous pore-fluid flow and the viscoelastic skeleton usually cannot be separately addressed in large strain experiments. Thus, based on suitable material tests that can be reproduced by coupled FE simulations, the application of numerical optimization techniques is inevitable. The challenge is to find a set of admissible material parameters such that the function of the squared deviations of simulation from experimental data becomes least. For this purpose, a constraint minimization strategy has to be applied. However, since it is out of the scope of the present work to discuss all available optimization techniques, the interested reader is referred to the textbooks by Luenberger [117], Fletcher [68], Spellucci [168], or Nocedal & Wright [132] among others. Here, following the works of Powell [143, 144], a derivative-free, direct search algorithm is used for the minimization of the least-squares functional, where a hierarchical simulation strategy keeps the computational overhead under an acceptable limit. In particular, Powell's *constrained optimization by linear approximations* (COBYLA) algorithm is used to adapt the viscoelastic model to a highly porous, open-celled polyurethane (PUR) foam.

In summary, to reach the goal of the present contribution, an interacting biphasic solid-fluid mixture is considered in the framework of the Theory of Porous Media. For simplicity, the presentation is restricted to isothermal conditions, and mass exchanges between the constituents, e. g., due to phase transitions or chemical reactions, are excluded. The macroscopic behavior of the materially incompressible, isotropic solid skeleton is described by a multiplicative finite viscoelasticity formulation based on extended *Ogden*-type strain energies. The interaction with the materially compressible or incompressible pore fluid is taken into account by a nonlinear viscous drag force, where a 3-d *Forchheimer*-type filter law with deformation-dependent permeability coefficients is finally used to govern the non-*Darcy* pore-gas or -liquid flow. Moreover, initial and deformation induced anisotropic permeability effects are included in the macroscopic formulation. All this is carried out within the background of a thermodynamically consistent theory, where the admissibility of the introduced constitutive relations is throughout guaranteed by the entropy principle. The numerical treatment is carried out through the FEM, where the solid displacement and the pore-fluid pressure as primary unknowns are approximated by stable mixed element formulations. The usage of *Runge-Kutta* time integration schemes for the global,

as well as for the local time discretization, allows for an efficient time-adaptive computation of large coupled viscoelastic systems. Finally, to show the overall applicability and the practical relevance of the presented macroscopic approach, the model is numerically adapted to the behavior of a soft cellular polymer foam, subsequently followed by two illustrative numerical examples. Thus, the present work delivers several new aspects to porous media theories concerning consistent modeling, efficient numerical treatment, and model adaption, where the overall combination defines the new state of the art in porous media viscoelasticity.

1.3 Overview

To begin with, in *Chapter 2*, the theoretical fundamentals of the TPM approach are briefly reviewed including the concept of volume fractions and the kinematics, the governing balance laws, and the entropy principle for mixtures. In this context, the particular focus is on a comprehensible introduction of the finite inelastic solid kinematics based on the multiplicative geometric concept in the framework of the natural basis representation.

The objective of *Chapter 3* is to present a convenient constitutive setting on the basis of a general biphasic solid-fluid mixture, which accounts for the coupled dissipative phenomena caused by the interplay of a viscous pore fluid streaming through a viscoelastic solid skeleton. Therefore, a thermodynamically consistent biphasic TPM model is introduced and admissible constitutive equations for the description of the finite viscoelastic deformation habits of the porous solid as well as the nonlinear percolation process of a general pore fluid are derived.

The numerical treatment of the viscoelastic two-phase model within the mixed finite element method is shown in *Chapter 4*. In this regard, the required weak formulations of the governing balance relations and their linearizations are presented, followed by appropriate techniques for the discretization in the space and the time domain including a convenient strategy for the treatment of the inelastic evolution equations. Finally, the algorithm for the nonlinear viscoelastic solid stress computation is described.

In *Chapter 5*, in order to demonstrate its practical applicability, the presented model is adapted for the description of a soft open-cell polyurethane (PUR) foam. Therefore, the model is correlated with experimental data by identifying the constitutively introduced material parameters with the help of the derivative-free optimization algorithm COBYLA. Finally, two numerical simulations are carried out to reveal the efficiency of the numerical implementation, the considerable influence of the pore fluid on the material response, and the overall applicability of the model to real engineering problems.

A final conclusion and discussion is given in the *last Chapter* including some statements on conceivable further developments and the future potential of the presented model in other disciplines, such as soft tissue biomechanics.

2 Theoretical Fundamentals

This section offers a brief review of the basic concepts of the Theory of Porous Media (TPM) including the concept of volume fractions and the kinematics, the governing balance laws, and the entropy principle for mixtures. Furthermore, in this context, the kinematical relations of finite inelasticity including the multiplicative decomposition of deformation gradients are reviewed and recast in descriptive tensorial form using local natural bases in curvilinear coordinates as well as the spectral representation.

2.1 Theory of Porous Media

2.1.1 Macroscopic Mixture Approach

In the framework of the Theory of Porous Media, a fluid-saturated porous medium can be treated as an immiscible binary mixture of constituents φ^α ($\alpha = S$: solid skeleton; $\alpha = F$: pore fluid), which are assumed to be in a state of ideal disarrangement. Following this, the prescription of a real or a virtual averaging process over a representative elementary volume (REV) leads to a model

$$\varphi = \bigcup_\alpha \varphi^\alpha = \varphi^S \cup \varphi^F \tag{2.1}$$

of superimposed and interacting continua (figure 2.1). In the arising macroscopic model, the incorporated physical quantities are then understood as the local averages of their microscopic representatives (Ehlers [54]).

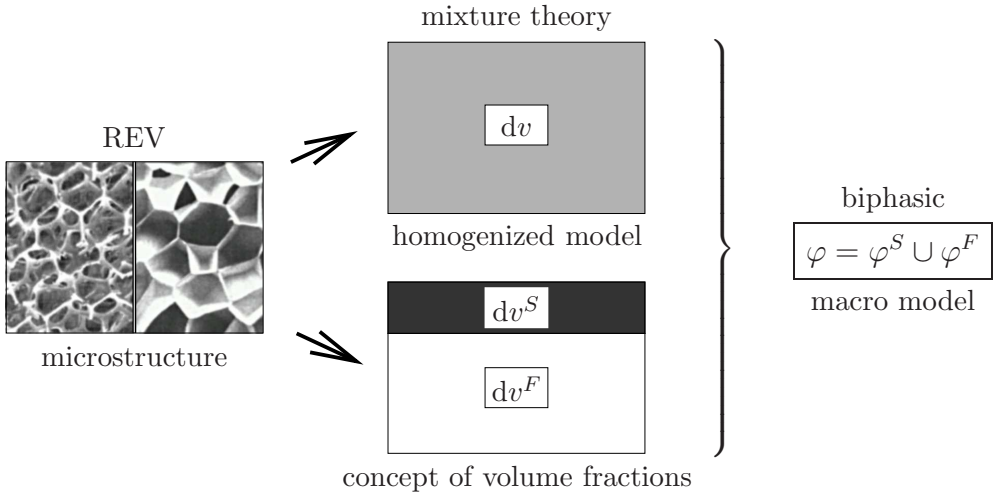

Figure 2.1: *REV with exemplary microstructures of open (left) and closed-celled (right) polymer foams and the biphasic TPM macro model including the volume fractions*

2.1.2 Volume Fractions and Density Functions

In order to account for the local composition of the mixture, local volumetric ratios are introduced according to the concept of volume fractions. The volume V of the overall medium $\mathcal{B}$ results from the sum of the partial volumes V^α of the constituent bodies $\mathcal{B}^\alpha$:

$$V = \int_{\mathcal{B}} \mathrm{d}v = \sum_\alpha V^\alpha \qquad \text{with} \qquad V^\alpha = \int_{\mathcal{B}^\alpha} \mathrm{d}v = \int_{\mathcal{B}} \mathrm{d}v^\alpha =: \int_{\mathcal{B}} n^\alpha \, \mathrm{d}v \,. \tag{2.2}$$

Following this, the volume fractions n^α of φ^α are defined as the local ratios of the partial volume elements $\mathrm{d}v^\alpha$ with respect to the volume element $\mathrm{d}v$ of the whole mixture φ:

$$n^\alpha := \frac{\mathrm{d}v^\alpha}{\mathrm{d}v} \,, \qquad \text{where} \qquad \begin{cases} n^S & : \text{solidity} \,, \\ n^F & : \text{porosity} \,. \end{cases} \tag{2.3}$$

As a further consequence of equations (2.2), assuming fully saturated conditions, i. e., avoiding any vacant space within the porous medium, the saturation constraint yields

$$\sum_\alpha n^\alpha = n^S + n^F = 1 \,. \tag{2.4}$$

Note that for some specific applications, where the pore fluid does not affect the mechanical properties of the porous medium, such as a pore gas in a stiff metal foam, an empty (non-saturated) solid matrix can be assumed, i. e., $\varphi = \varphi^S$ yielding $\sum_\alpha n^\alpha = n^S < 1$.

Proceeding from the definition of the volume fractions (2.3), associated with each constituent φ^α is a material (realistic or effective) density $\rho^{\alpha R}$ defined as the local mass $\mathrm{d}m^\alpha$ of φ^α per unit of $\mathrm{d}v^\alpha$, and a partial density ρ^α, where the local mass element $\mathrm{d}m^\alpha$ is related to the bulk volume element $\mathrm{d}v$. Moreover, the so-called mixture density can be introduced as the sum of the partial densities ρ^α. Thus, the density functions read

material density	partial density	mixture density
$\rho^{\alpha R} := \dfrac{\mathrm{d}m^\alpha}{\mathrm{d}v^\alpha}$	$\rho^\alpha := \dfrac{\mathrm{d}m^\alpha}{\mathrm{d}v}$	$\rho = \sum_\alpha \rho^\alpha$

$$\hookrightarrow \quad \rho^\alpha = n^\alpha \rho^{\alpha R} \quad \hookleftarrow \tag{2.5}$$

According to equations (2.5), it is obvious that the property of material incompressibility of a constituent φ^α (defined by $\rho^{\alpha R} = \text{const.}$) does not lead to macroscopic incompressibility, as the partial density ρ^α and thus ρ can still change through changes in the volume fractions n^α.

Remark: The fact that porous materials under drained conditions are in general macroscopically compressible, even if the single constituents are materially incompressible, is one important issue that must be taken into account for the development of an appropriate material law for the solid skeleton. Moreover, it is convenient to proceed from a materially incompressible solid constituent in regard to the large bulk compressibility of the porous medium. In this context, note that porous media models, where the fluid is

regarded as incompressible while the solid is considered as compressible, are not physically meaningful, as the bulk stiffness of dense solids is always greater than that of fluids. However, in the finite strain regime proceeding from $\rho^{SR} = \text{const.}$, the macroscopic material formulation for the solid skeleton must restrict the maximum volumetric contraction to the compaction point (Eipper [64]) given by $n^F = 0$ or $n^S = 1$, respectively, thereby describing the stiffening in the course of the densification of the material. ■

2.2 Kinematical Relations

2.2.1 Mixture Kinematics

Concerning the kinematics of mixtures, the idea of superimposed and interacting continua implies that, starting from different reference positions $\mathbf{X}_\alpha$ at time t_0, each constituent follows its individual *Lagrange*an motion function and has its own velocity and acceleration fields:

$$\mathbf{x} = \boldsymbol{\chi}_\alpha(\mathbf{X}_\alpha, t)\,, \quad \overset{\prime}{\mathbf{x}}_\alpha = \frac{\mathrm{d}\boldsymbol{\chi}_\alpha(\mathbf{X}_\alpha, t)}{\mathrm{d}t}\,, \quad \overset{\prime\prime}{\mathbf{x}}_\alpha = \frac{\mathrm{d}^2\boldsymbol{\chi}_\alpha(\mathbf{X}_\alpha, t)}{\mathrm{d}t^2}\,. \tag{2.6}$$

Following this, each spatial point $\mathbf{x}$ of the current configuration at time t is simultaneously occupied by material points $\mathcal{P}^\alpha$ of both constituents (figure 2.2)[1].

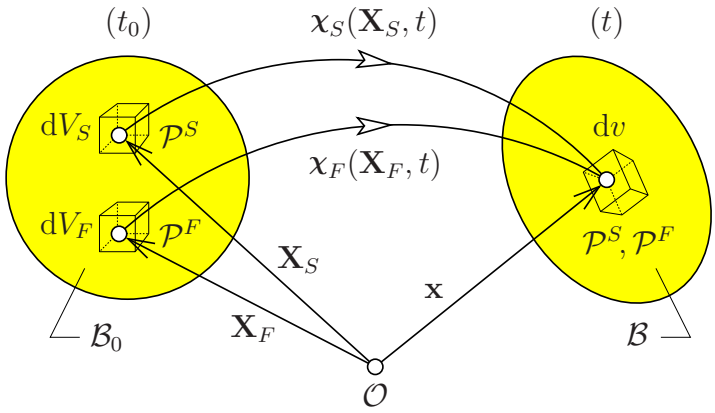

Figure 2.2: *Motion of a biphasic mixture*

Unique individual motions $\boldsymbol{\chi}_\alpha$ of the material points $\mathcal{P}^\alpha$ require the existence of unique inverse motion functions based on non-singular functional determinants (*Jacobi*ans) J_α:

$$\mathbf{X}_\alpha = \boldsymbol{\chi}_\alpha^{-1}(\mathbf{x}, t)\,, \quad \text{if} \quad J_\alpha := \det \frac{\partial \boldsymbol{\chi}_\alpha(\mathbf{X}_\alpha, t)}{\partial \mathbf{X}_\alpha} \neq 0\,. \tag{2.7}$$

[1] Concerning the notation, there is a break in the conventions declared on page XVII. Following the tradition, the reference position vectors are denoted by capital letters defined as $\mathbf{X}_\alpha := \mathbf{x}_{0\alpha}$ with $(\,\bullet\,)_{0\alpha}$ indicating an arbitrary initial state of the motion of φ^α at time t_0. Moreover, the common choice of capitals to indicate reference values is retained for line, area, and volume elements, e. g., $\mathrm{d}V_S := \mathrm{d}v_{0S}$ is the reference bulk volume element with respect to an initial (normally undeformed) solid state.

Thus, using the inverse motion functions $\boldsymbol{\chi}_\alpha^{-1}$, the *Euler*ian description of the velocity and the acceleration fields from equations (2.6) are given by

$$\overset{\prime}{\mathbf{x}}_\alpha = \overset{\prime}{\mathbf{x}}_\alpha(\mathbf{x}, t)\,, \quad \overset{\prime\prime}{\mathbf{x}}_\alpha = \overset{\prime\prime}{\mathbf{x}}_\alpha(\mathbf{x}, t)\,. \tag{2.8}$$

Furthermore, by use of the mixture density ρ from equations (2.5), the so-called mixture velocity $\dot{\mathbf{x}}$ describing the barycentric velocity of the overall medium and the diffusion velocity $\mathbf{d}_\alpha$ describing the relative velocity of φ^α with respect to φ can be introduced as

$$\dot{\mathbf{x}} = \frac{1}{\rho}\sum_\alpha \rho^\alpha \overset{\prime}{\mathbf{x}}_\alpha\,, \quad \mathbf{d}_\alpha = \overset{\prime}{\mathbf{x}}_\alpha - \dot{\mathbf{x}} \quad \text{with} \quad \sum_\alpha \rho^\alpha\, \mathbf{d}_\alpha = \mathbf{0}\,. \tag{2.9}$$

In the above equations, $(\,\cdot\,)'_\alpha$ indicates the material time derivative following the motion of φ_α and $(\,\cdot\,)^\cdot$ denotes the material time derivative following the barycentric motion of the whole mixture φ (mixture derivative). Suppose that Ψ and $\boldsymbol{\Psi}$ are arbitrary, steady and sufficiently steadily differentiable scalar and vector-valued field functions. Then, the respective derivatives are computed as follows:

$$\begin{aligned} \overset{\prime}{\Psi}_\alpha &= \frac{\mathrm{d}_\alpha \Psi}{\mathrm{d}t} = \frac{\partial \Psi}{\partial t} + \operatorname{grad}\Psi \cdot \overset{\prime}{\mathbf{x}}_\alpha\,, \quad \overset{\prime}{\boldsymbol{\Psi}}_\alpha = \frac{\mathrm{d}_\alpha \boldsymbol{\Psi}}{\mathrm{d}t} = \frac{\partial \boldsymbol{\Psi}}{\partial t} + (\operatorname{grad}\boldsymbol{\Psi})\,\overset{\prime}{\mathbf{x}}_\alpha\,, \\ \dot{\Psi} &= \frac{\mathrm{d}\Psi}{\mathrm{d}t} = \frac{\partial \Psi}{\partial t} + \operatorname{grad}\Psi \cdot \dot{\mathbf{x}}\,, \quad \dot{\boldsymbol{\Psi}} = \frac{\mathrm{d}\boldsymbol{\Psi}}{\mathrm{d}t} = \frac{\partial \boldsymbol{\Psi}}{\partial t} + (\operatorname{grad}\boldsymbol{\Psi})\,\dot{\mathbf{x}}\,. \end{aligned} \tag{2.10}$$

Therein, the differential operator $\operatorname{grad}(\,\cdot\,) := \partial(\,\cdot\,)/\partial\mathbf{x}$ denotes the partial derivative with respect to the actual position vector $\mathbf{x}$.

In porous media theories, it is generally convenient to proceed from a *Lagrange*an description of the solid matrix via the solid displacement vector $\mathbf{u}_S$ as the primary kinematical variable. In contrast, according to Gibson *et al.* [73], the pore-fluid flow is better expressed in a modified *Euler*ian setting via the seepage velocity $\mathbf{w}_{FR}$ describing the fluid motion relative to the deforming skeleton. Moreover, relating $\mathbf{w}_{FR}$ only to the fluid part of the mixture, the so-called filter or superficial velocity $\mathbf{w}_F$ can be introduced. Thus,

$$\mathbf{u}_S = \mathbf{x} - \mathbf{X}_S\,, \quad \mathbf{w}_{FR} = \mathbf{v}_F - \mathbf{v}_S \quad \text{with} \quad \mathbf{v}_\alpha := \overset{\prime}{\mathbf{x}}_\alpha\,, \quad \mathbf{w}_F = n^F\,\mathbf{w}_{FR}\,. \tag{2.11}$$

Given equations $(2.6)_1$ and $(2.7)_1$, the material deformation gradients and their inverses are defined by

$$\mathbf{F}_\alpha = \frac{\partial \mathbf{x}}{\partial \mathbf{X}_\alpha} =: \operatorname{Grad}_\alpha \mathbf{x}\,, \quad \mathbf{F}_\alpha^{-1} = \frac{\partial \mathbf{X}_\alpha}{\partial \mathbf{x}} = \operatorname{grad}\mathbf{X}_\alpha\,, \tag{2.12}$$

where the gradient operator $\operatorname{Grad}_\alpha(\,\cdot\,) := \partial(\,\cdot\,)/\partial\mathbf{X}_\alpha$ denotes the partial derivative with respect to the reference position vector $\mathbf{X}_\alpha$. Particularly, the solid deformation gradient $\mathbf{F}_S$, as a basic kinematical quantity of the large strain regime, can be expressed in terms of the solid displacement using equation $(2.11)_1$:

$$\mathbf{F}_S = \frac{\partial \mathbf{x}}{\partial \mathbf{X}_S} = \operatorname{Grad}_S \mathbf{x} = \mathbf{I} + \operatorname{Grad}_S \mathbf{u}_S\,. \tag{2.13}$$

According to equations (2.7), the existence of uniquely invertible motions requires non-zero *Jacobi*ans J_α. Starting the deformation process from an undeformed (natural) state at time t_0, the initial condition $\mathbf{F}_\alpha(t_0) = \mathbf{I}$ restricts the domain of $\det \mathbf{F}_\alpha$ to positive values

$$\det \mathbf{F}_\alpha = J_\alpha > 0 \quad \text{with} \quad \det \mathbf{F}_\alpha(t_0) = 1\,. \tag{2.14}$$

Moreover, following the remark on page 10, the assumption of solid incompressibility ($\rho^{SR} = \text{const.}$) implies that volumetric compression is only possible until the pore space is completely closed ($n^F = 0$). Therefore, the lower limit of the finite volume dilatation e_{VS} of the solid matrix is predefined by the initial porosity n^F_{0S}, i. e.,

$$\mathrm{e}_{VS} = \frac{\mathrm{d}v - \mathrm{d}V_S}{\mathrm{d}V_S} = \det \mathbf{F}_S - 1 > -n^F_{0S}\,, \tag{2.15}$$

thus, directly yielding the stronger restriction

$$\det \mathbf{F}_S = J_S > n^S_{0S} \quad \text{with} \quad n^S_{0S} = 1 - n^F_{0S}\,. \tag{2.16}$$

Therein, the transport property, $\mathrm{d}v = (\det \mathbf{F}_S)\,\mathrm{d}V_S$, of $\det \mathbf{F}_S$ is used (cf. relations (2.38)) describing the finite volume change of the reference volume element $\mathrm{d}V_S = \mathrm{d}v_{0S}$ to the volume element $\mathrm{d}v$ of the current configuration (figure 2.2). Furthermore, $(\,\cdot\,)_{0S}$ indicates initial values with respect to an undeformed solid state at time t_0. In particular, $n^S_{0S} = \mathrm{d}V^S_S/\mathrm{d}V_S$ and $n^F_{0S} = \mathrm{d}V^F_S/\mathrm{d}V_S$ are the initial solidity and porosity consistent with the saturation constraint (2.4).

2.2.2 Natural Basis Representation

In preparation for a comprehensible introduction of finite inelastic deformation and strain measures and their spatiotemporal derivatives (section 2.2.3), tensor formalisms with respect to bases in curvilinear coordinates provide an elegant alternative for the description (Bluhm [15]). Therefore, this section briefly recalls the required basics of the concept of the natural basis representation.

Proceeding from the 3-d physical space of our experience, the following considerations are based on a proper *Euclid*ean vector space $\mathcal{V}^3$, i. e., a set of vectors fulfilling the rules of elementary vector calculus and additionally $|\mathbf{v}|^2 = \mathbf{v} \cdot \mathbf{v} > 0\ \forall\, \mathbf{v} \neq \mathbf{0} \in \mathcal{V}^3$. In general, $\mathcal{V}^n$ is a n-dimensional vector space, if it admits only n linear independent vectors; these n vectors then build the basis of $\mathcal{V}^n$. Thus, an arbitrary vector $\mathbf{v} \in \mathcal{V}^3$ can be expressed as a linear combination of $n = 3$ basis vectors:

$$\lambda\,\mathbf{v} + \sum_{k=1}^{3} \lambda_k\,\mathbf{g}_k = \mathbf{0} \quad \longrightarrow \quad \mathbf{v} = \sum_{k=1}^{3} v^k\,\mathbf{g}_k = v^k\,\mathbf{g}_k\,. \tag{2.17}$$

Therein, $v^k = -\lambda_k/\lambda$ are the coefficients (of the vector components) with λ_k, λ as scalar factors, and $\mathbf{g}_k$ are general basis vectors forming a basis system $\{\mathbf{g}_k\}$. Note that the summation signs can be omitted implying *Einstein*'s summation convention (see conventions on page XVII).

Following this, supposing two arbitrary vectors $\mathbf{u} = u^k\,\mathbf{g}_k$ and $\mathbf{v} = v^l\,\mathbf{g}_l \in \mathcal{V}^3$, the scalar (dot) product is simply given by

$$\mathbf{u}\cdot\mathbf{v} = \mathrm{g}_{kl}\,u^k\,v^l\,, \quad \text{where} \quad \begin{cases} \mathrm{g}_{kl} = \mathbf{g}_k\cdot\mathbf{g}_l = \mathbf{g}_l\cdot\mathbf{g}_k = \mathrm{g}_{lk}\,, \\ \mathrm{g}_{kl} = |\mathbf{g}_k|\,|\mathbf{g}_l|\cos\sphericalangle(\mathbf{g}_k;\mathbf{g}_l)\,, \\ \det\mathrm{g}_{kl} =: \mathrm{g} > 0 \quad \text{(properness of } \mathcal{V}^3)\,. \end{cases} \tag{2.18}$$

Herein, g_{kl} denotes the so-called metric coefficients implying the geometric characteristics and thus, the comparability of the elements in $\mathcal{V}^3$. Note that in the special case of orthonormal basis vectors, the considerations simplify to a common rectangular *Cartesian* frame, viz., for $\mathbf{g}_k \perp \mathbf{g}_l\ \forall\, k \neq l$ and $|\mathbf{g}_k| = \sqrt{\mathbf{g}_k\cdot\mathbf{g}_k} = 1\ \sum\!\!\!\!\!\!\int k$ the general basis becomes a rectangular *Cartesian* basis $\{\mathbf{g}_k\} \rightarrow \{\mathbf{e}_k\}$ and the metric reduces to the *Kronecker* symbol $\mathrm{g}_{kl} = \delta_{kl}$ yielding 1 for $k = l$ and 0 for $k \neq l$.

In order to construct bases in a curvilinear frame, consider a set of general curvilinear coordinates θ^k $(k = 1,2,3)$ covering a region of $\mathcal{V}^3$ and a fixed origin $\mathcal{O}$. Then, the position vector of an arbitrary point $\mathcal{P} = \mathcal{P}(\theta^k)$ with respect to a global orthonormal basis $\{\mathcal{O};\mathbf{e}_k\}$, i. e., a rectangular *Cartesian* basis $\{\mathbf{e}_k\}$ with its origin in $\mathcal{O}$, is given by

$$\mathbf{x} = \mathbf{x}(\theta^k) = x^l(\theta^k)\,\mathbf{e}_l \quad \longleftrightarrow \quad \theta^k = \theta^k(\mathbf{x})\,, \tag{2.19}$$

where the unique inversions $\theta^k(\mathbf{x})$ are assumed to exist.

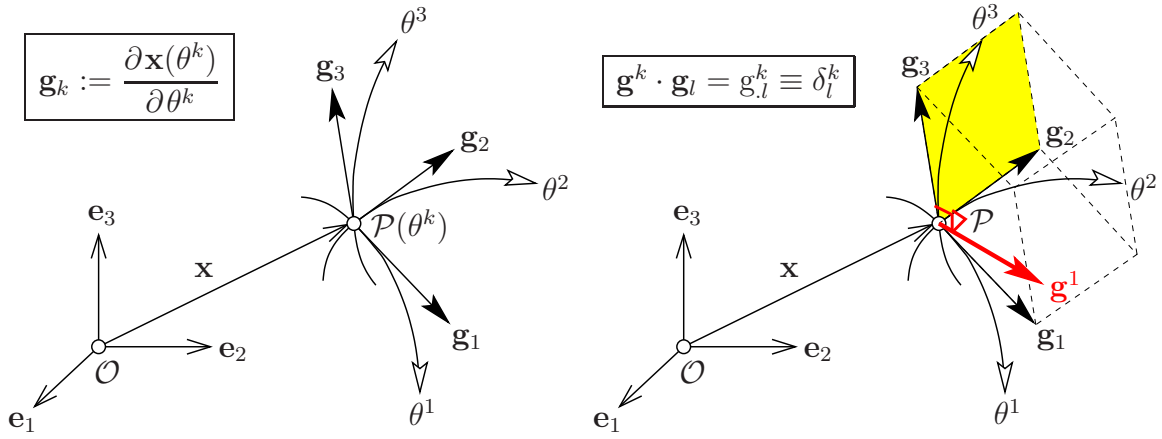

(a) Covariant local basis (b) Contravariant local basis

Figure 2.3: *Bases in curvilinear coordinates: (a) Fundamental natural or tangential covariant local basis; (b) Dual or reciprocal contravariant local basis*

Following this, a fundamental natural or tangential covariant local basis $\{\mathcal{P};\mathbf{g}_k\}$ is defined by the tangents to the coordinate lines θ^k in the point $\mathcal{P}$ (figure 2.3(a)):

$$\mathbf{g}_k := \frac{\partial\mathbf{x}(\theta^k)}{\partial\theta^k} = \frac{\partial x^l(\theta^k)}{\partial\theta^k}\,\mathbf{e}_l\,. \tag{2.20}$$

The local contravariant, dual, or reciprocal basis to $\mathbf{g}_k$ in $\mathcal{P}$, $\{\mathcal{P};\mathbf{g}^k\}$, is defined via

$$\mathbf{g}^k\cdot\mathbf{g}_l = \mathrm{g}^k_{.l} \equiv \delta^k_l\,. \tag{2.21}$$

Thus, the contravariant basis vectors $\mathbf{g}^k$ can be interpreted as normals of the surfaces $\theta^k = \text{const.}$ or as normals of the local tangential planes spanned by the covariant basis vectors $\mathbf{g}_k$, i. e., $\mathbf{g}^k \parallel \mathbf{g}_l \times \mathbf{g}_m$ with cyclic rotations of $k, l, m = 1, 2, 3$. This becomes clearer by regarding the tangential parallelepiped build by the $\mathbf{g}_k$ (figure 2.3(b)). With the volume of the parallelepiped $V_\square = (\mathbf{g}_1 \times \mathbf{g}_2) \cdot \mathbf{g}_3$ (scalar triple product of vectors), the reciprocal basis vectors can be calculated from

$$\mathbf{g}^1 = (\mathbf{g}_2 \times \mathbf{g}_3)/V_\square \,, \quad \mathbf{g}^2 = (\mathbf{g}_3 \times \mathbf{g}_1)/V_\square \,, \quad \mathbf{g}^3 = (\mathbf{g}_1 \times \mathbf{g}_2)/V_\square \,. \tag{2.22}$$

An alternative definition of $\{\mathcal{P}; \mathbf{g}^k\}$ is given by a *symbolic inversion* of definition (2.20)

$$\mathbf{g}^k := \Big(\frac{\partial \mathbf{x}(\theta^k)}{\partial \theta^k}\Big)^{-1} := \frac{\partial \theta^k(\mathbf{x})}{\partial \mathbf{x}} = \operatorname{grad} \theta^k(\mathbf{x}) = \frac{\partial \theta^k(x^l)}{\partial x^l}\, \mathbf{e}_l \,, \tag{2.23}$$

which directly reflects the mutual reciprocality of the co- and contravariant bases. Note that the introduced $\mathbf{g}_k$ and $\mathbf{g}^k$ are in general nonunit, nonorthogonal, and noncoplanar. In the special case of an orthonormal basis, it follows $\mathbf{g}^k = \mathbf{g}_k =: \mathbf{e}_k$, thus no distinction between co- and contravariance is necessary, as orthonormal bases are self-reciprocal.

Following the preceding, an arbitrary vector $\mathbf{v} \in \mathcal{V}^3$ can be expressed with respect to a co- or contravariant (local) basis, i. e., has a co- and contravariant representation:

$$\mathbf{v} = v^k\, \mathbf{g}_k = v_k\, \mathbf{g}^k \,. \tag{2.24}$$

Note that in this contribution, in contrast to, e. g., Holzapfel [93], p. 35, vectors and tensors are called co- or contravariant depending on the variant type of the basis vectors included in the vectorial and tensorial components. In this context, the raising and lowering of indices, i. e., the change of the variant type, plays an important role. Regarding the projections of $\mathbf{v}$ in the directions of $\mathbf{g}^l$ and $\mathbf{g}_l$ yields

$$v^l = \mathbf{v} \cdot \mathbf{g}^l = \mathrm{g}^{kl}\, v_k \,, \qquad v_l = \mathbf{v} \cdot \mathbf{g}_l = \mathrm{g}_{kl}\, v^k \,. \tag{2.25}$$

Moreover, with equation (2.24), it follows

$$\begin{aligned} \mathbf{v} = v^l\, \mathbf{g}_l = (\mathbf{v} \cdot \mathbf{g}^l)\, \mathbf{g}_l \overset{!}{=} v_l\, \mathbf{g}^l \quad &\longrightarrow \quad \mathbf{g}^l = \mathrm{g}^{kl}\, \mathbf{g}_k \,, \\ \mathbf{v} = v_l\, \mathbf{g}^l = (\mathbf{v} \cdot \mathbf{g}_l)\, \mathbf{g}^l \overset{!}{=} v^l\, \mathbf{g}_l \quad &\longrightarrow \quad \mathbf{g}_l = \mathrm{g}_{kl}\, \mathbf{g}^k \,. \end{aligned} \tag{2.26}$$

Thus, the co- and contravariant metric coefficients $\mathrm{g}_{kl} = \mathbf{g}_k \cdot \mathbf{g}_l$ and $\mathrm{g}^{kl} = \mathbf{g}^k \cdot \mathbf{g}^l$ act as operators that raise and lower the indices of coefficients and basis vectors. Furthermore, it can be easily shown that the following relations hold:

$$\begin{gathered} \mathrm{g}^{km}\, \mathrm{g}_{ml} = \mathrm{g}^k_{\cdot l} \equiv \delta^k_l \quad \longrightarrow \quad \mathrm{g}^{kl} = \mathrm{g}^{-1}_{kl} \,, \\ \overline{\mathrm{g}}\, \mathrm{g} \equiv 1 \quad \text{with} \quad \overline{\mathrm{g}} := \det \mathrm{g}^{kl} \,, \quad \mathrm{g} = \det \mathrm{g}_{kl} \,. \end{gathered} \tag{2.27}$$

Similarly to the representation of vectors in co- or contravariant basis systems, tensors can be expressed in the same manner. Proceeding from a polyadic product vector space $\mathcal{V}^3 \otimes \mathcal{V}^3 \otimes \cdots \otimes \mathcal{V}^3$, nth-order tensors can be expressed by $n-1$ dyadic tensor products

of n co- or contravariant basis vectors. Thus, equivalent co- and contravariant, as well as mixed-variant representations are possible. For an arbitrary rank-two tensor ($n = 2$) these are

$$\mathbf{T} = t^{kl}\,\mathbf{g}_k \otimes \mathbf{g}_l = t_{kl}\,\mathbf{g}^k \otimes \mathbf{g}^l = t^{k}_{.l}\,\mathbf{g}_k \otimes \mathbf{g}^l = t^{.l}_{k}\,\mathbf{g}^k \otimes \mathbf{g}_l \tag{2.28}$$

with t_{kl}, t^{kl} and $t^{k}_{.l}, t^{.l}_{k}$ as the co-, contra-, and mixed-variant coefficients of the tensor components. Waiving continuative details at this point, for further particulars of tensor formalisms in curvilinear coordinates, the reader is referred to the work of Green & Zerna [75], ch. 1 and the textbooks by de Boer [17] and Papastavridis [141].

2.2.3 Inelastic Solid Kinematics

For the description of the intrinsic relaxation and creep behavior, at first the basic frame for the inelastic kinematics of the solid skeleton must be provided. As mentioned in the introduction, benefitting from finite viscoelasticity of single-phase materials, the fundamental approach is principally based on the rheological structure of the generalized *Maxwell* model given in figure 2.4. This parallel assembly of one *Hooke* element and N *Maxwell* elements directly implies the internal variable concept with the dashpot deformations as the independently developing strain-equivalent internal variables. Note in passing that the overall behavior of viscoelastic solids can alternatively be described by the generalized *Kelvin-Voigt* model, i. e., one spring in series with several *Kelvin-Voigt* elements (spring and dashpot in parallel), which leads to a different interpretation of the elastic and inelastic strain measures (Huber & Tsakmakis [95]).

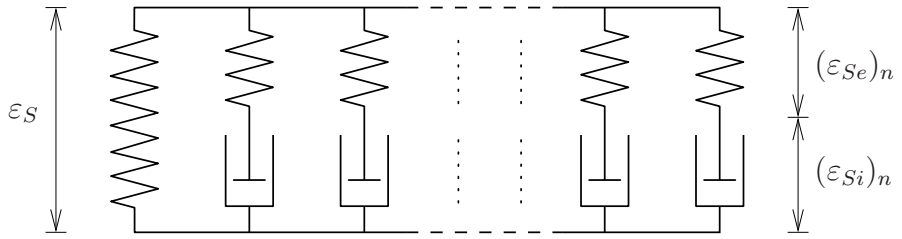

Figure 2.4: *Kinematics of the generalized Maxwell model (1+2N element viscoelastic solid)*

Proceeding from initially unitary lengths and cross-sections of the massless rheological elements, such that stresses and strains can be treated like forces and displacements, the $n = 1, ..., N$ parallel *Maxwell* branches meet the following kinematics:

$$\left.\begin{aligned} \varepsilon_S &= (\varepsilon_{Se})_n + (\varepsilon_{Si})_n \\ (\varepsilon_S)'_S &= [(\varepsilon_{Se})'_S]_n + [(\varepsilon_{Si})'_S]_n \end{aligned}\right\} \quad \overset{\text{3-d}}{\Longrightarrow} \quad \left\{\begin{aligned} \boldsymbol{\varepsilon}_S &= (\boldsymbol{\varepsilon}_{Se})_n + (\boldsymbol{\varepsilon}_{Si})_n\,, \\ (\boldsymbol{\varepsilon}_S)'_S &= [(\boldsymbol{\varepsilon}_{Se})_n]'_S + [(\boldsymbol{\varepsilon}_{Si})_n]'_S\,. \end{aligned}\right. \tag{2.29}$$

These additive decompositions of the total solid strain ε_S as well as the total solid strain rate $(\varepsilon_S)'_S$ into elastic parts $(\varepsilon_{Se})_n$ and $[(\varepsilon_{Se})_n]'_S$ and inelastic parts $(\varepsilon_{Si})_n$ and $[(\varepsilon_{Si})_n]'_S$, respectively, can be straightforwardly transferred to the 3-d infinitesimal theory. Therefore, the scalar quantities must be replaced with their corresponding tensorial counterparts. In this context, the geometric linear total strain and total strain rate tensors of the solid

skeleton are given by

$$\boldsymbol{\varepsilon}_S = \tfrac{1}{2}\left(\mathrm{Grad}_S\,\mathbf{u}_S + \mathrm{Grad}_S^T\,\mathbf{u}_S\right), \quad (\boldsymbol{\varepsilon}_S)'_S = \tfrac{1}{2}\left(\mathrm{Grad}_S\,\mathbf{v}_S + \mathrm{Grad}_S^T\,\mathbf{v}_S\right) \tag{2.30}$$

with $\mathbf{v}_S = (\mathbf{u}_S)'_S = \overset{\prime}{\mathbf{x}}_S$ representing the solid velocity vector (see also box (3.39) on page 55). Note that the dashpots can be generally replaced by arbitrary inelastic elements, such as friction elements for the description of plastic yielding, since the kinematics of the rheological structure is independent from the constitutive inelastic material formulations associated with the individual elements.

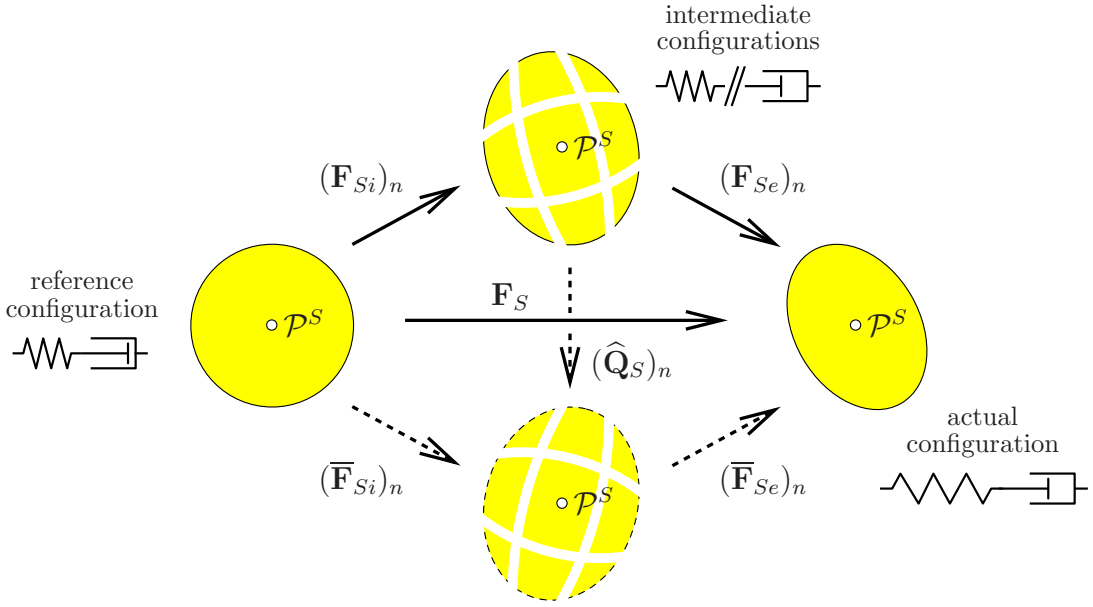

Figure 2.5: *Configurations of multiplicative solid inelasticity including a reference, an actual or current, as well as incompatible, stress-free intermediate configurations*

In the framework of a finite deformation theory of porous materials with elastic and inelastic behavior, it is convenient to proceed from a local multiplicative split of the solid deformation gradient

$$\mathbf{F}_S = (\mathbf{F}_{Se})_n\,(\mathbf{F}_{Si})_n\,, \quad n = 1, ..., N \tag{2.31}$$

into elastic parts $(\mathbf{F}_{Se})_n$ and inelastic parts $(\mathbf{F}_{Si})_n$. From elastoplasticity, it is commonly known that the concept of the multiplicative decomposition of deformation gradients is connected with the notion of a locally unloaded, stress-free intermediate configuration, where the purely inelastic state of deformation is frozen into the memory of the material (see, e. g., Kleiber [101]). In viscoelasticity, from a rheological point of view, in the intermediate states, the springs in the *Maxwell* models are assumed to be completely relaxed (i. e., stress-free), e. g., due to a virtual cut of the model, while the dashpot deformations remain (figure 2.5). Due to the independent local unloading (elastic release via $(\mathbf{F}_{Se}^{-1})_n$) of the usually non-uniformly strained solid skeleton at adjacent material points $\mathcal{P}^S$, the intermediate configurations are geometrically incompatible unless in the special case of homogeneous deformations. Thus, $(\mathbf{F}_{Se})_n$ and $(\mathbf{F}_{Si})_n$ generally do not have the character of gradient field functions; however, they are commonly termed elastic

and inelastic deformation gradients, which will, for convenience, also be retained in this contribution. Moreover, it is worth mentioning that the multiplicative decompositions (2.31) are not unique but can only be determined except for tensors $(\widehat{\mathbf{Q}}_S)_n$ of the special (proper) orthogonal group $\mathcal{SO}_3$ with the properties $(\widehat{\mathbf{Q}}_S^T)_n = (\widehat{\mathbf{Q}}_S^{-1})_n$ and $\det(\widehat{\mathbf{Q}}_S)_n = 1$, where $\widehat{(\bullet)}$ indicates their belonging to the inelastic intermediate configurations. It follows

$$\mathbf{F}_S = (\mathbf{F}_{Se})_n\,(\mathbf{F}_{Si})_n = (\overline{\mathbf{F}}_{Se})_n\,(\widehat{\mathbf{Q}}_S^T)_n\,(\widehat{\mathbf{Q}}_S)_n\,(\overline{\mathbf{F}}_{Si})_n = (\overline{\mathbf{F}}_{Se})_n\,(\overline{\mathbf{F}}_{Si})_n\,, \tag{2.32}$$

i. e., the intermediate configurations are defined up to superposed rigid-body rotations with unspecified $(\widehat{\mathbf{Q}}_S)_n$ (figure 2.5). Therefore, $(\mathbf{F}_{Se})_n$ and $(\mathbf{F}_{Si})_n$, respectively, must be regarded as representatives of the class of admissible decompositions. Note that this concept of the intermediate configuration is not mandatory. Some authors follow different concepts or completely avoid the notion of the intermediate configuration (see also remark on page 28). However, in this contribution, the multiplicative decompositions of the solid deformation gradient (2.31) are phenomenologically introduced without insisting on somehow abstract and somewhat controversial interpretations. Instead, they are understood as constitutive definitions that will consequently yield the additive decompositions of finite strain measures into elastic and inelastic parts (cf. Kleiber [101],Tsakmakis [182], or Ehlers [49]) and thus, directly reflect the structure of the underlying rheological model given in figure 2.4.

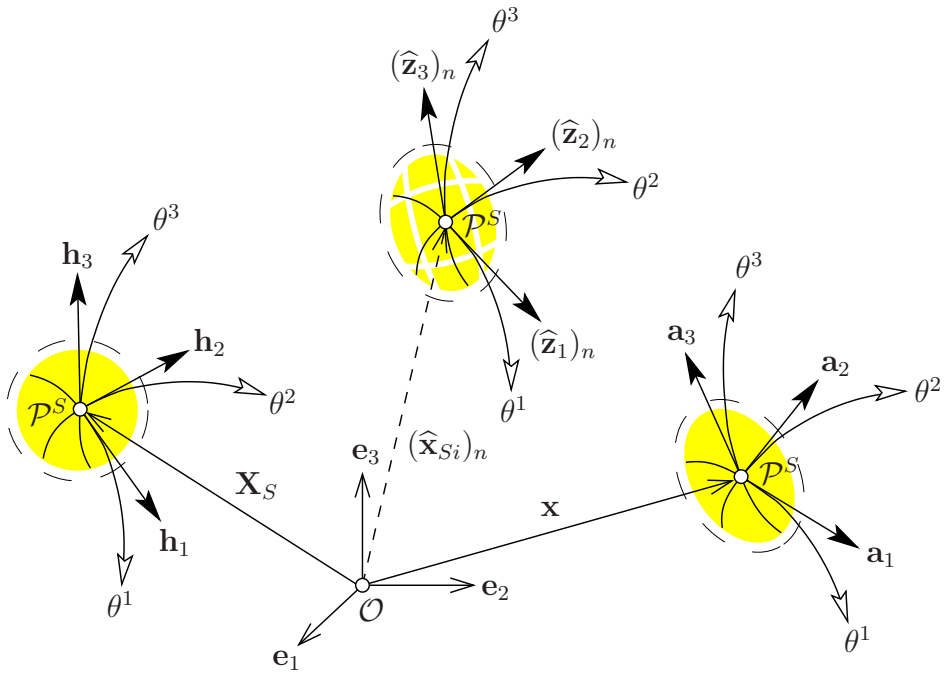

Figure 2.6: *Solid configurations with covariant local basis systems*

Following the preceding section 2.2.2, the solid configurations can be described within a local curvilinear frame with respect to a globally fixed *Cartesi*an basis system $\{\mathcal{O}; \mathbf{e}_k\}$ in $\mathcal{V}^3$ (see figure 2.6)[2]. The curvilinear coordinates $\theta^k = \theta^k(\mathbf{x}, t)$ are assumed to continuously

[2] For the sake of clarity, the solid constituent identifier $(\bullet)_S$ is omitted in connection with the natural basis representation.

follow the deforming material lines at each material point $\mathcal{P}^S$ of the solid skeleton body $\mathcal{B}^S$. In this context, some authors introduce the notion of *convective coordinates* to emphasize that the coordinate lines attached to the material lines deform with the material body respective to an undeformed reference state $\mathcal{B}_0^S$ at time t_0, where $\theta^k = \theta^k(\mathbf{X}_S, t_0)$ (see, e. g., Haupt [87]). According to definitions (2.20) and (2.23) together with the position vectors of the reference, intermediate, and actual configurations

$$\mathbf{X}_S = X_S^l(\theta^k, t_0)\,\mathbf{e}_l\,, \quad (\widehat{\mathbf{x}}_{Si})_n = (\widehat{x}_{Si}^{\,l})_n(\theta^k, t)\,\mathbf{e}_l\,, \quad \mathbf{x} = x^l(\theta^k, t)\,\mathbf{e}_l\,, \tag{2.33}$$

the following co- and contravariant local basis vectors can be defined:

covariant bases	configurations	contravariant bases
$\mathbf{h}_k := \dfrac{\partial \mathbf{X}_S}{\partial \theta^k} = \dfrac{\partial X_S^l}{\partial \theta^k}\,\mathbf{e}_l$	reference	$\mathbf{h}^k := \dfrac{\partial \theta^k}{\partial \mathbf{X}_S} = \dfrac{\partial \theta^k}{\partial X_S^l}\,\mathbf{e}_l$
$(\widehat{\mathbf{z}}_k)_n := \dfrac{\partial (\widehat{\mathbf{x}}_{Si})_n}{\partial \theta^k} = \dfrac{\partial (\widehat{x}_{Si}^{\,l})_n}{\partial \theta^k}\,\mathbf{e}_l$	intermediate	$(\widehat{\mathbf{z}}^k)_n := \dfrac{\partial \theta^k}{\partial (\widehat{\mathbf{x}}_{Si})_n} = \dfrac{\partial \theta^k}{\partial (\widehat{x}_{Si}^{\,l})_n}\,\mathbf{e}_l$
$\mathbf{a}_k := \dfrac{\partial \mathbf{x}}{\partial \theta^k} = \dfrac{\partial x^l}{\partial \theta^k}\,\mathbf{e}_l$	actual	$\mathbf{a}^k := \dfrac{\partial \theta^k}{\partial \mathbf{x}} = \dfrac{\partial \theta^k}{\partial x^l}\,\mathbf{e}_l$

(2.34)

Now, the introduced material deformation gradients and their inverses can be expressed in terms of the natural basis vectors (2.34), viz.:

$$\begin{aligned}
\mathbf{F}_S &= \mathrm{Grad}_S\,\mathbf{x} = \frac{\partial \mathbf{x}}{\partial \mathbf{X}_S} = \frac{\partial \mathbf{x}}{\partial \theta^k} \otimes \frac{\partial \theta^k}{\partial \mathbf{X}_S} = \mathbf{a}_k \otimes \mathbf{h}^k\,,\\
\mathbf{F}_S^{-1} &= \mathrm{grad}\,\mathbf{X}_S = \frac{\partial \mathbf{X}_S}{\partial \mathbf{x}} = \frac{\partial \mathbf{X}_S}{\partial \theta^k} \otimes \frac{\partial \theta^k}{\partial \mathbf{x}} = \mathbf{h}_k \otimes \mathbf{a}^k\,,\\
(\mathbf{F}_{Se})_n &= (\mathrm{grad}_{Si}\,\mathbf{x})_n = \frac{\partial \mathbf{x}}{\partial (\widehat{\mathbf{x}}_{Si})_n} = \frac{\partial \mathbf{x}}{\partial \theta^k} \otimes \frac{\partial \theta^k}{\partial (\widehat{\mathbf{x}}_{Si})_n} = \mathbf{a}_k \otimes (\widehat{\mathbf{z}}^k)_n\,,\\
(\mathbf{F}_{Se}^{-1})_n &= \mathrm{grad}\,(\widehat{\mathbf{x}}_{Si})_n = \frac{\partial (\widehat{\mathbf{x}}_{Si})_n}{\partial \mathbf{x}} = \frac{\partial (\widehat{\mathbf{x}}_{Si})_n}{\partial \theta^k} \otimes \frac{\partial \theta^k}{\partial \mathbf{x}} = (\widehat{\mathbf{z}}_k)_n \otimes \mathbf{a}^k\,,\\
(\mathbf{F}_{Si})_n &= \mathrm{Grad}_S(\widehat{\mathbf{x}}_{Si})_n = \frac{\partial (\widehat{\mathbf{x}}_{Si})_n}{\partial \mathbf{X}_S} = \frac{\partial (\widehat{\mathbf{x}}_{Si})_n}{\partial \theta^k} \otimes \frac{\partial \theta^k}{\partial \mathbf{X}_S} = (\widehat{\mathbf{z}}_k)_n \otimes \mathbf{h}^k\,,\\
(\mathbf{F}_{Si}^{-1})_n &= (\mathrm{grad}_{Si}\,\mathbf{X}_S)_n = \frac{\partial \mathbf{X}_S}{\partial (\widehat{\mathbf{x}}_{Si})_n} = \frac{\partial \mathbf{X}_S}{\partial \theta^k} \otimes \frac{\partial \theta^k}{\partial (\widehat{\mathbf{x}}_{Si})_n} = \mathbf{h}_k \otimes (\widehat{\mathbf{z}}^k)_n\,.
\end{aligned} \tag{2.35}$$

Therein, $(\mathrm{grad}_{Si}\,(\,\cdot\,))_n := \partial(\,\cdot\,)/\partial(\widehat{\mathbf{x}}_{Si})_n$ represent *fictitious* gradient operators with respect to the position vectors of the intermediate configurations. The term *fictitious* should emphasize that, in the inhomogeneous case, the $(\widehat{\mathbf{z}}_k)_n$ and $(\widehat{\mathbf{z}}^k)_n$, respectively, are not necessarily defined by some gradient-type equations, since gradients with respect to $(\widehat{\mathbf{x}}_{Si})_n$ as well as the inverse relations, in general, do not exist. More precisely, from a geometrical perspective, the intermediate configurations represent a 3-d proper *Riemann*ian manifold of material points $\mathcal{P}^S$ (Sidoroff [161]) with the intermediate metric coefficients $(\widehat{z}_{kl})_n = (\widehat{\mathbf{z}}_k)_n \cdot (\widehat{\mathbf{z}}_l)_n$ violating certain compatibility or integrability conditions (see Haupt [87] and Papastavridis [141]). However, every *Riemann*ian structure is locally flat (no cur-

vature), i. e., *Euclid*ean[3]. Accordingly, the introduction of local tangent (covariant) and cotangent (contravariant) *Euclid*ean bases in $\mathcal{P}^S$, almost promotes the presented approach to the inelastic intermediate configurations.

From equations (2.35), it is easy to recognize that, in terms of natural bases, the deformation gradients are mixed-variant, two-field or two-point tensors with identity metric, which directly implies their special property of acting as transport mechanisms between configurations (see also Ericksen [66], sec. III). This becomes clearer by applying $\mathbf{F}_S$ and $\mathbf{F}_S^{-1}$ as linear mappings to the covariant basis vectors $\mathbf{h}_l$ and $\mathbf{a}_l$ of the reference and the actual configuration, respectively. Thus, with definition (2.21), it follows

$$\begin{aligned} \mathbf{F}_S\,\mathbf{h}_l &= (\mathbf{a}_k \otimes \mathbf{h}^k)\,\mathbf{h}_l = \mathbf{a}_k\,\delta^k_l = \mathbf{a}_l\,, \\ \mathbf{F}_S^{-1}\,\mathbf{a}_l &= (\mathbf{h}_k \otimes \mathbf{a}^k)\,\mathbf{a}_l = \mathbf{h}_k\,\delta^k_l = \mathbf{h}_l\,. \end{aligned} \tag{2.36}$$

The transformations $(2.36)_1$ and $(2.36)_2$ are commonly known as covariant *push-forward* (reference $\rightarrow$ actual) and *pull-back* (actual $\rightarrow$ reference) operations. The respective contravariant transport mechanisms are simply given by applying the transposes of $\mathbf{F}_S^{-1}$ and $\mathbf{F}_S$ to the contravariant basis vectors $\mathbf{h}^l$ and $\mathbf{a}^l$:

$$\begin{aligned} \mathbf{F}_S^{T-1}\,\mathbf{h}^l &= (\mathbf{h}_k \otimes \mathbf{a}^k)^T\mathbf{h}^l = (\mathbf{a}^k \otimes \mathbf{h}_k)\,\mathbf{h}^l = \mathbf{a}^k\,\delta^l_k = \mathbf{a}^l\,, \\ \mathbf{F}_S^{T}\,\mathbf{a}^l &= (\mathbf{a}_k \otimes \mathbf{h}^k)^T\mathbf{a}^l = (\mathbf{h}^k \otimes \mathbf{a}_k)\,\mathbf{a}^l = \mathbf{h}^k\,\delta^l_k = \mathbf{h}^l\,. \end{aligned} \tag{2.37}$$

Following this, the transport mechanisms of material line, oriented area, and scalar volume elements of φ^S can be formulated:

$$\left.\begin{aligned} \mathrm{d}\mathbf{x}_{(k)} &= \mathbf{a}_k\,\mathrm{d}\theta^k = \mathbf{F}_S\,\mathbf{h}_k\,\mathrm{d}\theta^k = \mathbf{F}_S\,\mathrm{d}\mathbf{X}_{S(k)}\,, \\ \mathrm{d}\mathbf{a}_{(k)} &= \mathrm{d}\mathbf{x}_{(l)} \times \mathrm{d}\mathbf{x}_{(m)} = \mathbf{a}_l \times \mathbf{a}_m\,\mathrm{d}\theta^l\,\mathrm{d}\theta^m \\ &= (\mathbf{F}_S\,\mathbf{h}_l) \times (\mathbf{F}_S\,\mathbf{h}_m)\,\mathrm{d}\theta^l\,\mathrm{d}\theta^m \\ &= \tfrac{1}{2}\,(\mathbf{F}_S \barwedge \mathbf{F}_S)\,(\mathbf{h}_l \times \mathbf{h}_m)\,\mathrm{d}\theta^l\,\mathrm{d}\theta^m \\ &= \operatorname{cof}\mathbf{F}_S\,(\mathrm{d}\mathbf{X}_{S(l)} \times \mathrm{d}\mathbf{X}_{S(m)}) = \operatorname{cof}\mathbf{F}_S\,\mathrm{d}\mathbf{A}_{S(k)}\,, \\ \mathrm{d}v &= (\mathrm{d}\mathbf{x}_{(k)} \times \mathrm{d}\mathbf{x}_{(l)}) \cdot \mathrm{d}\mathbf{x}_{(m)} = (\mathbf{a}_k \times \mathbf{a}_l) \cdot \mathbf{a}_m\,\mathrm{d}\theta^k\,\mathrm{d}\theta^l\,\mathrm{d}\theta^m \\ &= [(\mathbf{F}_S\,\mathbf{h}_k) \times (\mathbf{F}_S\,\mathbf{h}_l)] \cdot (\mathbf{F}_S\,\mathbf{h}_m)\,\mathrm{d}\theta^k\,\mathrm{d}\theta^l\,\mathrm{d}\theta^m \\ &= \tfrac{1}{6}\,[(\mathbf{F}_S \barwedge \mathbf{F}_S) \cdot \mathbf{F}_S]\,(\mathbf{h}_k \times \mathbf{h}_l) \cdot \mathbf{h}_m\,\mathrm{d}\theta^k\,\mathrm{d}\theta^l\,\mathrm{d}\theta^m \\ &= \det\mathbf{F}_S\,(\mathrm{d}\mathbf{X}_{S(k)} \times \mathrm{d}\mathbf{X}_{S(l)}) \cdot \mathrm{d}\mathbf{X}_{S(m)} = \det\mathbf{F}_S\,\mathrm{d}V_S \end{aligned}\right\} \sum k,l,m\,. \tag{2.38}$$

Herein, $\mathrm{d}\mathbf{X}_{S(k)} := \mathrm{d}\mathbf{x}_{0S(k)}$, $\mathrm{d}\mathbf{x}_{(k)}$ and $\mathrm{d}\mathbf{A}_{S(k)} := \mathrm{d}\mathbf{a}_{0S(k)}$, $\mathrm{d}\mathbf{a}_{(k)}$ denote the covariant line and the contravariant area elements of the reference and the actual configuration. In

[3] This can be easily illustrated by regarding a triangle on a curved surface. The sum of bond angles in this triangle is in general unequal to 180° and thus, the *Pythagor*ean theorem cannot be applied. However, locally, on a tangential plane to that surface, the differential version of the *Pythagor*ean theorem can be formulated (cf. Papastavridis [141]).

particular, one finds

$$\left.\begin{aligned} \mathrm{d}\mathbf{A}_{S(k)} &= \mathbf{n}_{0S(k)}\,\mathrm{d}A_{S(k)} = \sqrt{h}\,\epsilon_{klm}\,\mathbf{h}^k\,\mathrm{d}\theta^l\,\mathrm{d}\theta^m\,, \\ \mathrm{d}\mathbf{a}_{(k)} &= \mathbf{n}_{(k)}\,\mathrm{d}a_{(k)} = \sqrt{a}\,\epsilon_{klm}\,\mathbf{a}^k\,\mathrm{d}\theta^l\,\mathrm{d}\theta^m \end{aligned}\right\} \sum\!\!\!\!\!\!\int k,l,m \tag{2.39}$$

with $\mathrm{d}A_{S(k)} := \mathrm{d}a_{0S(k)}$ and $\mathrm{d}a_{(k)}$ as the scalar area elements, $\mathbf{n}_{0S(k)}$ and $\mathbf{n}_{(k)}$ as the corresponding reference and actual outward oriented unit surface normals, the determinants of the metric coefficient matrices $h := \det h_{kl}$ and $a := \det a_{kl}$ (cf. relations (2.27)), and the *Levi-Cevita* permutation symbol

$$\epsilon_{klm} = \tfrac{1}{2}\,(k-l)\,(l-m)\,(m-k) = \begin{cases} +1 & : \textit{even} \text{ permutation, } \epsilon_{123} = \epsilon_{312} = \epsilon_{231}\,, \\ -1 & : \textit{odd} \text{ permutation, } \epsilon_{321} = \epsilon_{132} = \epsilon_{213}\,, \\ 0 & : \text{if } k,l,m \text{ are not all distinct}\,. \end{cases} \tag{2.40}$$

Furthermore, use was made of the outer (double cross) tensor product of tensors $(\,\cdot\,) \boxtimes (\,\cdot\,)$ (cf. appendix A), which allows a concise representation of cofactor tensors, such as $\operatorname{cof}\mathbf{F}_S = \frac{1}{2}\,(\mathbf{F}_S \boxtimes \mathbf{F}_S)$, and of determinants as the scalar triple product of tensors, such as $\det\mathbf{F}_S = \frac{1}{6}\,(\mathbf{F}_S \boxtimes \mathbf{F}_S) \cdot \mathbf{F}_S$ (see also de Boer [17]).

Next, the transport properties of the gradient operator are discussed. Proceeding from the natural basis representations of the material deformation gradients (2.35), depending on the type of the differentiable field function, the following contravariant transport mechanisms are apparent:

$$\begin{aligned} \operatorname{Grad}_S \Psi = \frac{\partial\Psi}{\partial\mathbf{X}_S} = \frac{\partial\Psi}{\partial\theta^k}\,\mathbf{h}^k \quad \underset{\mathbf{F}_S^T}{\overset{\mathbf{F}_S^{T-1}}{\rightleftarrows}} \quad \frac{\partial\Psi}{\partial\theta^k}\,\mathbf{a}^k = \frac{\partial\Psi}{\partial\mathbf{x}} = \operatorname{grad}\Psi\,, \\ \operatorname{Grad}_S \boldsymbol{\Psi} = \frac{\partial\boldsymbol{\Psi}}{\partial\mathbf{X}_S} = \frac{\partial\boldsymbol{\Psi}}{\partial\theta^k} \otimes \mathbf{h}^k \quad \underset{(\mathbf{I}\otimes\mathbf{F}_S^T)^{\overset{23}{T}}}{\overset{(\mathbf{I}\otimes\mathbf{F}_S^{T-1})^{\overset{23}{T}}}{\rightleftarrows}} \quad \frac{\partial\boldsymbol{\Psi}}{\partial\theta^k} \otimes \mathbf{a}^k = \frac{\partial\boldsymbol{\Psi}}{\partial\mathbf{x}} = \operatorname{grad}\boldsymbol{\Psi}\,. \end{aligned} \tag{2.41}$$

Herein, $(\,\cdot\,)^{\overset{kl}{T}}$ indicates an exchange of the kth and the lth basis vector included in the polyadic components of higher-order tensors. Following this, with the common rules of tensor calculus, transport mechanisms for tensors of arbitrary order can be defined including the inelastic and elastic transformations in the framework of the multiplicative geometric concept. A summary of the required co- and contravariant push-forward and pull-back operations is given in box (2.43), where, for clarity, the presentation is restricted to one *Maxwell* element ($N = 1$).

To continue, based on the multiplicative decomposition of $\mathbf{F}_S$ (2.31) with restriction to $N = 1$, the following right and left *Cauchy-Green* deformation tensors can be defined:

$$\begin{aligned} \mathbf{C}_S &= \mathbf{F}_S^T\,\mathbf{F}_S = a_{kl}\,\mathbf{h}^k \otimes \mathbf{h}^l\,, & \mathbf{B}_S &= \mathbf{F}_S\,\mathbf{F}_S^T = h^{kl}\,\mathbf{a}_k \otimes \mathbf{a}_l\,, \\ \widehat{\mathbf{C}}_{Se} &= \mathbf{F}_{Se}^T\,\mathbf{F}_{Se} = a_{kl}\,\widehat{\mathbf{z}}^k \otimes \widehat{\mathbf{z}}^l\,, & \mathbf{B}_{Se} &= \mathbf{F}_{Se}\,\mathbf{F}_{Se}^T = \widehat{z}^{kl}\,\mathbf{a}_k \otimes \mathbf{a}_l\,, \\ \mathbf{C}_{Si} &= \mathbf{F}_{Si}^T\,\mathbf{F}_{Si} = \widehat{z}_{kl}\,\mathbf{h}^k \otimes \mathbf{h}^l\,, & \widehat{\mathbf{B}}_{Si} &= \mathbf{F}_{Si}\,\mathbf{F}_{Si}^T = h^{kl}\,\widehat{\mathbf{z}}_k \otimes \widehat{\mathbf{z}}_l\,. \end{aligned} \tag{2.42}$$

Co- and contravariant transport mechanisms

1st-order tensors (vectors):

$$\mathbf{h}_k \underset{\mathbf{F}_{Si}^{-1}}{\overset{\mathbf{F}_{Si}}{\rightleftarrows}} \widehat{\mathbf{z}}_k \underset{\mathbf{F}_{Se}^{-1}}{\overset{\mathbf{F}_{Se}}{\rightleftarrows}} \mathbf{a}_k \qquad \mathbf{F}_S \,/\, \mathbf{F}_S^{-1}$$

$$\mathbf{h}^k \underset{\mathbf{F}_{Si}^{T}}{\overset{\mathbf{F}_{Si}^{T-1}}{\rightleftarrows}} \widehat{\mathbf{z}}^k \underset{\mathbf{F}_{Se}^{T}}{\overset{\mathbf{F}_{Se}^{T-1}}{\rightleftarrows}} \mathbf{a}^k \qquad \mathbf{F}_S^{T-1} \,/\, \mathbf{F}_S^{T}$$

2nd-order tensors:

$$\mathbf{h}_k \otimes \mathbf{h}_l \underset{\mathbf{F}_{Si}^{-1}(\,\widehat{\cdot}\,)\,\mathbf{F}_{Si}^{T-1}}{\overset{\mathbf{F}_{Si}(\,\cdot\,)\,\mathbf{F}_{Si}^{T}}{\rightleftarrows}} \widehat{\mathbf{z}}_k \otimes \widehat{\mathbf{z}}_l \underset{\mathbf{F}_{Se}^{-1}(\,\cdot\,)\,\mathbf{F}_{Se}^{T-1}}{\overset{\mathbf{F}_{Se}(\,\widehat{\cdot}\,)\,\mathbf{F}_{Se}^{T}}{\rightleftarrows}} \mathbf{a}_k \otimes \mathbf{a}_l \qquad \mathbf{F}_S(\,\cdot\,)\,\mathbf{F}_S^{T} \,/\, \mathbf{F}_S^{-1}(\,\cdot\,)\,\mathbf{F}_S^{T-1}$$

$$\mathbf{h}^k \otimes \mathbf{h}^l \underset{\mathbf{F}_{Si}^{T}(\,\widehat{\cdot}\,)\,\mathbf{F}_{Si}}{\overset{\mathbf{F}_{Si}^{T-1}(\,\cdot\,)\,\mathbf{F}_{Si}^{-1}}{\rightleftarrows}} \widehat{\mathbf{z}}^k \otimes \widehat{\mathbf{z}}^l \underset{\mathbf{F}_{Se}^{T}(\,\cdot\,)\,\mathbf{F}_{Se}}{\overset{\mathbf{F}_{Se}^{T-1}(\,\widehat{\cdot}\,)\,\mathbf{F}_{Se}^{-1}}{\rightleftarrows}} \mathbf{a}^k \otimes \mathbf{a}^l \qquad \mathbf{F}_S^{T}(\,\cdot\,)\,\mathbf{F}_S \,/\, \mathbf{F}_S^{T-1}(\,\cdot\,)\,\mathbf{F}_S^{-1}$$

4th-order tensors:

$$\overset{4}{\mathbf{H}}{}^{\sharp} \underset{(\mathbf{F}_{Si}^{-1}\otimes\mathbf{F}_{Si}^{-1})^{\overset{23}{T}}(\,\widehat{\cdot}\,)\,(\mathbf{F}_{Si}^{T-1}\otimes\mathbf{F}_{Si}^{T-1})^{\overset{23}{T}}}{\overset{(\mathbf{F}_{Si}\otimes\mathbf{F}_{Si})^{\overset{23}{T}}(\,\cdot\,)\,(\mathbf{F}_{Si}^{T}\otimes\mathbf{F}_{Si}^{T})^{\overset{23}{T}}}{\rightleftarrows}} \overset{4}{\widehat{\mathbf{Z}}}{}^{\sharp} \underset{(\mathbf{F}_{Se}^{-1}\otimes\mathbf{F}_{Se}^{-1})^{\overset{23}{T}}(\,\cdot\,)\,(\mathbf{F}_{Se}^{T-1}\otimes\mathbf{F}_{Se}^{T-1})^{\overset{23}{T}}}{\overset{(\mathbf{F}_{Se}\otimes\mathbf{F}_{Se})^{\overset{23}{T}}(\,\widehat{\cdot}\,)\,(\mathbf{F}_{Se}^{T}\otimes\mathbf{F}_{Se}^{T})^{\overset{23}{T}}}{\rightleftarrows}} \overset{4}{\mathbf{A}}{}^{\sharp} \qquad (\mathbf{F}_S\otimes\mathbf{F}_S)^{\overset{23}{T}}(\,\cdot\,)\,(\mathbf{F}_S^{T}\otimes\mathbf{F}_S^{T})^{\overset{23}{T}} \,/\, (\mathbf{F}_S^{-1}\otimes\mathbf{F}_S^{-1})^{\overset{23}{T}}(\,\cdot\,)\,(\mathbf{F}_S^{T-1}\otimes\mathbf{F}_S^{T-1})^{\overset{23}{T}}$$

$$\overset{4}{\mathbf{H}}{}^{\flat} \underset{(\mathbf{F}_{Si}^{T}\otimes\mathbf{F}_{Si}^{T})^{\overset{23}{T}}(\,\widehat{\cdot}\,)\,(\mathbf{F}_{Si}\otimes\mathbf{F}_{Si})^{\overset{23}{T}}}{\overset{(\mathbf{F}_{Si}^{T-1}\otimes\mathbf{F}_{Si}^{T-1})^{\overset{23}{T}}(\,\cdot\,)\,(\mathbf{F}_{Si}^{-1}\otimes\mathbf{F}_{Si}^{-1})^{\overset{23}{T}}}{\rightleftarrows}} \overset{4}{\widehat{\mathbf{Z}}}{}^{\flat} \underset{(\mathbf{F}_{Se}^{T}\otimes\mathbf{F}_{Se}^{T})^{\overset{23}{T}}(\,\cdot\,)\,(\mathbf{F}_{Se}\otimes\mathbf{F}_{Se})^{\overset{23}{T}}}{\overset{(\mathbf{F}_{Se}^{T-1}\otimes\mathbf{F}_{Se}^{T-1})^{\overset{23}{T}}(\,\widehat{\cdot}\,)\,(\mathbf{F}_{Se}^{-1}\otimes\mathbf{F}_{Se}^{-1})^{\overset{23}{T}}}{\rightleftarrows}} \overset{4}{\mathbf{A}}{}^{\flat} \qquad (\mathbf{F}_S^{T-1}\otimes\mathbf{F}_S^{T-1})^{\overset{23}{T}}(\,\cdot\,)\,(\mathbf{F}_S^{-1}\otimes\mathbf{F}_S^{-1})^{\overset{23}{T}} \,/\, (\mathbf{F}_S^{T}\otimes\mathbf{F}_S^{T})^{\overset{23}{T}}(\,\cdot\,)\,(\mathbf{F}_S\otimes\mathbf{F}_S)^{\overset{23}{T}}$$

(2.43)

where $\left\{ \begin{array}{l} \overset{4}{\mathbf{H}}{}^{\sharp} = \mathbf{h}_k \otimes \mathbf{h}_l \otimes \mathbf{h}_m \otimes \mathbf{h}_n \\ \overset{4}{\widehat{\mathbf{Z}}}{}^{\sharp} = \widehat{\mathbf{z}}_k \otimes \widehat{\mathbf{z}}_l \otimes \widehat{\mathbf{z}}_m \otimes \widehat{\mathbf{z}}_n \\ \overset{4}{\mathbf{A}}{}^{\sharp} = \mathbf{a}_k \otimes \mathbf{a}_l \otimes \mathbf{a}_m \otimes \mathbf{a}_n \end{array} \right\}$ and $\left\{ \begin{array}{l} \overset{4}{\mathbf{H}}{}^{\flat} = \mathbf{h}^k \otimes \mathbf{h}^l \otimes \mathbf{h}^m \otimes \mathbf{h}^n \\ \overset{4}{\widehat{\mathbf{Z}}}{}^{\flat} = \widehat{\mathbf{z}}^k \otimes \widehat{\mathbf{z}}^l \otimes \widehat{\mathbf{z}}^m \otimes \widehat{\mathbf{z}}^n \\ \overset{4}{\mathbf{A}}{}^{\flat} = \mathbf{a}^k \otimes \mathbf{a}^l \otimes \mathbf{a}^m \otimes \mathbf{a}^n \end{array} \right\}$ [a]

[a] Here, the identifiers $(\,\cdot\,)^{\sharp}$ and $(\,\cdot\,)^{\flat}$ are used to distinguish co- and contravariant tensors. Actually, the variant type of tensors follows directly from their natural basis representation. Hence, variant-type identifiers are usually omitted in this contribution.

The corresponding inverse relations read:

$$\begin{aligned}
\mathbf{C}_S^{-1} &= \mathbf{F}_S^{-1}\,\mathbf{F}_S^{T-1} = a^{kl}\,\mathbf{h}_k\otimes\mathbf{h}_l\,, \quad \mathbf{B}_S^{-1} = \mathbf{F}_S^{T-1}\,\mathbf{F}_S^{-1} = h_{kl}\,\mathbf{a}^k\otimes\mathbf{a}^l\,,\\
\widehat{\mathbf{C}}_{Se}^{-1} &= \mathbf{F}_{Se}^{-1}\,\mathbf{F}_{Se}^{T-1} = a^{kl}\,\widehat{\mathbf{z}}_k\otimes\widehat{\mathbf{z}}_l\,, \quad \mathbf{B}_{Se}^{-1} = \mathbf{F}_{Se}^{T-1}\,\mathbf{F}_{Se}^{-1} = \widehat{z}_{kl}\,\mathbf{a}^k\otimes\mathbf{a}^l\,,\\
\mathbf{C}_{Si}^{-1} &= \mathbf{F}_{Si}^{-1}\,\mathbf{F}_{Si}^{T-1} = \widehat{z}^{kl}\,\mathbf{h}_k\otimes\mathbf{h}_l\,, \quad \widehat{\mathbf{B}}_{Si}^{-1} = \mathbf{F}_{Si}^{T-1}\,\mathbf{F}_{Si}^{-1} = h_{kl}\,\widehat{\mathbf{z}}^k\otimes\widehat{\mathbf{z}}^l\,.
\end{aligned} \tag{2.44}$$

Given the definitions for the *Green-Lagrange*an and the *Almansi*an strains[4] together with the metric properties (2.26) and the identities

$$\begin{aligned}
&\mathbf{I} = \mathbf{F}_S^{-1}\,\mathbf{F}_S = \mathbf{F}_S^{T}\,\mathbf{F}_S^{T-1} = \mathbf{F}_S\,\mathbf{F}_S^{-1} = \mathbf{F}_S^{T-1}\,\mathbf{F}_S^{T} = \mathbf{F}_{Si}\,\mathbf{F}_{Si}^{-1} = \mathbf{F}_{Se}^{T}\,\mathbf{F}_{Se}^{T-1} = \dots\\
&\longrightarrow\quad \mathbf{I} = \mathbf{h}_k\otimes\mathbf{h}^k = \mathbf{h}^k\otimes\mathbf{h}_k = \mathbf{a}_k\otimes\mathbf{a}^k = \mathbf{a}^k\otimes\mathbf{a}_k = \widehat{\mathbf{z}}_k\otimes\widehat{\mathbf{z}}^k = \widehat{\mathbf{z}}^k\otimes\widehat{\mathbf{z}}_k\,,
\end{aligned} \tag{2.45}$$

one formally introduces

$$\begin{aligned}
\mathbf{E}_S &= \tfrac{1}{2}\,(\mathbf{C}_S - \mathbf{I}) = \tfrac{1}{2}\,(a_{kl} - h_{kl})\,\mathbf{h}^k\otimes\mathbf{h}^l\,,\\
\widehat{\mathbf{\Gamma}}_{Se} &= \tfrac{1}{2}\,(\widehat{\mathbf{C}}_{Se} - \mathbf{I}) = \tfrac{1}{2}\,(a_{kl} - \widehat{z}_{kl})\,\widehat{\mathbf{z}}^k\otimes\widehat{\mathbf{z}}^l\,,\\
\mathbf{E}_{Si} &= \tfrac{1}{2}\,(\mathbf{C}_{Si} - \mathbf{I}) = \tfrac{1}{2}\,(\widehat{z}_{kl} - h_{kl})\,\mathbf{h}^k\otimes\mathbf{h}^l\,,\\
\mathbf{A}_S &= \tfrac{1}{2}\,(\mathbf{I} - \mathbf{B}_S^{-1}) = \tfrac{1}{2}\,(a_{kl} - h_{kl})\,\mathbf{a}^k\otimes\mathbf{a}^l\,,\\
\mathbf{A}_{Se} &= \tfrac{1}{2}\,(\mathbf{I} - \mathbf{B}_{Se}^{-1}) = \tfrac{1}{2}\,(a_{kl} - \widehat{z}_{kl})\,\mathbf{a}^k\otimes\mathbf{a}^l\,,\\
\widehat{\mathbf{\Gamma}}_{Si} &= \tfrac{1}{2}\,(\mathbf{I} - \widehat{\mathbf{B}}_{Si}^{-1}) = \tfrac{1}{2}\,(\widehat{z}_{kl} - h_{kl})\,\widehat{\mathbf{z}}^k\otimes\widehat{\mathbf{z}}^l\,.
\end{aligned} \tag{2.46}$$

The remaining contravariant strain tensors hold the following additive relations:

$$\begin{aligned}
\mathbf{E}_{Se} &= \mathbf{E}_S - \mathbf{E}_{Si} = \tfrac{1}{2}\,(\mathbf{C}_S - \mathbf{C}_{Si}) = \tfrac{1}{2}\,(a_{kl} - \widehat{z}_{kl})\,\mathbf{h}^k\otimes\mathbf{h}^l\,,\\
\widehat{\mathbf{\Gamma}}_S &= \widehat{\mathbf{\Gamma}}_{Se} + \widehat{\mathbf{\Gamma}}_{Si} = \tfrac{1}{2}\,(\widehat{\mathbf{C}}_{Se} - \widehat{\mathbf{B}}_{Si}^{-1}) = \tfrac{1}{2}\,(a_{kl} - h_{kl})\,\widehat{\mathbf{z}}^k\otimes\widehat{\mathbf{z}}^l\,,\\
\mathbf{A}_{Si} &= \mathbf{A}_S - \mathbf{A}_{Se} = \tfrac{1}{2}\,(\mathbf{B}_{Se}^{-1} - \mathbf{B}_S^{-1}) = \tfrac{1}{2}\,(\widehat{z}_{kl} - h_{kl})\,\mathbf{a}^k\otimes\mathbf{a}^l\,.
\end{aligned} \tag{2.47}$$

Alternatively, they can be obtained from contravariant push-forward and pull-back operations, e. g., the total strain of the intermediate configuration $\widehat{\mathbf{\Gamma}}_S$ can be computed from an inelastic contravariant push-forward of $\mathbf{E}_S$ or an elastic contravariant pull-back of $\mathbf{A}_S$:

$$\begin{aligned}
\widehat{\mathbf{\Gamma}}_S &= \mathbf{F}_{Si}^{T-1}\,\mathbf{E}_S\,\mathbf{F}_{Si}^{-1} = \tfrac{1}{2}\,(a_{kl} - h_{kl})\,\mathbf{F}_{Si}^{T-1}\,\mathbf{h}^k\otimes\mathbf{F}_{Si}^{T-1}\,\mathbf{h}^l\\
&= \tfrac{1}{2}\,(a_{kl} - h_{kl})\,\widehat{\mathbf{z}}^k\otimes\widehat{\mathbf{z}}^l = \tfrac{1}{2}\,(a_{kl} - h_{kl})\,\mathbf{F}_{Se}^{T}\,\mathbf{a}^k\otimes\mathbf{F}_{Se}^{T}\,\mathbf{a}^l = \mathbf{F}_{Se}^{T}\,\mathbf{A}_S\,\mathbf{F}_{Se}\,.
\end{aligned} \tag{2.48}$$

Note that in this representation only the tensorial bases account for the difference of related strain measures while the metric coefficients are identical.

Analogously, the class of covariant *Karni-Reiner* strain tensors can be introduced by

[4] From the common definition by the differences of squares of line elements, e. g., with the squared lengths of the actual and reference line elements $\mathrm{d}s^2 = \mathrm{d}\mathbf{x}\cdot\mathrm{d}\mathbf{x}$ and $\mathrm{d}S_S^2 = \mathrm{d}\mathbf{X}_S\cdot\mathrm{d}\mathbf{X}_S$, one finds

$$\begin{aligned}
\mathrm{d}s^2 - \mathrm{d}S_S^2 &= (\mathbf{a}_k\cdot\mathbf{a}_l - \mathbf{h}_k\cdot\mathbf{h}_l)\,\mathrm{d}\theta^k\,\mathrm{d}\theta^l = (a_{kl} - h_{kl})\,\mathrm{d}\theta^k\,\mathrm{d}\theta^l = 2\,e_{kl}\,\mathrm{d}\theta^k\,\mathrm{d}\theta^l\\
&= (\mathbf{F}_S\,\mathbf{h}_k\cdot\mathbf{F}_S\,\mathbf{h}_l - \mathbf{h}_k\cdot\mathbf{h}_l)\,\mathrm{d}\theta^k\,\mathrm{d}\theta^l = \mathbf{h}_k\cdot(\mathbf{F}_S^T\,\mathbf{F}_S - \mathbf{I})\,\mathbf{h}_l\,\mathrm{d}\theta^k\,\mathrm{d}\theta^l = \mathbf{h}_k\cdot(2\,\mathbf{E}_S)\,\mathbf{h}_l\,\mathrm{d}\theta^k\,\mathrm{d}\theta^l\,.
\end{aligned}$$

formal definition[5]:

$$\begin{aligned}
\overset{\mathrm{R}}{\mathbf{K}}_S &= \tfrac{1}{2}\,(\mathbf{I}-\mathbf{C}_S^{-1}) = \tfrac{1}{2}\,(h^{kl}-a^{kl})\,\mathbf{h}_k\otimes\mathbf{h}_l\,,\\
\widehat{\mathbf{K}}_{Se} &= \tfrac{1}{2}\,(\mathbf{I}-\widehat{\mathbf{C}}_{Se}^{-1}) = \tfrac{1}{2}\,(\widehat{z}^{kl}-a^{kl})\,\widehat{\mathbf{z}}_k\otimes\widehat{\mathbf{z}}_l\,,\\
\overset{\mathrm{R}}{\mathbf{K}}_{Si} &= \tfrac{1}{2}\,(\mathbf{I}-\mathbf{C}_{Si}^{-1}) = \tfrac{1}{2}\,(h^{kl}-\widehat{z}^{kl})\,\mathbf{h}_k\otimes\mathbf{h}_l\,,\\
\mathbf{K}_S &= \tfrac{1}{2}\,(\mathbf{B}_S-\mathbf{I}) = \tfrac{1}{2}\,(h^{kl}-a^{kl})\,\mathbf{a}_k\otimes\mathbf{a}_l\,,\\
\mathbf{K}_{Se} &= \tfrac{1}{2}\,(\mathbf{B}_{Se}-\mathbf{I}) = \tfrac{1}{2}\,(\widehat{z}^{kl}-a^{kl})\,\mathbf{a}_k\otimes\mathbf{a}_l\,,\\
\widehat{\mathbf{K}}_{Si} &= \tfrac{1}{2}\,(\widehat{\mathbf{B}}_{Si}-\mathbf{I}) = \tfrac{1}{2}\,(h^{kl}-\widehat{z}^{kl})\,\widehat{\mathbf{z}}_k\otimes\widehat{\mathbf{z}}_l\,.
\end{aligned} \tag{2.49}$$

The remaining covariant strain measures follow then from the additive relations

$$\begin{aligned}
\overset{\mathrm{R}}{\mathbf{K}}_{Se} &= \overset{\mathrm{R}}{\mathbf{K}}_S - \overset{\mathrm{R}}{\mathbf{K}}_{Si} = \tfrac{1}{2}\,(\mathbf{C}_{Si}^{-1}-\mathbf{C}_S^{-1}) = \tfrac{1}{2}\,(\widehat{z}^{kl}-a^{kl})\,\mathbf{h}_k\otimes\mathbf{h}_l\,,\\
\widehat{\mathbf{K}}_S &= \widehat{\mathbf{K}}_{Se} + \widehat{\mathbf{K}}_{Si} = \tfrac{1}{2}\,(\widehat{\mathbf{B}}_{Si}-\widehat{\mathbf{C}}_{Se}^{-1}) = \tfrac{1}{2}\,(h^{kl}-a^{kl})\,\widehat{\mathbf{z}}_k\otimes\widehat{\mathbf{z}}_l\,,\\
\mathbf{K}_{Si} &= \mathbf{K}_S - \mathbf{K}_{Se} = \tfrac{1}{2}\,(\mathbf{B}_S-\mathbf{B}_{Se}) = \tfrac{1}{2}\,(h^{kl}-\widehat{z}^{kl})\,\mathbf{a}_k\otimes\mathbf{a}_l
\end{aligned} \tag{2.50}$$

or can be alternatively obtained from respective covariant transport operations, e. g.,

$$\begin{aligned}
\widehat{\mathbf{K}}_S &= \mathbf{F}_{Si}\,\overset{\mathrm{R}}{\mathbf{K}}_S\,\mathbf{F}_{Si}^T = \tfrac{1}{2}\,(h^{kl}-a^{kl})\,\mathbf{F}_{Si}\,\mathbf{h}_k\otimes\mathbf{F}_{Si}\,\mathbf{h}_l\\
&= \tfrac{1}{2}\,(h^{kl}-a^{kl})\,\widehat{\mathbf{z}}_k\otimes\widehat{\mathbf{z}}_l = \tfrac{1}{2}\,(h^{kl}-a^{kl})\,\mathbf{F}_{Se}^{-1}\,\mathbf{a}_k\otimes\mathbf{F}_{Se}^{-1}\,\mathbf{a}_l = \mathbf{F}_{Se}^{-1}\,\mathbf{K}_S\,\mathbf{F}_{Se}^{T-1}\,.
\end{aligned} \tag{2.51}$$

A complete summary of all introduced co- and contravariant strain tensors including the corresponding transport mechanisms is given in appendix B.1.

In order to formulate rate equations, time derivatives of the introduced deformation and strain measures are required. Proceeding from the material solid velocity gradient

$$\begin{aligned}
(\mathbf{F}_S)'_S = \frac{\mathrm{d}_S}{\mathrm{d}t}\Big(\frac{\partial\mathbf{x}}{\partial\mathbf{X}_S}\Big) = \frac{\partial\overset{\prime}{\mathbf{x}}_S}{\partial\mathbf{X}_S} = \frac{\partial\overset{\prime}{\mathbf{x}}_S}{\partial\theta^k}\otimes\frac{\partial\theta^k}{\partial\mathbf{X}_S} = (\mathbf{a}_k)'_S\otimes\mathbf{h}^k\\
= \mathrm{Grad}_S\,\overset{\prime}{\mathbf{x}}_S = \frac{\partial\overset{\prime}{\mathbf{x}}_S}{\partial\mathbf{x}}\,\frac{\partial\mathbf{x}}{\partial\mathbf{X}_S} =: \mathbf{L}_S\,\mathbf{F}_S\,,
\end{aligned} \tag{2.52}$$

the spatial solid velocity gradient is given by

$$\begin{aligned}
\mathbf{L}_S := \mathrm{grad}\,\overset{\prime}{\mathbf{x}}_S = \frac{\partial\overset{\prime}{\mathbf{x}}_S}{\partial\mathbf{x}} = \frac{\partial\overset{\prime}{\mathbf{x}}_S}{\partial\mathbf{X}_S}\,\frac{\partial\mathbf{X}_S}{\partial\mathbf{x}} = (\mathbf{F}_S)'_S\,\mathbf{F}_S^{-1}\\
= [(\mathbf{a}_k)'_S\otimes\mathbf{h}^k]\,\mathbf{F}_S^{-1} = (\mathbf{a}_k)'_S\otimes\mathbf{F}_S^{T-1}\,\mathbf{h}^k = (\mathbf{a}_k)'_S\otimes\mathbf{a}^k\,.
\end{aligned} \tag{2.53}$$

Additionally, following the multiplicative geometric concept (2.31), local inelastic material

[5] Commonly, based on the polar decomposition of the solid material deformation gradient, they are introduced by the differences of squares of rotated line elements (cf. section 2.2.4, equation (2.74)). Alternatively, this second family of strain tensors can also be motivated through the differences of squares of weighted vectorial area elements (see, e. g., Haupt & Tsakmakis [88]).

and spatial solid velocity gradients, can be introduced:

$$\begin{aligned}(\mathbf{F}_{Si})'_S = \frac{\mathrm{d}_S}{\mathrm{d}t}\Big(\frac{\partial \widehat{\mathbf{x}}_{Si}}{\partial \mathbf{X}_S}\Big) = \frac{\partial (\widehat{\mathbf{x}}_{Si})'_S}{\partial \mathbf{X}_S} = \frac{\partial (\widehat{\mathbf{x}}_{Si})'_S}{\partial \theta^k} \otimes \frac{\partial \theta^k}{\partial \mathbf{X}_S} = (\widehat{\mathbf{z}}_k)'_S \otimes \mathbf{h}^k \\ = \mathrm{Grad}_S\,(\widehat{\mathbf{x}}_{Si})'_S = \frac{\partial (\widehat{\mathbf{x}}_{Si})'_S}{\partial \widehat{\mathbf{x}}_{Si}} \frac{\partial \widehat{\mathbf{x}}_{Si}}{\partial \mathbf{X}_S} =: \widehat{\mathbf{L}}_{Si}\,\mathbf{F}_{Si}\,,\end{aligned} \tag{2.54}$$

$$\begin{aligned}\widehat{\mathbf{L}}_{Si} := \mathrm{grad}_{Si}\,(\widehat{\mathbf{x}}_{Si})'_S = \frac{\partial (\widehat{\mathbf{x}}_{Si})'_S}{\partial \widehat{\mathbf{x}}_{Si}} = \frac{\partial (\widehat{\mathbf{x}}_{Si})'_S}{\partial \mathbf{X}_S} \frac{\partial \mathbf{X}_S}{\partial \widehat{\mathbf{x}}_{Si}} = (\mathbf{F}_{Si})'_S\,\mathbf{F}_{Si}^{-1} \\ = [(\widehat{\mathbf{z}}_k)'_S \otimes \mathbf{h}^k]\,\mathbf{F}_{Si}^{-1} = (\widehat{\mathbf{z}}_k)'_S \otimes \mathbf{F}_{Si}^{T-1}\,\mathbf{h}^k = (\widehat{\mathbf{z}}_k)'_S \otimes \widehat{\mathbf{z}}^k\,.\end{aligned} \tag{2.55}$$

From the above together with the identities

$$\left.\begin{aligned}(\mathbf{F}_S\,\mathbf{F}_S^{-1})'_S = \mathbf{0} \\ (\mathbf{F}_{Si}\,\mathbf{F}_{Si}^{-1})'_S = \mathbf{0}\end{aligned}\right\} \quad \longrightarrow \quad \left\{\begin{aligned}\mathbf{L}_S &= -\mathbf{L}_S^{-1} = -\mathbf{a}_k \otimes (\mathbf{a}^k)'_S\,, \\ \widehat{\mathbf{L}}_{Si} &= -\widehat{\mathbf{L}}_{Si}^{-1} = -\widehat{\mathbf{z}}_k \otimes (\widehat{\mathbf{z}}^k)'_S\,,\end{aligned}\right. \tag{2.56}$$

provided that the inverses $[(\mathbf{F}_S)'_S]^{-1}$ and $[(\mathbf{F}_{Si})'_S]^{-1}$ exist[6], it is directly concluded that

$$\begin{aligned}(\mathbf{a}_k)'_S = \mathbf{L}_S\,\mathbf{a}_k = (\mathbf{F}_S)'_S\,\mathbf{h}_k\,, \quad (\mathbf{a}^k)'_S = -\mathbf{L}_S^T\,\mathbf{a}^k = (\mathbf{F}_S^{T-1})'_S\,\mathbf{h}^k\,, \\ (\widehat{\mathbf{z}}_k)'_S = \widehat{\mathbf{L}}_{Si}\,\widehat{\mathbf{z}}_k = (\mathbf{F}_{Si})'_S\,\mathbf{h}_k\,, \quad (\widehat{\mathbf{z}}^k)'_S = -\widehat{\mathbf{L}}_{Si}^T\,\widehat{\mathbf{z}}^k = (\mathbf{F}_{Si}^{T-1})'_S\,\mathbf{h}^k\,.\end{aligned} \tag{2.57}$$

In this context, note that the introduction of an elastic spatial solid velocity gradient $\mathbf{L}_{Se}$ is somehow artificial as it cannot be associated with a reasonable physical meaning comparable to the relations (2.57) (see also Ehlers [49, 50]). Moreover, for the sake of completeness, the material time derivatives of the infinitesimal line, area, and volume elements given in equations (2.38) can be expressed as

$$(\mathrm{d}\mathbf{x})'_S = \mathbf{L}_S\,\mathrm{d}\mathbf{x}\,, \quad (\mathrm{d}\mathbf{a})'_S = (\mathbf{L}_S \divideontimes \mathbf{I})\,\mathrm{d}\mathbf{a}\,, \quad (\mathrm{d}v)'_S = (\mathbf{L}_S \cdot \mathbf{I})\,\mathrm{d}v\,. \tag{2.58}$$

The symmetric and skew-symmetric parts of $\mathbf{L}_S$ and $\widehat{\mathbf{L}}_{Si}$, commonly termed total and inelastic solid stretching or deformation rate tensors and total and inelastic solid spin or vorticity tensors, read:

$$\begin{aligned}\mathbf{D}_S = \tfrac{1}{2}\,(\mathbf{L}_S + \mathbf{L}_S^T) = \mathbf{D}_S^T\,, \quad \widehat{\mathbf{D}}_{Si} = \tfrac{1}{2}\,(\widehat{\mathbf{L}}_{Si} + \widehat{\mathbf{L}}_{Si}^T) = \widehat{\mathbf{D}}_{Si}^T\,, \\ \mathbf{W}_S = \tfrac{1}{2}\,(\mathbf{L}_S - \mathbf{L}_S^T) = -\mathbf{W}_S^T\,, \quad \widehat{\mathbf{W}}_{Si} = \tfrac{1}{2}\,(\widehat{\mathbf{L}}_{Si} - \widehat{\mathbf{L}}_{Si}^T) = -\widehat{\mathbf{W}}_{Si}^T\,.\end{aligned} \tag{2.59}$$

In terms of natural bases, a special property of the deformation rates $\mathbf{D}_S$ and $\widehat{\mathbf{D}}_{Si}$ emerges. For example, with (2.26) and (2.56), one finds for the total solid deformation rate

$$\begin{aligned}\mathbf{D}_S &= \tfrac{1}{2}\,(\mathbf{L}_S + \mathbf{L}_S^T) = \tfrac{1}{2}\,(\mathbf{L}_S - \mathbf{L}_S^{T-1}) = \tfrac{1}{2}\,[(\mathbf{a}_l)'_S \otimes \mathbf{a}^l - (\mathbf{a}^l)'_S \otimes \mathbf{a}_l] \\ &= \tfrac{1}{2}\,[(a_{kl}\,\mathbf{a}^k)'_S \otimes \mathbf{a}^l - (\mathbf{a}^l)'_S \otimes \mathbf{a}_l] = \tfrac{1}{2}\,[(a_{kl})'_S\,\mathbf{a}^k \otimes \mathbf{a}^l + a_{kl}\,(\mathbf{a}^k)'_S \otimes \mathbf{a}^l - (\mathbf{a}^l)'_S \otimes \mathbf{a}_l] \\ &= \tfrac{1}{2}\,[(a_{kl})'_S\,\mathbf{a}^k \otimes \mathbf{a}^l + (\mathbf{a}^k)'_S \otimes \mathbf{a}_k - (\mathbf{a}^l)'_S \otimes \mathbf{a}_l] = \tfrac{1}{2}\,(a_{kl})'_S\,\mathbf{a}^k \otimes \mathbf{a}^l\end{aligned} \tag{2.60}$$

[6] As a counterexample, consider a pure shear deformation of φ^S with shear angle $\gamma = \gamma(t)$:

$$\mathbf{F}_S = \mathbf{I} + \gamma\,\mathbf{e}_1 \otimes \mathbf{e}_2 \;\longrightarrow\; (\mathbf{F}_S)'_S = \dot{\gamma}_S\,\mathbf{e}_1 \otimes \mathbf{e}_2 \;\longrightarrow\; \det(\mathbf{F}_S)'_S = 0 \;\longrightarrow\; \nexists\,[(\mathbf{F}_S)'_S]^{-1} \quad \text{q. e. d.}$$

but also

$$\begin{aligned}\mathbf{D}_S &= \tfrac{1}{2}\left[(\mathbf{a}_l)'_S \otimes \mathbf{a}^l - (a^{kl}\,\mathbf{a}_k)'_S \otimes \mathbf{a}_l\right] = \tfrac{1}{2}\left[(\mathbf{a}_l)'_S \otimes \mathbf{a}^l - (a^{kl})'_S\,\mathbf{a}_k \otimes \mathbf{a}_l - a^{kl}(\mathbf{a}_k)'_S \otimes \mathbf{a}_l\right] \\ &= \tfrac{1}{2}\left[(\mathbf{a}_l)'_S \otimes \mathbf{a}^l - (a^{kl})'_S\,\mathbf{a}_k \otimes \mathbf{a}_l - (\mathbf{a}_k)'_S \otimes \mathbf{a}^k\right] = -\tfrac{1}{2}\,(a^{kl})'_S\,\mathbf{a}_k \otimes \mathbf{a}_l\,.\end{aligned} \tag{2.61}$$

Thus, the deformation velocity tensors admit a co- and a contravariant representation in the frame of convected coordinates with the material time derivative acting only on the time-dependent metric coefficients:

$$\begin{aligned}\mathbf{D}_S &= -\tfrac{1}{2}\,(a^{kl})'_S\,\mathbf{a}_k \otimes \mathbf{a}_l = \tfrac{1}{2}\,(a_{kl})'_S\,\mathbf{a}^k \otimes \mathbf{a}^l\,, \\ \widehat{\mathbf{D}}_{Si} &= -\tfrac{1}{2}\,(\widehat{z}^{kl})'_S\,\widehat{\mathbf{z}}_k \otimes \widehat{\mathbf{z}}_l = \tfrac{1}{2}\,(\widehat{z}_{kl})'_S\,\widehat{\mathbf{z}}^k \otimes \widehat{\mathbf{z}}^l\,.\end{aligned} \tag{2.62}$$

Moreover, one finds

$$\begin{aligned}\mathbf{D}_S &= -\tfrac{1}{2}\,\mathbf{F}_S\,(\mathbf{C}_S^{-1})'_S\,\mathbf{F}_S^T = \tfrac{1}{2}\,\mathbf{F}_S^{T-1}\,(\mathbf{C}_S)'_S\,\mathbf{F}_S^{-1}\,, \\ \widehat{\mathbf{D}}_{Si} &= -\tfrac{1}{2}\,\mathbf{F}_{Si}\,(\mathbf{C}_{Si}^{-1})'_{Si}\,\mathbf{F}_{Si}^T = \tfrac{1}{2}\,\mathbf{F}_{Si}^{T-1}\,(\mathbf{C}_{Si})'_S\,\mathbf{F}_{Si}^{-1}\end{aligned} \tag{2.63}$$

with

$$\begin{aligned}(\mathbf{C}_S^{-1})'_S &= (a^{kl})'_S\,\mathbf{h}_k \otimes \mathbf{h}_l\,, \quad (\mathbf{C}_S)'_S = (a_{kl})'_S\,\mathbf{h}^k \otimes \mathbf{h}^l\,, \\ (\mathbf{C}_{Si}^{-1})'_S &= (\widehat{z}^{kl})'_S\,\mathbf{h}_k \otimes \mathbf{h}_l\,, \quad (\mathbf{C}_{Si})'_S = (\widehat{z}_{kl})'_S\,\mathbf{h}^k \otimes \mathbf{h}^l\end{aligned} \tag{2.64}$$

recalling that the reference basis vectors $\mathbf{h}_k$ and $\mathbf{h}^k$ are independent of time.

The above motivates the introduction of a special class of *objective* time derivatives. In continuum mechanics, the most familiar is the *convective* or *Oldroyd* derivative (Oldroyd [140]), which applied to a tensor field is essentially its *Lie* derivative along the velocity vector[7]. The procedure is to compute a pull-back to the reference configuration, take the material time derivative, and push-forward the result back to the actual configuration. Thus, one defines the *lower* (covariant) and the *upper* (contravariant) *Lie* or *Oldroyd* derivatives of φ^S via

$$\begin{aligned}(\,\bullet\,)_S^{\triangledown} &:= \mathcal{L}_{\mathbf{v}_S}(\,\bullet\,)^\sharp = \mathbf{F}_S\left(\frac{\mathrm{d}_S}{\mathrm{d}t}\left[\mathbf{F}_S^{-1}\,(\,\bullet\,)\,\mathbf{F}_S^{T-1}\right]\right)\mathbf{F}_S^T = (\,\bullet\,)'_S - \mathbf{L}_S\,(\,\bullet\,) - (\,\bullet\,)\,\mathbf{L}_S^T\,, \\ (\,\bullet\,)_S^{\triangle} &:= \mathcal{L}_{\mathbf{v}_S}(\,\bullet\,)^\flat = \mathbf{F}_S^{T-1}\left(\frac{\mathrm{d}_S}{\mathrm{d}t}\left[\mathbf{F}_S^T\,(\,\bullet\,)\,\mathbf{F}_S\right]\right)\mathbf{F}_S^{-1} = (\,\bullet\,)'_S + \mathbf{L}_S^T\,(\,\bullet\,) + (\,\bullet\,)\,\mathbf{L}_S\,.\end{aligned} \tag{2.65}$$

In analogy, convective inelastic time derivatives can be defined (Ehlers [49]):

$$\begin{aligned}(\,\widehat{\bullet}\,)_{Si}^{\triangledown} &:= (\,\widehat{\bullet}\,)'_S - \widehat{\mathbf{L}}_{Si}\,(\,\widehat{\bullet}\,) - (\,\widehat{\bullet}\,)\,\widehat{\mathbf{L}}_{Si}^T\,, \\ (\,\widehat{\bullet}\,)_{Si}^{\triangle} &:= (\,\widehat{\bullet}\,)'_S + \widehat{\mathbf{L}}_{Si}^T\,(\,\widehat{\bullet}\,) + (\,\widehat{\bullet}\,)\,\widehat{\mathbf{L}}_{Si}\,.\end{aligned} \tag{2.66}$$

In summary, the lower and upper *Lie* time derivatives are material time derivatives of the

[7] This becomes clear by rewriting the *Lie* time derivative in terms of a directional or *Gâteaux* derivative (cf. Hughes & Pister [97], Wriggers [194]). For example, for a covariant tensor field $\mathbf{T}(\mathbf{x},t)$, it holds

$$\mathcal{L}_{\mathbf{v}_S}\mathbf{T}(\mathbf{x},t) = \mathbf{F}_S\,[\mathcal{D}_{\mathbf{v}_S}\mathbf{T}(\mathbf{x},t)]\,\mathbf{F}_S^T \quad \text{with} \quad \mathcal{D}_{\mathbf{v}_S}\mathbf{T}(\mathbf{x},t) = \lim_{\epsilon\to 0}\frac{\mathbf{T}(\mathbf{X}_S + \epsilon\,\mathbf{v}_S, t_0) - \mathbf{T}(\mathbf{X}_S, t_0)}{\epsilon}\,.$$

tensorial components while keeping the co- and contravariant tensorial bases fixed (see box (2.67) for illustration).

Illustration of the *Lie* time derivative

Description:

Suppose a rotating disc (radius b) with its center mounted on a moving cantilever (length a). The relative motion of a material point $\mathcal{P}$ on the disc with respect to a fixed global basis system $\{\mathcal{O}, \mathbf{e}_k\}$ can then be described by help of a local basis system $\{\overset{*}{\mathcal{O}}, \overset{*}{\mathbf{e}}_k\}$ moving with the cantilever.

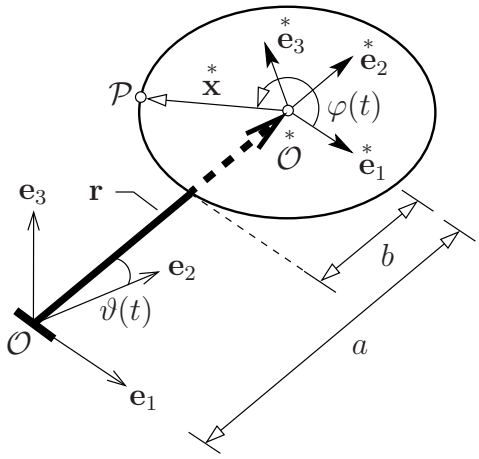

(2.67)

Position vector:

$$\mathbf{x} = \mathbf{r} + \overset{*}{\mathbf{x}} \quad \text{with} \quad \begin{cases} \mathbf{r} = r_k\,\mathbf{e}_k = a\,(\cos\vartheta\,\mathbf{e}_2 + \sin\vartheta\,\mathbf{e}_3) \\ \overset{*}{\mathbf{x}} = \overset{*}{x}_k\,\overset{*}{\mathbf{e}}_k = b\,(\cos\varphi\,\overset{*}{\mathbf{e}}_1 + \sin\varphi\,\overset{*}{\mathbf{e}}_2) \end{cases}$$

Absolute velocity:

$$\mathbf{v} = \dot{\mathbf{x}} = \dot{\mathbf{r}} + \boldsymbol{\omega} \times \overset{*}{\mathbf{x}} + \overset{*}{\mathbf{v}} \quad \text{with} \quad \begin{cases} \dot{\mathbf{r}} = \dot{r}_k\,\mathbf{e}_k \\ \boldsymbol{\omega} = \dot{\vartheta}\,\mathbf{e}_1 = \dot{\vartheta}\,\overset{*}{\mathbf{e}}_1 \\ \overset{*}{\mathbf{v}} = (\overset{*}{\mathbf{x}})^{\triangledown} = (\overset{*}{x}_k)^{\cdot}\,\overset{*}{\mathbf{e}}_k \end{cases}$$

Explanation:

$\overset{*}{\mathbf{v}} = (\overset{*}{\mathbf{x}})^{\triangledown}$ is the relative velocity of $\mathcal{P}$, i. e., the material time derivative of the position vector components, while the local basis is regarded as fixed.

Following the concept of the *Lie* time derivative, it is easily concluded that

$$\begin{aligned} (\mathbf{K}_S)^{\triangledown}_S = \mathbf{D}_S = -\tfrac{1}{2}\,(a^{kl})'_S\,\mathbf{a}_k \otimes \mathbf{a}_l\,, \quad (\mathbf{A}_S)^{\triangle}_S = \mathbf{D}_S = \tfrac{1}{2}\,(a_{kl})'_S\,\mathbf{a}^k \otimes \mathbf{a}^l\,, \\ (\widehat{\mathbf{K}}_{Si})^{\triangledown}_{Si} = \widehat{\mathbf{D}}_{Si} = -\tfrac{1}{2}\,(\widehat{z}^{kl})'_S\,\widehat{\mathbf{z}}_k \otimes \widehat{\mathbf{z}}_l\,, \quad (\widehat{\boldsymbol{\Gamma}}_{Si})^{\triangle}_{Si} = \widehat{\mathbf{D}}_{Si} = \tfrac{1}{2}\,(\widehat{z}_{kl})'_S\,\widehat{\mathbf{z}}^k \otimes \widehat{\mathbf{z}}^l\,. \end{aligned} \tag{2.68}$$

Now, convenient co- and contravariant strain rates can be introduced, which admit the same transport properties as the underlying strain measures. Moreover, the additive concept is kept consistent with the serial structure of the inelastic *Maxwell* branches. Thus, the respective co- and contravariant strain rates of the reference, intermediate, and actual configurations read:

$$\begin{aligned} (\overset{\mathrm{R}}{\mathbf{K}}_S)'_S = (\overset{\mathrm{R}}{\mathbf{K}}_{Se})'_S + (\overset{\mathrm{R}}{\mathbf{K}}_{Si})'_S = -\tfrac{1}{2}\,(\mathbf{C}_S^{-1})'_S = -\tfrac{1}{2}\,(a^{kl})'_S\,\mathbf{h}_k \otimes \mathbf{h}_l\,, \\ (\widehat{\mathbf{K}}_S)^{\triangledown}_{Si} = (\widehat{\mathbf{K}}_{Se})^{\triangledown}_{Si} + (\widehat{\mathbf{K}}_{Si})^{\triangledown}_{Si} = -\tfrac{1}{2}\,(\widehat{z}^{kl})'_S\,\widehat{\mathbf{z}}_k \otimes \widehat{\mathbf{z}}_l\,, \\ (\mathbf{K}_S)^{\triangledown}_S = (\mathbf{K}_{Se})^{\triangledown}_S + (\mathbf{K}_{Si})^{\triangledown}_S = \mathbf{D}_S = -\tfrac{1}{2}\,(a^{kl})'_S\,\mathbf{a}_k \otimes \mathbf{a}_l\,, \end{aligned} \tag{2.69}$$

$$
\begin{aligned}
(\mathbf{E}_S)'_S = (\mathbf{E}_{Se})'_S + (\mathbf{E}_{Si})'_S = \tfrac{1}{2}\,(\mathbf{C}_S)'_S = \tfrac{1}{2}\,(a_{kl})'_S\,\mathbf{h}^k \otimes \mathbf{h}^l\,,\\
(\widehat{\mathbf{\Gamma}}_S)^{\triangle}_{Si} = (\widehat{\mathbf{\Gamma}}_{Se})^{\triangle}_{Si} + (\widehat{\mathbf{\Gamma}}_{Si})^{\triangle}_{Si} = \tfrac{1}{2}\,(\widehat{z}_{kl})'_S\,\widehat{\mathbf{z}}^k \otimes \widehat{\mathbf{z}}^l\,,\\
(\mathbf{A}_S)^{\triangle}_S = (\mathbf{A}_{Se})^{\triangle}_S + (\mathbf{A}_{Si})^{\triangle}_S = \mathbf{D}_S = \tfrac{1}{2}\,(a_{kl})'_S\,\mathbf{a}^k \otimes \mathbf{a}^l\,.
\end{aligned}
\tag{2.70}
$$

For the sake of completeness, a complete summary of the *Green-Almansi* and the *Karni-Reiner* strain rates including their transport mechanisms is provided in appendix B.2.

Remark: As already mentioned, the multiplicative geometric concept of deformation gradients associated with the suggestion of locally unloaded intermediate configurations is not mandatory. Particularly, the shortcoming of unspecified rotations (cf. equation (2.32)) in regard to certain invariance requirements led to diverse discussions in the related literature (see Green & Naghdi [74], Sidoroff [161], and Haupt [85] among others). Therefore, two alternative approaches are worth mentioning:

(*i*) A more abstract interpretation of the intermediate configuration is given by the concept of *elastic material isomorphisms* (Bertram [8], Svendsen [172], and quotations therein). From a mathematical point of view, an isomorphism is a mapping that preserves sets and relations among elements. In the context of finite inelasticity, an elastic material isomorphism is understood as a mapping that does not affect the elastic properties at material points. This can be illustrated by comparison of the basic deformation tensors $\mathbf{C}_S = a_{kl}\,\mathbf{h}^k \otimes \mathbf{h}^l$ of the reference and $\widehat{\mathbf{C}}_{Se} = \mathbf{F}_{Si}^{T-1}\,\mathbf{C}_S\,\mathbf{F}_{Si}^{-1} = a_{kl}\,\widehat{\mathbf{z}}^k \otimes \widehat{\mathbf{z}}^l$ of the intermediate configuration. From the natural basis representation, it can be directly observed that the actual metric a_{kl}, which is associated with the deformation of the actual line elements, is generally unaltered due to a transport with $\mathbf{F}_{Si} = \widehat{\mathbf{z}}_k \otimes \mathbf{h}^k$. Thus, if in addition, the inelastic deformation gradient does not influence the shape of the constitutive elastic material formulation, i. e., purely acts as an inelastic transport operator, then $\mathbf{F}_{Si}$ is an elastic material isomorphism.

(*ii*) Another approach to finite inelasticity is based on the constitutive introduction of an *inelastic metric* to locally govern the inelastic deformation process in the sense of an internal variable (Miehe [122, 123]). Following this, the introduction of multiplicative decompositions of deformation gradients and associated inelastic intermediate configurations is not necessarily required. This can be motivated from a computational perspective, since neither a multiplicative split is explicitly computed nor any equation is evaluated or solved with respect to an intermediate configuration. However, in the frame of natural coordinates, it turns out that the inelastic metric somehow coincides with the intermediate metric $\widehat{z}_{kl} = \widehat{\mathbf{z}}_k \cdot \widehat{\mathbf{z}}_l$ of the multiplicative concept. Thus, one may introduce an inelastic reference metric tensor of the form $\mathbf{G}_{Si} = \widehat{z}_{kl}\,\mathbf{h}^k \otimes \mathbf{h}^l$, which is actually identical to the naturally symmetric and positive definite, inelastic *Cauchy-Green* deformation tensor $\mathbf{C}_{Si} = \mathbf{F}_{Si}^T\,\mathbf{F}_{Si}$. Following Sidoroff [161], sec. 3.1, the introduction of $\mathbf{C}_{Si}$ or $\widehat{z}_{kl}$, respectively, as an internal variable with six internal degrees of freedom implies an *equivalence class* of intermediate configurations, where two configurations are said to be equivalent if they can be obtained by mutual rotations. Consequently, concerning the description of inelastic material behavior, it is mostly sufficient to postulate an evolution equation for the intermediate metric $\widehat{z}_{kl}$ (or a related quantity) as the developing variable during an inelastic deformation process (see also Haupt [87], sec. 1.10.3). ■

2.2.4 Polar Decomposition and Spectral Representation

In order to allow for a concise formulation of the subsequent constitutive material equations, it is, for some applications, of considerable assistance to express the deformation tensors by means of their eigenvalues and eigenvectors or eigentensors, respectively. Moreover, from a computational perspective, the spectral representation enables an efficient algorithmic treatment of potential high-grade nonlinear material functions within large strain finite element implementations.

Proceeding from the fundamental theorem of polar decomposition, the solid deformation gradient (as any other linear mapping) can be multiplicatively split into a proper orthogonal rotation tensor $\mathbf{R}_S \in \mathcal{SO}_3$ and a symmetric, positive definite right (material) or left (spatial) stretch tensor $\mathbf{U}_S$ or $\mathbf{V}_S$, respectively:

$$\begin{aligned} \mathbf{F}_S &= \mathbf{R}_S\,\mathbf{U}_S = \mathbf{V}_S\,\mathbf{R}_S \\ \text{with}\quad \mathbf{R}_S^T &= \mathbf{R}_S^{-1}\,, \quad \mathbf{U}_S^T = \mathbf{U}_S\,, \quad \mathbf{V}_S^T = \mathbf{V}_S\,. \end{aligned} \tag{2.71}$$

Following this, the solid deformation tensors and their inverses can be expressed as

$$\begin{aligned} \mathbf{C}_S = \mathbf{F}_S^T\,\mathbf{F}_S = \mathbf{U}_S\,\mathbf{U}_S = \mathbf{U}_S^2\,, \quad \mathbf{B}_S = \mathbf{F}_S\,\mathbf{F}_S^T = \mathbf{V}_S\,\mathbf{V}_S = \mathbf{V}_S^2\,, \\ \mathbf{C}_S^{-1} = (\mathbf{U}_S^{-1})^2 = (\mathbf{U}_S^2)^{-1}\,, \quad \mathbf{B}_S^{-1} = (\mathbf{V}_S^{-1})^2 = (\mathbf{V}_S^2)^{-1}\,. \end{aligned} \tag{2.72}$$

Moreover, with the rotation tensor, one finds the relationships

$$\begin{aligned} \mathbf{V}_S = \mathbf{R}_S\,\mathbf{U}_S\,\mathbf{R}_S^T\,, \quad \mathbf{U}_S = \mathbf{R}_S^T\,\mathbf{V}_S\,\mathbf{R}_S\,, \\ \mathbf{B}_S = \mathbf{R}_S\,\mathbf{C}_S\,\mathbf{R}_S^T\,, \quad \mathbf{C}_S = \mathbf{R}_S^T\,\mathbf{B}_S\,\mathbf{R}_S\,, \\ \mathbf{V}_S^{-1} = \mathbf{R}_S\,\mathbf{U}_S^{-1}\,\mathbf{R}_S^T\,, \quad \mathbf{U}_S^{-1} = \mathbf{R}_S^T\,\mathbf{V}_S^{-1}\,\mathbf{R}_S\,, \\ \mathbf{B}_S^{-1} = \mathbf{R}_S\,\mathbf{C}_S^{-1}\,\mathbf{R}_S^T s\,, \quad \mathbf{C}_S^{-1} = \mathbf{R}_S^T\,\mathbf{B}_S^{-1}\,\mathbf{R}_S \end{aligned} \tag{2.73}$$

and thus, a transformation rule between the co- and contravariant strain tensors

$$\begin{aligned} \mathbf{K}_S = \mathbf{R}_S\,\underset{\text{R}}{\mathbf{E}}_S\,\mathbf{R}_S^T\,, \quad \underset{\text{R}}{\mathbf{E}}_S = \mathbf{R}_S^T\,\mathbf{K}_S\,\mathbf{R}_S\,, \\ \mathbf{A}_S = \mathbf{R}_S\,\underset{\text{R}}{\mathbf{K}}_S\,\mathbf{R}_S^T\,, \quad \underset{\text{R}}{\mathbf{K}}_S = \mathbf{R}_S^T\,\mathbf{A}_S\,\mathbf{R}_S\,. \end{aligned} \tag{2.74}$$

In this connection, $\mathbf{R}_S\,(\,\cdot\,)\,\mathbf{R}_S^T$ and $\mathbf{R}_S^T\,(\,\cdot\,)\,\mathbf{R}_S$ denote so-called push-forward and pull-back rotations, which are special transport mechanisms that simultaneously alter the variant type of the argument due to the orthogonality property $\mathbf{R}_S = \mathbf{R}_S^{T-1}$. From this, it also becomes clear that the two-field character of $\mathbf{F}_S$ is included in the rotation tensor $\mathbf{R}_S$ rather than in the stretch tensors $\mathbf{U}_S$ or $\mathbf{V}_S$, respectively.

It is now easily concluded that $\mathbf{C}_S$ and $\mathbf{B}_S$ obey the same eigenvalues, which are the squares of the principal stretches, i. e., the eigenvalues of $\mathbf{U}_S$ or $\mathbf{V}_S$, respectively. Moreover, the principal directions, i. e., the eigenvectors, of $\mathbf{C}_S$ and $\mathbf{U}_S$ as well as of $\mathbf{B}_S$ and $\mathbf{V}_S$ coincide. For the purpose of this contribution, it is sufficient to consider the eigenvalue problems of the *Cauchy-Green* deformation tensors only. They read:

$$\left.\begin{aligned} (\mathbf{C}_S - \lambda_S\,\mathbf{I})\,\mathbf{m}_S = \mathbf{0} \\ (\mathbf{B}_S - \lambda_S\,\mathbf{I})\,\mathbf{n}_S = \mathbf{0} \end{aligned}\right\} \quad \longleftrightarrow \quad \left\{\begin{aligned} \mathbf{C}_S\,\mathbf{m}_{S(k)} = \lambda_{S(k)}\,\mathbf{m}_{S(k)}\,, \\ \mathbf{B}_S\,\mathbf{n}_{S(k)} = \lambda_{S(k)}\,\mathbf{n}_{S(k)} \end{aligned}\right. \tag{2.75}$$

with $\lambda_{S(k)} := \lambda_{\mathbf{C}_S(k)} = \lambda_{\mathbf{B}_S(k)} = (\lambda_{\mathbf{U}_S(k)})^2 = (\lambda_{\mathbf{V}_S(k)})^2 \in \mathbb{R}^+$ $(k = 1, 2, 3)$ as the three real, positive eigenvalues of the symmetric and positive definite deformation tensors $\mathbf{C}_S$ or $\mathbf{B}_S$, respectively, and $\mathbf{m}_{S(k)}$ and $\mathbf{n}_{S(k)}$ as the corresponding orthonormal eigenvectors of the reference and the actual configuration with the property $\mathbf{m}_{S(k)} \cdot \mathbf{m}_{S(l)} = \mathbf{n}_{S(k)} \cdot \mathbf{n}_{S(l)} = \delta_{kl}$. The non-trivial solution of (2.75) requires the characteristic polynomial to be zero, i. e.,

$$\det(\mathbf{C}_S - \lambda_S \mathbf{I}) = \det(\mathbf{B}_S - \lambda_S \mathbf{I}) = \lambda_S^3 - I_S \lambda_S^2 + II_S \lambda_S - III_S = 0 \tag{2.76}$$

with the principal invariants of the solid deformation tensors given as

$$\begin{aligned} I_S &:= I_{\mathbf{C}_S} = I_{\mathbf{B}_S} = \tfrac{1}{2} (\mathbf{C}_S \divideontimes \mathbf{I}) \cdot \mathbf{I} = \operatorname{tr} \mathbf{C}_S = \mathbf{C}_S \cdot \mathbf{I} = \mathbf{F}_S \cdot \mathbf{F}_S \,, \\ II_S &:= II_{\mathbf{C}_S} = II_{\mathbf{B}_S} = \tfrac{1}{2} (\mathbf{C}_S \divideontimes \mathbf{C}_S) \cdot \mathbf{I} = \operatorname{cof} \mathbf{C}_S \cdot \mathbf{I} = \operatorname{cof} \mathbf{F}_S \cdot \operatorname{cof} \mathbf{F}_S \,, \\ III_S &:= III_{\mathbf{C}_S} = III_{\mathbf{B}_S} = \tfrac{1}{6} (\mathbf{C}_S \divideontimes \mathbf{C}_S) \cdot \mathbf{C}_S = \det \mathbf{C}_S = (\det \mathbf{F}_S)^2 \,. \end{aligned} \tag{2.77}$$

Note that the representation of the principal invariants by means of $\mathbf{F}_S$, $\operatorname{cof} \mathbf{F}_S$, and $\det \mathbf{F}_S$ is of special interest in regard to certain stability requirements (keyword *polyconvexity*) of the to-be defined constitutive functions (see section 3.2.2). In this context, recall that the transport mechanisms of the material line, area, and volume elements of φ^S (2.38) are defined by exactly these terms.

If the eigenvalues $\lambda_{S(k)}$ are known, the principal invariants can also be obtained from

$$\begin{aligned} I_S &= \sum_{k=1}^{3} \lambda_{S(k)} = \lambda_{S(1)} + \lambda_{S(2)} + \lambda_{S(3)} \,, \\ II_S &= \tfrac{1}{2} \sum_{\substack{k,l=1 \\ l \neq k}}^{3} \lambda_{S(k)} \lambda_{S(l)} = \lambda_{S(1)} \lambda_{S(2)} + \lambda_{S(2)} \lambda_{S(3)} + \lambda_{S(3)} \lambda_{S(1)} \,, \\ III_S &= \prod_{k=1}^{3} \lambda_{S(k)} = \lambda_{S(1)} \lambda_{S(2)} \lambda_{S(3)} \end{aligned} \tag{2.78}$$

with the products $\lambda_{S(1)} \lambda_{S(2)}$, $\lambda_{S(2)} \lambda_{S(3)}$, and $\lambda_{S(3)} \lambda_{S(1)}$ precisely representing the eigenvalues of $\operatorname{cof} \mathbf{C}_S$ or $\operatorname{cof} \mathbf{B}_S$, respectively. Moreover, knowing the eigenvectors, the symmetric eigentensors or eigenbases of the reference and the actual configuration are introduced via

$$\mathbf{M}_{S(k)} := \mathbf{m}_{S(k)} \otimes \mathbf{m}_{S(k)} \quad \text{and} \quad \mathbf{N}_{S(k)} := \mathbf{n}_{S(k)} \otimes \mathbf{n}_{S(k)} \,, \tag{2.79}$$

which accordingly obey the following properties:

$$\begin{aligned} \sum_{k=1}^{3} \mathbf{M}_{S(k)} &= \mathbf{I} \,, & \sum_{k=1}^{3} \mathbf{N}_{S(k)} &= \mathbf{I} \,, \\ \mathbf{M}_{S(k)} \cdot \mathbf{M}_{S(l)} &= \delta_{kl} \,, & \mathbf{N}_{S(k)} \cdot \mathbf{N}_{S(l)} &= \delta_{kl} \,, \\ \mathbf{M}_{S(k)} \, \mathbf{M}_{S(l)} &= \mathbf{0} \quad \forall\, k \neq l \,, & \mathbf{N}_{S(k)} \, \mathbf{N}_{S(l)} &= \mathbf{0} \quad \forall\, k \neq l \,, \\ (\mathbf{M}_{S(k)})^m &= \mathbf{M}_{S(k)} \quad \forall\, m \in \mathbb{R}^+ \,, & (\mathbf{N}_{S(k)})^m &= \mathbf{N}_{S(k)} \quad \forall\, m \in \mathbb{R}^+ \,, \\ \mathbf{C}_S \, \mathbf{M}_{S(k)} &= \mathbf{M}_{S(k)} \, \mathbf{C}_S = \lambda_{S(k)} \, \mathbf{M}_{S(k)} \,, & \mathbf{B}_S \, \mathbf{N}_{S(k)} &= \mathbf{N}_{S(k)} \, \mathbf{B}_S = \lambda_{S(k)} \, \mathbf{N}_{S(k)} \,. \end{aligned} \tag{2.80}$$

Remark: Proceeding from three distinct roots $\lambda_{S(1)} \neq \lambda_{S(2)} \neq \lambda_{S(3)} \neq \lambda_{S(1)}$ of the characteristic polynomial (2.76), the eigentensors can be directly determined from

$$\mathbf{M}_{S(k)} = \prod_{\substack{l=1 \\ l\neq k}}^{3} \frac{(\mathbf{C}_S - \lambda_{S(l)}\,\mathbf{I})}{(\lambda_{S(k)} - \lambda_{S(l)})}\,, \quad \mathbf{N}_{S(k)} = \prod_{\substack{l=1 \\ l\neq k}}^{3} \frac{(\mathbf{B}_S - \lambda_{S(l)}\,\mathbf{I})}{(\lambda_{S(k)} - \lambda_{S(l)})} \tag{2.81}$$

without computing the eigenvectors first[8]. However, the existence of three distinct eigenvalues of $\mathbf{C}_S$ or $\mathbf{B}_S$ throughout the mechanical process (except the undeformed initial state at time t_0, where $\mathbf{F}_S = \mathbf{I}$ and all $\lambda_{S(k)} = 1$), requires the deformation to be *isochoric*, i. e., volume preserving, which obviously cannot be reconciled with general porous media applications. Moreover, the sophisticated numerical solution of symmetric eigenvalue problems, e. g., by the *Householder-QL* algorithm, delivers the corresponding eigenvectors as a computational byproduct (see paragraph on page 109). Thus, closed-form equations for the computation of the eigenbases such as (2.81) are, in principle, dispensable. ■

Thus, the spectral representations of arbitrary real-valued powers $m \in \mathbb{R}$ of the solid deformation tensors are given by

$$(\mathbf{C}_S)^m = \sum_{k=1}^{3} (\lambda_{S(k)})^m\, \mathbf{M}_{S(k)}\,, \quad (\mathbf{B}_S)^m = \sum_{k=1}^{3} (\lambda_{S(k)})^m\, \mathbf{N}_{S(k)}\,. \tag{2.82}$$

Following this, the right and left solid stretch tensors take the form

$$\mathbf{U}_S = (\mathbf{C}_S)^{1/2} = \sum_{k=1}^{3} \sqrt{\lambda_{S(k)}}\, \mathbf{M}_{S(k)}\,, \quad \mathbf{V}_S = (\mathbf{B}_S)^{1/2} = \sum_{k=1}^{3} \sqrt{\lambda_{S(k)}}\, \mathbf{N}_{S(k)}\,, \tag{2.83}$$

and it can be directly deduced that

$$\mathbf{R}_S = \sum_{k=1}^{3} \mathbf{n}_{S(k)} \otimes \mathbf{m}_{S(k)} \quad \longrightarrow \quad \mathbf{F}_S = \sum_{k=1}^{3} \sqrt{\lambda_{S(k)}}\, \mathbf{n}_{S(k)} \otimes \mathbf{m}_{S(k)}\,. \tag{2.84}$$

In particular, $\mathbf{R}_S$ and $\mathbf{R}_S^T = \mathbf{R}_S^{-1}$ act as transport mechanisms (cf. equations (2.73) and (2.74)) by rotating the principal directions of the reference (i. e., of $\mathbf{C}_S$ or $\mathbf{U}_S$) into those

[8] This can be easily deduced from the spectral representations of $\mathbf{C}_S$ and $\mathbf{B}_S$ (2.82) and the properties of the eigentensors (2.80). As an example, regard the derivation of $\mathbf{M}_{S(3)}$:

$$\begin{aligned}
\mathbf{C}_S - \lambda_{S(1)}\,\mathbf{I} &= (\lambda_{S(2)} - \lambda_{S(1)})\,\mathbf{M}_{S(2)} + (\lambda_{S(3)} - \lambda_{S(1)})\,\mathbf{M}_{S(3)}\,,\\
\mathbf{C}_S - \lambda_{S(2)}\,\mathbf{I} &= (\lambda_{S(1)} - \lambda_{S(2)})\,\mathbf{M}_{S(1)} + (\lambda_{S(3)} - \lambda_{S(2)})\,\mathbf{M}_{S(3)}\,,\\
(\mathbf{C}_S - \lambda_{S(1)}\,\mathbf{I})\,(\mathbf{C}_S - \lambda_{S(2)}\,\mathbf{I}) &= (\lambda_{S(3)} - \lambda_{S(1)})\,(\lambda_{S(3)} - \lambda_{S(2)})\,\mathbf{M}_{S(3)}\\
\longrightarrow \quad \mathbf{M}_{S(3)} &= \frac{(\mathbf{C}_S - \lambda_{S(1)}\,\mathbf{I})\,(\mathbf{C}_S - \lambda_{S(2)}\,\mathbf{I})}{(\lambda_{S(3)} - \lambda_{S(1)})\,(\lambda_{S(3)} - \lambda_{S(2)})} \quad \text{q. e. d.}
\end{aligned}$$

of the actual configuration (i. e., of $\mathbf{B}_S$ or $\mathbf{V}_S$) and *vice versa*, viz.,

$$\mathbf{m}_{S(k)} \underset{\mathbf{R}_S^T}{\overset{\mathbf{R}_S}{\rightleftharpoons}} \mathbf{n}_{S(k)}\,, \qquad \mathbf{M}_{S(k)} \underset{\mathbf{R}_S^T\,(\,\cdot\,)\,\mathbf{R}_S}{\overset{\mathbf{R}_S\,(\,\cdot\,)\,\mathbf{R}_S^T}{\rightleftharpoons}} \mathbf{N}_{S(k)}\,. \tag{2.85}$$

Note that due to the orthogonality of the principal axes, in the context of the spectral representation no distinction between co- and contravariant is necessary comparable to the self-reciprocal rectangular *Cartesi*an basis vectors $\mathbf{e}_k$ (cf. section 2.2.2). However, concerning the complete transport property of eigenvectors and eigentensors including both rotation and stretch, it turns out as a kinematical consequence of

$$\mathbf{B}_S = \mathbf{F}_S\,\mathbf{F}_S^T = \mathbf{F}_S\,\mathbf{I}\,\mathbf{F}_S^T = \mathbf{F}_S\Big(\sum_{k=1}^{3}\mathbf{M}_{S(k)}\Big)\,\mathbf{F}_S^T = \sum_{k=1}^{3}\mathbf{F}_S\,\mathbf{M}_{S(k)}\,\mathbf{F}_S^T = \sum_{k=1}^{3}\lambda_{S(k)}\,\mathbf{N}_{S(k)} \tag{2.86}$$

that they accordingly obey a covariant transformation behavior. Thus,

$$\mathbf{m}_{S(k)} \underset{\mathbf{F}_S^{-1}}{\overset{\mathbf{F}_S}{\rightleftharpoons}} \sqrt{\lambda_{S(k)}}\,\mathbf{n}_{S(k)}\,, \quad \mathbf{M}_{S(k)} \underset{\mathbf{F}_S^{-1}\,(\,\cdot\,)\,\mathbf{F}_S^{T-1}}{\overset{\mathbf{F}_S\,(\,\cdot\,)\,\mathbf{F}_S^T}{\rightleftharpoons}} \lambda_{S(k)}\,\mathbf{N}_{S(k)}\,. \tag{2.87}$$

Remark: In the context of multiplicative finite inelasticity associated with $\mathbf{F}_S = \mathbf{F}_{Se}\,\mathbf{F}_{Si}$ (cf. section 2.2.3), the presented polar and spectral decompositions can be applied straightforwardly to both the elastic and the inelastic parts of $\mathbf{F}_S$. Following this, respective elastic and inelastic stretch and rotation tensors can be directly introduced via

$$\mathbf{F}_{Se} = \mathbf{R}_{Se}\,\widehat{\mathbf{U}}_{Se} = \mathbf{V}_{Se}\,\mathbf{R}_{Se}\,, \quad \mathbf{F}_{Si} = \mathbf{R}_{Si}\,\mathbf{U}_{Si} = \widehat{\mathbf{V}}_{Si}\,\mathbf{R}_{Si}\,, \tag{2.88}$$

which obviously obey properties equivalent to relations (2.71 – 2.73). Furthermore, the eigenvalue problems of $\widehat{\mathbf{C}}_{Se} = \widehat{\mathbf{U}}_{Se}^2$ and $\mathbf{B}_{Se} = \mathbf{V}_{Se}^2$ as well as of $\mathbf{C}_{Si} = \mathbf{U}_{Si}^2$ and $\widehat{\mathbf{B}}_{Si} = \widehat{\mathbf{V}}_{Si}^2$ are treated analogously to those of $\mathbf{C}_S$ and $\mathbf{B}_S$ yielding the corresponding spectral representations. For the purpose of this contribution, the spectral forms of the elastic deformation tensors are of particular interest for the formulation of the inelastic constitutive material law. Accordingly, they read

$$\widehat{\mathbf{C}}_{Se} = \sum_{k=1}^{3}\lambda_{Se(k)}\,\widehat{\mathbf{M}}_{Se(k)}\,, \quad \mathbf{B}_{Se} = \sum_{k=1}^{3}\lambda_{Se(k)}\,\mathbf{N}_{Se(k)} \tag{2.89}$$

with $\lambda_{Se(k)}$ representing the eigenvalues of the elastic deformation tensors $\widehat{\mathbf{C}}_{Se}$ or $\mathbf{B}_{Se}$ (i. e., the squares of the purely elastic principal stretches), respectively, and $\widehat{\mathbf{M}}_{Se(k)} = \widehat{\mathbf{m}}_{Se(k)} \otimes \widehat{\mathbf{m}}_{Se(k)}$ and $\mathbf{N}_{Se(k)} = \mathbf{n}_{Se(k)} \otimes \mathbf{n}_{Se(k)}$ as the elastic eigentensors built by the dyadic products of the elastic intermediate eigenvectors $\widehat{\mathbf{m}}_{Se(k)}$ and the elastic principal axes of the actual frame $\mathbf{n}_{Se(k)}$. ■

To continue, for the entire formulation of constitutive material functions in spectral representation, additionally, the partial derivatives of the eigenvalues, eigenvectors, and

eigentensors with respect to the corresponding deformation tensors are required. For their derivation, one initially proceeds from the general case of three distinct eigenvalues $\lambda_{S(1)} \neq \lambda_{S(2)} \neq \lambda_{S(3)} \neq \lambda_{S(1)}$. Necessary modifications for the special cases of equal values of the $\lambda_{S(k)}$ will be discussed in the context of a specific application at the end of this section.

At first, in order to find those derivatives of the reference frame with respect to $\mathbf{C}_S$, it is assumed that the principal referential directions $\mathbf{m}_{S(k)}$ can be determined from a time-dependent rotation $\mathbf{Q}_S = \mathbf{Q}_S(t) \in \mathcal{SO}_3$ of the spatially fixed orthonormal basis vectors $\mathbf{e}_k$, i. e., $\mathbf{m}_{S(k)} = \mathbf{Q}_S\,\mathbf{e}_k$. Taking the material time derivative, it is easily deduced that

$$(\mathbf{m}_{S(k)})'_S = (\mathbf{Q}_S)'_S\,\mathbf{e}_k = \mathbf{\Omega}_S\,\mathbf{m}_{S(k)} \quad \text{with} \quad \mathbf{\Omega}_S := (\mathbf{Q}_S)'_S\,\mathbf{Q}_S^T = -\mathbf{\Omega}_S^T \tag{2.90}$$

representing the skew-symmetric gyration tensor of the principal directions of $\mathbf{C}_S$ or $\mathbf{U}_S$, respectively. In particular, the gyration tensor takes the form

$$\mathbf{\Omega}_S = \sum_{k=1}^{3} (\mathbf{m}_{S(k)})'_S \otimes \mathbf{m}_{S(k)} = \sum_{k,l=1}^{3} \Omega_{kl}\,\mathbf{e}_k \otimes \mathbf{e}_l\,, \tag{2.91}$$

so that

$$(\mathbf{m}_{S(l)})'_S = \mathbf{\Omega}_S\,\mathbf{m}_{S(l)} = \sum_{\substack{k=1 \\ k\neq l}}^{3} \Omega_{kl}\,\mathbf{m}_{S(k)}\,, \tag{2.92}$$

where Ω_{kl} are the coefficients of $\mathbf{\Omega}_S$ in the fixed *Cartesi*an frame $\{\mathbf{e}_k\}$. These coefficients, although not explicitly required for the following considerations, may be obtained from

$$\begin{gathered} \Omega_{kl} = \mathbf{m}_{S(k)} \cdot (\mathbf{m}_{S(l)})'_S = \mathbf{m}_{S(k)} \cdot \mathbf{\Omega}_S\,\mathbf{m}_{S(l)} = -\Omega_{lk} \\ \text{with} \quad \Omega_{kk} = \mathbf{m}_{S(k)} \cdot (\mathbf{m}_{S(k)})'_S = 0\,. \end{gathered} \tag{2.93}$$

For the determination of the partial derivatives of $\lambda_{S(k)}$, $\mathbf{m}_{S(k)}$, and $\mathbf{M}_{S(k)}$ with respect to $\mathbf{C}_S$, use will be made of the following rate formulations:

$$(\lambda_{S(k)})'_S = \frac{\partial \lambda_{S(k)}}{\partial \mathbf{C}_S} \cdot (\mathbf{C}_S)'_S\,, \quad (\mathbf{m}_{S(k)})'_S = \frac{\partial \mathbf{m}_{S(k)}}{\partial \mathbf{C}_S}\,(\mathbf{C}_S)'_S\,. \tag{2.94}$$

Hence, if the left hand sides of these equations as well as $(\mathbf{C}_S)'_S$ are known, the respective partial derivatives can be deduced by comparison.

Starting with the derivative of the eigenvalues, with the symmetry property $\mathbf{C}_S = \mathbf{C}_S^T$ and the orthogonality condition $(2.93)_2$, the left hand side of $(2.94)_1$ can be found as

$$(\lambda_{S(k)})'_S = (\mathbf{m}_{S(k)} \cdot \mathbf{C}_S\,\mathbf{m}_{S(k)})'_S = \mathbf{m}_{S(k)} \cdot (\mathbf{C}_S)'_S\,\mathbf{m}_{S(k)} = (\mathbf{m}_{S(k)} \otimes \mathbf{m}_{S(k)}) \cdot (\mathbf{C}_S)'_S\,. \tag{2.95}$$

Comparison with the right hand side of the rate formulation directly yields the result

$$\frac{\partial \lambda_{S(k)}}{\partial \mathbf{C}_S} = \mathbf{m}_{S(k)} \otimes \mathbf{m}_{S(k)} = \mathbf{M}_{S(k)}\,. \tag{2.96}$$

Next, regarding the derivative of the eigenvectors, the left hand side of $(2.94)_2$ is already

given by equation (2.92). Taking the material time derivative of $\mathbf{C}_S$ in form of $(2.82)_1$ by means of the gyration tensor $\boldsymbol{\Omega}_S$ yields

$$(\mathbf{C}_S)'_S = \sum_{k=1}^{3} (\lambda_{S(k)})'_S \, \mathbf{m}_{S(k)} \otimes \mathbf{m}_{S(k)} + \overbrace{\sum_{\substack{k,l=1 \\ l\neq k}}^{3} \Omega_{kl} \, (\lambda_{S(l)} - \lambda_{S(k)}) \, \mathbf{m}_{S(k)} \otimes \mathbf{m}_{S(l)}}^{\boldsymbol{\Omega}_S \, \mathbf{C}_S \, - \, \mathbf{C}_S \, \boldsymbol{\Omega}_S} \, . \tag{2.97}$$

Under consideration of the orthonormality condition $\mathbf{m}_{S(k)} \cdot \mathbf{m}_{S(l)} = \delta_{kl}$ and the skew-symmetry of the gyration tensor coefficients $(2.93)_1$, by comparison of the terms in the rate formulation $(2.94)_2$, one finds the 3rd-order tensor

$$\frac{\partial \mathbf{m}_{S(k)}}{\partial \mathbf{C}_S} = \tfrac{1}{2} \sum_{\substack{l=1 \\ l\neq k}}^{3} \frac{1}{\lambda_{S(k)} - \lambda_{S(l)}} \overset{3}{\mathbf{M}}_{S[lk]} =: \overset{3}{\mathbf{M}}_{S(k)} \tag{2.98}$$

with the abbreviation

$$\overset{3}{\mathbf{M}}_{S[lk]} = (\mathbf{M}_{S(l)} \otimes \mathbf{m}_{S(k)})^{\overset{23}{T}} + \mathbf{M}_{S(l)} \otimes \mathbf{m}_{S(k)} \, . \tag{2.99}$$

Thereafter, the partial derivative of the eigenbases with respect to $\mathbf{C}_S$ is directly computed from

$$\begin{aligned} \frac{\partial \mathbf{M}_{S(k)}}{\partial \mathbf{C}_S} &= \frac{\partial (\mathbf{m}_{S(k)} \otimes \mathbf{m}_{S(k)})}{\partial \mathbf{C}_S} \\ &= \Big[\Big(\frac{\partial \mathbf{m}_{S(k)}}{\partial \mathbf{C}_S} \Big)^{\overset{23}{T}} \otimes \mathbf{m}_{S(k)} \Big]^{\overset{24}{T}} + \mathbf{m}_{S(k)} \otimes \frac{\partial \mathbf{m}_{S(k)}}{\partial \mathbf{C}_S} \\ &= \tfrac{1}{2} \sum_{\substack{l=1 \\ l\neq k}}^{3} \frac{1}{\lambda_{S(k)} - \lambda_{S(l)}} \big(\overset{4}{\mathbf{M}}_{S[kl]} + \overset{4}{\mathbf{M}}_{S[lk]} \big) =: \overset{4}{\mathbf{M}}_{S(k)} \end{aligned} \tag{2.100}$$

with the abbreviation

$$\overset{4}{\mathbf{M}}_{S[kl]} = (\mathbf{M}_{S(k)} \otimes \mathbf{M}_{S(l)})^{\overset{23}{T}} + (\mathbf{M}_{S(k)} \otimes \mathbf{M}_{S(l)})^{\overset{24}{T}} . \tag{2.101}$$

Note that in the above equations, the defined tensors possess the following symmetries:

$$\overset{3}{\mathbf{M}}_{S(k)} = \overset{3}{\mathbf{M}}{}^{\overset{23}{T}}_{S(k)} \, , \quad \overset{4}{\mathbf{M}}_{S(k)} = \overset{4}{\mathbf{M}}{}^{\overset{12}{T}}_{S(k)} = \overset{4}{\mathbf{M}}{}^{\overset{34}{T}}_{S(k)} = (\overset{4}{\mathbf{M}}{}^{\overset{13}{T}}_{S(k)})^{\overset{24}{T}} . \tag{2.102}$$

In analogy, the corresponding derivatives of the actual frame are introduced

$$\begin{aligned} \frac{\partial \lambda_{S(k)}}{\partial \mathbf{B}_S} &= \mathbf{n}_{S(k)} \otimes \mathbf{n}_{S(k)} = \mathbf{N}_{S(k)} \, , \\ \frac{\partial \mathbf{n}_{S(k)}}{\partial \mathbf{B}_S} &= \tfrac{1}{2} \sum_{\substack{l=1 \\ l\neq k}}^{3} \frac{1}{\lambda_{S(k)} - \lambda_{S(l)}} \overset{3}{\mathbf{N}}_{S[lk]} =: \overset{3}{\mathbf{N}}_{S(k)} \, , \\ \frac{\partial \mathbf{N}_{S(k)}}{\partial \mathbf{B}_S} &= \tfrac{1}{2} \sum_{\substack{l=1 \\ l\neq k}}^{3} \frac{1}{\lambda_{S(k)} - \lambda_{S(l)}} \big(\overset{4}{\mathbf{N}}_{S[kl]} + \overset{4}{\mathbf{N}}_{S[lk]} \big) =: \overset{4}{\mathbf{N}}_{S(k)} \end{aligned} \tag{2.103}$$

with the abbreviations

$$\begin{aligned}\overset{3}{\mathbf{N}}_{S[lk]} &= \left(\mathbf{N}_{S(l)} \otimes \mathbf{n}_{S(k)}\right)^{\overset{23}{T}} + \mathbf{N}_{S(l)} \otimes \mathbf{n}_{S(k)}\,,\\ \overset{4}{\mathbf{N}}_{S[kl]} &= \left(\mathbf{N}_{S(k)} \otimes \mathbf{N}_{S(l)}\right)^{\overset{23}{T}} + \left(\mathbf{N}_{S(k)} \otimes \mathbf{N}_{S(l)}\right)^{\overset{24}{T}}.\end{aligned} \tag{2.104}$$

Note that the introduced abbreviations may be regarded as fundamental tensors of the spectral representation, as they are only composed of dyads of eigenvectors. According to the covariant transport behavior (2.87) and the relations in box (2.43), one finds

$$\begin{aligned}\left(\mathbf{F}_S \otimes \mathbf{F}_S\right)^{\overset{23}{T}} \overset{3}{\mathbf{M}}_{S[lk]}\, \mathbf{F}_S^T &= \lambda_{S(l)}\, \sqrt{\lambda_{S(k)}}\, \overset{3}{\mathbf{N}}_{S[lk]}\,,\\ \left(\mathbf{F}_S \otimes \mathbf{F}_S\right)^{\overset{23}{T}} \overset{4}{\mathbf{M}}_{S[kl]}\, \left(\mathbf{F}_S^T \otimes \mathbf{F}_S^T\right)^{\overset{23}{T}} &= \lambda_{S(k)}\, \lambda_{S(l)}\, \overset{4}{\mathbf{N}}_{S[kl]}\,.\end{aligned} \tag{2.105}$$

As an important application of the preceding, regard a scalar-valued, *isotropic*[9] tensor function of the solid deformation tensors, which in spectral representation takes the form

$$\Psi = \Psi(\mathbf{C}_S) = \Psi(\mathbf{B}_S) = \Psi(I_S, II_S, III_S) \quad \longrightarrow \quad \Psi = \Psi(\lambda_{S(1)}, \lambda_{S(2)}, \lambda_{S(3)})\,. \tag{2.106}$$

Then, the first and second derivatives with respect to $\mathbf{C}_S$ read:

$$\begin{aligned}\frac{\partial \Psi}{\partial \mathbf{C}_S} &= \sum_{k=1}^{3} \frac{\partial \Psi}{\partial \lambda_{S(k)}}\, \frac{\partial \lambda_{S(k)}}{\partial \mathbf{C}_S} = \sum_{k=1}^{3} \frac{\partial \Psi}{\partial \lambda_{S(k)}}\, \mathbf{M}_{S(k)}\,,\\ \frac{\partial^2 \Psi}{\partial \mathbf{C}_S \otimes \partial \mathbf{C}_S} &= \sum_{k,l=1}^{3} \frac{\partial^2 \Psi}{\partial \lambda_{S(k)}\, \partial \lambda_{S(l)}}\, \frac{\partial \lambda_{S(k)}}{\partial \mathbf{C}_S} \otimes \frac{\partial \lambda_{S(l)}}{\partial \mathbf{C}_S} + \sum_{k=1}^{3} \frac{\partial \Psi}{\partial \lambda_{S(k)}}\, \frac{\partial \mathbf{M}_{S(k)}}{\partial \mathbf{C}_S}\\ &= \sum_{k,l=1}^{3} \frac{\partial^2 \Psi}{\partial \lambda_{S(k)}\, \partial \lambda_{S(l)}}\, \mathbf{M}_{S(k)} \otimes \mathbf{M}_{S(l)} + \sum_{k=1}^{3} \frac{\partial \Psi}{\partial \lambda_{S(k)}}\, \overset{4}{\mathbf{M}}_{S(k)}\\ &= \sum_{k,l=1}^{3} \frac{\partial^2 \Psi}{\partial \lambda_{S(k)}\, \partial \lambda_{S(l)}}\, \mathbf{M}_{S(k)} \otimes \mathbf{M}_{S(l)} + \tfrac{1}{2} \sum_{\substack{k,l=1\\ l \neq k}}^{3} \frac{\frac{\partial \Psi}{\partial \lambda_{S(k)}} - \frac{\partial \Psi}{\partial \lambda_{S(l)}}}{\lambda_{S(k)} - \lambda_{S(l)}}\, \overset{4}{\mathbf{M}}_{S[kl]}\,.\end{aligned} \tag{2.107}$$

The corresponding relations in the actual configuration result from a covariant push-forward of the previous results, but may also be obtained from equations (2.103), i. e.,

$$\begin{aligned}&\mathbf{F}_S\, \frac{\partial \Psi}{\partial \mathbf{C}_S}\, \mathbf{F}_S^T = \frac{\partial \Psi}{\partial \mathbf{B}_S}\, \mathbf{B}_S = \mathbf{B}_S\, \frac{\partial \Psi}{\partial \mathbf{B}_S} = \sum_{k=1}^{3} \frac{\partial \Psi}{\partial \lambda_{S(k)}}\, \lambda_{S(k)}\, \mathbf{N}_{S(k)}\,,\\ &\left(\mathbf{F}_S \otimes \mathbf{F}_S\right)^{\overset{23}{T}} \frac{\partial^2 \Psi}{\partial \mathbf{C}_S \otimes \partial \mathbf{C}_S}\, \left(\mathbf{F}_S^T \otimes \mathbf{F}_S^T\right)^{\overset{23}{T}} = \left[\mathbf{B}_S\, \frac{\partial^2 \Psi}{\partial \mathbf{B}_S \otimes \partial \mathbf{B}_S}\, \mathbf{B}_S\right]^{\underline{4}} =\\ &= \sum_{k,l=1}^{3} \frac{\partial^2 \Psi}{\partial \lambda_{S(k)}\, \partial \lambda_{S(l)}}\, \lambda_{S(k)}\, \lambda_{S(l)}\, \mathbf{N}_{S(k)} \otimes \mathbf{N}_{S(l)} + \tfrac{1}{2} \sum_{\substack{k,l=1\\ l \neq k}}^{3} \frac{\frac{\partial \Psi}{\partial \lambda_{S(k)}} - \frac{\partial \Psi}{\partial \lambda_{S(l)}}}{\lambda_{S(k)} - \lambda_{S(l)}}\, \lambda_{S(k)}\, \lambda_{S(l)}\, \overset{4}{\mathbf{N}}_{S[kl]}\,.\end{aligned} \tag{2.108}$$

[9] The term *isotropy* stands for the uniformity of the physical properties in a material body, i. e., characterizes orientation-independent material behavior. In this context, a tensor function is said to be isotropic if it is invariant due to any superimposed rigid-body motions on the reference configuration (cf. page 63).

Herein, $(\,\cdot\,)^{\underline{n}}$ indicates that the tensor product in the argument has to be carried out so that it yields a tensor of nth order. Note that the representation by means of $\mathbf{B}_S$ can be achieved by some algebraic transformations and usage of relations (2.71 – 2.73)[10].

Since the above relations are developed for the case of distinct roots, special modifications must be provided for the case of multiple eigenvalues. It is easily observed that, if $\lambda_{S(k)} = \lambda_{S(l)}$, the fractions in the second sums of equations $(2.107)_2$ and $(2.108)_2$ yield undetermined expressions. However, the limits of the rational expressions can be computed by exploiting *l'Hôpital*'s rule. Hence, the fraction of the reference frame yields

$$\lim_{\lambda_{S(k)} \to \lambda_{S(l)}} \frac{\frac{\partial \Psi}{\partial \lambda_{S(k)}} - \frac{\partial \Psi}{\partial \lambda_{S(l)}}}{\lambda_{S(k)} - \lambda_{S(l)}} = \frac{\partial^2 \Psi}{\partial \lambda_{S(k)}^2} - \frac{\partial^2 \Psi}{\partial \lambda_{S(l)}\, \partial \lambda_{S(k)}} \tag{2.109}$$

and the limit of the rational expression of the actual frame results in

$$\begin{aligned} &\lim_{\lambda_{S(k)} \to \lambda_{S(l)}} \frac{\left(\frac{\partial \Psi}{\partial \lambda_{S(k)}} - \frac{\partial \Psi}{\partial \lambda_{S(l)}}\right) \lambda_{S(k)}\, \lambda_{S(l)}}{\lambda_{S(k)} - \lambda_{S(l)}} = \\ &\quad = \left(\frac{\partial \Psi}{\partial \lambda_{S(k)}} - \frac{\partial \Psi}{\partial \lambda_{S(l)}}\right) \lambda_{S(l)} + \left(\frac{\partial^2 \Psi}{\partial \lambda_{S(k)}^2} - \frac{\partial^2 \Psi}{\partial \lambda_{S(l)}\, \partial \lambda_{S(k)}}\right) \lambda_{S(k)}\, \lambda_{S(l)}\,. \end{aligned} \tag{2.110}$$

Note that the above limits are valid for the case of double roots $\lambda_{S(k)} = \lambda_{S(l)} \neq \lambda_{S(m)}$ $(k \neq l \neq m \neq k)$ as well as for the case of three identical eigenvalues $\lambda_{S(1)} = \lambda_{S(2)} = \lambda_{S(3)}$.

For further details concerning the eigenvalue problems of deformation gradients and tensors, and the spectral representation of tensor functions and their derivatives, the interested reader is referred to the works of Morman [126], Ogden [139], Šilhavý [163] and Lambrecht [106] among others.

2.3 Balance Relations

In this section, the fundamental balance principles of continuum mechanics applied to mixtures are briefly summarized. Therefore, the basic stress measures are introduced and the specific balances of the overall mixture as well as of the individual constituents are discussed in the framework of the master balance principle. Moreover, the entropy principle for mixtures is prepared for later use. For a more detailed discussion of the continuum mechanical basics, the reader should refer to the classical works of Truesdell &

[10] As an example, regard the procedure for the first derivative (see also Miehe [121]):

$$\mathbf{F}_S\, \frac{\partial \Psi}{\partial \mathbf{C}_S}\, \mathbf{F}_S^T = (\mathbf{F}_S \otimes \mathbf{F}_S)^{\overset{23}{T}}\, \frac{\partial \Psi}{\partial \mathbf{C}_S} = (\mathbf{F}_S \otimes \mathbf{F}_S)^{\overset{23}{T}} \left(\frac{\partial \mathbf{B}_S}{\partial \mathbf{C}_S}\right)^T \frac{\partial \Psi}{\partial \mathbf{B}_S}$$

$$\text{with} \quad \begin{cases} \left(\frac{\partial \mathbf{B}_S}{\partial \mathbf{C}_S}\right)^T = \left[\frac{\partial (\mathbf{R}_S\, \mathbf{C}_S\, \mathbf{R}_S^T)}{\partial \mathbf{C}_S}\right]^T = \left[(\mathbf{R}_S \otimes \mathbf{R}_S)^{\overset{23}{T}}\right]^T = (\mathbf{R}_S^T \otimes \mathbf{R}_S^T)^{\overset{23}{T}}, \\ (\mathbf{F}_S \otimes \mathbf{F}_S)^{\overset{23}{T}}\, (\mathbf{R}_S^T \otimes \mathbf{R}_S^T)^{\overset{23}{T}} = (\mathbf{F}_S\, \mathbf{R}_S^T \otimes \mathbf{F}_S\, \mathbf{R}_S^T)^{\overset{23}{T}} = (\mathbf{V}_S \otimes \mathbf{V}_S)^{\overset{23}{T}} \end{cases}$$

$$\longrightarrow \quad \mathbf{F}_S\, \frac{\partial \Psi}{\partial \mathbf{C}_S}\, \mathbf{F}_S^T = (\mathbf{V}_S \otimes \mathbf{V}_S)^{\overset{23}{T}}\, \frac{\partial \Psi}{\partial \mathbf{B}_S} = \mathbf{V}_S\, \frac{\partial \Psi}{\partial \mathbf{B}_S}\, \mathbf{V}_S = \frac{\partial \Psi}{\partial \mathbf{B}_S}\, \mathbf{B}_S = \mathbf{B}_S\, \frac{\partial \Psi}{\partial \mathbf{B}_S} \quad \text{q. e. d.}$$

Toupin [181], Coleman & Noll [36], as well as Truesdell & Noll [180]. Concerning mixture theories, a comprehensive description of the balance principles can be found in the works of Ehlers [53, 54].

2.3.1 Stress Concept and Dual Variables

According to the intersection (free-body) principle, each partial body $\mathcal{B}^\alpha \subset \mathcal{B}$ of φ is subjected to an external mass-specific body (volume) force $\mathbf{b}^\alpha = \mathbf{b}^\alpha(\mathbf{x}, t)$ and an external traction (contact) force $\mathbf{t}^\alpha = \mathbf{t}^\alpha(\mathbf{x}, t, \mathbf{n})$ acting on parts or the whole of the boundary surface $\mathcal{S}^\alpha \subset \mathcal{S}$ with orientation $\mathbf{n}$. Then, the whole mixture body $\mathcal{B} = \bigcup_\alpha \mathcal{B}^\alpha$ is exposed to the total body force $\rho\,\mathbf{b} = \sum_\alpha \rho^\alpha\,\mathbf{b}^\alpha$ and the total surface traction $\mathbf{t} = \sum_\alpha \mathbf{t}^\alpha$ on the entire surface $\mathcal{S} = \bigcup_\alpha \mathcal{S}^\alpha$. In conclusion, one finds the resultant force vectors $\mathbf{f}$ and $\mathbf{f}^\alpha$ acting on the overall medium φ and on the constituents φ^α to

$$\mathbf{f} = \underbrace{\int_{\mathcal{B}} \rho\,\mathbf{b}\,\mathrm{d}v}_{\mathbf{f}_v} + \underbrace{\int_{\mathcal{S}} \mathbf{t}\,\mathrm{d}a}_{\mathbf{f}_a}\,, \qquad \mathbf{f}^\alpha = \underbrace{\int_{\mathcal{B}} \rho^\alpha\,\mathbf{b}^\alpha\,\mathrm{d}v}_{\mathbf{f}_v^\alpha} + \underbrace{\int_{\mathcal{S}} \mathbf{t}^\alpha\,\mathrm{d}a}_{\mathbf{f}_a^\alpha}\,. \tag{2.111}$$

Applying *Cauchy*'s theorem, one recovers the *Cauchy* stress tensor of the mixture $\mathbf{T} = \mathbf{T}(\mathbf{x}, t)$ and the partial *Cauchy* stress tensor $\mathbf{T}^\alpha = \mathbf{T}^\alpha(\mathbf{x}, t)$ of φ^α from

$$\mathbf{t}(\mathbf{x}, t, \mathbf{n}) = \mathbf{T}(\mathbf{x}, t)\,\mathbf{n}\,, \quad \mathbf{t}^\alpha(\mathbf{x}, t, \mathbf{n}) = \mathbf{T}^\alpha(\mathbf{x}, t)\,\mathbf{n}\,. \tag{2.112}$$

The total *Cauchy* stress may also be expressed by means of partial quantities, viz.,

$$\mathbf{T} = \sum_\alpha (\mathbf{T}^\alpha - \rho^\alpha \mathbf{d}_\alpha \otimes \mathbf{d}_\alpha)\,, \tag{2.113}$$

where $\rho^\alpha \mathbf{d}_\alpha \otimes \mathbf{d}_\alpha$ represents an apparent stress comparable to the *Reynolds* stress in turbulent flows (cf. Prandtl [146], Schlichting [157]), which is caused by fluctuations of the entire velocity field due to the diffusion velocities $\mathbf{d}_\alpha$ superimposed on the averaged velocity of the whole mixture $\dot{\mathbf{x}}$ given in equations (2.9).

Following the above, the *Cauchy* stresses as the true stresses represent the current stress state at material points by describing the surface force acting on an area element in the actual configuration. Proceeding from the solid incremental surface force on $\mathcal{S}$, additional solid stress tensors are introduced via

$$\mathrm{d}\mathbf{f}_a^S = \mathbf{t}^S\,\mathrm{d}a = \mathbf{T}^S\,\mathrm{d}\mathbf{a} = \mathbf{T}^S \operatorname{cof}\mathbf{F}_S\,\mathrm{d}\mathbf{A}_S = \underbrace{\overbrace{\mathbf{T}^S\,(\det\mathbf{F}_S)}^{\boldsymbol{\tau}^S}\,\mathbf{F}_S^{T-1}}_{\mathbf{P}^S}\,\mathrm{d}\mathbf{A}_S\,, \tag{2.114}$$

where in terms of natural basis vectors

$$\begin{aligned}
\mathbf{T}^S &= t^{kl}\,\mathbf{a}_k \otimes \mathbf{a}_l && : \textit{Cauchy} \text{ stress (true stress)}\,,\\
\boldsymbol{\tau}^S = (\det\mathbf{F}_S)\,\mathbf{T}^S &= \tau^{kl}\,\mathbf{a}_k \otimes \mathbf{a}_l && : \textit{Kirchhoff} \text{ stress (weighted } \textit{Cauchy} \text{ stress)}\,,\\
\mathbf{P}^S = \boldsymbol{\tau}^S\,\mathbf{F}_S^{T-1} &= \tau^{kl}\,\mathbf{a}_k \otimes \mathbf{h}_l && : 1\text{st } \textit{Piola-Kirchhoff} \text{ stress (nominal stress)}\,.
\end{aligned} \tag{2.115}$$

Moreover, it is of considerable assistance to formally introduce two further stress tensors,

which operate on the reference and the inelastic intermediate configuration, respectively:

$$\begin{aligned} \mathbf{S}^S &= \mathbf{F}_S^{-1}\,\mathbf{P}^S = \mathbf{F}_S^{-1}\,\boldsymbol{\tau}^S\,\mathbf{F}_S^{T-1} = \tau^{kl}\,\mathbf{h}_k \otimes \mathbf{h}_l \quad : 2\text{nd } \textit{Piola-Kirchhoff} \text{ stress}\,, \\ \widehat{\boldsymbol{\tau}}^S &= \mathbf{F}_{Si}\,\mathbf{S}^S\,\mathbf{F}_{Si}^T = \mathbf{F}_{Se}^{-1}\,\boldsymbol{\tau}^S\,\mathbf{F}_{Se}^{T-1} = \tau^{kl}\,\widehat{\mathbf{z}}_k \otimes \widehat{\mathbf{z}}_l \quad : \text{intermediate stress}\,. \end{aligned} \tag{2.116}$$

Note that the covariant representation of the introduced stress measures is a direct consequence of the contravariant nature of the oriented area elements and the corresponding surface normals (recall equations (2.38 – 2.39); see also Haupt [87]).

In analogy to the covariant strain rates given in equations $(2.69)_{1,2,3}$, by use of the lower *Oldroyd* derivatives $(2.65)_1$ and $(2.66)_1$, convenient stress rates, which obey the same transport mechanisms as the corresponding stresses, can be introduced (see box (2.117)).

Solid stress tensors and solid stress rates

$$\begin{array}{ccccc} & & \xrightarrow{\quad\mathbf{F}_S\,(\,\cdot\,)\,\mathbf{F}_S^T\quad} & & \\ \mathbf{S}^S & \xrightarrow[\mathbf{F}_{Si}^{-1}(\,\widehat{\cdot}\,)\,\mathbf{F}_{Si}^{T-1}]{\mathbf{F}_{Si}\,(\,\cdot\,)\,\mathbf{F}_{Si}^T} & \widehat{\boldsymbol{\tau}}^S & \xrightarrow[\mathbf{F}_{Se}^{-1}(\,\cdot\,)\,\mathbf{F}_{Se}^{T-1}]{\mathbf{F}_{Se}\,(\,\widehat{\cdot}\,)\,\mathbf{F}_{Se}^T} & \boldsymbol{\tau}^S \\ (\mathbf{S}^S)'_S & & (\widehat{\boldsymbol{\tau}}^S)^{\triangledown}_{Si} & & (\boldsymbol{\tau}^S)^{\triangledown}_S \\ & & \xleftarrow{\quad\mathbf{F}_S^{-1}(\,\cdot\,)\,\mathbf{F}_S^{T-1}\quad} & & \end{array} \tag{2.117}$$

The natural bond between certain stresses and strains is best described by the concept of *dual variables* stating that physically relevant scalar products between associated (conjugate) stress-strain pairs, such as the rate of internal mechanical work (stress power), stay invariant due to any transport operation between configurations (Haupt [87]). One finds,

$$\begin{aligned} \mathbf{S}^S \cdot \mathbf{E}_S &= \widehat{\boldsymbol{\tau}}^S \cdot \widehat{\boldsymbol{\Gamma}}_S = \boldsymbol{\tau}^S \cdot \mathbf{A}_S = \tfrac{1}{2}\,\tau^{kl}\,(a_{kl} - h_{kl})\,, \\ \mathbf{S}^S \cdot (\mathbf{E}_S)'_S &= \widehat{\boldsymbol{\tau}}^S \cdot (\widehat{\boldsymbol{\Gamma}}_S)^{\triangle}_{Si} = \boldsymbol{\tau}^S \cdot (\mathbf{A}_S)^{\triangle}_S = \tfrac{1}{2}\,\tau^{kl}\,(a_{kl})'_S\,, \\ (\mathbf{S}^S)'_S \cdot \mathbf{E}_S &= (\widehat{\boldsymbol{\tau}}^S)^{\triangledown}_{Si} \cdot \widehat{\boldsymbol{\Gamma}}_S = (\boldsymbol{\tau}^S)^{\triangledown}_S \cdot \mathbf{A}_S = \tfrac{1}{2}\,(\tau^{kl})'_S\,(a_{kl} - h_{kl})\,, \\ (\mathbf{S}^S)'_S \cdot (\mathbf{E}_S)'_S &= (\widehat{\boldsymbol{\tau}}^S)^{\triangledown}_{Si} \cdot (\widehat{\boldsymbol{\Gamma}}_S)^{\triangle}_{Si} = (\boldsymbol{\tau}^S)^{\triangledown}_S \cdot (\mathbf{A}_S)^{\triangle}_S = \tfrac{1}{2}\,(\tau^{kl})'_S\,(a_{kl})'_S\,. \end{aligned} \tag{2.118}$$

Note that the scalar products of equations (2.118) including strain rates may also be expressed by means of the 1st *Piola-Kirchhoff* stress. For example, assuming that $\boldsymbol{\tau}^S = (\boldsymbol{\tau}^S)^T$ (see remark on page 42), the volume-specific stress power can be rewritten as

$$\boldsymbol{\tau}^S \cdot (\mathbf{A}_S)^{\triangle}_S = \boldsymbol{\tau}^S \cdot \mathbf{D}_S = \boldsymbol{\tau}^S \cdot \mathbf{L}_S = (\mathbf{P}^S\,\mathbf{F}_S^T) \cdot [(\mathbf{F}_S)'_S\,\mathbf{F}_S^{-1}] = \mathbf{P}^S \cdot (\mathbf{F}_S)'_S \tag{2.119}$$

with $\{\mathbf{P}^S, (\mathbf{F}_S)'_S\}$ as a so-called work conjugate pair, which is obviously not consistent with all of the invariance conditions of dual variables (2.118).

2.3.2 Master Balance Principle for Mixtures

According to *Truesdell*'s *metaphysical principles* given in box (2.120), each constituent φ^α can be described by individual balance equations accounting for interactions between

them by additional production terms. The balance equations of the whole mixture are obtained as the sum of the balance equations of the constituents and must have the same form as the respective balance equations of a single-phase material. Due to the fact that the mathematical structure of the fundamental balance relations, namely of mass, linear momentum, moment of momentum (m. o. m.), energy, and entropy, is in principle identical, they can be formulated within the concise shape of a master balance.

***Truesdell*'s metaphysical principles**

(1) All properties of the mixture must be mathematical consequences of properties of the constituents.

(2) So as to describe the motion of a constituent, we may in imagination isolate it from the rest of the mixture, provided we allow properly for the actions of the other constituents upon it.

(3) The motion of a mixture is governed by the same equations as is a single body.

(Truesdell, 1984, p. 221 [179]) (2.120)

To begin with, let Ψ and $\boldsymbol{\Psi}$ be volume-specific scalar- and vector-valued densities of a physical quantity to be balanced. Then, proceeding from classical continuum mechanics of single-phase materials, the general balance relations of a multiphasic mixture $\varphi = \sum_\alpha \varphi^\alpha$ take the global (integral) form:

$$\begin{aligned} \frac{\mathrm{d}}{\mathrm{d}t}\int_{\mathcal{B}} \Psi \,\mathrm{d}v &= \int_{\mathcal{S}} (\boldsymbol{\phi}\cdot\mathbf{n})\,\mathrm{d}a + \int_{\mathcal{B}} \sigma \,\mathrm{d}v + \int_{\mathcal{B}} \hat{\Psi}\,\mathrm{d}v\,, \\ \frac{\mathrm{d}}{\mathrm{d}t}\int_{\mathcal{B}} \boldsymbol{\Psi} \,\mathrm{d}v &= \int_{\mathcal{S}} (\boldsymbol{\Phi}\,\mathbf{n})\,\mathrm{d}a + \int_{\mathcal{B}} \boldsymbol{\sigma} \,\mathrm{d}v + \int_{\mathcal{B}} \hat{\boldsymbol{\Psi}}\,\mathrm{d}v\,. \end{aligned} \tag{2.121}$$

Herein, $\boldsymbol{\phi}\cdot\mathbf{n}$ and $\boldsymbol{\Phi}\,\mathbf{n}$ are the surface densities defined per unit current area representing the efflux of the physical quantity over the surface $\mathcal{S}$ of $\mathcal{B}$, σ and $\boldsymbol{\sigma}$ are the volume densities describing the supply (external source) of the physical quantity, and $\hat{\Psi}$ and $\hat{\boldsymbol{\Psi}}$ represent the productions of the physical quantity due to couplings of φ with its environment. Supposing adequate continuity properties for all occurring fields, the equivalent local (differential) form of the master balance equations (2.121) results from differentiation of the left-hand sides and transformation of the surface integrals into volume integrals on the right-hand sides of (2.121):

$$\begin{aligned} \dot{\Psi} + \Psi \operatorname{div}\dot{\mathbf{x}} &= \operatorname{div}\boldsymbol{\phi} + \sigma + \hat{\Psi}\,, \\ \dot{\boldsymbol{\Psi}} + \boldsymbol{\Psi} \operatorname{div}\dot{\mathbf{x}} &= \operatorname{div}\boldsymbol{\Phi} + \boldsymbol{\sigma} + \hat{\boldsymbol{\Psi}}\,. \end{aligned} \tag{2.122}$$

Proceeding from the axiomatically introduced balance principles, namely of mass, linear momentum, moment of momentum (m. o. m.), energy, and entropy, one identifies the

quantities in equations (2.121) and (2.122) according to the following table (Ehlers [53]):

	Ψ, $\boldsymbol{\Psi}$	$\boldsymbol{\phi}$, $\boldsymbol{\Phi}$	σ, $\boldsymbol{\sigma}$	$\hat{\Psi}$, $\hat{\boldsymbol{\Psi}}$
mass	ρ	$\mathbf{0}$	0	0
momentum	$\rho\,\dot{\mathbf{x}}$	$\mathbf{T}$	$\rho\,\mathbf{b}$	$\mathbf{0}$
m. o. m.	$\mathbf{x}\times(\rho\,\dot{\mathbf{x}})$	$\mathbf{x}\times\mathbf{T}$	$\mathbf{x}\times(\rho\,\mathbf{b})$	$\mathbf{0}$
energy	$\rho\,\varepsilon+\frac{1}{2}\,\dot{\mathbf{x}}\cdot(\rho\,\dot{\mathbf{x}})$	$\mathbf{T}^T\,\dot{\mathbf{x}}-\mathbf{q}$	$\dot{\mathbf{x}}\cdot(\rho\,\mathbf{b})+\rho\,r$	0
entropy	$\rho\,\eta$	$\boldsymbol{\phi}_\eta$	σ_η	$\hat{\eta}$

(2.123)

Herein, $\rho\,\dot{\mathbf{x}}$ is the momentum of the entire mixture and $\mathbf{x}\times(\rho\,\dot{\mathbf{x}})$ is the corresponding moment of momentum. Concerning the energy and the entropy balances, ε is the internal energy, $\mathbf{q}$ is the heat influx vector, and r is the external heat supply. Moreover, η is the entropy, $\boldsymbol{\phi}_\eta$ and σ_η are the efflux of entropy and the external entropy supply, and $\hat{\eta}\geq 0$ is the non-negative entropy production, which considers the irreversibility of the overall thermodynamical process. Furthermore, regarding the mixture as a closed system, all remaining production terms are equal to zero. By inserting the respective quantities of table (2.123) into the local master balances (2.122), one recovers the specific balance relations known from classical continuum mechanics of single-phase materials:

Mixture balance relations

$$
\begin{aligned}
&\textit{mass:} && \dot{\rho}+\rho\,\operatorname{div}\dot{\mathbf{x}}=0\\
&\textit{momentum:} && \rho\,\ddot{\mathbf{x}}=\operatorname{div}\mathbf{T}+\rho\,\mathbf{b}\\
&\textit{m. o. m.:} && \mathbf{0}=\mathbf{I}\times\mathbf{T}\quad\longrightarrow\quad\mathbf{T}=\mathbf{T}^T\\
&\textit{energy:} && \rho\,\dot{\varepsilon}=\mathbf{T}\cdot\mathbf{L}-\operatorname{div}\mathbf{q}+\rho\,r\quad\text{with}\quad\mathbf{L}=\operatorname{grad}\dot{\mathbf{x}}\\
&\textit{entropy:} && \rho\,\dot{\eta}\geq\operatorname{div}\boldsymbol{\phi}_\eta+\sigma_\eta
\end{aligned}
\tag{2.124}
$$

Furthermore, following *Truesdell*'s principles (2.120), the general balances of the individual constituents yield, in analogy to (2.121), the global form

$$
\begin{aligned}
\frac{\mathrm{d}_\alpha}{\mathrm{d}t}\int_{\mathcal{B}}\Psi^\alpha\,\mathrm{d}v&=\int_{\mathcal{S}}(\boldsymbol{\phi}^\alpha\cdot\mathbf{n})\,\mathrm{d}a+\int_{\mathcal{B}}\sigma^\alpha\,\mathrm{d}v+\int_{\mathcal{B}}\hat{\Psi}^\alpha\,\mathrm{d}v\,,\\
\frac{\mathrm{d}_\alpha}{\mathrm{d}t}\int_{\mathcal{B}}\boldsymbol{\Psi}^\alpha\,\mathrm{d}v&=\int_{\mathcal{S}}(\boldsymbol{\Phi}^\alpha\,\mathbf{n})\,\mathrm{d}a+\int_{\mathcal{B}}\boldsymbol{\sigma}^\alpha\,\mathrm{d}v+\int_{\mathcal{B}}\hat{\boldsymbol{\Psi}}^\alpha\,\mathrm{d}v
\end{aligned}
\tag{2.125}
$$

and according to (2.122) the local form

$$
\begin{aligned}
(\Psi^\alpha)'_\alpha+\Psi^\alpha\operatorname{div}\mathbf{x}'_\alpha&=\operatorname{div}\boldsymbol{\phi}^\alpha+\sigma^\alpha+\hat{\Psi}^\alpha\,,\\
(\boldsymbol{\Psi}^\alpha)'_\alpha+\boldsymbol{\Psi}^\alpha\operatorname{div}\mathbf{x}'_\alpha&=\operatorname{div}\boldsymbol{\Phi}^\alpha+\boldsymbol{\sigma}^\alpha+\hat{\boldsymbol{\Psi}}^\alpha\,.
\end{aligned}
\tag{2.126}
$$

In the above equations, the partial quantities $(\,\bullet\,)^\alpha$ have the same physical meaning as the quantities included in the master balances of the overall mixture. However, they have to satisfy additional conditions such that summation of a partial balance of all φ^α yields

the respective fields of the multiphasic continuum φ:

$$\begin{aligned}
&\Psi = \sum_\alpha \Psi^\alpha\,, \quad \boldsymbol{\phi}\cdot\mathbf{n} = \sum_\alpha (\boldsymbol{\phi}^\alpha - \Psi^\alpha\,\mathbf{d}_\alpha)\cdot\mathbf{n}\,, \quad \sigma = \sum_\alpha \sigma^\alpha\,, \quad \hat{\Psi} = \sum_\alpha \hat{\Psi}^\alpha\,,\\
&\boldsymbol{\Psi} = \sum_\alpha \boldsymbol{\Psi}^\alpha\,, \quad \boldsymbol{\Phi}\,\mathbf{n} = \sum_\alpha (\boldsymbol{\Phi}^\alpha - \boldsymbol{\Psi}^\alpha\otimes\mathbf{d}_\alpha)\,\mathbf{n}\,, \quad \boldsymbol{\sigma} = \sum_\alpha \boldsymbol{\sigma}^\alpha\,, \quad \hat{\boldsymbol{\Psi}} = \sum_\alpha \hat{\boldsymbol{\Psi}}^\alpha\,.
\end{aligned} \tag{2.127}$$

The specific balance equations of the constituents are then derived in analogy to those of single-phase materials accounting for the interaction mechanisms by additional production terms. Actually, the local partial continua can be regarded as open systems staying in thermodynamical exchange with each other. In particular, one identifies the partial physical quantities according to the following table (Ehlers [54]):

	$\Psi^\alpha,\ \boldsymbol{\Psi}^\alpha$	$\boldsymbol{\phi}^\alpha,\ \boldsymbol{\Phi}^\alpha$	$\sigma^\alpha,\ \boldsymbol{\sigma}^\alpha$	$\hat{\Psi}^\alpha,\ \hat{\boldsymbol{\Psi}}^\alpha$
mass	ρ^α	$\mathbf{0}$	0	$\hat{\rho}^\alpha$
momentum	$\rho^\alpha\,\overset{\prime}{\mathbf{x}}_\alpha$	$\mathbf{T}^\alpha$	$\rho^\alpha\,\mathbf{b}^\alpha$	$\hat{\mathbf{s}}^\alpha$
m. o. m.	$\mathbf{x}\times(\rho^\alpha\,\overset{\prime}{\mathbf{x}}_\alpha)$	$\mathbf{x}\times\mathbf{T}^\alpha$	$\mathbf{x}\times(\rho^\alpha\,\mathbf{b}^\alpha)$	$\hat{\mathbf{h}}^\alpha$
energy	$\rho^\alpha\,\varepsilon^\alpha + \frac{1}{2}\,\overset{\prime}{\mathbf{x}}_\alpha\cdot(\rho^\alpha\,\overset{\prime}{\mathbf{x}}_\alpha)$	$(\mathbf{T}^\alpha)^T\,\overset{\prime}{\mathbf{x}}_\alpha - \mathbf{q}^\alpha$	$\overset{\prime}{\mathbf{x}}_\alpha\cdot(\rho^\alpha\,\mathbf{b}^\alpha) + \rho^\alpha\,r^\alpha$	$\hat{e}^\alpha$
entropy	$\rho^\alpha\,\eta^\alpha$	$\boldsymbol{\phi}^\alpha_\eta$	σ^α_η	$\hat{\eta}^\alpha$

(2.128)

Herein, $\hat{\rho}^\alpha$ is the mass production describing mass exchanges or phase transitions between the constituents, $\hat{\mathbf{s}}^\alpha$ is the total momentum production of φ^α, and $\hat{\mathbf{h}}^\alpha$ is the total production of angular momentum. Moreover, $\hat{e}^\alpha$ and $\hat{\eta}^\alpha$ are the total energy and entropy productions of φ^α. In mixture theories, it is convenient to split the total production terms into direct parts and parts including productions of the preceding (lower) balances:

$$\begin{aligned}
\hat{\mathbf{s}}^\alpha &= \hat{\mathbf{p}}^\alpha + \hat{\rho}^\alpha\,\overset{\prime}{\mathbf{x}}_\alpha\,, \quad \hat{\mathbf{h}}^\alpha = \hat{\mathbf{m}}^\alpha + \mathbf{x}\times(\hat{\mathbf{p}}^\alpha + \hat{\rho}^\alpha\,\overset{\prime}{\mathbf{x}}_\alpha)\,,\\
\hat{e}^\alpha &= \hat{\varepsilon}^\alpha + \hat{\mathbf{p}}^\alpha\cdot\overset{\prime}{\mathbf{x}}_\alpha + \hat{\rho}^\alpha\,(\varepsilon^\alpha + \tfrac{1}{2}\,\overset{\prime}{\mathbf{x}}_\alpha\cdot\overset{\prime}{\mathbf{x}}_\alpha)\,, \quad \hat{\eta}^\alpha = \hat{\zeta}^\alpha + \hat{\rho}^\alpha\,\eta^\alpha\,.
\end{aligned} \tag{2.129}$$

In equations (2.129), $\hat{\mathbf{p}}^\alpha$ denotes the direct momentum production, which can be interpreted as the volume-specific local interaction force between φ^α and the other constituents of φ, and $\hat{\mathbf{m}}^\alpha$ represents the direct moment of momentum production describing the angular momentum couplings between the constituents. Moreover, $\hat{\varepsilon}^\alpha$ and $\hat{\zeta}^\alpha$ are the direct terms of the energy and the entropy productions. As is usual in the framework of single-phase continua, one proceeds from an *a priori* constitutive assumption for the partial entropy efflux and the external entropy supply, viz.,

$$\boldsymbol{\phi}^\alpha_\eta = -\frac{1}{\Theta^\alpha}\,\mathbf{q}^\alpha\,, \quad \sigma^\alpha_\eta = \frac{1}{\Theta^\alpha}\,\rho^\alpha\,r^\alpha\,, \tag{2.130}$$

where different absolute *Kelvin*'s temperatures $\Theta^\alpha > 0$ allow for an individual temperature field for each constituent. Following this, the final form of the specific partial balance relations is obtained in analogy to those of the whole mixture (2.124):

Constituent balance relations

$$
\begin{aligned}
&\textit{mass:} && (\rho^\alpha)'_\alpha + \rho^\alpha \operatorname{div} \overset{\prime}{\mathbf{x}}_\alpha = \hat{\rho}^\alpha \\
&\textit{momentum:} && \rho^\alpha \overset{\prime\prime}{\mathbf{x}}_\alpha = \operatorname{div} \mathbf{T}^\alpha + \rho^\alpha \mathbf{b}^\alpha + \hat{\mathbf{p}}^\alpha \\
&\textit{m. o. m.:} && \mathbf{0} = \mathbf{I} \times \mathbf{T}^\alpha + \hat{\mathbf{m}}^\alpha \\
&\textit{energy:} && \rho^\alpha \, (\varepsilon^\alpha)'_\alpha = \mathbf{T}^\alpha \cdot \mathbf{L}_\alpha - \operatorname{div} \mathbf{q}^\alpha + \rho^\alpha \, r^\alpha + \hat{\varepsilon}^\alpha \\
&\textit{entropy:} && \rho^\alpha \, (\eta^\alpha)'_\alpha = \operatorname{div} \left(-\frac{1}{\Theta^\alpha} \, \mathbf{q}^\alpha\right) + \frac{1}{\Theta^\alpha} \, \rho^\alpha \, r^\alpha + \hat{\zeta}^\alpha
\end{aligned}
\tag{2.131}
$$

According to the sum relations (2.127), the physical quantities of the mixture can be expressed by means of the respective partial quantities extended by a diffusion term in the case of the surface densities. As an example, recall the previously introduced total *Cauchy* stress tensor $\mathbf{T}$ of equation (2.113). Moreover, one finds the following restrictions for the partial production terms:

$$
\sum_\alpha \hat{\rho}^\alpha = 0 \,, \quad \sum_\alpha \hat{\mathbf{s}}^\alpha = \mathbf{0} \,, \quad \sum_\alpha \hat{\mathbf{h}}^\alpha = \mathbf{0} \,, \quad \sum_\alpha \hat{e}^\alpha = 0 \,, \quad \sum_\alpha \hat{\eta}^\alpha \geq 0 \,. \tag{2.132}
$$

Remark: In this contribution, only non-polar materials (*Boltzmann* continua) are considered. Thus, proceeding from non-polar mixtures, evaluation of the mixture balance of angular momentum yields the symmetry of the total *Cauchy* stress tensor, $\mathbf{T} = \mathbf{T}^T$, as depicted in box $(2.124)_3$. However, regarding the partial moment of momentum balances of the non-polar φ^α $(2.131)_3$, direct angular momentum couplings $\hat{\mathbf{m}}^\alpha$ must be considered yielding non-symmetric partial *Cauchy* stresses[11], $\mathbf{T}^\alpha \neq (\mathbf{T}^\alpha)^T$. Nevertheless, proceeding from intrinsically non-polar materials associated with symmetric *Cauchy* stresses on the microscale, it can be shown by homogenization that the macroscopic stresses must also be symmetric (Ehlers [54]; see also Hassanizadeh & Gray [84]). Thus,

$$
\mathbf{T}^\alpha = (\mathbf{T}^\alpha)^T \quad \longrightarrow \quad \hat{\mathbf{m}}^\alpha \equiv \mathbf{0} \,. \tag{2.133}
$$

Accordingly, the partial *Kirchhoff* and 2nd *Piola-Kirchhoff* stresses $\boldsymbol{\tau}^\alpha$ and $\mathbf{S}^\alpha$ are also symmetric, while the 1st *Piola-Kirchhoff* stress $\mathbf{P}^\alpha$ is generally not. For specific extensions of the balance principles for mixtures to micropolar materials (*Cosserat* continua), the interested reader is referred to the works of Diebels [43], Diebels & Ehlers [45], Ehlers [54], and the quotations therein. ■

[11] The direct angular momentum production $\hat{\mathbf{m}}^\alpha$ represents twice the negative axial vector $\overset{\mathrm{A}}{\mathbf{t}}{}^\alpha$ associated with the skew-symmetric properties of $\mathbf{T}^\alpha$. It can be shown that (cf. de Boer [17])

$$
\hat{\mathbf{m}}^\alpha = -\mathbf{I} \times \operatorname{skw} \mathbf{T}^\alpha = \overset{3}{\mathbf{E}} \operatorname{skw} \mathbf{T}^\alpha = -2 \, \overset{\mathrm{A}}{\mathbf{t}}{}^\alpha \,, \quad \operatorname{skw} \mathbf{T}^\alpha = -\tfrac{1}{2} \, (\hat{\mathbf{m}}^\alpha \times \mathbf{I}) = -\tfrac{1}{2} \, [\overset{3}{\mathbf{E}} \, (\hat{\mathbf{m}}^\alpha \otimes \mathbf{I})]^{\underline{2}} .
$$

2.3.3 Entropy Principle for Mixtures

In order to formulate admissible constitutive relations for the description of specific material behavior, evaluation of the entropy principle for mixtures provides the thermodynamical restrictions (see chapter 3). According to inequality $(2.132)_5$ together with $(2.129)_4$ and the partial entropy balance $(2.131)_5$, the entropy principle for mixtures takes the form

$$\sum_{\alpha} \left[\rho^{\alpha} \left(\eta^{\alpha}\right)'_{\alpha} + \hat{\rho}^{\alpha}\, \eta^{\alpha} + \operatorname{div}\left(\frac{1}{\Theta^{\alpha}}\, \mathbf{q}^{\alpha}\right) - \frac{1}{\Theta^{\alpha}}\, \rho^{\alpha}\, r^{\alpha} \right] \geq 0\,. \tag{2.134}$$

Next, by formal introduction of the *Helmholtz* free-energy density[12]

$$\psi^{\alpha} := \varepsilon^{\alpha} - \Theta^{\alpha}\, \eta^{\alpha} \tag{2.135}$$

and by use of the partial energy balance $(2.131)_4$, the entropy principle can be rephrased in the most common *Clausius-Duhem* representation

$$\begin{aligned} \sum_{\alpha} \frac{1}{\Theta^{\alpha}} \Big\{ \mathbf{T}^{\alpha} \cdot \mathbf{L}_{\alpha} - \rho^{\alpha} \left[\left(\psi^{\alpha}\right)'_{\alpha} + \left(\Theta^{\alpha}\right)'_{\alpha}\, \eta^{\alpha} \right] - \hat{\mathbf{p}}^{\alpha} \cdot \overset{\prime}{\mathbf{x}}_{\alpha} - \\ - \hat{\rho}^{\alpha} \left(\psi^{\alpha} + \tfrac{1}{2}\, \overset{\prime}{\mathbf{x}}_{\alpha} \cdot \overset{\prime}{\mathbf{x}}_{\alpha} \right) - \frac{1}{\Theta^{\alpha}}\, \mathbf{q}^{\alpha} \cdot \operatorname{grad} \Theta^{\alpha} + \hat{e}^{\alpha} \Big\} \geq 0\,. \end{aligned} \tag{2.136}$$

Assuming that all constituents have the same constant *Kelvin*'s temperature $\Theta^{\alpha} \equiv \Theta = \text{const.}$, the above inequality reduces to the so-called *Clausius-Planck* inequality

$$\mathcal{D}_{\text{int}} = \sum_{\alpha} \left[\mathbf{T}^{\alpha} \cdot \mathbf{L}_{\alpha} - \rho^{\alpha} \left(\psi^{\alpha}\right)'_{\alpha} - \hat{\mathbf{p}}^{\alpha} \cdot \overset{\prime}{\mathbf{x}}_{\alpha} - \hat{\rho}^{\alpha} \left(\psi^{\alpha} + \tfrac{1}{2}\, \overset{\prime}{\mathbf{x}}_{\alpha} \cdot \overset{\prime}{\mathbf{x}}_{\alpha} \right) \right] \geq 0\,, \tag{2.137}$$

which actually represents the non-negative internal dissipation $\mathcal{D}_{\text{int}} \geq 0$ of the overall isothermal process. Furthermore, if the constituents undergo neither an exchange of matter nor phase transitions due to any biological, chemical, or physical process, the mass production terms can be excluded, i. e., $\hat{\rho}^{\alpha} \equiv 0$. Thus, proceeding from non-polar φ^{α} yielding $\mathbf{T}^{\alpha} = (\mathbf{T}^{\alpha})^{T}$ (see remark on page 42), the mixture entropy inequality of the purely mechanical process simplifies to

$$\mathcal{D}_{\text{int}} = \sum_{\alpha} \left[\mathbf{T}^{\alpha} \cdot \mathbf{D}_{\alpha} - \rho^{\alpha} \left(\psi^{\alpha}\right)'_{\alpha} - \hat{\mathbf{p}}^{\alpha} \cdot \overset{\prime}{\mathbf{x}}_{\alpha} \right] \geq 0\,, \tag{2.138}$$

where the interaction mechanisms are solely considered by the momentum productions $\hat{\mathbf{p}}^{\alpha}$. As examples of conceivable processes with $\hat{\rho}^{\alpha} \neq 0$, think of the growing of cells governed by metabolism or the melting of ice, where solid ice transforms into liquid water.

[12] In classical equilibrium thermodynamics, the *Helmholtz* free energy as a thermodynamical potential is derived from the internal energy by *Legendre* transformation between the energetically conjugate variables temperature and entropy.

3 Constitutive Modeling

Based on the theoretical fundamentals of the preceding chapter, a manifold of distinct multiphasic models can be defined. However, it is out of the scope of the present contribution to list all possible variations. In fact, it is the objective to present on the basis of a general biphasic solid-fluid mixture a convenient constitutive setting, which accounts for the coupled dissipative phenomena caused by the interplay of a viscous pore fluid streaming through a viscoelastic solid skeleton. Therefore, a thermodynamically consistent biphasic TPM model is introduced and admissible constitutive equations for the description of the finite viscoelastic deformation habits of the porous solid as well as the nonlinear percolation process of a general pore fluid are derived.

3.1 The General Biphasic TPM Model

In this section, the entropy principle for mixtures is evaluated for a general binary porous medium and prepared for the formulation of specific constitutive material equations. In particular, the general biphasic model incorporates the standard incompressible model, which proceeds from materially incompressible constituents, as well as the so-called hybrid model, which additionally considers the compressibility of the fluid phase. Thus, the general biphasic model is capable of describing liquid and gas flows through deformable porous solids, such as they occur, e. g., in open-celled polymer foams.

3.1.1 Preliminaries

With regard to a comprehensible thermodynamical treatment, the biphasic model excludes thermal effects as well as any mass exchanges. In particular, the arising purely mechanical binary model is subject to the following assumptions:

- saturated solid-fluid mixture: $n^S + n^F = 1\,,$
- materially incompressible solid: $\rho^{SR} = \text{const.}\,,$
- materially compressible or incompressible pore fluid,
- no mass production: $\hat{\rho}^\alpha \equiv 0\,,$
- dissipative solid material,
- non-polar materials: $\mathbf{T}^\alpha = (\mathbf{T}^\alpha)^T\,,$
- uniform body force: $\mathbf{b}^\alpha = \mathbf{b}\,,$
- quasi-static conditions[1]: $\overset{\prime\prime}{\mathbf{x}}_\alpha \equiv \mathbf{0}\,, \quad \ddot{\mathbf{x}} \equiv \mathbf{0}\,,$ (3.1)
- isothermal process: $\Theta^\alpha \equiv \Theta = \text{const.}\,,$
- viscous pore-fluid flow.

[1] See remark on page 46.

Following this, according to section 2.3, the governing partial balance relations and the entropy principle for mixtures read:

- Solid mass balance $\longrightarrow$ solid volume balance:

$$(\rho^S)'_S + \rho^S \operatorname{div} \overset{\prime}{\mathbf{x}}_S = 0 \quad \longrightarrow \quad (n^S)'_S + n^S \operatorname{div} \overset{\prime}{\mathbf{x}}_S = 0\,, \tag{3.2}$$

- Fluid mass balance:

$$(\rho^F)'_F + \rho^F \operatorname{div} \overset{\prime}{\mathbf{x}}_F = 0\,, \tag{3.3}$$

- Partial momentum balances:

$$\mathbf{0} = \operatorname{div} \mathbf{T}^S + \rho^S \mathbf{b} - \hat{\mathbf{p}}^F\,, \quad \mathbf{0} = \operatorname{div} \mathbf{T}^F + \rho^F \mathbf{b} + \hat{\mathbf{p}}^F\,, \tag{3.4}$$

- *Clausius-Planck* inequality:

$$\mathbf{T}^S \cdot \mathbf{D}_S + \mathbf{T}^F \cdot \mathbf{D}_F - \rho^S (\psi^S)'_S - \rho^F (\psi^F)'_F - \hat{\mathbf{p}}^F \cdot \mathbf{w}_{FR} \geq 0\,. \tag{3.5}$$

Herein, proceeding from the convenient assumption of a materially incompressible solid skeleton (cf. remark on page 10), the solid mass balance degenerates to a volume balance, since $(n^S \rho^{SR})'_S = (n^S)'_S \rho^{SR}$ due to $(\rho^{SR})'_S \equiv 0$. Thus, one directly finds a conditional equation for the solidity n^S by analytical integration[2]:

$$(n^S)'_S = -n^S \operatorname{div} \overset{\prime}{\mathbf{x}}_S \quad \longrightarrow \quad n^S = n^S_{0S} \det \mathbf{F}_S^{-1}\,. \tag{3.6}$$

Furthermore, according to equations $(2.129)_1$ and $(2.132)_2$ together with the assumption $\hat{\rho}^\alpha \equiv 0$, $\hat{\mathbf{p}}^S = -\hat{\mathbf{p}}^F$ must hold due to the overall conservation of momentum. Moreover, note that proceeding from an overall isothermal, purely mechanical process, the energy balances are not considered.

Remark: Proceeding from quasi-static conditions by neglecting the constituent as well as the mixture accelerations and excluding any mass exchanges between the φ^α (cf. assumptions (3.1)), moreover implies consequences for the diffusion processes described by $\mathbf{d}_\alpha$ according to equation $(2.9)_2$. It can be shown that (cf. Ehlers [49], p. 49)

$$\rho\, \ddot{\mathbf{x}} = \sum_\alpha \left[\rho^\alpha \overset{\prime\prime}{\mathbf{x}}_\alpha - \operatorname{div} (\rho^\alpha \mathbf{d}_\alpha \otimes \mathbf{d}_\alpha) + \hat{\rho}^\alpha \overset{\prime}{\mathbf{x}}_\alpha\right] \tag{3.7}$$

and thus,

$$\operatorname{div} \Big(\sum_\alpha \rho^\alpha \mathbf{d}_\alpha \otimes \mathbf{d}_\alpha \Big) \equiv \mathbf{0} \quad \text{if} \quad \overset{\prime\prime}{\mathbf{x}}_\alpha = \ddot{\mathbf{x}} \equiv \mathbf{0} \ \wedge \ \hat{\rho}^\alpha \equiv 0\,. \tag{3.8}$$

[2] Proceeding from the volume balance $(3.2)_2$, the divergence term is rewritten by means of the solid *Jacobi*an $J_S = \det \mathbf{F}_S$ and, after separation of variables, the solution is found by analytical integration:

$$\operatorname{div} \overset{\prime}{\mathbf{x}}_S = \mathbf{L}_S \cdot \mathbf{I} = (J_S)'_S J_S^{-1} \quad \longrightarrow \quad \frac{(n^S)'_S}{n^S} = -\frac{(J_S)'_S}{J_S} \quad \longrightarrow \quad \frac{1}{n^S} \frac{\mathrm{d}_S(n^S)}{\mathrm{d}t} = -\frac{1}{J_S} \frac{\mathrm{d}_S(J_S)}{\mathrm{d}t}\,,$$

$$\int_{n^S_{0S}}^{n^S} \frac{1}{n^S}\, \mathrm{d}_S(n^S) = -\int_1^{J_S} \frac{1}{J_S}\, \mathrm{d}_S(J_S) \quad \longrightarrow \quad \ln\Big(\frac{n^S}{n^S_{0S}}\Big) = \ln\Big(\frac{1}{J_S}\Big) \quad \longrightarrow \quad n^S = n^S_{0S}\, J_S^{-1} \quad \text{q. e. d.}$$

Consequently, the *Reynolds*-like contributions to the total *Cauchy* stress in equation (2.113) can be dropped as $\mathbf{T}$ will only be used in divergence form. ■

3.1.2 Saturation Constraint and Effective Stress Principle

Throughout the thermodynamical process, the saturation constraint (2.4) must be fulfilled. This is guaranteed by adding the derivation of the saturation condition weighted by a *Lagrange*an multiplier $\mathcal{P}$ to the entropy inequality of the biphasic model (3.5):

$$\mathbf{T}^S \cdot \mathbf{D}_S + \mathbf{T}^F \cdot \mathbf{D}_F - \rho^S \, (\psi^S)'_S - \rho^F \, (\psi^F)'_F - \hat{\mathbf{p}}^F \cdot \mathbf{w}_{FR} - \mathcal{P} \, (n^S + n^F)'_S \geq 0 \,. \tag{3.9}$$

Therein, the additional constraint has the nature of a volume balance and thus, $\mathcal{P}$ will be easily identified as the excess pore-fluid pressure. For further investigations, the volumetric constraint is rewritten by replacing the derivatives $(n^\alpha)'_S$ with respective evolution equations. Since the volume fractions represent additional independent variables describing the local composition of the porous microstructure, there generally exist no distinct balance relations for the determination. However, due to the assumed solid incompressibility, $(n^S)'_S$ can be directly substituted by the solid volume balance $(3.6)_1$. Concerning the evolution of n^F, the concurrent consideration of compressible as well as incompressible pore-fluid behavior demands for a particular treatment. Therefore, the rate of change of the effective fluid density $(\rho^{FR})'_F$ is regarded as a free variable of the overall thermodynamical process. Then, after applying the product rule to $(\rho^F)'_F = (n^F \rho^{FR})'_F$, the fluid balance of mass (3.3) yields a conditional equation for the porosity evolution[3], viz.:

$$(n^F)'_F = -\frac{n^F}{\rho^{FR}} \, (\rho^{FR})'_F - n^F \operatorname{div} \overset{\prime}{\mathbf{x}}_F \quad \text{with} \quad \rho^{FR} > 0 \,. \tag{3.10}$$

Note that the treatment of $(\rho^{FR})'_F$ as a free variable is not a precarious assumption. Actually, it is a direct consequence of exploiting the fluid mass balance as an evolution equation for n^F, since obviously no further balance exists for the determination of $(\rho^{FR})'_F$. Thus, with equations $(3.6)_1$, (3.10), and the relations

$$\operatorname{div} \overset{\prime}{\mathbf{x}}_\alpha = \mathbf{L}_\alpha \cdot \mathbf{I} = \mathbf{D}_\alpha \cdot \mathbf{I} \,, \quad (n^F)'_S = (n^F)'_F - \operatorname{grad} n^F \cdot \mathbf{w}_{FR} \,, \tag{3.11}$$

the additional constraint can be rewritten as

$$-\mathcal{P} \, (n^S + n^F)'_S = \mathcal{P} \left[n^S \, \mathbf{D}_S \cdot \mathbf{I} + n^F \, \mathbf{D}_F \cdot \mathbf{I} + \frac{n^F}{\rho^{FR}} \, (\rho^{FR})'_F + \operatorname{grad} n^F \cdot \mathbf{w}_{FR} \right] . \tag{3.12}$$

Note in passing that, in the case of an incompressible pore fluid, i. e., $\rho^{FR} = \text{const.}$ yielding $(\rho^{FR})'_F \equiv 0$, the expression $(n^S + n^F)'_S$ naturally reduces to a continuity-like equation,

[3] An alternative approach is described by Diebels [43] in connection with a materially compressible solid constituent. In particular, the solid mass balance is constitutively split, based on the introduction of an additional distribution function, which governs the way of change of the partial solid density. However, this unspecified function, although not explicitly required, is of purely constitutive nature and entails further assumptions.

viz., the volume balance of the standard incompressible biphasic model (e. g., Ehlers [54]):

$$-(n^S + n^F)'_S = \operatorname{div}\left[(\mathbf{u}_S)'_S + n^F \mathbf{w}_{FR}\right] = 0\,. \tag{3.13}$$

Finally, inserting relation (3.12) into the dissipation inequality (3.9) yields

$$\begin{aligned} &\overbrace{(\mathbf{T}^S + \mathcal{P}\, n^S\, \mathbf{I})}^{\mathbf{T}^S_E} \cdot \mathbf{D}_S + \overbrace{(\mathbf{T}^F + \mathcal{P}\, n^F\, \mathbf{I})}^{\mathbf{T}^F_E} \cdot \mathbf{D}_F - \rho^S\, (\psi^S)'_S - \\ &-\rho^F\, (\psi^F)'_F + \mathcal{P}\, \frac{n^F}{\rho^{FR}}\, (\rho^{FR})'_F - \underbrace{(\hat{\mathbf{p}}^F - \mathcal{P}\, \operatorname{grad} n^F)}_{\hat{\mathbf{p}}^F_E} \cdot \mathbf{w}_{FR} \geq 0\,, \end{aligned} \tag{3.14}$$

where $\mathbf{T}^S_E$, $\mathbf{T}^F_E$, and $\hat{\mathbf{p}}^F_E$ are the so-called extra quantities, which act as substitutes for the respective over- and underbraced terms. This is in full agreement with the classical concept of effective stresses, which originally presumes that the effective soil stress in a geotechnical consolidation problem is determined by the total stress minus the excess pore pressure (Bishop [13], Skempton [167], de Boer & Ehlers [20]). Accordingly, the extra terms

$$\mathbf{T}^S_E = \mathbf{T}^S + \mathcal{P}\, n^S\, \mathbf{I}\,, \quad \mathbf{T}^F_E = \mathbf{T}^F + \mathcal{P}\, n^F\, \mathbf{I}\,, \quad \hat{\mathbf{p}}^F_E = \hat{\mathbf{p}}^F - \mathcal{P}\, \operatorname{grad} n^F \tag{3.15}$$

represent effective field quantities for which suitable constitutive equations must be found. Thus, the effective stress principle enables the modular treatment of specific solid skeleton, pore-fluid, and interaction properties. For example, having defined $\mathbf{T}^S_E$ by an appropriate viscoelastic material law (see section 3.2), it can straightforwardly be exploited in any other multiphasic TPM model.

3.1.3 Constitutive Variables

To close the general biphasic model under study, a convenient set of constitutive relations must be found for the energy functions and the extra quantities satisfying the entropy principle in form of (3.14). Thus, based on the fundamental principles of constitutive modeling, namely *determinism*, *local action*, *equipresence*, *frame indifference*, and *dissipation*[4], the following set of response functions must be determined:

$$\mathcal{R} = \{\psi^S,\, \psi^F,\, \mathbf{T}^S_E,\, \mathbf{T}^F_E,\, \hat{\mathbf{p}}^F_E\}\,. \tag{3.16}$$

According to the principle of equipresence, each of these response functions may depend on a common set $\mathcal{V}$ of independent constitutive or process variables, i. e.,

$$\mathcal{R} := \mathcal{R}(\mathcal{V}) \quad \text{with} \quad \mathcal{V} = \mathcal{V}^S \cup \mathcal{V}^F \tag{3.17}$$

as the union of sets of independent state variables of the solid and the fluid constituent. Following the arguments of Ehlers [54], proceeding from assumptions (3.1) and initially

[4] For reference, see the classical articles of Truesdell [178], Noll [133, 134], and Coleman & Noll [36].

homogeneous constituents φ^α, the partial set of process variables describing the behavior of a potentially inelastic solid skeleton with dissipative properties is found as

$$\mathcal{V}^S = \{\mathbf{F}_S,\, \mathrm{Grad}_S\mathbf{F}_S,\, \boldsymbol{\mathcal{Q}}_n^S,\, \mathrm{Grad}_S\boldsymbol{\mathcal{Q}}_n^S\}\,. \tag{3.18}$$

Therein, based on the thermodynamics with internal state variables (Coleman & Gurtin [34], Valanis [184]), $\boldsymbol{\mathcal{Q}}_n^S$ represents a finite number of independent internal state or history variables, which have to be implicitly defined via respective evolution equations:

$$(\boldsymbol{\mathcal{Q}}_n^S)'_S = \boldsymbol{\mathcal{F}}_n(\mathcal{V}^S)\,, \quad n = 1, ..., N\,. \tag{3.19}$$

Hence, the internal variables are assumed to govern the inelastic state of the solid matrix, i. e., they represent the memory of φ^S depending on the process history (cf. Lubliner [115]). Here, they are introduced as tensor-valued fields, but, in general, also scalar or vector-valued functions can be introduced. Moreover, the set of objective (frame-indifferent) constitutive variables for a possibly compressible pore fluid reads

$$\mathcal{V}^F = \{\mathbf{w}_{FR},\, \mathbf{D}_F,\, n^F,\, \mathrm{grad}\, n^F,\, \rho^{FR},\, \mathrm{grad}\, \rho^{FR}\}\,. \tag{3.20}$$

Thus, the overall set of independent process variables is found as

$$\mathcal{V} = \{\mathbf{F}_S,\, \mathrm{Grad}_S\mathbf{F}_S,\, \boldsymbol{\mathcal{Q}}_n^S,\, \mathrm{Grad}_S\boldsymbol{\mathcal{Q}}_n^S,\, \mathbf{w}_{FR},\, \mathbf{D}_F,\, \rho^{FR},\, \mathrm{grad}\, \rho^{FR}\}\,, \tag{3.21}$$

where n^F and $\mathrm{grad}\, n^F$ are removed from the list, as they are directly coupled to the skeleton deformation via the saturation constraint. In particular, with the aid of relation $(3.6)_2$, it can be shown[5] that

$$\begin{aligned} n^F &= 1 - n^S = 1 - n_{0S}^S\, \det \mathbf{F}_S^{-1}\,, \\ \mathrm{grad}\, n^F &= -\mathrm{grad}\, n^S = n_{0S}^S\, (\det \mathbf{F}_S^{-1})\, \mathbf{F}_S^{T-1}\, (\mathbf{F}_S^{T-1}\, \mathrm{Grad}_S\mathbf{F}_S)^{\underline{1}}\,. \end{aligned} \tag{3.22}$$

Moreover, it is easily concluded that in the case of a materially incompressible pore fluid, additionally, ρ^{FR} and $\mathrm{grad}\, \rho^{FR}$ can be removed from $\mathcal{V}^F$ and $\mathcal{V}$, respectively. In this context, note that $\mathcal{V}^S$, $\mathcal{V}^F$, and, as a consequence, $\mathcal{V}$ only represent specific subsets of the fundamental constitutive variables for general mixtures. However, the second-grade character of multiphasic materials remains by inclusion of the gradients of the considered basic variables. For further particulars, the interested reader is referred to the more

[5] The second relation can be obtained as follows (see also Ehlers [49]):

Starting from

$$\mathrm{grad}\, n^F = -\mathrm{grad}\, n^S = -n_{0S}^S\, \mathrm{grad}\, (\det \mathbf{F}_S^{-1}) = -n_{0S}^S\, \frac{\partial (\det \mathbf{F}_S^{-1})}{\partial \mathbf{x}}$$

with

$$\frac{\partial (\det \mathbf{F}_S^{-1})}{\partial \mathbf{x}} = \frac{\partial (\det \mathbf{F}_S^{-1})}{\partial \mathbf{F}_S}\, \frac{\partial \mathbf{F}_S}{\partial \mathbf{X}_S}\, \frac{\partial \mathbf{X}_S}{\partial \mathbf{x}} = -(\det \mathbf{F}_S^{-1})\, \mathbf{F}_S^{T-1}\, (\mathbf{F}_S^{T-1}\, \mathrm{Grad}_S\, \mathbf{F}_S)^{\underline{1}},$$

where

$$\frac{\partial (\det \mathbf{F}_S^{-1})}{\partial \mathbf{F}_S} = -(\mathbf{F}_S^{T-1} \otimes \mathbf{F}_S^{-1})^{\overset{23}{T}}\, \mathrm{cof}\, \mathbf{F}_S^{-1} = -(\det \mathbf{F}_S^{-1})\, \mathbf{F}_S^{T-1}\,,$$

finally yields

$$\mathrm{grad}\, n^F = n_{0S}^S\, (\det \mathbf{F}_S^{-1})\, \mathbf{F}_S^{T-1}\, (\mathbf{F}_S^{T-1}\, \mathrm{Grad}_S\, \mathbf{F}_S)^{\underline{1}} \quad \text{q. e. d.}$$

comprehensive works of Ehlers [49, 50, 54].

To continue, regarding the constituent free energies, further *a priori* constitutive assumptions can be made. Proceeding from the *principle of phase separation* (Ehlers [49]), the energy potential ψ^α of a given constituent φ^α only depends on the non-dissipative variables included into the process by the respective constituent itself without circumventing the principle of equipresence. Moreover, following a statement of Bowen [22, 23], the second-grade character of multiphasic mixtures is only associated with the involved production terms. Thus, it is supposed that

$$\left.\begin{array}{l}\psi^S = \psi^S(\mathcal{V}^S)\\ \psi^F = \psi^F(\mathcal{V}^F)\end{array}\right\} \quad \longrightarrow \quad \left\{\begin{array}{lll}\psi^S = \psi^S(\mathbf{F}_S, \boldsymbol{\mathcal{Q}}_n^S) & \text{with} & n = 1, ..., N\,,\\ \psi^F = \psi^F(n^F, \rho^{FR}) & \longrightarrow & \psi^F = \psi^F(\rho^{FR})\,,\end{array}\right. \tag{3.23}$$

where, additionally, the dependence of ψ^F on the porosity n^F is constitutively neglected because of the assumption that the energy potential of a fluid does not recognize the domain on which the fluid exists (Ehlers [54]). Note that a general evaluation of the mixture entropy principle with $\psi^\alpha = \psi^\alpha(\mathcal{V})$ would recover assumptions (3.23) as a natural result of the binary model under study.

3.1.4 Evaluation of the Entropy Inequality

In the preceding, a convenient reduction of the set of process variables is achieved by *a priori* constitutive assumptions based on logical deduction and experience. Hence, the effort to evaluate the entropy principle is kept to a minimum. It is now the goal of the evaluation procedure to derive logical consequences from the mixture entropy inequality in order to find constitutive equations, which restrict the admissible processes in the mixture body $\mathcal{B} = \mathcal{B}^S \cup \mathcal{B}^F$ consisting of the supposed constituent materials. Here, in order to satisfy the dissipation inequality in form of (3.14), the approved evaluation procedure of Coleman & Noll [36] is applied. Note that, alternatively, the more demanding Liu-Müller procedure (Liu [113], Liu & Müller [114]) can be used, which basically yields similar results. For a more detailed discussion of the evaluation of the entropy principle for mixtures see, e. g., Bowen [21], Ehlers [49], or Diebels [43].

To begin with, proceeding from the assumed functional dependencies of the constituent free energy densities (3.23), the corresponding material time derivatives read

$$(\psi^S)'_S = \frac{\partial \psi^S}{\partial \mathbf{F}_S} \cdot (\mathbf{F}_S)'_S + \sum_{n=1}^{N} \frac{\partial \psi^S}{\partial \boldsymbol{\mathcal{Q}}_n^S} \cdot (\boldsymbol{\mathcal{Q}}_n^S)'_S\,, \quad (\psi^F)'_F = \frac{\partial \psi^F}{\partial \rho^{FR}} (\rho^{FR})'_F\,. \tag{3.24}$$

By inserting the above derivatives into the dissipation inequality (3.14) together with the definition of the spatial velocity gradient (2.53), one obtains

$$\begin{aligned}&\left(\mathbf{T}_E^S - \rho^S \frac{\partial \psi^S}{\partial \mathbf{F}_S} \mathbf{F}_S^T\right) \cdot \mathbf{L}_S - \rho^S \sum_{n=1}^{N} \frac{\partial \psi^S}{\partial \boldsymbol{\mathcal{Q}}_n^S} \cdot (\boldsymbol{\mathcal{Q}}_n^S)'_S +\\ &+ \mathbf{T}_E^F \cdot \mathbf{D}_F + \left(\mathcal{P} \frac{n^F}{\rho^{FR}} - \rho^F \frac{\partial \psi^F}{\partial \rho^{FR}}\right) (\rho^{FR})'_F - \hat{\mathbf{p}}_E^F \cdot \mathbf{w}_{FR} \geq 0\,.\end{aligned} \tag{3.25}$$

The validity of this inequality can now be guaranteed following the standard arguments. Accordingly, at a particular time, the included constitutive variables are locally determined, but their temporal derivatives as free variables can be assigned arbitrarily depending on the ongoing process. Thus, the factors belonging to the free variables $\mathbf{L}_S = (\mathbf{F}_S)'_S \, \mathbf{F}_S^{-1}$ and $(\rho^{FR})'_F$ must vanish in order to satisfy the equality condition, which holds in the state of thermodynamic equilibrium. Note in passing that the rates of the internal variables $(\boldsymbol{\mathcal{Q}}_n^S)'_S$ are not to be considered as free variables of the process, since they have to be defined by evolution equations associated with the intrinsic dissipation mechanisms of φ^S. However, according to Coleman & Gurtin [34], each dissipative system tends towards thermodynamic equilibrium ($\mathcal{D}_{\text{int}} = 0$) implying that also the internal state variables reach equilibrium, i. e.,

$$\lim_{t \to \infty} \boldsymbol{\mathcal{Q}}_n^S = \overset{*}{\boldsymbol{\mathcal{Q}}}{}_n^S \,, \quad n = 1, ..., N \,. \tag{3.26}$$

Thus, the considered biphasic mixture is in an equilibrium state, whenever

$$(\overset{*}{\boldsymbol{\mathcal{Q}}}{}_n^S)'_S = \boldsymbol{\mathcal{F}}_n(\overset{*}{\mathbf{F}}_S, \overset{*}{\boldsymbol{\mathcal{Q}}}{}_n^S) = \mathbf{0} \,, \quad \overset{*}{\mathbf{D}}_F = \mathbf{0} \,, \quad \overset{*}{\mathbf{w}}_{FR} = \mathbf{0} \,, \tag{3.27}$$

where $\overset{*}{(\,\cdot\,)}$ indicates the equilibrium quantities. Then, from Coleman & Gurtin's *equation of internal equilibrium* [34, p. 602], it can be consequently deduced that

$$\left. \frac{\partial \psi^S(\mathbf{F}_S, \boldsymbol{\mathcal{Q}}_n^S)}{\partial \boldsymbol{\mathcal{Q}}_n^S} \right|_{\boldsymbol{\mathcal{Q}}_n^S \, = \, \overset{*}{\boldsymbol{\mathcal{Q}}}{}_n^S} = \mathbf{0} \quad \longrightarrow \quad \overset{*}{\psi}{}^S = \overset{*}{\psi}{}^S(\overset{*}{\mathbf{F}}_S) \,, \tag{3.28}$$

which means that for a sufficiently slow process or as $t \to \infty$, the dissipative solid skeleton actually behaves perfectly elastic.

Following the above, by claiming the terms in parentheses to vanish, the solid extra stress tensor is determined by

$$\mathbf{T}_E^S = \rho^S \, \frac{\partial \psi^S}{\partial \mathbf{F}_S} \, \mathbf{F}_S^T \tag{3.29}$$

or equivalently by (cf. section 2.3.1)

$$\boldsymbol{\tau}_E^S = \rho_{0S}^S \, \frac{\partial \psi^S}{\partial \mathbf{F}_S} \, \mathbf{F}_S^T \quad \longleftrightarrow \quad \mathbf{P}_E^S = \rho_{0S}^S \, \frac{\partial \psi^S}{\partial \mathbf{F}_S} \quad \longleftrightarrow \quad \mathbf{S}_E^S = \rho_{0S}^S \, \mathbf{F}_S^{-1} \, \frac{\partial \psi^S}{\partial \mathbf{F}_S} \,, \tag{3.30}$$

where $\rho_{0S}^S = n_{0S}^S \, \rho^{SR}$ is the partial solid density with respect to the solid reference configuration. Note that in the context of *hyperelasticity*[6], one commonly proceeds from the existence of a scalar-valued strain-energy function

$$\mathcal{W}^S := \rho_{0S}^S \, \psi^S \,, \tag{3.31}$$

[6] The concept of hyperelasticity (*Green* elasticity) claims that the conditional equation for the stress is derivable from a potential. Thus, hyperelasticity implies a conservative framework, i. e., the conservation of mechanical energy and reversibility or, in other words, the path-independence of the work done by the stress field, which are properties commonly associated with elasticity (Ogden [139]).

which represents the elastic potential or the stored elastic energy and is defined per unit reference volume rather than per unit mass (cf. Ogden [139]). To continue, from the second term in parentheses of equation (3.25) the *Lagrange*an multiplier $\mathcal{P}$ is easily identified as the effective pore-fluid pressure p^{FR} or simply p:

$$p = p^{FR} := \mathcal{P} = (\rho^{FR})^2 \, \frac{\partial \psi^F}{\partial \rho^{FR}} \, . \tag{3.32}$$

Note that this reproduces the result known from fluid thermodynamics. There, proceeding from the fundamental energy potential of a compressible fluid, $\psi^F = \psi^F(\Theta^F, \mathcal{V}^{FR})$, formulated in the absolute temperature Θ^F and the effective specific volume $\mathcal{V}^{FR}$, the effective fluid pressure is found as the conjugate variable to the specific volume. Thus,

$$p^{FR} = -\frac{\partial \psi^F}{\partial \mathcal{V}^{FR}} = (\rho^{FR})^2 \, \frac{\partial \psi^F}{\partial \rho^{FR}} \quad \text{with} \quad \mathcal{V}^{FR} = \frac{1}{\rho^{FR}} \, . \tag{3.33}$$

In the case of an incompressible pore fluid, it is easily deduced that $p = p^{FR}$ degenerates to an unspecified pore-fluid pressure in the sense of a constraining force, which has to be determined from the boundary conditions of the boundary-value problem under study.

The remainder of the *Clausius-Planck* inequality (3.25), the so-called *residual* inequality,

$$-\rho^S \sum_{n=1}^{N} \frac{\partial \psi^S}{\partial \boldsymbol{\mathcal{Q}}_n^S} \cdot (\boldsymbol{\mathcal{Q}}_n^S)'_S + \mathbf{T}_E^F \cdot \mathbf{D}_F - \hat{\mathbf{p}}_E^F \cdot \mathbf{w}_{FR} \geq 0 \, , \tag{3.34}$$

represents the irreversible or dissipative parts responsible for the non-equilibrium states ($\mathcal{D}_{\text{int}} > 0$) of the binary model. The residual inequality essentially serves as a restrictive condition for the formulation of admissible constitutive laws for $(\boldsymbol{\mathcal{Q}}_n^S)'_S$, $\mathbf{T}_E^F$, and $\hat{\mathbf{p}}_E^F$. Moreover, it reveals the overlay of the dissipative solid and fluid properties during general deformation processes, which gives rise to a challenging model adaption when applied to real material behavior (see section 5.2). For the subsequent treatment, it is convenient to proceed from the sufficient condition that each expression of the residual inequality (3.34) satisfies the inequality itself. This is guaranteed if each expression yields a positive definite quadratic form, which can be accomplished by assuming the following natural proportionalities:

$$(\boldsymbol{\mathcal{Q}}_n^S)'_S \propto -\rho^S \, \frac{\partial \psi^S}{\partial \boldsymbol{\mathcal{Q}}_n^S} \, , \quad \mathbf{T}_E^F \propto \mathbf{D}_F \, , \quad \hat{\mathbf{p}}_E^F \propto -\mathbf{w}_{FR} \, . \tag{3.35}$$

However, further investigations require detailed information about the constituent materials, particularly concerning the type of solid inelasticity, the pore-fluid behavior, and the solid-fluid interaction mechanisms. Therefore, based on the above findings, in the forthcoming sections, appropriate constitutive equations will be derived for the description of a viscoelastic solid skeleton (section 3.2) and the nonlinear percolation process of a compressible or incompressible pore fluid (section 3.3).

3.2 Viscoelastic Solid Constituent

This section is concerned with the formulation of a suitable viscoelastic material law for the intrinsically dissipative solid constituent, which accounts for all relevant nonlinearities that may occur during finite distortions of the macroscopically compressible skeleton. Therefore, at first, the basic approach to solid viscoelasticity is reviewed within the geometrically linear regime, where the generalized *Maxwell* model consistently serves as the constitutive phenomenological basis. In addition to the convenient kinematics of its rheological structure (cf. section 2.2.3), the stress conditions of the generalized *Maxwell* model also allow for a physically meaningful interpretation and can straightforwardly be transferred to the finite deformation theory. Following this, accounting for all mathematical and physical requirements, an appropriate solid strain-energy function and consistent evolution equations for the inelastic solid deformation tensors as the strain-equivalent internal variables are defined.

3.2.1 Introduction to Solid Viscoelasticity

A solid material is said to be viscoelastic, if it exhibits a rate-dependent material response without showing an equilibrium hysteresis (cf. Haupt [86]). Accordingly, viscoelastic solids show distinct relaxation and creep behavior as well as frequency-dependent stiffness and damping effects, which makes them indispensable for applications, where continual energy absorption is demanded. Particularly, the relaxation and creep response originally led to the description as *materials with fading memory*, with the fading memory represented by means of rate-dependent functionals implying that the current state of stress (or strain) depends on the whole strain (or stress) history (Coleman & Noll [35]).

Following this, to formally establish the 1-d effective stress response $\sigma_E^S(t)$ of a linear viscoelastic solid skeleton to a strain-driven uniaxial process, the current stress can be expressed as a functional of the whole solid strain history

$$\sigma_E^S(t) = \mathcal{F}[\varepsilon_S(\tau)] \quad \text{with} \quad -\infty < \tau \leq t\,. \tag{3.36}$$

Excluding aging effects and assuming that the functional is linear and the strain history is represented by a series of steps, application of the *Boltzmann* superposition principle yields the known integral representation of linear solid viscoelasticity (Christensen [30]):

$$\sigma_E^S(t) := \mathcal{G}^S(t-\tau) * \mathrm{d}\sigma_E^S(\tau) = \int_{-\infty}^{t} \mathcal{G}^S(t-\tau)\,\frac{\mathrm{d}\varepsilon_S(\tau)}{\mathrm{d}\tau}\,\mathrm{d}\tau\,. \tag{3.37}$$

Therein, $\mathcal{G}^S$ represents a constitutive relaxation function, which essentially serves as a weighting function for the past deformation process and thus, represents the memory of the material. Note that the symbol "$*$" denotes a convolution product, which in an integral sense expresses the amount of overlap of one function as it is shifted over another function (cf. Gurtin & Sternberg [78]). By analogous considerations, one finds the dual formulation for seeking the linear solid strain response $\varepsilon_S(t)$ to a subjected effective stress

on the solid skeleton as

$$\varepsilon_S(t) := \mathcal{J}^S(t-\tau) * \mathrm{d}\varepsilon_S(\tau) = \int_{-\infty}^{t} \mathcal{J}^S(t-\tau)\,\frac{\mathrm{d}\sigma_E^S(\tau)}{\mathrm{d}\tau}\,\mathrm{d}\tau \tag{3.38}$$

with $\mathcal{J}^S$ representing the so-called creep or retardation function. However, in order to render the fading memory property more precisely, the relaxation and creep functions $\mathcal{G}^S$ and $\mathcal{J}^S$, respectively, have to be specified. Note that in the context of linear viscoelasticity, as far as $\sigma_E^S(t) = \varepsilon_S(t) \equiv 0\ \forall\, t \leq 0$, the fundamental constitutive relations are invertible, i. e., $\mathcal{G}^S$ is uniquely defined by $\mathcal{J}^S$ and *vice versa*, which can be shown by *Laplace* transformation (Tschoegl [183]). In principle, any form of the relaxation or creep function is conceivable, if it fits the observed material behavior. Accordingly, many different empirical formulations have been suggested ranging from error functions of probability theory (Bischoff *et al.* [12]) over fractional power forms (Williams & Watts [192]) to finite uniform relaxation spectra (Fung [71]). However, a more physically-based selection of $\mathcal{G}^S$ and $\mathcal{J}^S$ can be motivated by reverting to rheological models, where, in this contribution, the generalized *Maxwell* model as depicted in box (3.39) is the convenient choice. The usage of rheological models to phenomenologically display viscoelastic material behavior is directly connected with the differential representation of the material equations, which is given preference for the following considerations.

Proceeding from the notions and the governing equations on the left hand side in box (3.39), it is seen that in addition to the additive kinematics in the *Maxwell* elements, the parallel structure yields an additive composition of the stresses. In particular, the linear solid extra stress is composed of the elastic stress response σ_{EQ}^S of the single spring and the sum of the transient viscoelastic overstresses σ_n^S $(n = 1, ..., N)$ collected in σ_{NEQ}^S. Usually, σ_{EQ}^S is referred to as equilibrium (EQ) stress associated with the time infinity property of the single spring, whereas σ_{NEQ}^S represents the non-equilibrium (NEQ) part describing the perturbation away from thermodynamic equilibrium. Following this, the linear viscoelastic material response can be easily visualized. For example, taking only one *Maxwell* element into consideration $(N = 1)$, i. e., restricting the presentation to the so-called *Poynting-Thomson* model (cf. box (3.39)), the descriptive differential equation is found by rephrasing the time derivative of the equilibrium condition for the solid extra stress by use of the compatibility and constitutive relations such that only the external state variables σ_E^S and ε_S as well as their rates remain. Thus, assuming constant spring elasticities $E_0^S, E_1^S > 0$ and a constant dashpot viscosity $D_1^S > 0$, it is easily deduced that

$$\begin{aligned}
(\sigma_E^S)'_S &= (\sigma_{EQ}^S)'_S + (\sigma_{NEQ}^S)'_S \\
&= E_0^S\,(\varepsilon_S)'_S + E_1^S\,(\varepsilon_{Se})'_S \\
&= E_0^S\,(\varepsilon_S)'_S + E_1^S\,[(\varepsilon_S)'_S - (\varepsilon_{Si})'_S] \\
&= (E_0^S + E_1^S)\,(\varepsilon_S)'_S - (\tau_1^S)^{-1}\,\sigma_{NEQ}^S \\
&= (E_0^S + E_1^S)\,(\varepsilon_S)'_S - (\tau_1^S)^{-1}\,(\sigma_E^S - \sigma_{EQ}^S) \\
&= (E_0^S + E_1^S)\,(\varepsilon_S)'_S - (\tau_1^S)^{-1}\,\sigma_E^S + (\tau_1^S)^{-1}\,E_0^S\,\varepsilon_S
\end{aligned} \tag{3.40}$$

1- and 3-d linear solid viscoelasticity

Rheological model:

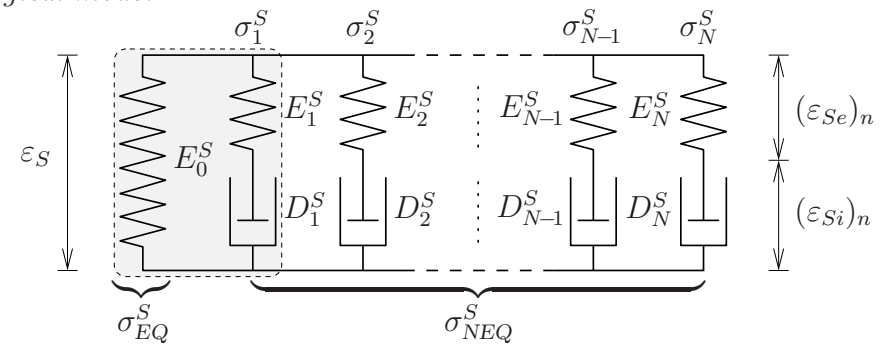

- generalized *Maxwell* model (1+2N element linear viscoelastic solid)
- $N = 1$: *Poynting-Thomson* model (standard linear viscoelastic solid)

Equilibrium:

$$\begin{aligned} \sigma_E^S &= \sigma_{EQ}^S + \sigma_{NEQ}^S & \boldsymbol{\sigma}_E^S &= \boldsymbol{\sigma}_{EQ}^S + \boldsymbol{\sigma}_{NEQ}^S \\ \sigma_{NEQ}^S &= \sum_{n=1}^{N} \sigma_n^S & \boldsymbol{\sigma}_{NEQ}^S &= \sum_{n=1}^{N} \boldsymbol{\sigma}_n^S \\ \sigma_n^S &= (\sigma_{Se}^S)_n = (\sigma_{Si}^S)_n & \boldsymbol{\sigma}_n^S &= (\boldsymbol{\sigma}_{Se}^S)_n = (\boldsymbol{\sigma}_{Si}^S)_n \end{aligned} \qquad \left\{ \begin{array}{c} n = 1, ..., N \\ \textit{Maxwell} \text{ elements} \end{array} \right\} \tag{3.39}$$

Kinematics: (cf. section 2.2.3)

$$\varepsilon_S = (\varepsilon_{Se})_n + (\varepsilon_{Si})_n \qquad \boldsymbol{\varepsilon}_S = (\boldsymbol{\varepsilon}_{Se})_n + (\boldsymbol{\varepsilon}_{Si})_n$$

Constitutive laws[a]*:*

$$\begin{aligned} \sigma_{EQ}^S &= E_0^S \, \varepsilon_S & \boldsymbol{\sigma}_{EQ}^S &= \overset{4}{\mathbf{E}}{}_0^S \, \boldsymbol{\varepsilon}_S \,, \; \overset{4}{\mathbf{E}}{}_0^S = 2\mu_0^S \, \overset{4}{\mathbf{I}} + \Lambda_0^S \, \overset{4}{\mathbf{I}}_{\mathrm{tr}} \\ (\sigma_{Se}^S)_n &= E_n^S \, (\varepsilon_{Se})_n & (\boldsymbol{\sigma}_{Se}^S)_n &= \overset{4}{\mathbf{E}}{}_n^S \, (\boldsymbol{\varepsilon}_{Se})_n \,, \; \overset{4}{\mathbf{E}}{}_n^S = 2\mu_n^S \, \overset{4}{\mathbf{I}} + \Lambda_n^S \, \overset{4}{\mathbf{I}}_{\mathrm{tr}} \\ (\sigma_{Si}^S)_n &= D_n^S \, [(\varepsilon_{Si})_n]'_S & (\boldsymbol{\sigma}_{Si}^S)_n &= \overset{4}{\mathbf{D}}{}_n^S \, [(\boldsymbol{\varepsilon}_{Si})_n]'_S \,, \; \overset{4}{\mathbf{D}}{}_n^S = 2\eta_n^S \, \overset{4}{\mathbf{I}} + \zeta_n^S \, \overset{4}{\mathbf{I}}_{\mathrm{tr}} \end{aligned}$$

Evolution equations:

$$\begin{aligned} [(\varepsilon_{Si})_n]'_S &= (\tau_n^S)^{-1} \, [\varepsilon_S - (\varepsilon_{Si})_n] & [(\boldsymbol{\varepsilon}_{Si})_n]'_S &= (\overset{4}{\boldsymbol{\tau}}{}_n^S)^{-1} \, [\boldsymbol{\varepsilon}_S - (\boldsymbol{\varepsilon}_{Si})_n] \\ \tau_n^S &:= D_n^S / E_n^S : \text{relaxation times} & \overset{4}{\boldsymbol{\tau}}{}_n^S &:= (\overset{4}{\mathbf{E}}{}_n^S)^{-1} \, \overset{4}{\mathbf{D}}{}_n^S : \text{relaxation tensors} \end{aligned}$$

[a] With the fundamental tensors $\overset{4}{\mathbf{I}} := (\mathbf{I} \otimes \mathbf{I})^{\overset{23}{T}}$ and $\overset{4}{\mathbf{I}}_{\mathrm{tr}} := (\mathbf{I} \otimes \mathbf{I})$ (cf. appendix A)

finally yielding the first-order ordinary differential equation (ODE)

$$\sigma_E^S + \tau_1^S \, (\sigma_E^S)'_S = E_0^S \, \varepsilon_S + \tau_1^S \, (E_0^S + E_1^S) \, (\varepsilon_S)'_S \tag{3.41}$$

with $\tau_1^S = D_1^S / E_1^S > 0$ representing the relaxation time constant of the single *Maxwell* element. The characteristic behavior of the standard linear viscoelastic model described by the above differential equation is best displayed by regarding its response to subjected

step loads in the strain or the stress variable. By *Laplace* transformation or, alternatively, by integration with the aid of an integrating factor, the readily determined solution of the ODE (3.41) due to a strain step $\varepsilon_S(t) = \varepsilon_{S0}\, H(t)$ takes the form

$$\sigma_E^S(t) = \underbrace{\left(E_0^S + E_1^S\, e^{-t/\tau_1^S}\right)}_{\mathcal{G}^S(t)}\, \varepsilon_{S0}\, H(t) \tag{3.42}$$

and for a prescribed stress step $\sigma_E^S(t) = \sigma_{E0}^S\, H(t)$, it follows

$$\varepsilon_S(t) = \underbrace{\left(\frac{1}{E_0^S + E_1^S} + \frac{E_1^S}{E_0^S\,(E_0^S + E_1^S)}\,(1 - e^{-t/\overline{\tau}_1^S})\right)}_{\mathcal{J}^S(t)}\, \sigma_{E0}^S\, H(t)\,. \tag{3.43}$$

Herein, $H(t)$ is the *Heaviside* step function with the properties $H(t) = 0$ if $t < 0$ and $H(t) = 1$ if $t \geq 0$, ε_{S0} and σ_{E0}^S are the respective strain and stress amplitudes, and $\overline{\tau}_1^S = \tau_1^S\,(E_0^S + E_1^S)/E_0^S > 0$ denotes the retardation time constant. In equations (3.42) and (3.43), the constitutive relaxation and retardation functions $\mathcal{G}^{\mathcal{S}}(t)$ and $\mathcal{J}^{\mathcal{S}}(t)$ are now easily identified. It is directly seen that they describe an instantaneous elastic response followed by a time-delayed monotonic relaxation or creep behavior with the decaying exponential function representing the fading memory. The general behavior of the *Poynting-Thomson* model is depicted in figure 3.1. The subfigures (a) and (b) show the distinct relaxation and retardation (creep) responses to subjected step loads as given in equations (3.42) and (3.43), where the relaxation and retardation times can directly be identified. Moreover, subfigure (c) shows the hysteretic stress response due to a cyclic loading at a constant strain rate. The area enclosed by the hysteresis curve is a measure of the dissipated energy during the deformation process. Subfigure (d) finally displays the frequency dependent stiffness and damping effects of viscoelastic solid materials. It is seen that the hysteresis loop expands, if the strain rate is increased, thereby increasing the energy absorption and the transient stiffness.

Remark: Note that the consideration of more *Maxwell* elements ($N > 1$) does not change the principle shape of the relaxation and creep curves given in figure 3.1. Actually, the order of the ODE (3.41) is increased by one with each additional *Maxwell* branch but relaxation functions $\mathcal{G}^S$ always decrease monotonously to an asymptotic end value $\mathcal{G}_{EQ}^S(t \to \infty)$, i. e., $(\mathcal{G}^S)'_S \leq 0$, whereas retardation functions $\mathcal{J}^S$ are monotone increasing functions with an asymptotic end value $\mathcal{J}_{EQ}^S(t \to \infty)$, i. e., $(\mathcal{J}^S)'_S \geq 0$. Typically, the number of *Maxwell* elements is chosen according to the considered frequency range[7] (cf. Lion [112]). However, one has to be aware of the identification problem of the included material parameters, which is the major drawback compared to the integral formulations with continuous relaxation spectra. Moreover, it is worth mentioning that dynamic viscoelastic material response is often studied for the special case of harmonic loading situations. Therefore, particular quantities, the so-called storage and loss moduli, are introduced, which govern the stiffness and dissipation properties depending on

[7] Approximately one *Maxwell* element per decade in the frequency range.

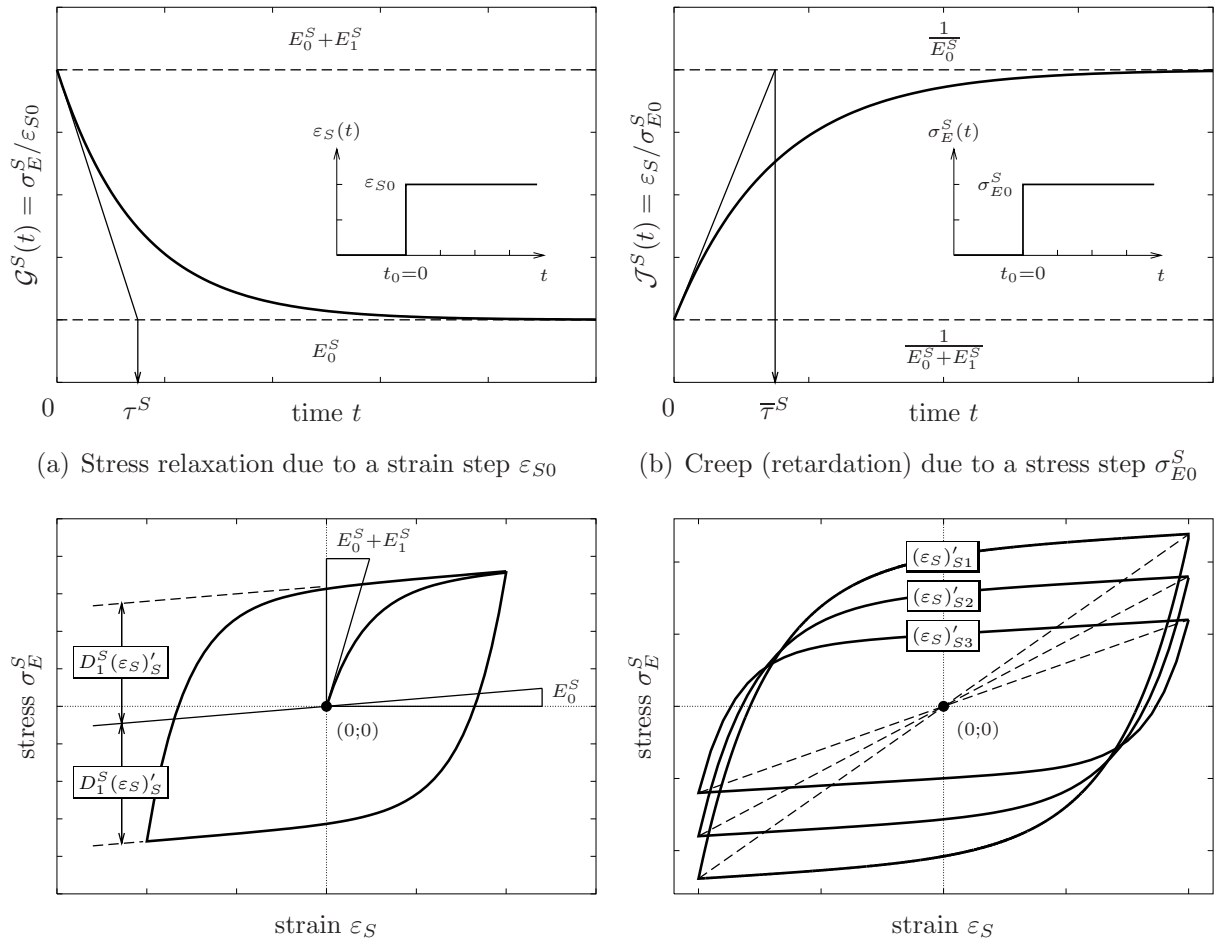

(a) Stress relaxation due to a strain step ε_{S0}

(b) Creep (retardation) due to a stress step σ_{E0}^S

(c) Hysteretic stress response to a cyclic process at a constant strain rate $(\varepsilon_S)'_S = \text{const.}$

(d) Hysteretic stress responses to cyclic processes at different strain rates $(\varepsilon_S)'_{S1} > (\varepsilon_S)'_{S2} > (\varepsilon_S)'_{S3}$

Figure 3.1: *Characteristic behavior of the standard linear viscoelastic solid model: (a) and (b) are the plots of the solution functions (3.42) and (3.43), (c) and (d) are achieved through numerical integration of the differential equation (3.41)*

the frequency of the periodic load. However, for general 3-d applications with arbitrary loading conditions, their usage is not meaningful. For more details, see, e. g., Tschoegl [183], Haupt [87], pp. 215, or Wineman & Rajagopal [193], ch. 6. ■

Recalling section 3.1.3 on constitutive variables, the simple linear 1-d model can further be used to find additional assumptions for the solid free energy. Particularly, from the additive composition of the solid extra stress, it is easily deduced that

$$\sigma_E^S = \sigma_{EQ}^S + \sigma_{NEQ}^S = E_0^S\,\varepsilon_S + E_1^S\,\varepsilon_{Se} = \frac{\partial}{\partial \varepsilon_S}\underbrace{\left(\tfrac{1}{2}\,E_0^S\,\varepsilon_S^2\right)}_{\psi_{EQ}^S(\varepsilon_S)} + \frac{\partial}{\partial \varepsilon_{Se}}\underbrace{\left(\tfrac{1}{2}\,E_1^S\,\varepsilon_{Se}^2\right)}_{\psi_{NEQ}^S(\varepsilon_{Se})}. \tag{3.44}$$

Thus, in view of the fact that energy can only be stored in the elastic springs, the consti-

tutive split of the solid energy potential in analogy to the stresses into an equilibrium part $\psi^S_{EQ}(\varepsilon_S)$ and a non-equilibrium part $\psi^S_{NEQ}(\varepsilon_{Se})$ is a natural choice. However, based on the internal variable concept, the reasonably reduced dependencies of the solid free energy given in equation (3.23) must be brought into accordance with the above findings. This can be accomplished by formal decomposition of the infinitesimal 1-d representation of ψ^S into an equilibrium part and a *pseudo potential*[8] depending on the internal variables:

$$\psi^S = \psi^S(\mathbf{F}_S, \boldsymbol{\mathcal{Q}}^S_n) \quad \longrightarrow \quad \psi^S(\varepsilon_S, \mathcal{Q}^S_n) = \psi^S_{EQ}(\varepsilon_S) + \psi^S(\mathcal{Q}^S_n)\,. \tag{3.45}$$

Then, identifying the dashpot deformation as the scalar-valued, strain-equivalent internal variable of the *Poynting-Thomson* model, i. e., $\mathcal{Q}^S_1 = \varepsilon_{Si}$, the dependency of the pseudo potential $\psi(\mathcal{Q}^S_1) = \psi(\varepsilon_{Si})$ is rewritten by use of the additive kinematics yielding

$$\psi^S(\varepsilon_{Si}) \quad \longrightarrow \quad \psi^S(\varepsilon_S, \varepsilon_{Se}) \quad \longrightarrow \quad \psi^S_{NEQ}(\varepsilon_{Se})\,, \tag{3.46}$$

where it is assumed that the dependency on the total solid strain ε_S is completely included in the equilibrium part $\psi^S_{EQ}(\varepsilon_S)$. This is in full agreement with Coleman & Gurtin's equation of internal equilibrium (3.28) as in the state of thermodynamic equilibrium with $\tau^S_1 > 0$ the following relations hold:

$$\begin{aligned} (\overset{*}{\varepsilon}_{Si})'_S = (\tau^S_1)^{-1}\,(\overset{*}{\varepsilon}_S - \overset{*}{\varepsilon}_{Si}) = 0 \quad \longrightarrow \quad \overset{*}{\varepsilon}_{Si} \equiv \overset{*}{\varepsilon}_S = \text{const.} \quad \longrightarrow \quad \overset{*}{\varepsilon}_{Se} \equiv 0\,, \\ \overset{*}{\psi}{}^S = \overset{*}{\psi}{}^S(\overset{*}{\varepsilon}_S, \overset{*}{\varepsilon}_{Se}) = \overset{*}{\psi}{}^S(\overset{*}{\varepsilon}_S) \equiv \overset{*}{\psi}{}^S_{EQ}(\overset{*}{\varepsilon}_S)\,, \quad \overset{*}{\psi}{}^S_{NEQ}(\overset{*}{\varepsilon}_{Se}) \equiv 0\,. \end{aligned} \tag{3.47}$$

Note in passing that a theoretical relaxation time $\tau^S_1 = 0$ due to $D^S_1 = 0$ would imply instantaneous relaxation meaning that the *Maxwell* element does not contribute to the response of the model. Thus, the model would behave purely elastic governed by the single spring and hence, is always in equilibrium. In conclusion, it is convenient to proceed from the following form of the free energy for the 1+2N element linear viscoelastic solid model:

$$\psi^S[\varepsilon_S, \mathcal{Q}^S_n = (\varepsilon_{Si})_n] \quad \longrightarrow \quad \psi^S[\varepsilon_S, (\varepsilon_{Se})_n] = \psi^S_{EQ}(\varepsilon_S) + \psi^S_{NEQ}[(\varepsilon_{Se})_n]\,. \tag{3.48}$$

Moreover, based on the 1-d rheological structure of the generalized *Maxwell* model, 3-d linear viscoelastic material behavior can be described by formal extension of the governing scalar equations to three dimensions. As depicted on the right hand side in box (3.39), the 3-d extension of the infinitesimal theory is straightforward by simply replacing the scalar quantities with their tensorial counterparts. In addition to the already defined infinitesimal strain tensors given in equations (2.29) and (2.30), $\boldsymbol{\sigma}^S_E \approx \mathbf{T}^S_E$ denotes the linear solid extra stress tensor of the infinitesimal theory with $\boldsymbol{\sigma}^S_{EQ}$ and $\boldsymbol{\sigma}^S_{NEQ} = \sum_n \boldsymbol{\sigma}^S_n$ as the equilibrium and non-equilibrium parts. The elastic stresses are determined by linear *Hooke*-type elasticity laws with the positive definite 4th-order elasticity tensors[9] $(\mathbf{E}^S_0)^{\underline{4}}$ and $(\mathbf{E}^S_n)^{\underline{4}}$, wherein μ^S_0, Λ^S_0 and μ^S_n, Λ^S_n are the respective *Lamé* constants. As isotropic tensor functions, the positive definite viscosity tensors $(\mathbf{D}^S_n)^{\underline{4}}$ are given analogously to the elasticity tensors with η^S_n and ζ^S_n representing the viscosity parameters. Thus, the porous

[8] Also known under the somehow self-contradictory term *dissipation potential*.

[9] For lack of space, $(\,\bullet\,)^{\underline{n}}$ is also used to indicate higher-order tensors within the text, e. g., $(\mathbf{E}^S_0)^{\underline{4}} := \overset{4}{\mathbf{E}}{}^S_0$.

solid matrix is allowed to be linear viscoelastic in both shear and bulk deformation with independent relaxation and retardation properties. This motivates the introduction of 4th-order relaxation tensors $(\boldsymbol{\mathcal{T}}_n^S)^{\underline{4}}$ to control the rate of the 3-d inelastic strain evolution instead of using scalar relaxation constants such as in the 1-d case. In this context, it should be noted that by decomposition of the solid extra stress tensor into *deviatoric* and *spheric*[10] parts, it is possible to uncouple the governing viscoelastic equations in order to handle them separately in analogy to the 1-d formulation. A more detailed discussion of the procedure, its numerical treatment and application within the TPM approach, e. g., for the description of soft biological tissues, can be found in Ehlers & Markert [59, 60].

However, as this contribution is primarily concerned with the highly nonlinear response of saturated porous materials, which suffer large viscoelastic deformations, continuative details of the linear viscoelasticity theory are not presented at this point. For further particulars, it is referred to the standard works of Christensen [30], Findley *et al.* [67], Gurtin & Sternberg [78], and Tschoegl [183] among others.

3.2.2 Aspects of Finite Solid Viscoelasticity

For the description of the intrinsic dissipative phenomena of the porous solid skeleton, an appropriate finite viscoelastic material formulation is required. Therefore, the solid strain energy $\mathcal{W}^S$, as the response function that governs the hyperelastic solid material behavior, must be specified accounting for all essential large strain properties of φ^S. Proceeding from the generalized *Maxwell* model as the convenient phenomenological basis, one can directly follow the arguments of the 1-d linear viscoelasticity theory given in equations (3.45 – 3.48). Accordingly, the dependencies of the solid free energy function of the finite theory are rewritten by use of the multiplicative geometric concept (2.31) with the inelastic deformation gradients $(\mathbf{F}_{Si})_n$ identified as the internal variables associated with the dashpot deformations in the *Maxwell* elements:

$$\psi^S(\mathbf{F}_S, \boldsymbol{\mathcal{Q}}_n^S) \quad \longrightarrow \quad \psi^S[\mathbf{F}_S, (\mathbf{F}_{Si})_n] \quad \longrightarrow \quad \psi^S[\mathbf{F}_S, (\mathbf{F}_{Se})_n]\,. \tag{3.49}$$

Moreover, adopting the constitutive split of ψ^S of the 1-d infinitesimal case (3.48) together with the definition (3.31), one assumes a solid strain-energy function of the form

$$\mathcal{W}^S[\mathbf{F}_S, (\mathbf{F}_{Se})_n] = \mathcal{W}^S_{EQ}(\mathbf{F}_S) + \mathcal{W}^S_{NEQ}[(\mathbf{F}_{Se})_n]\,. \tag{3.50}$$

Before proceeding, it should be noted that the specific choice of $\mathcal{W}^S_{EQ}$ and $\mathcal{W}^S_{NEQ}$ is constrained by certain important properties, which are not to be sacrificed for obtaining rigorous results. In particular, the strain-energy function must ensure *polyconvexity*, certain *growth conditions* (*coerciveness*), and *objectivity* (frame indifference). For the sake of completeness, these conditions and the resulting restrictions on the constitutive shape of $\mathcal{W}^S$ are briefly discussed in the following paragraphs.

[10] The deviator (traceless tensor) $\boldsymbol{\sigma}^D$ and the spherical tensor $\boldsymbol{\sigma}^K$ of a 2nd-order tensor $\boldsymbol{\sigma}$ read:

$$\boldsymbol{\sigma}^D = \boldsymbol{\sigma} - \tfrac{1}{3}(\boldsymbol{\sigma}\cdot\mathbf{I})\,\mathbf{I}\,, \quad \boldsymbol{\sigma}^K = \tfrac{1}{3}(\boldsymbol{\sigma}\cdot\mathbf{I})\,\mathbf{I} \quad \longrightarrow \quad \boldsymbol{\sigma} = \boldsymbol{\sigma}^D + \boldsymbol{\sigma}^K\,, \quad \boldsymbol{\sigma}^D\cdot\mathbf{I} \equiv 0\,.$$

Polyconvexity: The solution of boundary-value problems (BVP) using the presented model will be based on the solution of some *variational problem* by searching a deformed configuration in which the energy of the system is a minimum under prescribed boundary conditions. Therefore, the stored energy must be chosen in such a way that the existence of minimizers of the energy functional is guaranteed. A necessary and sufficient condition is quasiconvexity introduced by Morrey [127] claiming isothermal stability of an all-round fixed homogeneous body of hyperelastic material by ensuring the energy functional to be weakly lower semicontinuous. However, quasiconvexity as an integral inequality is complicated to handle and disallows singularities, which cannot be reconciled with finite material behavior. In this regard, Ball [5] established the more practical notion of polyconvexity, which is a sufficient condition for quasiconvex functions that can be evaluated locally and allows infinite function values. In particular, a scalar-valued tensor function $\Psi(\mathbf{F}_S)$ is said to be polyconvex, if it can be expressed as a convex function of subdeterminants of its tensorial variables, viz.,

$$\Psi(\mathbf{F}_S) = \Psi(\mathbf{F}_S, \operatorname{cof}\mathbf{F}_S, \det\mathbf{F}_S) \quad \text{or} \quad \Psi(\mathbf{F}_S) = \Psi_l(\mathbf{F}_S) + \Psi_a(\operatorname{cof}\mathbf{F}_S) + \Psi_v(\det\mathbf{F}_S)\,, \tag{3.51}$$

where the second equality denotes an additive polyconvex function with each part convex in the associated variable. Assuming Ψ to be twice differentiable, the convexity is easily verified by showing that the second derivative with respect to each variable is positive semidefinite:

$$\left.\begin{aligned} \frac{\partial^2\Psi}{\partial\mathbf{F}_S\otimes\partial\mathbf{F}_S}\cdot(\mathbf{H}\otimes\mathbf{H}) \geq 0\,, \\ \frac{\partial^2\Psi}{\partial\operatorname{cof}\mathbf{F}_S\otimes\partial\operatorname{cof}\mathbf{F}_S}\cdot(\mathbf{H}\otimes\mathbf{H}) \geq 0\,, \\ \frac{\partial^2\Psi}{\partial(\det\mathbf{F}_S)^2} \geq 0 \end{aligned}\right\} \quad \forall\ \mathbf{H}\neq\mathbf{0}\,. \tag{3.52}$$

Following this, $\mathcal{W}^S$ is polyconvex by choosing the equilibrium and non-equilibrium stored energies of the form

$$\begin{aligned} \mathcal{W}^S_{EQ}(\mathbf{F}_S) &= \mathcal{W}^S_{EQ}(\mathbf{F}_S, \operatorname{cof}\mathbf{F}_S, \det\mathbf{F}_S)\,, \\ \mathcal{W}^S_{NEQ}[(\mathbf{F}_{Se})_n] &= \mathcal{W}^S_{NEQ}[(\mathbf{F}_{Se})_n, \operatorname{cof}(\mathbf{F}_{Se})_n, \det(\mathbf{F}_{Se})_n] \end{aligned} \tag{3.53}$$

with the properties

$$\begin{aligned} &\frac{\partial^2\mathcal{W}^S_{EQ}}{\partial\mathbf{F}_S\otimes\partial\mathbf{F}_S}\cdot(\mathbf{H}\otimes\mathbf{H}) \geq 0\,, \quad \frac{\partial^2\mathcal{W}^S_{NEQ}}{\partial(\mathbf{F}_{Se})_n\otimes\partial(\mathbf{F}_{Se})_n}\cdot(\mathbf{H}\otimes\mathbf{H}) \geq 0\,, \\ &\frac{\partial^2\mathcal{W}^S_{EQ}}{\partial\operatorname{cof}\mathbf{F}_S\otimes\partial\operatorname{cof}\mathbf{F}_S}\cdot(\mathbf{H}\otimes\mathbf{H}) \geq 0\,, \quad \frac{\partial^2\mathcal{W}^S_{NEQ}}{\partial\operatorname{cof}(\mathbf{F}_{Se})_n\otimes\partial\operatorname{cof}(\mathbf{F}_{Se})_n}\cdot(\mathbf{H}\otimes\mathbf{H}) \geq 0\,, \\ &\frac{\partial^2\mathcal{W}^S_{EQ}}{\partial(\det\mathbf{F}_S)^2} \geq 0\,, \quad \frac{\partial^2\mathcal{W}^S_{NEQ}}{\partial[(\det\mathbf{F}_{Se})_n]^2} \geq 0\,. \end{aligned} \tag{3.54}$$

From a continuum mechanical perspective, polyconvexity claims local material stability with regard to perturbations in length, area, and volume as $\mathbf{F}_S$, $\operatorname{cof}\mathbf{F}_S$, and $\det\mathbf{F}_S$ as well as the elastic counterparts, respectively, govern the changes of the corresponding

material elements (cf. relations (2.38)). In this context note that the stronger condition of convexity of the solid strain-energy function would be too restrictive for the description of real material behavior since (strict) convexity, e. g., induces uniqueness, i. e., precludes stability problems in nominal description based on the conjugate pair $\{\mathbf{P}^S, \mathbf{F}_S\}$, and is incompatible with the principle of frame indifference. For a more comprehensive discussion of convexity conditions and constitutive inequalities see, e. g., Baker & Ericksen [4], Ball [5], Ciarlet [32], Dacorogna [40], Marsden & Hughes [120], and Šilhavý [163]. Comprehensible summaries of the different notions of convexity can be found in the monographs of Schröder [158] and Lambrecht [106]. □

Growth conditions: It is quite an obvious physical fact that extreme values in stress are accompanied by extreme values in strain. In the case of a hyperelastic solid material this corresponds to the requirement that total compression and infinite distortion or expansion must yield infinite values of the strain energy. Thus, for the equilibrium part it follows

$$\mathcal{W}^S_{EQ} \to +\infty \quad \text{as} \quad \left\{ \begin{array}{l} \det \mathbf{F}_S \to n^S_{0S}\,, \\ \big(\|\mathbf{F}_S\| + \|\mathrm{cof}\,\mathbf{F}_S\| + \det \mathbf{F}_S\big) \to +\infty\,, \end{array} \right. \tag{3.55}$$

where $\|(\,\cdot\,)\|$ indicates the norm of a tensor, e. g., $\|\mathbf{F}_S\| = \sqrt{\mathbf{F}_S \cdot \mathbf{F}_S}$. The first condition differs from the one of singlephasic materials ($\det \mathbf{F} \to 0^+$) insofar as the volumetric compression of the materially incompressible solid skeleton is limited to the point of compaction, i. e., the transition point to a dense solid material associated with $n^S = 1$. In this context recall the remark on page 10 and the relations (2.15) and (2.16). Following Ciarlet [32], sec. 4.6, the second condition can be expressed in the sharper form of a *coerciveness inequality* describing the rate of growth of the strain-energy function:

$$\mathcal{W}^S_{EQ} \geq \alpha \left[\, \|\mathbf{F}_S\|^p + \|\mathrm{cof}\,\mathbf{F}_S\|^q + (\det \mathbf{F}_S)^r \right] + \beta \quad \exists\, \{\alpha, p, q, r > 0\,,\ \beta\} \in \mathbb{R}\,. \tag{3.56}$$

In particular, the inequality guarantees that the strain energy grows sufficiently rapid with its variables such that equilibrium solutions exist even under extreme loading conditions (see, e. g., Antman [1]). For the non-equilibrium part analogous considerations yield

$$\mathcal{W}^S_{NEQ} \to +\infty \quad \text{as} \quad \left\{ \begin{array}{l} \det(\mathbf{F}_{Se})_n \to (n^S_{Si})_n\,, \\ \big[\, \|(\mathbf{F}_{Se})_n\| + \|\mathrm{cof}(\mathbf{F}_{Se})_n\| + \det(\mathbf{F}_{Se})_n \big] \to +\infty\,. \end{array} \right. \tag{3.57}$$

Herein, the finite elastic volume compressions in the associated *Maxwell* elements are limited by the inelastic solid volume fractions $(n^S_{Si})_n$ resulting from preceding inelastic volume contractions. In fact, the inelastic intermediate configurations act as reference configurations for the subsequent elastic deformation processes (cf. figure 2.5). Thus, the $(n^S_{Si})_n$ can be regarded as referential solidities for the elastic volume contractions, in the same way as n^S_{0S} represents the initial value for the total volume deformation of φ^S. Proceeding from the multiplicative decompositions of $\mathbf{F}_S$ (2.31), elastic and inelastic solid *Jacobi*an determinants can be introduced:

$$\begin{gathered} J_S = \det \mathbf{F}_S = \det[(\mathbf{F}_{Se})_n\,(\mathbf{F}_{Si})_n] = \det[(\mathbf{F}_{Se})_n]\ \det[(\mathbf{F}_{Si})_n] = (J_{Se})_n\,(J_{Si})_n \\ \text{with} \quad (J_{Se})_n := \det[(\mathbf{F}_{Se})_n]\,, \quad (J_{Si})_n := \det[(\mathbf{F}_{Si})_n]\,. \end{gathered} \tag{3.58}$$

Then, the conditional equation for the intermediate solid volume fractions is found by inserting the above result into the conditional equation of n^S $(3.6)_2$ yielding

$$n^S = n^S_{0S}\, J_S^{-1} = n^S_{0S}\,[(J^{-1}_{Se})_n\,(J^{-1}_{Si})_n] = (n^S_{Si})_n\,(J^{-1}_{Se})_n \quad \text{with} \quad (n^S_{Si})_n := n^S_{0S}\,(J^{-1}_{Si})_n\,. \tag{3.59}$$

In analogy, elastic volume fractions can be defined as $(n^S_{Se})_n := n^S_{0S}\,(J^{-1}_{Se})_n$, so that a relation between the current solidity and its elastic and inelastic parts can be formulated:

$$\frac{n^S}{n^S_{0S}} = \frac{(n^S_{Se})_n}{n^S_{0S}}\,\frac{(n^S_{Si})_n}{n^S_{0S}} \quad \Leftrightarrow \quad n^S\,n^S_{0S} = (n^S_{Se})_n\,(n^S_{Si})_n\,. \tag{3.60}$$

□

Objectivity: Material objectivity or material frame indifference postulates that the constitutive material equations are independent of the current frame of reference. In other words, the described material properties remain unaltered due to changes of the observer (observer-invariance). Following this, in the case of hyperelastic material behavior, the strain-energy function is assumed to be invariant with respect to any superimposed rigid-body motions on the current configuration. Accordingly, the invariance conditions for the equilibrium and non-equilibrium energies can be expressed as

$$\overset{\star}{\mathcal{W}}{}^S_{EQ}(\mathbf{F}_S) = \mathcal{W}^S_{EQ}(\overset{\star}{\mathbf{F}}_S)\,, \quad \overset{\star}{\mathcal{W}}{}^S_{NEQ}[(\mathbf{F}_{Se})_n] = \mathcal{W}^S_{NEQ}[(\overset{\star}{\mathbf{F}}_{Se})_n]\,, \tag{3.61}$$

where $(\overset{\star}{\bullet})$ indicates the quantities of the translated and/or rotated actual configuration. With the rigid-body rotations represented by arbitrary proper orthogonal tensors $\mathbf{Q}_S \in \mathcal{SO}_3$, the covariant transformation mechanisms read

$$\begin{aligned} \overset{\star}{\mathbf{F}}_S &= \overset{\star}{\mathbf{a}}_k \otimes \mathbf{h}^k = (\mathbf{Q}_S\,\mathbf{a}_k) \otimes \mathbf{h}^k = \mathbf{Q}_S\,(\mathbf{a}_k \otimes \mathbf{h}^k) = \mathbf{Q}_S\,\mathbf{F}_S\,, \\ \overset{\star}{\mathbf{F}}_{Se} &= \overset{\star}{\mathbf{a}}_k \otimes \widehat{\mathbf{z}}^k = (\mathbf{Q}_S\,\mathbf{a}_k) \otimes \widehat{\mathbf{z}}^k = \mathbf{Q}_S\,(\mathbf{a}_k \otimes \widehat{\mathbf{z}}^k) = \mathbf{Q}_S\,\mathbf{F}_{Se}\,, \end{aligned} \tag{3.62}$$

so that with the natural objectivity of scalar-valued quantities, $\overset{\star}{\Psi}(\bullet) = \Psi(\bullet)$, it follows

$$\mathcal{W}^S_{EQ}(\mathbf{F}_S) = \mathcal{W}^S_{EQ}(\mathbf{Q}_S\,\mathbf{F}_S)\,, \quad \mathcal{W}^S_{NEQ}[(\mathbf{F}_{Se})_n] = \mathcal{W}^S_{NEQ}[(\mathbf{Q}_S)_n\,(\mathbf{F}_{Se})_n]\,. \tag{3.63}$$

Then, with the special choices $\mathbf{Q}_S = \mathbf{R}^T_S$ and $(\mathbf{Q}_S)_n = (\mathbf{R}^T_{Se})_n$ and use of the right polar decompositions of $\mathbf{F}_S$ $(2.71)_1$ and $(\mathbf{F}_{Se})_n$ $(2.88)_1$, respectively, one finds

$$\mathcal{W}^S_{EQ}(\mathbf{F}_S) = \mathcal{W}^S_{EQ}(\mathbf{U}_S)\,, \quad \mathcal{W}^S_{NEQ}[(\mathbf{F}_{Se})_n] = \mathcal{W}^S_{NEQ}[(\widehat{\mathbf{U}}_{Se})_n]\,. \tag{3.64}$$

Following this, the solid strain energies depend only on the stretching parts of the deformation gradients and hence, it is convenient to express $\mathcal{W}^S_{EQ}$ and $\mathcal{W}^S_{NEQ}$ in terms of the deformation tensors $\mathbf{C}_S = \mathbf{U}^2_S$ and $(\widehat{\mathbf{C}}_{Se})_n = (\widehat{\mathbf{U}}^2_{Se})_n$ or the related strain measures $\mathbf{E}_S$ and $(\widehat{\mathbf{\Gamma}}_{Se})_n$ (cf. equations $(2.46)_{1,2}$), respectively:

$$\begin{aligned} \mathcal{W}^S_{EQ}(\mathbf{F}_S) &= \mathcal{W}^S_{EQ}(\mathbf{C}_S) = \mathcal{W}^S_{EQ}(\mathbf{E}_S)\,, \\ \mathcal{W}^S_{NEQ}[(\mathbf{F}_{Se})_n] &= \mathcal{W}^S_{NEQ}[(\widehat{\mathbf{C}}_{Se})_n] = \mathcal{W}^S_{NEQ}[(\widehat{\mathbf{\Gamma}}_{Se})_n]\,. \end{aligned} \tag{3.65}$$

Note that the representation by means of the right *Cauchy-Green* deformation or the *Green-Lagrange*an strain tensors is a natural consequence as these are the basic deformation and strain measures of the reference and the intermediate configurations and thus, are unaffected by changes to the actual configuration. □

In addition to the above discussed conditions, which must be fulfilled independent of the considered material behavior, the present work proceeds from further additional assumptions. For obvious reasons, in the undeformed initial or natural state at time $t = t_0$, where $\mathbf{F}_S = (\mathbf{F}_{Se})_n = (\mathbf{F}_{Si})_n \equiv \mathbf{I}$, the solid strain energy is assumed to vanish, which furthermore implies a stress-free reference configuration[11]:

$$\mathcal{W}_{0S}^S(\,\mathbf{I}\,) = 0\,, \quad \mathbf{T}_{E0}^S(\mathcal{W}_{0S}^S) \equiv \mathbf{0}\,. \tag{3.66}$$

Following these *normalization* assumptions together with the polyconvexity and growth conditions, the strain energy has its global minimum in the undeformed reference state, i. e., $\mathcal{W}^S[\mathbf{F}_S, (\mathbf{F}_{Se})_n] \geq 0$ must hold for all conceivable processes. Moreover, the *downward compatibility* of the constitutive material equations to the *Hooke*-type formulations of the linear viscoelasticity theory (box (3.39) right) is demanded at the transition to the small strain regime, which yields further restrictions on the class of admissible constitutive functions. Beside these self-evident assumptions, the following considerations proceed from *isotropy*, i. e., the simplification to orientation-independent, uniform material properties, which is a special case of *anisotropy*. Basically, this reduces to some extent the applicability of the viscoelastic solid model but does not generally disable future improvements for the description of anisotropic behavior. However, although it is not the objective of this contribution, in the following paragraph, some particulars on the property of *material symmetry* are presented to theoretically illustrate the restriction to isotropic material response.

Material symmetry and isotropy: By studying the orientation-dependency of the material behavior, one seeks for the properties of material symmetry, i. e., the inherent type of anisotropy of the material. In general, every material can be associated with a material symmetry group $\mathcal{MG}_3$ including all symmetry-preserving transformations in order to characterize the material and its constitutive equations (Truesdell & Noll [180]). Mathematically, the symmetry group is defined by the invariance of constitutive equations due to transformations of the body in the reference configuration. Such a change of the reference configuration can be interpreted as an imaginary rigid-body motion $\overset{\diamond}{\boldsymbol{\chi}}_S\,(\mathbf{X}_S, t_0)$ that is superimposed on the real motion. The associated new reference configuration is then related to the original reference configuration by a volume preserving mapping

$$\mathbf{H}_S = \mathrm{Grad}_S\, \overset{\diamond}{\boldsymbol{\chi}}_S \quad \in \mathcal{SU}_3\,, \tag{3.67}$$

where $\mathcal{SU}_3$ represents the special unitary group of proper unimodular transformations with $\det \mathbf{H}_S = 1\ \forall\, \mathbf{H}_S \in \mathcal{SU}_3$. Proceeding from the concept of hyperelasticity, the prop-

[11] For some specific applications, such as for the description of swelling phenomena in ionized porous media (cf. Ehlers *et al.* [61]), it can be of considerable assistance to proceed from an initially prestressed solid skeleton, which is in equilibrium with an initial pore-fluid pressure p_0, e. g., $\mathbf{T}_{E0}^S = -p_0\,\mathbf{I}$.

erty of anisotropy associated with preferred directions at material points of the reference configuration can be described by covariant 2nd-order *structural tensors*[12] $\boldsymbol{\mathcal{M}}^S$. Following this, let $\Psi(\mathbf{F}_S, \boldsymbol{\mathcal{M}}^S)$ be an energy potential of an anisotropic elastic solid. The invariance condition can then be formulated as

$$\Psi(\mathbf{F}_S, \boldsymbol{\mathcal{M}}^S) = \Psi(\overset{\diamond}{\mathbf{F}}_S, \overset{\diamond}{\boldsymbol{\mathcal{M}}}^S) \tag{3.68}$$

claiming the original and the changed reference configuration to yield the same material response in the current configuration. By use of the transport mechanisms

$$\begin{aligned} \overset{\diamond}{\mathbf{F}}_S = \mathbf{a}_k \otimes \overset{\diamond}{\mathbf{h}}^k = \mathbf{a}_k \otimes (\mathbf{H}_S^{T-1}\,\mathbf{h}^k) = (\mathbf{a}_k \otimes \mathbf{h}^k)\,\mathbf{H}_S^{-1} = \mathbf{F}_S\,\mathbf{H}_S^{-1}\,, \\ \overset{\diamond}{\boldsymbol{\mathcal{M}}}^S = \mathbf{H}_S\,\boldsymbol{\mathcal{M}}^S\,\mathbf{H}_S^T\,, \end{aligned} \tag{3.69}$$

the material symmetry group $\mathcal{MG}_3$ can be found by evaluation of

$$\left.\begin{aligned} \Psi(\mathbf{F}_S, \boldsymbol{\mathcal{M}}^S) = \Psi(\mathbf{F}_S\,\mathbf{H}_S^{-1}, \mathbf{H}_S\,\boldsymbol{\mathcal{M}}^S\,\mathbf{H}_S^T)\,, \\ \boldsymbol{\mathcal{M}}^S = \mathbf{H}_S\,\boldsymbol{\mathcal{M}}^S\,\mathbf{H}_S^T \end{aligned}\right\} \quad \forall\,\mathbf{F}_S\,,\ \forall\,\mathbf{H}_S \in \mathcal{MG}_3 \subset \mathcal{SU}_3\,. \tag{3.70}$$

In particular, the first condition is used for the definition of the material symmetry group, while condition $(3.70)_2$ serves to specify the structural tensors $\boldsymbol{\mathcal{M}}^S$ such that they are invariant with respect to the found transformations in $\mathcal{MG}_3$. Following this, proceeding from uniform (isotropic) solid properties, the material symmetry group is the whole group of proper orthogonal mappings (rotations). This means that the material response is invariant to any rigid-body rotations of the reference configuration, reflecting that an isotropic material has no preferred directions (orientation-independence), i. e., possesses complete material symmetry. Thus, in the special case of isotropic behavior, it holds

$$\Psi(\mathbf{F}_S) = \Psi(\mathbf{F}_S\,\mathbf{H}_S^T) \quad \forall\,\mathbf{H}_S \in \mathcal{MG}_3 = \mathcal{SO}_3 \subset \mathcal{SU}_3\,, \quad \boldsymbol{\mathcal{M}}^S \equiv \mathbf{I}\,. \tag{3.71}$$

For more details on the theoretical treatment of general anisotropic material behavior, it is referred to the fundamental works of Boehler [16], Spencer [169], Truesdell & Noll [180] or the more recent article of Schröder & Neff [159] among others.

To continue, applying the above findings to the equilibrium and non-equilibrium strain energies of the considered isotropic viscoelastic solid skeleton, the invariance conditions read

$$\mathcal{W}_{EQ}^S(\mathbf{F}_S) = \mathcal{W}_{EQ}^S(\overset{\diamond}{\mathbf{F}}_S)\,, \quad \mathcal{W}_{NEQ}^S[(\mathbf{F}_{Se})_n] = \mathcal{W}_{NEQ}^S[(\overset{\circ}{\mathbf{F}}_{Se})_n]\,, \tag{3.72}$$

where $(\overset{\diamond}{\bullet})$ and $(\overset{\circ}{\bullet})$ indicate the quantities of the rotated solid reference and intermediate configurations[13]. According to relation $(3.71)_1$, with the rigid-body rotations represented

[12] As an example, assume a fiber-reinforced solid with a single family of fibers locally having an initial orientation given by some unit vector $\mathbf{a}_0$ pointing in the fiber direction. Then, the structural tensor takes the simple form $\boldsymbol{\mathcal{M}}^S = \mathbf{a}_0 \otimes \mathbf{a}_0$ (see, e. g., Spencer [170] among others).

[13] It is assumed that no anisotropy is induced by the inelastic deformation process, such as it may occur during texture developments in crystal plasticity (Bertram & Böhlke [9], Kocks *et al.* [103]). Thus, the inelastic intermediate configurations in the sense of reference configurations remain the property of material symmetry and do not affect the subsequent elastic deformation processes.

by arbitrary proper orthogonal tensors $\mathbf{H}_S$ and $\widehat{\mathbf{H}}_S \in \mathcal{SO}_3$, it holds

$$\overset{\diamond}{\mathbf{F}}_S = \mathbf{F}_S\,\mathbf{H}_S^T\,, \quad \overset{\circ}{\mathbf{F}}_{Se} = \mathbf{F}_{Se}\,\widehat{\mathbf{H}}_S^T\,. \tag{3.73}$$

Then, with the special choices $\mathbf{H}_S = \mathbf{R}_S$ and $(\widehat{\mathbf{H}}_S)_n = (\mathbf{R}_{Se})_n$ and the left polar decompositions of $\mathbf{F}_S$ $(2.71)_1$ and $(\mathbf{F}_{Se})_n$ $(2.88)_1$, respectively, one finds with arguments similar to those used for the evaluation of the principle of frame indifference

$$\begin{aligned} \mathcal{W}_{EQ}^S(\mathbf{F}_S) = \mathcal{W}_{EQ}^S(\mathbf{V}_S) = \mathcal{W}_{EQ}^S(\mathbf{B}_S)\,, \\ \mathcal{W}_{NEQ}^S[(\mathbf{F}_{Se})_n] = \mathcal{W}_{NEQ}^S[(\mathbf{V}_{Se})_n] = \mathcal{W}_{NEQ}^S[(\mathbf{B}_{Se})_n]\,. \end{aligned} \tag{3.74}$$

Note in passing that the formulation of the energies by means of the left *Cauchy-Green* deformation tensors is a natural consequence as $\mathbf{B}_S$ and $(\mathbf{B}_{Se})_n$ are tensor fields living on the current configuration and thus, are invariant due to alterations of the reference and the intermediate configurations, respectively.

In conclusion, together with the objectivity requirements (3.65), the dependency of the solid strain energies on $\mathbf{F}_S$ and $(\mathbf{F}_{Se})_n$, respectively, must be equally expressible in both the corresponding right and left *Cauchy-Green* deformation tensors. This can be accomplished, if $\mathcal{W}_{EQ}^S$ and $\mathcal{W}_{NEQ}^S$ take the form of isotropic tensor functions formulated in the principal invariants or the eigenvalues of the deformation tensors as already shown in relation (2.106):

$$\begin{aligned} &\mathcal{W}_{EQ}^S(\mathbf{F}_S) = \mathcal{W}_{EQ}^S(\mathbf{C}_S) = \mathcal{W}_{EQ}^S(\mathbf{B}_S) \quad \longrightarrow \quad \mathcal{W}_{EQ}^S(I_S, II_S, III_S) = \mathcal{W}_{EQ}^S(\lambda_{S(k)})\,, \\ &\mathcal{W}_{NEQ}^S[(\mathbf{F}_{Se})_n] = \mathcal{W}_{NEQ}^S[(\widehat{\mathbf{C}}_{Se})_n] = \mathcal{W}_{NEQ}^S[(\mathbf{B}_{Se})_n] \\ &\qquad\qquad \longrightarrow \quad \mathcal{W}_{NEQ}^S[(I_{Se})_n, (II_{Se})_n, (III_{Se})_n] = \mathcal{W}_{NEQ}^S[(\lambda_{Se(k)})_n]\,. \end{aligned} \tag{3.75}$$

Herein, $(I_{Se})_n$, $(II_{Se})_n$, and $(III_{Se})_n$ represent the elastic principal invariants of $(\widehat{\mathbf{C}}_{Se})_n$ or $(\mathbf{B}_{Se})_n$, respectively, and are computed analogously to the principal invariants given in equations (2.77). □

The next step before specifying the strain-energy functions and the inelastic evolution equations is the identification of the stress tensors of the finite theory. Proceeding from the objective form of the strain energy $\mathcal{W}^S[\mathbf{E}_S, (\widehat{\mathbf{\Gamma}}_{Se})_n]$ given in equations (3.65), time derivation yields the effective solid stress power including the intrinsic dissipative contributions of φ^S:

$$(\mathcal{W}^S)'_S = \frac{\partial \mathcal{W}_{EQ}^S}{\partial \mathbf{E}_S} \cdot (\mathbf{E}_S)'_S + \sum_{n=1}^{N} \frac{\partial \mathcal{W}_{NEQ}^S}{\partial (\widehat{\mathbf{\Gamma}}_{Se})_n} \cdot [(\widehat{\mathbf{\Gamma}}_{Se})_n]'_S\,. \tag{3.76}$$

Then, by use of the upper inelastic *Oldroyd* derivative $(2.66)_2$, the elastic strain rate tensors of the $n = 1, ..., N$ intermediate configurations can be rewritten as

$$\begin{aligned} (\widehat{\mathbf{\Gamma}}_{Se})'_S &= (\widehat{\mathbf{\Gamma}}_{Se})_{Si}^{\triangle} - \widehat{\mathbf{L}}_{Si}^T\,\widehat{\mathbf{\Gamma}}_{Se} - \widehat{\mathbf{\Gamma}}_{Se}\,\widehat{\mathbf{L}}_{Si} \\ &= (\widehat{\mathbf{\Gamma}}_S)_{Si}^{\triangle} - \widehat{\mathbf{D}}_{Si} - \widehat{\mathbf{L}}_{Si}^T\,\widehat{\mathbf{\Gamma}}_{Se} - \widehat{\mathbf{\Gamma}}_{Se}\,\widehat{\mathbf{L}}_{Si} \\ &= \mathbf{F}_{Si}^{T-1}\,(\mathbf{E}_S)'_S\,\mathbf{F}_{Si}^{-1} - \tfrac{1}{2}\,(\widehat{\mathbf{L}}_{Si}^T\,\widehat{\mathbf{C}}_{Se} + \widehat{\mathbf{C}}_{Se}\,\widehat{\mathbf{L}}_{Si})\,, \end{aligned} \tag{3.77}$$

where, moreover, the transport property and the additive composition of the contravariant strain rates are exploited (cf. appendix B.2). By insertion of the result into equation (3.76), one finally obtains

$$\begin{aligned}(\mathcal{W}^S)'_S = \Big[\frac{\partial \mathcal{W}^S_{EQ}}{\partial \mathbf{E}_S} + \sum_{n=1}^{N} (\mathbf{F}^{-1}_{Si})_n \frac{\partial \mathcal{W}^S_{NEQ}}{\partial (\widehat{\mathbf{\Gamma}}_{Se})_n} (\mathbf{F}^{T-1}_{Si})_n\Big] \cdot (\mathbf{E}_S)'_S - \\ - \sum_{n=1}^{N} \frac{\partial \mathcal{W}^S_{NEQ}}{\partial (\widehat{\mathbf{\Gamma}}_{Se})_n} \cdot [(\widehat{\mathbf{C}}_{Se})_n (\widehat{\mathbf{L}}_{Si})_n]\,.\end{aligned} \tag{3.78}$$

Herein, the second term has been simplified utilizing the symmetry properties of $\widehat{\mathbf{C}}_{Se}$ and $\partial \mathcal{W}^S_{NEQ}/\partial \widehat{\mathbf{\Gamma}}_{Se}$, which yields the scalar identity

$$\frac{\partial \mathcal{W}^S_{NEQ}}{\partial \widehat{\mathbf{\Gamma}}_{Se}} \cdot (\widehat{\mathbf{L}}^T_{Si}\, \widehat{\mathbf{C}}_{Se}) = \frac{\partial \mathcal{W}^S_{NEQ}}{\partial \widehat{\mathbf{\Gamma}}_{Se}} \cdot (\widehat{\mathbf{C}}_{Se}\, \widehat{\mathbf{L}}_{Si})\,. \tag{3.79}$$

Next, recalling the evaluation procedure of the *Clausius-Planck* inequality of section 3.1.4 together with $(\mathcal{W}^S)'_S$ of equation (3.78), the expression for the determination of the solid extra stress tensor in terms of the reference configuration is given by

$$\Big[\mathbf{S}^S_E - \underbrace{\frac{\partial \mathcal{W}^S_{EQ}}{\partial \mathbf{E}_S}}_{\mathbf{S}^S_{EQ}} - \underbrace{\sum_{n=1}^{N} \overbrace{(\mathbf{F}^{-1}_{Si})_n \frac{\partial \mathcal{W}^S_{NEQ}}{(\widehat{\mathbf{\Gamma}}_{Se})_n} (\mathbf{F}^{T-1}_{Si})_n}^{\mathbf{S}^S_n}}_{\mathbf{S}^S_{NEQ}}\Big] \cdot (\mathbf{E}_S)'_S \geq 0 \quad \forall\, (\mathbf{E}_S)'_S\,. \tag{3.80}$$

In regard of the additive stress composition associated with the parallel rheological structure of the generalized *Maxwell* model (cf. box (3.39)) and the fact that the above expression sufficiently fulfills the dissipation inequality for arbitrary values of the free variable $(\mathbf{E}_S)'_S$ if the term in brackets vanishes, the following relations are postulated[14]:

$$\mathbf{S}^S_E := \mathbf{S}^S_{EQ} + \mathbf{S}^S_{NEQ} \quad \text{with} \quad \mathbf{S}^S_{EQ} := \frac{\partial \mathcal{W}^S_{EQ}}{\partial \mathbf{E}_S}\,, \quad \mathbf{S}^S_{NEQ} := \sum_{n=1}^{N} \mathbf{S}^S_n = \sum_{n=1}^{N} \frac{\partial \mathcal{W}^S_{NEQ}}{\partial (\mathbf{E}_{Se})_n}\,. \tag{3.81}$$

Moreover, following section 2.3.1, in particular box (2.117) and the concept of dual vari-

[14] The change of the variables in the derivatives of $\mathcal{W}^S_{NEQ}$ is carried out as follows (here for $N = 1$):

$$\mathbf{S}^S_{NEQ} = \mathbf{F}^{-1}_{Si} \frac{\partial \mathcal{W}^S_{NEQ}}{\partial \widehat{\mathbf{\Gamma}}_{Se}} \mathbf{F}^{T-1}_{Si} = (\mathbf{F}^{-1}_{Si} \otimes \mathbf{F}^{-1}_{Si})^{\overset{23}{T}} \frac{\partial \mathcal{W}^S_{NEQ}}{\partial \widehat{\mathbf{\Gamma}}_{Se}} = (\mathbf{F}^{-1}_{Si} \otimes \mathbf{F}^{-1}_{Si})^{\overset{23}{T}} \Big(\frac{\partial \mathbf{E}_{Se}}{\partial \widehat{\mathbf{\Gamma}}_{Se}}\Big)^T \frac{\partial \mathcal{W}^S_{NEQ}}{\partial \mathbf{E}_{Se}}$$

$$\text{with} \quad \begin{cases} \Big(\frac{\partial \mathbf{E}_{Se}}{\partial \widehat{\mathbf{\Gamma}}_{Se}}\Big)^T = \Big[\frac{\partial (\mathbf{F}^T_{Si}\, \widehat{\mathbf{\Gamma}}_{Se}\, \mathbf{F}_{Si})}{\partial \widehat{\mathbf{\Gamma}}_{Se}}\Big]^T = \big[(\mathbf{F}^T_{Si} \otimes \mathbf{F}^T_{Si})^{\overset{23}{T}}\big]^T = (\mathbf{F}_{Si} \otimes \mathbf{F}_{Si})^{\overset{23}{T}}\,, \\ (\mathbf{F}^{-1}_{Si} \otimes \mathbf{F}^{-1}_{Si})^{\overset{23}{T}} (\mathbf{F}_{Si} \otimes \mathbf{F}_{Si})^{\overset{23}{T}} = (\mathbf{F}^{-1}_{Si}\, \mathbf{F}_{Si} \otimes \mathbf{F}^{-1}_{Si}\, \mathbf{F}_{Si})^{\overset{23}{T}} = (\mathbf{I} \otimes \mathbf{I})^{\overset{23}{T}} = \overset{4}{\mathbf{I}} \end{cases}$$

$$\longrightarrow \quad \mathbf{S}^S_{NEQ} = \mathbf{S}^S_1 = \mathbf{F}^{-1}_{Si} \frac{\partial \mathcal{W}^S_{NEQ}}{\partial \widehat{\mathbf{\Gamma}}_{Se}} \mathbf{F}^{T-1}_{Si} = \frac{\partial \mathcal{W}^S_{NEQ}}{\partial \mathbf{E}_{Se}} \quad \text{q. e. d.}$$

ables (2.118), the intermediate and *Kirchhoff* solid extra stress tensors are found as

$$
\begin{aligned}
&(\widehat{\boldsymbol{\tau}}^{\,S}_{EQ})_n := \frac{\partial \mathcal{W}^S_{EQ}}{\partial (\widehat{\boldsymbol{\Gamma}}_S)_n}\,, \quad (\widehat{\boldsymbol{\tau}}^{\,S}_{NEQ})_n := \widehat{\boldsymbol{\tau}}^{\,S}_n := \frac{\partial \mathcal{W}^S_{NEQ}}{\partial (\widehat{\boldsymbol{\Gamma}}_{Se})_n}\,, \\
&\boldsymbol{\tau}^S_E := \boldsymbol{\tau}^S_{EQ} + \boldsymbol{\tau}^S_{NEQ} \quad \text{with} \quad \boldsymbol{\tau}^S_{EQ} := \frac{\partial \mathcal{W}^S_{EQ}}{\partial \mathbf{A}_S}\,, \quad \boldsymbol{\tau}^S_{NEQ} := \sum_{n=1}^{N} \boldsymbol{\tau}^S_n = \sum_{n=1}^{N} \frac{\partial \mathcal{W}^S_{NEQ}}{\partial (\mathbf{A}_{Se})_n}\,.
\end{aligned}
\tag{3.82}
$$

Note in passing that in the general case of multiple *Maxwell* elements ($N > 1$), the individual intermediate stress tensors cannot be added to a total solid extra stress tensor $\widehat{\boldsymbol{\tau}}^{\,S}_E$, as they are not referring to one and the same configuration.

To continue, the second term of equation (3.78) inserted into the *Clausius-Planck* inequality represents the intrinsic dissipative solid part remaining in the residual inequality. To make this point clearer, one can alternatively proceed from the first term of the basic residual inequality (3.34). Following this, with $\boldsymbol{\mathcal{Q}}^S_n = (\mathbf{F}_{Si})_n$ and multiplied by $J_S > n^S_{0S} > 0$, the original dissipative solid term becomes

$$
-\rho^S \sum_{n=1}^{N} \frac{\partial \psi^S}{\partial \boldsymbol{\mathcal{Q}}^S_n} \cdot (\boldsymbol{\mathcal{Q}}^S_n)'_S \geq 0 \quad \longrightarrow \quad -\rho^S_{0S} \sum_{n=1}^{N} \frac{\partial \psi^S}{\partial (\mathbf{F}_{Si})_n} \cdot [(\mathbf{F}_{Si})_n]'_S \geq 0\,. \tag{3.83}
$$

Then, utilizing the objective non-equilibrium strain energy $(3.65)_2$ and the definition of the non-equilibrium intermediate stresses $(3.82)_1$, which are conjugate to $(\widehat{\boldsymbol{\Gamma}}_{Se})_n$, yields

$$
\begin{aligned}
-\sum_{n=1}^{N} \frac{\partial \mathcal{W}^S_{NEQ}[(\widehat{\boldsymbol{\Gamma}}_{Se})_n]}{\partial (\mathbf{F}_{Si})_n} \cdot [(\mathbf{F}_{Si})_n]'_S &= -\sum_{n=1}^{N} \Big[\frac{\partial (\widehat{\boldsymbol{\Gamma}}_{Se})_n}{\partial (\mathbf{F}_{Si})_n}\Big]^T \frac{\partial \mathcal{W}^S_{NEQ}}{\partial [(\widehat{\boldsymbol{\Gamma}}_{Se})_n]} \cdot [(\mathbf{F}_{Si})_n]'_S = \\
&= -\sum_{n=1}^{N} \widehat{\boldsymbol{\tau}}^{\,S}_n \cdot \frac{\partial (\widehat{\boldsymbol{\Gamma}}_{Se})_n}{\partial (\mathbf{F}_{Si})_n} [(\widehat{\mathbf{L}}_{Si})_n (\mathbf{F}_{Si})_n] \geq 0\,.
\end{aligned}
\tag{3.84}
$$

The right hand side of the scalar product is then rewritten using the derivative[15]

$$
\frac{\partial \widehat{\boldsymbol{\Gamma}}_{Se}}{\partial \mathbf{F}_{Si}} = \tfrac{1}{2} \frac{\partial \widehat{\mathbf{C}}_{Se}}{\partial \mathbf{F}_{Si}} = \tfrac{1}{2} \frac{\partial (\mathbf{F}^{T-1}_{Si} \mathbf{C}_S \mathbf{F}^{-1}_{Si})}{\partial \mathbf{F}_{Si}} = -\tfrac{1}{2} \left[(\mathbf{F}^{T-1}_{Si} \otimes \widehat{\mathbf{C}}_{Se})^{\overset{24}{T}} + (\widehat{\mathbf{C}}_{Se} \otimes \mathbf{F}^{T-1}_{Si})^{\overset{23}{T}} \right], \tag{3.85}
$$

which, multiplied by the inelastic solid material velocity gradient $(\mathbf{F}_{Si})'_S = \widehat{\mathbf{L}}_{Si} \mathbf{F}_{Si}$ (cf. equation (2.54)), results in

$$
-\tfrac{1}{2} \left[(\mathbf{F}^{T-1}_{Si} \otimes \widehat{\mathbf{C}}_{Se})^{\overset{24}{T}} + (\widehat{\mathbf{C}}_{Se} \otimes \mathbf{F}^{T-1}_{Si})^{\overset{23}{T}} \right] (\widehat{\mathbf{L}}_{Si} \mathbf{F}_{Si}) = -\tfrac{1}{2} (\widehat{\mathbf{L}}^T_{Si} \widehat{\mathbf{C}}_{Se} + \widehat{\mathbf{C}}_{Se} \widehat{\mathbf{L}}_{Si})\,. \tag{3.86}
$$

[15] In particular, it holds (cf. appendix A)

$$
\frac{\partial (\mathbf{F}^{T-1}_{Si} \mathbf{C}_S \mathbf{F}^{-1}_{Si})}{\partial \mathbf{F}_{Si}} = \frac{\partial (\mathbf{F}^{T-1}_{Si} \mathbf{C}_S \mathbf{F}^{-1}_{Si})}{\partial \mathbf{F}^{-1}_{Si}} \frac{\partial \mathbf{F}^{-1}_{Si}}{\partial \mathbf{F}_{Si}} = -(\mathbf{F}^{T-1}_{Si} \otimes \mathbf{F}^{T-1}_{Si} \mathbf{C}_S \mathbf{F}^{-1}_{Si})^{\overset{24}{T}} - (\mathbf{F}^{T-1}_{Si} \mathbf{C}_S \mathbf{F}^{-1}_{Si} \otimes \mathbf{F}^{T-1}_{Si})^{\overset{23}{T}}
$$

$$
\text{with} \quad \frac{\partial (\mathbf{F}^{T-1}_{Si} \mathbf{C}_S \mathbf{F}^{-1}_{Si})}{\partial \mathbf{F}^{-1}_{Si}} = (\mathbf{I} \otimes \mathbf{C}_S \mathbf{F}^{-1}_{Si})^{\overset{24}{T}} + (\mathbf{F}^{T-1}_{Si} \mathbf{C}_S \otimes \mathbf{I})^{\overset{23}{T}}\,, \quad \frac{\partial \mathbf{F}^{-1}_{Si}}{\partial \mathbf{F}_{Si}} = -(\mathbf{F}^{-1}_{Si} \otimes \mathbf{F}^{T-1}_{Si})^{\overset{23}{T}}\,.
$$

By insertion into relation (3.84) and use of the symmetry of the non-equilibrium intermediate stresses, $\widehat{\boldsymbol{\tau}}{}^S_n = (\widehat{\boldsymbol{\tau}}{}^S_n)^T$, one likewise recovers the residual solid term as if equation (3.78) is inserted into the dissipation inequality, viz.,

$$\sum_{n=1}^{N} \widehat{\boldsymbol{\tau}}{}^S_n \cdot [(\widehat{\mathbf{C}}_{Se})_n \, (\widehat{\mathbf{L}}_{Si})_n] = \sum_{n=1}^{N} [(\widehat{\mathbf{C}}_{Se})_n \, \widehat{\boldsymbol{\tau}}{}^S_n] \cdot (\widehat{\mathbf{L}}_{Si})_n \geq 0 \,. \tag{3.87}$$

For the considered special case of isotropic skeleton properties, $(\widehat{\mathbf{C}}_{Se})_n$ and $\widehat{\boldsymbol{\tau}}{}^S_n$ commute yielding the symmetry of the *Mandel* stress tensors[16] $(\widehat{\mathbf{C}}_{Se})_n \, \widehat{\boldsymbol{\tau}}{}^S_n$. Consequently, only the symmetric part of the inelastic spatial velocity gradients $(\widehat{\mathbf{D}}_{Si})_n = \frac{1}{2}\,[(\widehat{\mathbf{L}}_{Si})_n + (\widehat{\mathbf{L}}{}^T_{Si})_n]$ complies and thus, the isotropic representation of the solid residual inequality becomes

$$\sum_{n=1}^{N} \widehat{\boldsymbol{\tau}}{}^S_n \cdot [(\widehat{\mathbf{C}}_{Se})_n \, (\widehat{\mathbf{D}}_{Si})_n] = \sum_{n=1}^{N} \widehat{\boldsymbol{\tau}}{}^S_n \cdot \{(\widehat{\mathbf{C}}_{Se})_n \, [(\widehat{\boldsymbol{\Gamma}}_{Si})^{\triangle}_{Si}]_n\} \geq 0 \,. \tag{3.88}$$

By use of the respective transport mechanisms, the corresponding relations of the reference and the intermediate configurations are then found as

$$\sum_{n=1}^{N} \mathbf{S}^S_n \cdot \{\mathbf{C}_S \, (\mathbf{C}^{-1}_{Si})_n \, [(\mathbf{E}_{Si})_n]'_S\} \geq 0 \,, \quad \sum_{n=1}^{N} \boldsymbol{\tau}^S_n \cdot \{(\mathbf{B}_{Se})_n \, [(\mathbf{A}_{Si})_n]^{\triangle}_S\} \geq 0 \,. \tag{3.89}$$

From the above inequalities, it is obvious that in the case of isotropy the inelastic deformation tensors $(\mathbf{C}_{Si})_n = (\mathbf{U}_{Si})^2_n$ take over the role of the strain-equivalent internal variables as they are invariant due to any rotations superimposed on the intermediate configurations. For the case of singlephasic materials comparable results can be found, e. g., in the works of Huber & Tsakmakis [95], Reese & Govindjee [151], and Reese [149].

Remark: Note that the residual solid inequality can also be expressed by means of covariant strain measures by exploiting the special property of the deformation velocities, which have a co- as well as a contravariant representation in terms of convective coordinates (see equations (2.62)). From the kinematical relations presented in section 2.2.3, it is easily deduced that

$$(\widehat{\mathbf{D}}_{Si})_n = [(\widehat{\mathbf{K}}_{Si})^{\triangledown}_{Si}]_n = -\tfrac{1}{2}\,(\mathbf{F}^{-1}_{Se})_n \, [(\mathbf{B}_{Se})_n]^{\triangledown}_S \, (\mathbf{F}^{T-1}_{Se})_n = -\tfrac{1}{2}\,(\widehat{z}^{kl})'_S \, \widehat{\mathbf{z}}_k \otimes \widehat{\mathbf{z}}_l \,. \tag{3.90}$$

Insertion into (3.88) and substitution of the non-equilibrium intermediate stresses with the elastic covariant pull-backs of the *Kirchhoff* solid extra stresses, $\widehat{\boldsymbol{\tau}}{}^S_n = (\mathbf{F}^{-1}_{Se})_n \, \boldsymbol{\tau}^S_n \, (\mathbf{F}^{T-1}_{Se})_n$, yields the alternative representation

$$-\tfrac{1}{2} \sum_{n=1}^{N} \boldsymbol{\tau}^S_n \cdot [\mathcal{L}_{\mathbf{v}_S}(\mathbf{B}_{Se})_n \, (\mathbf{B}^{-1}_{Se})_n] \geq 0 \,, \tag{3.91}$$

[16] Proceeding from the isotropic strain energy $(3.75)_2$, one finds in analogy to footnote 10 on page 36

$$\widehat{\mathbf{C}}_{Se} \, \frac{\partial \mathcal{W}^S_{NEQ}}{\partial \widehat{\mathbf{C}}_{Se}} = \widehat{\mathbf{U}}_{Se} \, \frac{\partial \mathcal{W}^S_{NEQ}}{\partial \widehat{\mathbf{C}}_{Se}} \, \widehat{\mathbf{U}}_{Se} = \frac{\partial \mathcal{W}^S_{NEQ}}{\partial \widehat{\mathbf{C}}_{Se}} \, \widehat{\mathbf{C}}_{Se} \quad \Leftrightarrow \quad (\widehat{\mathbf{C}}_{Se} \, \widehat{\boldsymbol{\tau}}_{Se})^T = \widehat{\mathbf{C}}_{Se} \, \widehat{\boldsymbol{\tau}}_{Se} \,.$$

where the covariant *Lie* time derivative in the form of $\mathcal{L}_{\mathbf{v}_S}(\mathbf{B}_{Se})_n = [(\mathbf{B}_{Se})_n]_S^{\triangledown}$ (cf. equation $(2.65)_1$) is frequently used. Note that this representation of the residual inequality is expedient to find evolution equations that allow for an efficient algorithmic treatment based on an *operator split* and an *exponential mapping* as originally proposed by Weber & Anand [188] in the context of finite elastoplasticity. In the framework of finite viscoelasticity such a strategy is successfully applied by Reese & Govindjee [151]. ■

3.2.3 An Appropriate Porous Media Viscoelasticity Law

In the following, the nonlinear model of the viscoelastic porous solid matrix will be closed by specifying the solid strain-energy function $\mathcal{W}^S$ and the evolution equations for the internal variables consistent with the conditions and assumptions discussed in the previous section. As large deformations of a porous solid matrix are accompanied by considerably larger distortions of the pore space, the macroscopic response of the entire material can be extremely nonlinear. These nonlinearities are particularly caused by deformation-induced instabilities and stiffening effects of the skeleton structure, such as buckling, alignment, or compaction of pore edges and walls, which can be very well observed in high-porosity foams (cf. section 5.1). Thus, a suitable material formulation must be provided that can be successfully correlated with distinct nonlinear experimental observations. This draws the attention to an established class of constitutive models of finite isotropic elasticity, the so-called *Ogden*-type formulations, originally proposed by Ogden [135, 136] for the description of the nonlinear stress-strain response of rubber (cf. Treloar [177]).

For an isotropic hyperelastic solid skeleton, a general form of such an *Ogden*-type formulation, which *a priori* satisfies the normalization assumption $(3.66)_1$, is given by

$$\mathcal{W}^S(I_{\mathbf{F}_S}, II_{\mathbf{F}_S}, III_{\mathbf{F}_S}) = \sum_{m=1}^{M_I} \frac{\overline{\mu}_m}{\alpha_m} \left(I_{\mathbf{F}_S}^{\alpha_m} - 3\right) + \sum_{m=1}^{M_{II}} \frac{\overline{\overline{\mu}}_m}{\beta_m} \left(II_{\mathbf{F}_S}^{\beta_m} - 3\right) + \mathcal{U}^S(III_{\mathbf{F}_S})\,. \tag{3.92}$$

Typically, the *Ogden* strain energy is expressed in terms of the principal invariants of the solid deformation gradient $\mathbf{F}_S$ rather than of the deformation tensors $\mathbf{C}_S$ or $\mathbf{B}_S$, namely

$$I_{\mathbf{F}_S} = \operatorname{tr} \mathbf{F}_S\,, \quad II_{\mathbf{F}_S} = \operatorname{tr} (\operatorname{cof} \mathbf{F}_S)\,, \quad III_{\mathbf{F}_S} = J_S = \det \mathbf{F}_S\,, \tag{3.93}$$

which are of course identical to those of the right or left solid stretch tensors $\mathbf{U}_S$ or $\mathbf{V}_S$, respectively (cf. section 2.2.4)[17]. Moreover, in equation (3.92), $\overline{\mu}_m$, $\alpha_m \neq 0$ and $\overline{\overline{\mu}}_m$, $\beta_m \neq 0$ are material constants, $M_I, M_{II} \in \mathbb{N}^+$ denote positive integers, and $\mathcal{U}^S$ represents a convex volumetric response function describing the compressible material behavior, where $\mathcal{U}^S(III_{\mathbf{F}_S} = 1) = 0$. As negative combinations of the *Ogden* parameters are generally valid, in order to have $\mathcal{W}^S$ strictly positive, the following sufficient conditions are apparent (Ogden [136]):

$$\overline{\mu}_m\, \alpha_m > 0\,, \qquad \overline{\overline{\mu}}_m\, \beta_m > 0\,. \tag{3.94}$$

[17] Basically, the solid strain energy may be treated as a function of any three invariants of the skeleton deformation.

However, in regard to the stability requirements, it is easily recognized that $\mathcal{W}^S$ possesses a form similar to equation $(3.51)_2$ and hence, represents an additive polyconvex function provided that each term is convex in the associated variable. According to relations (3.52), this is guaranteed, if the respective second derivatives are positive semidefinite[18], which finally yields the essential restrictions (cf. also Ogden [137])

$$\begin{gathered} \overline{\mu}_m\,(\alpha_m-1)\geq 0\,, \qquad \overline{\overline{\mu}}_m\,(\beta_m-1)\geq 0 \\ \longrightarrow \quad \left\{ \begin{array}{llll} \overline{\mu}_m>0\,, & \alpha_m\geq 1 & \vee & \overline{\mu}_m<0\,,\ \alpha_m\leq 1\ \wedge\ \alpha_m\neq 0\,, \quad m=1,...,M_I\,, \\ \overline{\overline{\mu}}_m>0\,, & \beta_m\geq 1 & \vee & \overline{\overline{\mu}}_m<0\,,\ \beta_m\leq 1\ \wedge\ \beta_m\neq 0\,, \quad m=1,...,M_{II}\,. \end{array} \right. \end{gathered} \tag{3.95}$$

Moreover, following Ciarlet [32], the strain energy (3.92) fulfills the growth conditions in form of the coerciveness inequality (3.56) if $\mathcal{U}^S(J_S\to n_{0S}^S)\to+\infty$ is satisfied. Further particulars on the general requirements of $\mathcal{U}^S$ will be discussed later in this section.

Equally, the strain energy can be expressed by means of the principal stretches, which, for convenience, are represented by the square roots of the eigenvalues $\lambda_{S(k)}$ of $\mathbf{C}_S$ or $\mathbf{B}_S$, respectively, yielding the more common representation

$$\mathcal{W}^S(\lambda_{S(k)})=\sum_{m=1}^{M_I}\sum_{k=1}^{3}\frac{\overline{\mu}_m}{\alpha_m}\left(\lambda_{S(k)}^{\alpha_m/2}-1\right)+\tfrac{1}{2}\sum_{m=1}^{M_{II}}\sum_{\substack{k,l=1\\ l\neq k}}^{3}\frac{\overline{\overline{\mu}}_m}{\beta_m}\left[\left(\lambda_{S(k)}\,\lambda_{S(l)}\right)^{\beta_m/2}-2\right]+\mathcal{U}^S(J_S) \tag{3.96}$$

with $J_S=\sqrt{\lambda_{S(1)}\,\lambda_{S(2)}\,\lambda_{S(3)}}$ according to equations $(2.77)_3$ and $(2.78)_3$. A simplified version of this strain energy, which avoids products of eigenvalues, is proved to be very successful in describing the nonlinear large strain response of rubber-like materials (Ogden [138, 139]). Hence, we proceed from a reduced constitutive function of the form

$$\mathcal{W}^S(\lambda_{S(k)})=\mu^S\sum_{m=1}^{M_I}\Big(\sum_{k=1}^{3}\frac{\mu_m^*}{\alpha_m}\left(\lambda_{S(k)}^{\alpha_m/2}-1\right)-\mu_m^*\ln J_S\Big)+\overline{\mathcal{U}}^S(J_S)\,, \tag{3.97}$$

where $\mu^S>0$ is identified as the 1st *Lamé* constant, i. e., the conventional positive shear modulus of the linear theory, such that both $\mu_m^*=\overline{\mu}_m/\mu^S$ and α_m represent dimensionless, real-valued parameters. In this regard, by comparison with the geometrically linear theory[19], the downward compatibility to a linear *Hooke*an-type elasticity formulation is satisfied if

$$\sum_{m=1}^{M_I}\mu_m^*\,\alpha_m=2\,. \tag{3.98}$$

Moreover, in the strain-energy function (3.97), the additional logarithmic term is separated from $\mathcal{U}^S$ in order to make the unstrained reference state stress-free, independent of the actual choice of the volumetric extension term $\overline{\mathcal{U}}^S(J_S)$ (cf. Ogden [135]). Consequently,

[18] The positive semidefiniteness, e. g., of the first term with $I_{\mathbf{F}_S}^{\alpha_m}=(\mathbf{F}_S\cdot\mathbf{I})^{\alpha_m}>0$ is verified via

$$\frac{\overline{\mu}_m}{\alpha_m}\frac{\partial(\mathbf{F}_S\cdot\mathbf{I})^{\alpha_m}}{\partial\mathbf{F}_S\otimes\partial\mathbf{F}_S}\cdot(\mathbf{H}\otimes\mathbf{H})=\overline{\mu}_m\frac{\partial(\mathbf{F}_S\cdot\mathbf{I})^{\alpha_m-1}}{\partial\mathbf{F}_S}\cdot\mathbf{H}\,(\mathbf{H}\cdot\mathbf{I})=\overline{\mu}_m\,(\alpha_m-1)\,(\mathbf{F}_S\cdot\mathbf{I})^{\alpha_m-2}\,\|\mathbf{H}\|^2\geq 0\,.$$

[19] See the paragraph on linearized theories on page 79.

to further maintain polyconvexity, it must be additionally ensured that

$$\frac{\partial^2}{\partial J_S^2}\Big(-\sum_{m}^{M_I}\mu_m^*\,\ln J_S\Big)=\sum_{m}^{M_I}\mu_m^*\,\frac{1}{J_S^2}\geq 0\quad\longrightarrow\quad\sum_{m=1}^{M_I}\mu_m^*\geq 0\,. \tag{3.99}$$

Remark: In this context, it should be noted that the single *Ogden* parameters generally cannot be associated with a distinct physical meaning as μ_m^* represent the coefficients of a trivariate polynomial in the variables $\lambda_{S(k)}$ $(k=1,2,3)$, whereas the powers α_m govern the actual nonlinearity. The required number of polynomial terms in the strain-energy function determined by M_I depends on the complexity of the response of the considered material. It emerges that in the case of rubber-like materials a number of $M_I=3$ is sufficient to give an excellent correlation with the experimental data (Ogden [136, 139]). Moreover, by specific choices of the parameters μ_m^* and α_m, it turns out that the *Ogden* law comprises other well-known finite elasticity models (see table (3.100) below), such as the *Varga*, neo-*Hooke*, or *Mooney-Rivlin* model (cf. Mooney [125], Rivlin [152], Varga [186], and Treloar [177]).

model	M_I	μ_m^*	α_m
Varga	1	$\mu_1^*=2$	$\alpha_1=1$
neo-*Hooke*	1	$\mu_1^*=1$	$\alpha_1=2$
Mooney-Rivlin	2	$\mu_1^*-\mu_2^*=1$	$\alpha_1=2\,,\ \alpha_2=-2$

(3.100)

Moreover, it is worth mentioning that the *Ogden* model in the form of (3.97) incorporates as a special case the experimentally validated *Valanis-Landel hypothesis* (Valanis & Landel [185]), which claims the strain energy of rubber to be of an additive separable form, viz.:

$$\mathcal{W}^S(\lambda_{S(k)})=\mathcal{W}^S(\lambda_{S(1)})+\mathcal{W}^S(\lambda_{S(2)})+\mathcal{W}^S(\lambda_{S(3)})\,. \tag{3.101}$$

■

In a next step, a volumetric extension term $\overline{\mathcal{U}}^S(J_S)$ must be derived, such that the requirements depicted in box (3.103) are met. Therein, in regard to the classical definition of a positive ground-state solid bulk modulus, one has

$$\mathcal{K}^S:=\left.\frac{\partial^2\mathcal{W}^S}{\partial J_S^2}\right|_{\lambda_{S(k)}=1}=\tfrac{2}{3}\,\mu^S+\Lambda^S>0 \tag{3.102}$$

for physical reasons. Thus, the second *Lamé* constant must satisfy $\Lambda^S>-\frac{2}{3}\,\mu^S$. Of course the convexity condition $(3.103)_1$ yielding the stronger restriction $\Lambda^S\geq 0$ together with the first classical inequality $\mu^S>0$ renders the above inequality (3.102) redundant and moreover, embraces the natural assumption of a positive *Poisson*'s ratio. Following this, Eipper [64] extended the volumetric strain-energy function proposed by Ogden [135] to porous media problems through incorporation of the compaction point accounting for all conditions given in box (3.103) (see also Ehlers & Eipper [55]). The resulting volumetric

Conditions for the volumetric extension term

convexity condition:	$\dfrac{\partial^2 \overline{U}^S}{\partial J_S^2} \geq 0$	$\forall\, J_S > n_{0S}^S > 0$
growth conditions:	$\overline{U}^S \to +\infty\,, \quad \dfrac{\partial \overline{U}^S}{\partial J_S} \to -\infty$	as $J_S \to n_{0S}^S$
	$\overline{U}^S \to +\infty\,, \quad \dfrac{\partial \overline{U}^S}{\partial J_S} \to +\infty$	as $J_S \to +\infty$
normalization assumption:	$\overline{U}^S = 0\,, \quad \dfrac{\partial \overline{U}^S}{\partial J_S} = 0$	as $J_S = 1$
compatibility assumption:	$\left.\dfrac{\partial^2 \overline{U}^S}{\partial J_S^2}\right\vert_{J_S=1} =: \Lambda^S$	: 2nd *Lamé* constant

(3.103)

extension term and its derivatives read

$$
\begin{aligned}
\overline{U}^S &= \frac{\Lambda^S}{\gamma^S \left(\gamma^S - 1 + \frac{1}{[1-n_{0S}^S]^2}\right)} \left(J_S^{\gamma^S} - 1 - \gamma^S \, \ln \frac{J_S - n_{0S}^S}{1 - n_{0S}^S} + \gamma^S \, n_{0S}^S \, \frac{J_S - 1}{1 - n_{0S}^S} \right), \\
\frac{\partial \overline{U}^S}{\partial J_S} &= \frac{\Lambda^S}{\gamma^S - 1 + \frac{1}{[1-n_{0S}^S]^2}} \left(J_S^{\gamma^S - 1} - \frac{1}{J_S - n_{0S}^S} + \frac{n_{0S}^S}{1 - n_{0S}^S} \right), \\
\frac{\partial^2 \overline{U}^S}{\partial J_S^2} &= \frac{\Lambda^S}{\gamma^S - 1 + \frac{1}{[1-n_{0S}^S]^2}} \left((\gamma^S - 1)\, J_S^{\gamma^S - 2} + \frac{1}{(J_S - n_{0S}^S)^2} \right),
\end{aligned}
\tag{3.104}
$$

where γ^S represents an additional dimensionless solid parameter to govern the compressive stiffening behavior of the skeleton. From the second derivative $(3.104)_3$, it is apparent that $\gamma^S \geq 1$ must hold to satisfy the convexity condition. However, applied to real porous materials, it turns out that the stress increase towards the point of compaction is not sufficiently fast. Therefore, the formulation is improved by replacing the logarithmic term by an inverse power expression[20]. Following this, the new volumetric response function and its derivatives take the form

$$
\begin{aligned}
\overline{U}^S &= \frac{\Lambda^S}{\gamma^S \left(\gamma^S - 1 + \frac{\gamma^S + 1}{[1-n_{0S}^S]^2}\right)} \left(J_S^{\gamma^S} - 2 + \left[\frac{1 - n_{0S}^S}{J_S - n_{0S}^S}\right]^{\gamma^S} + \gamma^S \, n_{0S}^S \, \frac{J_S - 1}{1 - n_{0S}^S} \right), \\
\frac{\partial \overline{U}^S}{\partial J_S} &= \frac{\Lambda^S}{\gamma^S - 1 + \frac{\gamma^S + 1}{[1-n_{0S}^S]^2}} \left(J_S^{\gamma^S - 1} - \frac{(1 - n_{0S}^S)^{\gamma^S}}{(J_S - n_{0S}^S)^{\gamma^S + 1}} + \frac{n_{0S}^S}{1 - n_{0S}^S} \right), \\
\frac{\partial^2 \overline{U}^S}{\partial J_S^2} &= \frac{\Lambda^S}{\gamma^S - 1 + \frac{\gamma^S + 1}{[1-n_{0S}^S]^2}} \left((\gamma^S - 1)\, J_S^{\gamma^S - 2} + (\gamma^S + 1) \, \frac{(1 - n_{0S}^S)^{\gamma^S}}{(J_S - n_{0S}^S)^{\gamma^S + 2}} \right),
\end{aligned}
\tag{3.105}
$$

[20] Volumetric strain energies including some logarithm of the deformation gradient are commonly used for the description of *nearly incompressible* materials. For references, see, e. g., Hartmann & Neff [83].

where likewise convexity is guaranteed for $\gamma^S \geq 1$. Thus, proceeding from the *Ogden* strain-energy function (3.97) in combination with the volumetric extension term $(3.105)_1$, the equilibrium response of the solid skeleton is appropriately described by the formulation given in box (3.106). Therein, the additional subscript $(\,\cdot\,)_0$ indicates the belonging of

Equilibrium strain energy of the solid skeleton

$$\mathcal{W}^S_{EQ}(\mathbf{C}_S) = \overline{\mathcal{W}}^S_{EQ}(\lambda_{S(k)}) + \overline{\mathcal{U}}^S_{EQ}(J_S) \quad \text{with}$$

$$\overline{\mathcal{W}}^S_{EQ} = \mu^S_0 \sum_{m=1}^{M_0} \Big(\sum_{k=1}^{3} \frac{\mu^*_{0(m)}}{\alpha_{0(m)}} \left(\lambda_{S(k)}^{\alpha_{0(m)}/2} - 1\right) - \mu^*_{0(m)} \ln J_S \Big) \tag{3.106}$$

$$\overline{\mathcal{U}}^S_{EQ} = \frac{\Lambda^S_0}{\gamma^S_0 \left(\gamma^S_0 - 1 + \frac{\gamma^S_0 + 1}{[1 - n^S_{0S}]^2}\right)} \Big(J_S^{\gamma^S_0} - 2 + \Big[\frac{1 - n^S_{0S}}{J_S - n^S_{0S}}\Big]^{\gamma^S_0} + \gamma^S_0\, n^S_{0S}\, \frac{J_S - 1}{1 - n^S_{0S}} \Big)$$

the material parameters to the equilibrium branch associated with the single spring of the generalized *Maxwell* model (see box (3.39)). The hyperelastic equilibrium solid extra stress tensor of the reference configuration is then computed from

$$\mathbf{S}^S_{EQ} = \frac{\partial \mathcal{W}^S_{EQ}}{\partial \mathbf{E}_S} = 2\, \frac{\partial \mathcal{W}^S_{EQ}}{\partial \mathbf{C}_S} = 2 \Big(\sum_{k=1}^{3} \frac{\partial \overline{\mathcal{W}}^S_{EQ}}{\partial \lambda_{S(k)}} \frac{\partial \lambda_{S(k)}}{\partial \mathbf{C}_S} + \frac{\partial \overline{\mathcal{U}}^S_{EQ}}{\partial J_S} \frac{\partial J_S}{\partial \mathbf{C}_S} \Big), \tag{3.107}$$

so that with the partial derivatives (2.96), $(3.105)_2$, and[21]

$$\frac{\partial \overline{\mathcal{W}}^S_{EQ}}{\partial \lambda_{S(k)}} = \mu^S_0 \sum_{m=1}^{M_0} \tfrac{1}{2}\, \mu^*_{0(m)}\, \lambda^{-1}_{S(k)} \left(\lambda_{S(k)}^{\alpha_{0(m)}/2} - 1\right), \tag{3.108}$$

the equilibrium 2nd *Piola-Kirchhoff* stress finally becomes

$$\begin{aligned} \mathbf{S}^S_{EQ} = \mu^S_0 \sum_{m=1}^{M_0} \sum_{k=1}^{3} \mu^*_{0(m)}\, \lambda^{-1}_{S(k)} \left(\lambda_{S(k)}^{\alpha_{0(m)}/2} - 1\right) \mathbf{M}_{S(k)} + \\ + \frac{\Lambda^S_0}{\gamma^S_0 - 1 + \frac{\gamma^S_0 + 1}{[1 - n^S_{0S}]^2}} \Big(J_S^{\gamma^S_0} - \frac{J_S\,(1 - n^S_{0S})^{\gamma^S_0}}{(J_S - n^S_{0S})^{\gamma^S_0 + 1}} + \frac{J_S\, n^S_{0S}}{1 - n^S_{0S}} \Big) \mathbf{C}_S^{-1}\,. \end{aligned} \tag{3.109}$$

The corresponding stress tensor of the current frame results from a covariant push-forward

[21] Moreover, the following derivatives of the solid *Jacobi*an are used (see also appendix A):

$$\frac{\partial J_S}{\partial \lambda_{S(k)}} = \frac{\partial \sqrt{\lambda_{S(j)}\, \lambda_{S(k)}\, \lambda_{S(l)}}}{\partial \lambda_{S(k)}} = \tfrac{1}{2}\, \frac{\lambda_{S(j)}\, \lambda_{S(l)}}{\sqrt{\lambda_{S(j)}\, \lambda_{S(k)}\, \lambda_{S(l)}}} = \tfrac{1}{2}\, \frac{1}{\lambda_{S(k)}}\, J_S\,, \quad \{j \neq k \neq l \neq j\} = 1,2,3\,,$$

$$\frac{\partial J_S}{\partial \mathbf{C}_S} = \frac{\partial \sqrt{\det \mathbf{C}_S}}{\partial \mathbf{C}_S} = \tfrac{1}{2}\, \frac{1}{\sqrt{\det \mathbf{C}_S}}\, \mathrm{cof}\, \mathbf{C}_S = \tfrac{1}{2}\, J_S\, \mathbf{C}_S^{-1} \quad \text{with} \quad \mathrm{cof}\, \mathbf{C}_S = (\det \mathbf{C}_S)\, \mathbf{C}_S^{-1}\,.$$

of $\mathbf{S}^S_{EQ}$ (3.109) or from the related derivatives $(3.82)_2$ or $(2.108)_1$ (in the isotropic case):

$$\boldsymbol{\tau}^S_{EQ} = \mathbf{F}_S\,\mathbf{S}^S_{EQ}\,\mathbf{F}_S^T = \frac{\partial \mathcal{W}^S_{EQ}}{\partial \mathbf{A}_S} = 2\,\mathbf{B}_S\,\frac{\partial \mathcal{W}^S_{EQ}}{\partial \mathbf{B}_S} = 2\,\frac{\partial \mathcal{W}^S_{EQ}}{\partial \mathbf{B}_S}\,\mathbf{B}_S\,. \tag{3.110}$$

Thus, the equilibrium *Kirchhoff* solid extra stress is found as

$$\begin{aligned}\boldsymbol{\tau}^S_{EQ} = \mu^S_0 \sum_{m=1}^{M_0}\sum_{k=1}^{3} \mu^*_{0(m)}\,\big(\lambda^{\alpha_{0(m)}/2}_{S(k)} - 1\big)\,\mathbf{N}_{S(k)} + \\ + \frac{\Lambda^S_0}{\gamma^S_0 - 1 + \frac{\gamma^S_0+1}{[1-n^S_{0S}]^2}}\Big(J_S^{\gamma^S_0} - \frac{J_S\,(1-n^S_{0S})^{\gamma^S_0}}{(J_S - n^S_{0S})^{\gamma^S_0+1}} + \frac{J_S\,n^S_{0S}}{1-n^S_{0S}}\Big)\,\mathbf{I}\,.\end{aligned} \tag{3.111}$$

In addition, although not explicitly required, the equilibrium solid extra stress tensor related to the nth intermediate configuration may be determined from

$$(\widehat{\boldsymbol{\tau}}^S_{EQ})_n = (\mathbf{F}_{Si})_n\,\mathbf{S}^S_{EQ}\,(\mathbf{F}^T_{Si})_n = \frac{\partial \mathcal{W}^S_{EQ}}{\partial (\widehat{\boldsymbol{\Gamma}}_S)_n} = (\mathbf{F}^{-1}_{Se})_n\,\boldsymbol{\tau}^S_{EQ}\,(\mathbf{F}^{T-1}_{Se})_n\,. \tag{3.112}$$

Analogously, the stress tensors associated with the springs in the *Maxwell* elements are obtained from appropriate elastic potentials similar to the one of the equilibrium part given in box (3.106). Thus, proceeding from the non-equilibrium strain-energy function

Non-equilibrium strain energy of the solid skeleton

$$\begin{aligned}\mathcal{W}^S_{NEQ}[(\widehat{\mathbf{C}}_{Se})_n] &= \overline{\mathcal{W}}^S_{NEQ}[(\lambda_{Se(k)})_n] + \overline{\mathcal{U}}^S_{NEQ}[(J_{Se})_n] \quad \text{with}\\
\overline{\mathcal{W}}^S_{NEQ} &= \sum_{n=1}^{N}\mu^S_n \sum_{m=1}^{M_n}\Big(\sum_{k=1}^{3}\frac{\mu^*_{n(m)}}{\alpha_{n(m)}}\,\big[(\lambda^{\alpha_{n(m)}/2}_{Se(k)})_n - 1\big] - \mu^*_{n(m)}\ln(J_{Se})_n\Big)\\
\overline{\mathcal{U}}^S_{NEQ} &= \sum_{n=1}^{N}\frac{\Lambda^S_n}{\gamma^S_n\,\big(\gamma^S_n - 1 + \frac{\gamma^S_n+1}{[1-(n^S_{Si})_n]^2}\big)}\\
&\qquad\Big((J^{\gamma^S_n}_{Se})_n - 2 + \Big[\frac{1-(n^S_{Si})_n}{(J_{Se})_n - (n^S_{Si})_n}\Big]^{\gamma^S_n} + \gamma^S_n\,(n^S_{Si})_n\,\frac{(J_{Se})_n - 1}{1-(n^S_{Si})_n}\Big)\end{aligned} \tag{3.113}$$

depicted in box (3.113), where the inelastic solidities $(n^S_{Si})_n$ serve as constant reference values for the elastic volume deformations, the individual intermediate and the total *Kirchhoff* non-equilibrium solid extra stress tensors take the form

$$\begin{aligned}\widehat{\boldsymbol{\tau}}^S_n = \mu^S_n \sum_{m=1}^{M_n}\sum_{k=1}^{3}\mu^*_{n(m)}\,(\lambda^{-1}_{Se(k)})_n\,\big[(\lambda^{\alpha_{n(m)}/2}_{Se(k)})_n - 1\big]\,(\widehat{\mathbf{M}}_{Se(k)})_n + \\ + \frac{\Lambda^S_n}{\gamma^S_n - 1 + \frac{\gamma^S_n+1}{[1-(n^S_{Si})_n]^2}}\Big((J^{\gamma^S_n}_{Se})_n - \frac{(J_{Se})_n\,[1-(n^S_{Si})_n]^{\gamma^S_n}}{[(J_{Se})_n - (n^S_{Si})_n]^{\gamma^S_n+1}} + \frac{(J_{Se})_n\,(n^S_{Si})_n}{1-(n^S_{Si})_n}\Big)\,(\widehat{\mathbf{C}}^{-1}_{Se})_n\,,\end{aligned} \tag{3.114}$$

$$\boldsymbol{\tau}^S_{NEQ} = \sum_{n=1}^{N} \Big[\mu^S_n \sum_{m=1}^{M_n} \sum_{k=1}^{3} \mu^*_{n(m)} \left[(\lambda^{\alpha_{n(m)}/2}_{Se(k)})_n - 1 \right] (\mathbf{N}_{Se(k)})_n + \\ + \frac{\Lambda^S_n}{\gamma^S_n - 1 + \frac{\gamma^S_n + 1}{[1-(n^S_{Si})_n]^2}} \Big((J^{\gamma^S_n}_{Se})_n - \frac{(J_{Se})_n \left[1 - (n^S_{Si})_n \right]^{\gamma^S_n}}{\left[(J_{Se})_n - (n^S_{Si})_n \right]^{\gamma^S_n + 1}} + \frac{(J_{Se})_n \, (n^S_{Si})_n}{1 - (n^S_{Si})_n} \Big) \mathbf{I} \Big] . \tag{3.115}$$

By use of the covariant transport properties of the stress tensors (2.117), the corresponding total overstress related to the reference configuration can be obtained from

$$\mathbf{S}^S_{NEQ} = \sum_{n=1}^{N} \frac{\partial \mathcal{W}^S_{NEQ}}{\partial (\mathbf{E}_{Se})_n} = \sum_{n=1}^{N} (\mathbf{F}^{-1}_{Si})_n \, \widehat{\boldsymbol{\tau}}^S_n \, (\mathbf{F}^{T-1}_{Si})_n = \mathbf{F}^{-1}_S \, \boldsymbol{\tau}^S_{NEQ} \, \mathbf{F}^{T-1}_S . \tag{3.116}$$

Note that the formulation of an entire intermediate-state overstress tensor is not possible for $N > 1$, as the individual intermediate stresses $\widehat{\boldsymbol{\tau}}^S_n$ operate on different configurations.

In addition to the conditional equations for the stresses, the efficient numerical treatment of the nonlinear problem by an iterative solution technique, such as the *Newton-Raphson* method, requires the linearization of the constitutive material equations. Therefore, the equilibrium and non-equilibrium *continuum tangents* or *material moduli*[22], which relate the changes of the respective stresses to the changes of the conjugate strain variables, must be provided. Accordingly, the equilibrium solid elasticity tensor of the reference configuration can be introduced by regarding the total differential of the equilibrium part of the 2nd *Piola-Kirchhoff* extra stress:

$$\mathrm{d}\mathbf{S}^S_{EQ}(\mathbf{E}_S) = \frac{\partial \mathbf{S}^S_{EQ}}{\partial \mathbf{E}_S} \, \mathrm{d}\mathbf{E}_S = \overset{4}{\mathbf{B}}{}^S_{EQ} \, \mathrm{d}\mathbf{E}_S \quad \text{with} \quad \overset{4}{\mathbf{B}}{}^S_{EQ} := \frac{\partial \mathbf{S}^S_{EQ}}{\partial \mathbf{E}_S} . \tag{3.117}$$

Thus, following the concept of hyperelasticity, one finds

$$\overset{4}{\mathbf{B}}{}^S_{EQ} = \frac{\partial^2 \mathcal{W}^S_{EQ}}{\partial \mathbf{E}_S \otimes \partial \mathbf{E}_S} = 4 \, \frac{\partial^2 \mathcal{W}^S_{EQ}}{\partial \mathbf{C}_S \otimes \partial \mathbf{C}_S} = 4 \Big(\frac{\partial^2 \overline{\mathcal{W}}^S_{EQ}}{\partial \mathbf{C}_S \otimes \partial \mathbf{C}_S} + \frac{\partial^2 \overline{\mathcal{U}}^S_{EQ}}{\partial \mathbf{C}_S \otimes \partial \mathbf{C}_S} \Big) \tag{3.118}$$

where, in particular, according to the spectral representation $(2.107)_2$

$$\frac{\partial^2 \overline{\mathcal{W}}^S_{EQ}}{\partial \mathbf{C}_S \otimes \partial \mathbf{C}_S} = \sum_{k,l=1}^{3} \frac{\partial^2 \overline{\mathcal{W}}^S_{EQ}}{\partial \lambda_{S(k)} \, \partial \lambda_{S(l)}} \, \mathbf{M}_{S(k)} \otimes \mathbf{M}_{S(l)} + \tfrac{1}{2} \sum_{\substack{k,l=1 \\ l \neq k}}^{3} \frac{\frac{\partial \overline{\mathcal{W}}^S_{EQ}}{\partial \lambda_{S(k)}} - \frac{\partial \overline{\mathcal{W}}^S_{EQ}}{\partial \lambda_{S(l)}}}{\lambda_{S(k)} - \lambda_{S(l)}} \, \overset{4}{\mathbf{M}}_{S[kl]} \tag{3.119}$$

with $\partial \overline{W}^S_{EQ} / \partial \lambda_{S(k)}$ from equation (3.108) and

$$\frac{\partial^2 \overline{\mathcal{W}}^S_{EQ}}{\partial \lambda_{S(k)} \, \partial \lambda_{S(l)}} = \begin{cases} \mu^S_0 \sum_{m=1}^{M_0} \tfrac{1}{4} \, \mu^*_{0(m)} \, \lambda^{-2}_{S(k)} \left[(\alpha_{0(m)} - 2) \, \lambda^{\alpha_{0(m)}/2}_{S(k)} + 2 \right] & \text{if} \quad l = k , \\ 0 & \text{if} \quad l \neq k , \end{cases} \tag{3.120}$$

[22] In this context, the continuum tangent is not to be confused with the finally required *consistent* or *algorithmic tangent*, which is based on a complete (consistent) equal-order linearization (Hughes & Pister [97]) of the governing field equations with respect to all occurring unknowns (see section 4.2).

as well as

$$\frac{\partial^2 \overline{U}^S_{EQ}}{\partial \mathbf{C}_S \otimes \partial \mathbf{C}_S} = \tfrac{1}{4}\left(J_S \, \frac{\partial \overline{U}^S_{EQ}}{\partial J_S} + J_S^2 \, \frac{\partial^2 \overline{U}^S_{EQ}}{\partial J_S^2} \right) \mathbf{C}_S^{-1} \otimes \mathbf{C}_S^{-1} - \tfrac{1}{2} \, J_S \, \frac{\partial \overline{U}^S_{EQ}}{\partial J_S} \, (\mathbf{C}_S^{-1} \otimes \mathbf{C}_S^{-1})^{\overset{23}{T}} \quad (3.121)$$

with the derivatives of $\overline{U}^S_{EQ}$ in analogy to equations $(3.105)_{2,3}$. The corresponding elasticity tensor of the actual frame is then obtained from a covariant push-forward operation of $(\mathbf{B}^S_{EQ})^{\underline{4}}$ (cf. box (2.43)) or from the related 2nd-order derivatives, viz.,

$$\overset{4}{\mathbf{C}}{}^S_{EQ} = (\mathbf{F}_S \otimes \mathbf{F}_S)^{\overset{23}{T}} \, \overset{4}{\mathbf{B}}{}^S_{EQ} \, (\mathbf{F}_S^T \otimes \mathbf{F}_S^T)^{\overset{23}{T}} = \frac{\partial^2 \mathcal{W}^S_{EQ}}{\partial \mathbf{A}_S \otimes \partial \mathbf{A}_S} = 4 \left[\mathbf{B}_S \, \frac{\partial^2 \mathcal{W}^S_{EQ}}{\partial \mathbf{B}_S \otimes \partial \mathbf{B}_S} \, \mathbf{B}_S \right]^{\underline{4}}, \quad (3.122)$$

where the derivative formulated in $\mathbf{B}_S$ holds in the case of isotropy (cf. relation $(2.108)_2$). Thus, one finally obtains

$$\begin{aligned} \overset{4}{\mathbf{C}}{}^S_{EQ} = 4 \sum_{k,l=1}^{3} \frac{\partial^2 \overline{\mathcal{W}}^S_{EQ}}{\partial \lambda_{S(k)} \, \partial \lambda_{S(l)}} \, \lambda_{S(k)} \, \lambda_{S(l)} \, \mathbf{N}_{S(k)} \otimes \mathbf{N}_{S(l)} + \\ + 2 \sum_{\substack{k,l=1 \\ l \neq k}}^{3} \frac{\frac{\partial \overline{\mathcal{W}}^S_{EQ}}{\partial \lambda_{S(k)}} - \frac{\partial \overline{\mathcal{W}}^S_{EQ}}{\partial \lambda_{S(l)}}}{\lambda_{S(k)} - \lambda_{S(l)}} \, \lambda_{S(k)} \, \lambda_{S(l)} \, \overset{4}{\mathbf{N}}_{S[kl]} + \\ + \left(J_S \, \frac{\partial \overline{U}^S_{EQ}}{\partial J_S} + J_S^2 \, \frac{\partial^2 \overline{U}^S_{EQ}}{\partial J_S^2} \right) \overset{4}{\mathbf{I}}_{\mathrm{tr}} - 2 \, J_S \, \frac{\partial \overline{U}^S_{EQ}}{\partial J_S} \, \overset{4}{\mathbf{I}} \, . \end{aligned} \quad (3.123)$$

Note that in the special cases of identical eigenvalues, in the tangent moduli (3.119) and (3.123) the rational expressions with $\lambda_{S(k)} - \lambda_{S(l)}$ in the denominator must be replaced by the limits (2.109) and (2.110), respectively. Moreover, it should be mentioned that the hyperelastic continuum tangents possess the minor and major symmetries (cf. relation $(2.102)_2$), viz.:

$$\begin{aligned} \overset{4}{\mathbf{B}}{}^S_{EQ} = (\overset{4}{\mathbf{B}}{}^S_{EQ})^{\overset{12}{T}} = (\overset{4}{\mathbf{B}}{}^S_{EQ})^{\overset{34}{T}} = [(\overset{4}{\mathbf{B}}{}^S_{EQ})^{\overset{13}{T}}]^{\overset{24}{T}} , \\ \overset{4}{\mathbf{C}}{}^S_{EQ} = (\overset{4}{\mathbf{C}}{}^S_{EQ})^{\overset{12}{T}} = (\overset{4}{\mathbf{C}}{}^S_{EQ})^{\overset{34}{T}} = [(\overset{4}{\mathbf{C}}{}^S_{EQ})^{\overset{13}{T}}]^{\overset{24}{T}} . \end{aligned} \quad (3.124)$$

Thus, at each strain state they only have 21 instead of 36 independent coefficients, which in the linearized isotropic case can be traced back to just two parameters, namely the *Lamé* constants μ_0^S and Λ_0^S. In this context, see also the paragraph on linearized theories on page 79.

Concerning the non-equilibrium part, the individual elasticity tensors of the intermediate configurations associated with the springs in the *Maxwell* elements can analogously be motivated from the total differential of the related stress tensors:

$$\mathrm{d}\widehat{\boldsymbol{\tau}}^S_n = \overset{4}{\widehat{\mathbf{C}}}{}^S_n \, \mathrm{d}(\widehat{\boldsymbol{\Gamma}}_{Se})_n \quad \text{with} \quad \overset{4}{\widehat{\mathbf{C}}}{}^S_n := \frac{\partial \widehat{\boldsymbol{\tau}}^S_n}{\partial (\widehat{\boldsymbol{\Gamma}}_{Se})_n} = 4 \, \frac{\partial^2 \mathcal{W}^S_{NEQ}}{\partial (\widehat{\mathbf{C}}_{Se})_n \otimes \partial (\widehat{\mathbf{C}}_{Se})_n} \, . \quad (3.125)$$

Thus, proceeding from the non-equilibrium strain-energy function (3.113), one finds

$$\begin{aligned}
\overset{4}{\widehat{\mathbf{C}}}{}^{S}_{n} &= 4 \sum_{k,l=1}^{3} \frac{\partial^2 \overline{\mathcal{W}}^{S}_{NEQ}}{\partial (\lambda_{Se(k)})_n \, \partial (\lambda_{Se(l)})_n} \, (\mathbf{M}_{Se(k)})_n \otimes (\mathbf{M}_{Se(l)})_n + \\
&+ 2 \sum_{\substack{k,l=1 \\ l \neq k}}^{3} \frac{\frac{\partial \overline{\mathcal{W}}^{S}_{NEQ}}{\partial (\lambda_{Se(k)})_n} - \frac{\partial \overline{\mathcal{W}}^{S}_{NEQ}}{\partial (\lambda_{Se(l)})_n}}{(\lambda_{Se(k)})_n - (\lambda_{Se(l)})_n} \, \overset{4}{(\mathbf{M}_{Se[kl]})_n} + \\
&+ \Big((J_{Se})_n \frac{\partial \overline{\mathcal{U}}^{S}_{NEQ}}{\partial (J_{Se})_n} + (J^2_{Se})_n \frac{\partial^2 \overline{\mathcal{U}}^{S}_{NEQ}}{\partial (J^2_{Se})_n} \Big) \, (\widehat{\mathbf{C}}^{-1}_{Se})_n \otimes (\widehat{\mathbf{C}}^{-1}_{Se})_n - \\
&- 2 \, (J_{Se})_n \frac{\partial \overline{\mathcal{U}}^{S}_{NEQ}}{\partial (J_{Se})_n} \left[(\widehat{\mathbf{C}}^{-1}_{Se})_n \otimes (\widehat{\mathbf{C}}^{-1}_{Se})_n \right]^{23}_{T}
\end{aligned} \tag{3.126}$$

with the partial derivatives

$$\begin{aligned}
\frac{\partial \overline{\mathcal{W}}^{S}_{NEQ}}{\partial (\lambda_{Se(k)})_n} &= \mu^{S}_{n} \sum_{m=1}^{M_n} \tfrac{1}{2} \, \mu^{*}_{n(m)} \, (\lambda^{-1}_{Se(k)})_n \left[(\lambda^{\alpha_{n(m)}/2}_{Se(k)})_n - 1 \right] , \\
\frac{\partial^2 \overline{\mathcal{W}}^{S}_{NEQ}}{\partial (\lambda_{Se(k)})_n \, \partial (\lambda_{Se(l)})_n} &= \begin{cases} \mu^{S}_{n} \sum_{m=1}^{M_n} \tfrac{1}{4} \, \mu^{*}_{n(m)} \, (\lambda^{-2}_{Se(k)})_n \left[(\alpha_{n(m)} - 2) \, (\lambda^{\alpha_{n(m)}/2}_{Se(k)})_n + 2 \right] & \text{if } \; l = k \, , \\ 0 & \text{if } \; l \neq k \, . \end{cases}
\end{aligned} \tag{3.127}$$

The individual tangent moduli of the current frame are determined from

$$\begin{aligned}
\overset{4}{\mathbf{C}}{}^{S}_{n} &= \left[(\mathbf{F}_{Se})_n \otimes (\mathbf{F}_{Se})_n \right]^{23}_{T} \overset{4}{\widehat{\mathbf{C}}}{}^{S}_{n} \left[(\mathbf{F}^{T}_{Se})_n \otimes (\mathbf{F}^{T}_{Se})_n \right]^{23}_{T} \\
&= \frac{\partial^2 \mathcal{W}^{S}_{NEQ}}{\partial (\mathbf{A}_{Se})_n \otimes \partial (\mathbf{A}_{Se})_n} = 4 \Big[(\mathbf{B}_{Se})_n \frac{\partial^2 \mathcal{W}^{S}_{NEQ}}{\partial (\mathbf{B}_{Se})_n \otimes \partial (\mathbf{B}_{Se})_n} \, (\mathbf{B}_{Se})_n \Big]^{\underline{4}} ,
\end{aligned} \tag{3.128}$$

finally yielding

$$\begin{aligned}
\overset{4}{\mathbf{C}}{}^{S}_{n} &= 4 \sum_{k,l=1}^{3} \frac{\partial^2 \overline{\mathcal{W}}^{S}_{NEQ}}{\partial (\lambda_{Se(k)})_n \, \partial (\lambda_{Se(l)})_n} \, (\lambda_{Se(k)})_n \, (\lambda_{Se(l)})_n \, (\mathbf{N}_{Se(k)})_n \otimes (\mathbf{N}_{Se(l)})_n + \\
&+ 2 \sum_{\substack{k,l=1 \\ l \neq k}}^{3} \frac{\frac{\partial \overline{\mathcal{W}}^{S}_{NEQ}}{\partial (\lambda_{Se(k)})_n} - \frac{\partial \overline{\mathcal{W}}^{S}_{NEQ}}{\partial (\lambda_{Se(l)})_n}}{(\lambda_{Se(k)})_n - (\lambda_{Se(l)})_n} \, (\lambda_{Se(k)})_n \, (\lambda_{Se(l)})_n \, \overset{4}{(\mathbf{N}_{Se[kl]})_n} + \\
&+ \Big((J_{Se})_n \frac{\partial \overline{\mathcal{U}}^{S}_{NEQ}}{\partial (J_{Se})_n} + (J^2_{Se})_n \frac{\partial^2 \overline{\mathcal{U}}^{S}_{NEQ}}{\partial (J^2_{Se})_n} \Big) \, \overset{4}{\mathbf{I}}_{\mathrm{tr}} - 2 \, (J_{Se})_n \frac{\partial \overline{\mathcal{U}}^{S}_{NEQ}}{\partial (J_{Se})_n} \, \overset{4}{\mathbf{I}} \, .
\end{aligned} \tag{3.129}$$

The corresponding non-equilibrium material tangents of the referential frame are then

obtained from respective covariant fourth-order pull-backs, viz.,

$$\begin{aligned}\overset{4}{\mathbf{B}}{}^{S}_{n} &= [(\mathbf{F}^{-1}_{Si})_n \otimes (\mathbf{F}^{-1}_{Si})_n]^{\overset{23}{T}}\, \overset{4}{\widehat{\mathbf{C}}}{}^{S}_{n}\, [(\mathbf{F}^{T-1}_{Si})_n \otimes (\mathbf{F}^{T-1}_{Si})_n]^{\overset{23}{T}} \\ &= (\mathbf{F}^{-1}_{S} \otimes \mathbf{F}^{-1}_{S})^{\overset{23}{T}}\, \overset{4}{\mathbf{C}}{}^{S}_{n}\, (\mathbf{F}^{T-1}_{S} \otimes \mathbf{F}^{T-1}_{S})^{\overset{23}{T}}\,.\end{aligned} \tag{3.130}$$

Note that similar to the total non-equilibrium stresses $\mathbf{S}^{S}_{NEQ}$ and $\boldsymbol{\tau}^{S}_{NEQ}$, entire tangent moduli can be introduced as

$$\overset{4}{\mathbf{B}}{}^{S}_{NEQ} = \sum_{n=1}^{N} \overset{4}{\mathbf{B}}{}^{S}_{n}\,, \quad \overset{4}{\mathbf{C}}{}^{S}_{NEQ} = \sum_{n=1}^{N} \overset{4}{\mathbf{C}}{}^{S}_{n}\,, \tag{3.131}$$

which, for obvious reasons, is not possible for the intermediate states. Similar to the equilibrium elasticity tensors, the hyperelastic continuum tangents of the non-equilibrium parts exhibit the minor and major symmetries (cf. relations (3.124)). However, also here, a special treatment of multiple eigenvalues $(\lambda_{Se(k)})_n$ is required according to equations (2.109) and (2.110), respectively.

The final task in order to complete the finite viscoelastic solid model is the specification of the inelastic evolution equations, i. e., the flow rules that govern the temporal development of the inelastic deformations. Proceeding from the solid residual inequality (3.88) and following the arguments of section 3.1.4, the dissipation inequality is sufficiently satisfied if the individual terms of the residual inequality possess a positive quadratic form. Accordingly, in regard to the positive definiteness of $(\widehat{\mathbf{C}}_{Se})_n$, this can be accomplished by choosing the simple ansatz[23]

$$(\widehat{\mathbf{D}}_{Si})_n \propto \widehat{\boldsymbol{\tau}}^{S}_{n} \quad \longrightarrow \quad (\widehat{\mathbf{D}}_{Si})_n = (\overset{4}{\widehat{\mathbf{D}}}{}^{S}_{n})^{-1}\, \widehat{\boldsymbol{\tau}}^{S}_{n}\,, \tag{3.132}$$

where $(\overset{4}{\widehat{\mathbf{D}}}{}^{S}_{n})^{-1}$ are positive definite, isotropic tensor functions of fourth order. Actually, they represent the viscous compliances associated with the dashpots of the underlying *Maxwell* elements and are chosen in such a way that their inverses are identical to the isotropic viscosity tensors of the linear theory presented in box (3.39), viz.:

$$(\overset{4}{\widehat{\mathbf{D}}}{}^{S}_{n})^{-1} = \frac{1}{2\,\eta^{S}_{n}}\,\overset{4}{\mathbf{I}} - \frac{\zeta^{S}_{n}}{2\,\eta^{S}_{n}\,(2\,\eta^{S}_{n} + 3\,\zeta^{S}_{n})}\,\overset{4}{\mathbf{I}}_{\mathrm{tr}} \quad \Leftrightarrow \quad \overset{4}{\widehat{\mathbf{D}}}{}^{S}_{n} = 2\,\eta^{S}_{n}\,\overset{4}{\mathbf{I}} + \zeta^{S}_{n}\,\overset{4}{\mathbf{I}}_{\mathrm{tr}}\,. \tag{3.133}$$

Therein, the viscosities possibly depend on the individual overstresses[24], which is appropriate if nonlinear rate-dependent behavior has to be modeled (cf. Haupt [87]). Moreover, it is apparent that they must satisfy

$$\eta^{S}_{n} = \eta^{S}_{n}(\widehat{\boldsymbol{\tau}}^{S}_{n}) > 0\,, \quad \zeta^{S}_{n} = \zeta^{S}_{n}(\widehat{\boldsymbol{\tau}}^{S}_{n}) > -\tfrac{2}{3}\,\eta^{S}_{n} \quad \text{as} \quad \xi^{S}_{n} := \tfrac{2}{3}\,\eta^{S}_{n} + \zeta^{S}_{n} > 0\,, \tag{3.134}$$

[23] Some authors proceed from an alternative ansatz based on the *Mandel* stress tensors $(\widehat{\mathbf{C}}_{Se})_n\,\widehat{\boldsymbol{\tau}}^{S}_{n}$ (e. g., Huber & Tsakmakis [95] or Reese & Govindjee [151]). Following this, one may likewise choose

$$(\widehat{\mathbf{D}}_{Si})_n \propto (\widehat{\mathbf{C}}_{Se})_n\,\widehat{\boldsymbol{\tau}}^{S}_{n} \quad \Leftrightarrow \quad -\tfrac{1}{2}\,[(\mathbf{B}_{Se})_n]^{\triangledown}_{S}\,(\mathbf{B}^{-1}_{Se})_n \propto \boldsymbol{\tau}^{S}_{n}\,.$$

[24] In general, according to the principle of equipresence, the viscosities as any other introduced material parameter may depend on the whole set of process variables.

where ξ_n^S denotes the macroscopic bulk viscosities of the skeleton. The inelastic evolution equations (3.132) describe the temporal changes of the strain-equivalent internal variables depending on their current values including the history information. Thus, it appears to be natural to formulate the evolution laws with respect to the intermediate configurations as they represent the actual frame for the inelastic deformation process. However, with regards to the numerical evaluation of the evolution equations, for the sake of convenience, the spatiotemporal discretization is usually carried out on the constant reference configuration (see section 4.3). Therefore, the constitutive evolution laws (3.132) must be rephrased by means of referential quantities, which can be accomplished using the known transport mechanisms. Thus, the conditional differential equations for the inelastic deformation tensors become

$$\begin{aligned} [(\mathbf{C}_{Si})_n]'_S &= \frac{1}{\eta_n^S}\,(\mathbf{C}_{Si})_n\,\mathbf{S}_n^S\,(\mathbf{C}_{Si})_n - \frac{\zeta_n^S}{\eta_n^S\,(2\,\eta_n^S + 3\,\zeta_n^S)}\left[\mathbf{S}_n^S \cdot (\mathbf{C}_{Si})_n\right](\mathbf{C}_{Si})_n\,, \\ \mathbf{h}^k \otimes \mathbf{h}^l :\quad [(\widehat{z}_{kl})_n]'_S &= \frac{1}{\eta_n^S}\,(\widehat{z}_{ki})_n\,(\tau^{ij})_n\,(\widehat{z}_{jl})_n - \frac{\zeta_n^S}{\eta_n^S\,(2\,\eta_n^S + 3\,\zeta_n^S)}\left[(\tau^{ij})_n\,(\widehat{z}_{ij})_n\right](\widehat{z}_{kl})_n \end{aligned} \tag{3.135}$$

or, equivalently, in covariant representation

$$\begin{aligned} [(\mathbf{C}_{Si}^{-1})_n]'_S &= -\frac{1}{\eta_n^S}\,\mathbf{S}_n^S + \frac{\zeta_n^S}{\eta_n^S\,(2\,\eta_n^S + 3\,\zeta_n^S)}\left[\mathbf{S}_n^S \cdot (\mathbf{C}_{Si})_n\right](\mathbf{C}_{Si}^{-1})_n\,, \\ \mathbf{h}_k \otimes \mathbf{h}_l :\quad [(\widehat{z}^{kl})_n]'_S &= -\frac{1}{\eta_n^S}\,(\tau^{kl})_n + \frac{\zeta_n^S}{\eta_n^S\,(2\,\eta_n^S + 3\,\zeta_n^S)}\left[(\tau^{ij})_n\,(\widehat{z}_{ij})_n\right](\widehat{z}^{kl})_n\,. \end{aligned} \tag{3.136}$$

The formulation in terms of the reference configuration is favorable as all dependencies on the internal variables are explicit, which is apparently not the case, if the intermediate configurations are used. Moreover, from the natural basis representations $(3.135)_2$ and $(3.136)_2$, it is seen that the evolution laws actually determine the six independent intermediate metric coefficients $(\widehat{z}_{kl})_n$ or $(\widehat{z}^{kl})_n$, respectively. In this context, note that the choice of the preferred representation of the evolution equations is a computational rather than a physical question depending on the algorithmic implementation of the internal variable concept. For the sake of completeness, a summary of the different representations of the evolution equations is provided in boxes (B.5) and (B.6) of appendix B.3.

Linearized theories: This paragraph is concerned with the downward compatibility of the presented finite solid viscoelasticity model to linear theories. As pointed out by Reese & Govindjee [151], the required linearization procedure can be carried out in two steps. In a first step, a linearization can be performed about the thermodynamic equilibrium state, which can be regarded as a linearization about the intermediate configurations representing the reference states of the elastic deformation processes associated with totally relaxed springs in the *Maxwell* elements, i. e., $(\widehat{\mathbf{\Gamma}}_{Se})_n = \mathbf{0}$ (cf. also relations (3.47)). The resulting semi-linear model is then said to belong to the theory of *finite linear viscoelasticity*, which is restricted to slow deformation or fast relaxation processes that take place close to thermodynamic equilibrium, but is still valid for large deformations. In a second step, the linearization procedure can be completed through linearization about the undeformed reference (natural) state implying $\mathbf{E}_S = \mathbf{0}$ and $(\mathbf{E}_{Se})_n = \mathbf{0}$, finally yielding

the linear viscoelasticity model of the infinitesimal theory. For the sake of clarity, in the sequel, $(\,\cdot\,)_{\widehat{\text{lin}}}$ is used to indicate linearizations about the intermediate configurations and $(\,\cdot\,)_{\text{lin}}$ denotes linearizations with respect to the natural state.

To begin with, the linearization of the intermediate overstresses about the thermodynamic equilibrium state is carried out by a *Taylor* series expansion up to the first order

$$(\widehat{\boldsymbol{\tau}}_n^S)_{\widehat{\text{lin}}} = \widehat{\boldsymbol{\tau}}_n^S\Big|_{(\widehat{\boldsymbol{\Gamma}}_{Se})_n=\mathbf{0}} + \frac{\partial \widehat{\boldsymbol{\tau}}_n^S}{\partial(\widehat{\boldsymbol{\Gamma}}_{Se})_n}\Big|_{(\widehat{\boldsymbol{\Gamma}}_{Se})_n=\mathbf{0}} (\widehat{\boldsymbol{\Gamma}}_{Se})_n\,, \tag{3.137}$$

where $(\widehat{\boldsymbol{\Gamma}}_{Se})_n = \mathbf{0}$ implies

$$(\widehat{\mathbf{C}}_{Se})_n = \mathbf{I} \quad \Leftrightarrow \quad (\widehat{\mathbf{F}}_{Se})_n = \mathbf{I} \quad \Leftrightarrow \quad (\lambda_{Se(k)})_n = 1\,,\ (J_{Se})_n = 1\,. \tag{3.138}$$

Thus, with

$$\begin{aligned} \widehat{\boldsymbol{\tau}}_n^S[(\widehat{\boldsymbol{\Gamma}}_{Se})_n = \mathbf{0}] &= \mathbf{0}\,, \\ \overset{4}{\mathbf{E}}{}_n^S := \frac{\partial \widehat{\boldsymbol{\tau}}_n^S}{\partial(\widehat{\boldsymbol{\Gamma}}_{Se})_n}\Big|_{(\widehat{\boldsymbol{\Gamma}}_{Se})_n=\mathbf{0}} &= \overset{4}{\widehat{\mathbf{C}}}{}_n^S[(\widehat{\boldsymbol{\Gamma}}_{Se})_n = \mathbf{0}] = 2\,\mu_n^S\,\overset{4}{\mathbf{I}} + \Lambda_n^S\,\overset{4}{\mathbf{I}}_{\text{tr}}\,, \end{aligned} \tag{3.139}$$

one finds the linear relationship

$$(\widehat{\boldsymbol{\tau}}_n^S)_{\widehat{\text{lin}}} = \overset{4}{\mathbf{E}}{}_n^S\,(\widehat{\boldsymbol{\Gamma}}_{Se})_n = 2\,\mu_n^S\,(\widehat{\boldsymbol{\Gamma}}_{Se})_n + \Lambda_n^S\,\big[(\widehat{\boldsymbol{\Gamma}}_{Se})_n \cdot \mathbf{I}\big]\,\mathbf{I}\,. \tag{3.140}$$

Next, linearization of the evolution equations (3.132) yields

$$\begin{aligned} [(\widehat{\mathbf{D}}_{Si})_n]_{\widehat{\text{lin}}} &= (\widehat{\mathbf{D}}_{Si})_n\Big|_{(\widehat{\boldsymbol{\Gamma}}_{Se})_n=\mathbf{0}} + \frac{\partial(\widehat{\mathbf{D}}_{Si})_n}{\partial(\widehat{\boldsymbol{\Gamma}}_{Se})_n}\Big|_{(\widehat{\boldsymbol{\Gamma}}_{Se})_n=\mathbf{0}} (\widehat{\boldsymbol{\Gamma}}_{Se})_n = \\ &= \Big[(\overset{4}{\widehat{\mathbf{D}}}{}_n^S)^{-1}\,\widehat{\boldsymbol{\tau}}_n^S\Big]\Big|_{(\widehat{\boldsymbol{\Gamma}}_{Se})_n=\mathbf{0}} + \Big[\frac{\partial(\overset{4}{\widehat{\mathbf{D}}}{}_n^S)^{-1}}{\partial(\widehat{\boldsymbol{\Gamma}}_{Se})_n}\,\widehat{\boldsymbol{\tau}}_n^S + (\overset{4}{\widehat{\mathbf{D}}}{}_n^S)^{-1}\,\frac{\partial \widehat{\boldsymbol{\tau}}_n^S}{\partial(\widehat{\boldsymbol{\Gamma}}_{Se})_n}\Big]\Big|_{(\widehat{\boldsymbol{\Gamma}}_{Se})_n=\mathbf{0}} (\widehat{\boldsymbol{\Gamma}}_{Se})_n\,, \end{aligned} \tag{3.141}$$

so that together with the results (3.139) and

$$(\overset{4}{\mathbf{D}}{}_n^S)^{-1} := (\overset{4}{\widehat{\mathbf{D}}}{}_n^S)^{-1}[(\widehat{\boldsymbol{\Gamma}}_{Se})_n = \mathbf{0}] = \frac{1}{2\,\eta_n^S}\,\overset{4}{\mathbf{I}} - \frac{\zeta_n^S}{2\,\eta_n^S\,(2\,\eta_n^S + 3\,\zeta_n^S)}\,\overset{4}{\mathbf{I}}_{\text{tr}}\,, \tag{3.142}$$

one obtains the linearized evolution equations

$$[(\widehat{\mathbf{D}}_{Si})_n]_{\widehat{\text{lin}}} = \{[(\widehat{\boldsymbol{\Gamma}}_{Si})^{\triangle}_{Si}]_n\}_{\widehat{\text{lin}}} = (\overset{4}{\mathbf{D}}{}_n^S)^{-1}\,\overset{4}{\mathbf{E}}{}_n^S\,(\widehat{\boldsymbol{\Gamma}}_{Se})_n = (\overset{4}{\boldsymbol{\tau}}{}_n^S)^{-1}\,\big[\widehat{\boldsymbol{\Gamma}}_S - (\widehat{\boldsymbol{\Gamma}}_{Si})_n\big]\,. \tag{3.143}$$

Alternatively, in terms of the reference and the actual configuration, they read

$$\begin{aligned} \{[(\mathbf{E}_{Si})_n]'_S\}_{\widehat{\text{lin}}} &= (\overset{4}{\boldsymbol{\tau}}{}_n^S)^{-1}\,\big[\mathbf{E}_S - (\mathbf{E}_{Si})_n\big]\,, \\ \{[(\mathbf{A}_{Si})_n]^{\triangle}_S\}_{\widehat{\text{lin}}} &= (\overset{4}{\boldsymbol{\tau}}{}_n^S)^{-1}\,\big[\mathbf{A}_S - (\mathbf{A}_{Si})_n\big]\,. \end{aligned} \tag{3.144}$$

Therein, the positive definite, inverse 4th-order relaxation tensors $(\overset{4}{\boldsymbol{\tau}}{}^{S}_{n})^{-1} = (\overset{4}{\mathbf{D}}{}^{S}_{n})^{-1}\,\overset{4}{\mathbf{E}}{}^{S}_{n}$ are identical to those of the geometrically linear theory presented in box (3.39). A meaningful representation of the individual relaxation tensors is, for instance, given by

$$(\overset{4}{\boldsymbol{\tau}}{}^{S}_{n})^{-1} = \frac{1}{(\tau^{S}_{\mathrm{dev}})_{n}}\left(\overset{4}{\mathbf{I}} - \tfrac{1}{3}\,\overset{4}{\mathbf{I}}_{\mathrm{tr}}\right) + \frac{1}{3\,(\tau^{S}_{\mathrm{vol}})_{n}}\,\overset{4}{\mathbf{I}}_{\mathrm{tr}} \tag{3.145}$$

with the deviatoric and volumetric relaxation time constants

$$(\tau^{S}_{\mathrm{dev}})_{n} = \frac{\eta^{S}_{n}}{\mu^{S}_{n}} > 0\,, \quad (\tau^{S}_{\mathrm{vol}})_{n} = \frac{\xi^{S}_{n}}{\mathcal{K}^{S}_{n}} = \frac{\frac{2}{3}\,\eta^{S}_{n} + \zeta^{S}_{n}}{\frac{2}{3}\,\mu^{S}_{n} + \Lambda^{S}_{n}} > 0\,. \tag{3.146}$$

In this context, some authors proceed from unique relaxation times, i. e., $\tau^{S}_{n} := (\tau^{S}_{\mathrm{dev}})_{n} = (\tau^{S}_{\mathrm{vol}})_{n}$, which, e. g., proceeding from equation $(3.144)_1$, yields exactly the simplified evolution equations proposed by Lubliner [116]:

$$(\overset{4}{\boldsymbol{\tau}}{}^{S}_{n})^{-1} = \frac{1}{\tau^{S}_{n}}\,\overset{4}{\mathbf{I}} \quad \longrightarrow \quad \{[(\mathbf{C}_{Si})_{n}]'_{S}\}_{\widehat{\mathrm{lin}}} = \frac{1}{\tau^{S}_{n}}\left[\mathbf{C}_{S} - (\mathbf{C}_{Si})_{n}\right]. \tag{3.147}$$

From the above equations, it is directly seen that the finite linear model proceeds from a linearization of the constitutive laws associated with the inelastic *Maxwell* branches. Accordingly, the semi-linear formulation in some respect represents the viscoelastic counterpart to the *St. Venant-Kirchhoff* elasticity law, which is valid for large deformations but obeys a constant continuum tangent[25]. Following this, finite linear viscoelasticity can only be expected to be useful in a narrow range of small perturbations away from thermodynamic equilibrium such that the intermediate configurations are adjacent to the current configuration, i. e., $(\mathbf{F}_{Si})_{n} \approx \mathbf{F}_{S}$ as $[(\mathbf{F}_{Se})_{n}]_{\widehat{\mathrm{lin}}} \approx \mathbf{I}$. However, note that the equilibrium part is not affected by this first linearization step and hence, still describes a spontaneous nonlinear elastic response. For further particulars including a comparative literature review of large deformation viscoelasticity models, it is referred to the monograph of Reese [149].

To continue, according to condition (3.98) and the proposed form of the volumetric extensions (3.105), the complete linearization about the unstrained reference state reveals the downward compatibility to the linear viscoelasticity model of the infinitesimal theory as depicted in box (3.39). In detail, application of the linearization procedure yields

$$(\mathbf{S}^{S}_{E})_{\mathrm{lin}} = (\mathbf{S}^{S}_{EQ})_{\mathrm{lin}} + \sum_{n=1}^{N}(\mathbf{S}^{S}_{n})_{\mathrm{lin}} \left\{\begin{array}{l} (\mathbf{S}^{S}_{EQ})_{\mathrm{lin}} = \mathbf{S}^{S}_{EQ}\Big|^{\mathbf{E}_{S}=\mathbf{0}}_{(\mathbf{E}_{Se})_{n}=\mathbf{0}} + \dfrac{\partial \mathbf{S}^{S}_{EQ}}{\partial \mathbf{E}_{S}}\Big|^{\mathbf{E}_{S}=\mathbf{0}}_{(\mathbf{E}_{Se})_{n}=\mathbf{0}} \mathbf{E}_{S}\,, \\[2ex] (\mathbf{S}^{S}_{n})_{\mathrm{lin}} = \mathbf{S}^{S}_{n}\Big|^{\mathbf{E}_{S}=\mathbf{0}}_{(\mathbf{E}_{Se})_{n}=\mathbf{0}} + \dfrac{\partial \mathbf{S}^{S}_{n}}{\partial (\mathbf{E}_{Se})_{n}}\Big|^{\mathbf{E}_{S}=\mathbf{0}}_{(\mathbf{E}_{Se})_{n}=\mathbf{0}} (\mathbf{E}_{Se})_{n}\,, \end{array}\right. \tag{3.148}$$

[25] For details, see, e. g., Ciarlet [32], sec. 3.9.

where, in particular,

$$\mathbf{S}^S_{EQ}(\mathbf{E}_S = \mathbf{0}) = \mathbf{0}\,,$$

$$\mathbf{S}^S_n\Big|^{\mathbf{E}_S=\mathbf{0}}_{(\mathbf{E}_{Se})_n=\mathbf{0}} = \big[(\mathbf{F}^{-1}_{Si})_n\,\widehat{\boldsymbol{\tau}}^S_n\,(\mathbf{F}^{T-1}_{Si})_n\big]\Big|^{(\mathbf{E}_{Si})_n=\mathbf{0}}_{(\widehat{\boldsymbol{\Gamma}}_{Se})_n=\mathbf{0}} = \mathbf{0}\,,$$

$$\overset{4}{\mathbf{E}}{}^S_0 := \frac{\partial \mathbf{S}^S_{EQ}}{\partial \mathbf{E}_S}\Big|^{\mathbf{E}_S=\mathbf{0}}_{(\mathbf{E}_{Se})_n=\mathbf{0}} = \overset{4}{\mathbf{B}}{}^S_{EQ}(\mathbf{E}_S = \mathbf{0}) = 2\,\mu^S_0\,\overset{4}{\mathbf{I}} + \Lambda^S_0\,\overset{4}{\mathbf{I}}_{\mathrm{tr}}\,,$$

$$\frac{\partial \mathbf{S}^S_n}{\partial (\mathbf{E}_{Se})_n}\Big|^{\mathbf{E}_S=\mathbf{0}}_{(\mathbf{E}_{Se})_n=\mathbf{0}} = \Big\{\big[(\mathbf{F}^{-1}_{Si})_n \otimes (\mathbf{F}^{-1}_{Si})_n\big]^{\overset{23}{T}} \frac{\partial \widehat{\boldsymbol{\tau}}^S_n}{\partial (\widehat{\boldsymbol{\Gamma}}_{Se})_n}\,\big[(\mathbf{F}^{T-1}_{Si})_n \otimes (\mathbf{F}^{T-1}_{Si})_n\big]^{\overset{23}{T}}\Big\}\Big|^{(\mathbf{E}_{Si})_n=\mathbf{0}}_{(\widehat{\boldsymbol{\Gamma}}_{Se})_n=\mathbf{0}} = \overset{4}{\mathbf{E}}{}^S_n\,. \tag{3.149}$$

Note that a further linearization of the referential evolution equations $(3.144)_1$ is not necessary as they already possess a linear shape. However, in the context of a geometrical linearization procedure, one proceeds from small deformations, which can be expressed by $\mathbf{u}_S = \epsilon\,\mathbf{u}_S$, where ϵ denotes a small positive infinitesimal quantity with the properties $\epsilon \ll 1$ and $\epsilon^{n+1} \ll \epsilon^n$. Following this, it is easily concluded that

$$\begin{aligned}(\mathbf{F}_S)_{\mathrm{lin}} &= \mathbf{I} + \epsilon\,\mathrm{Grad}_S\mathbf{u}_S \approx \mathbf{I}\,,\\ (\mathbf{E}_S)_{\mathrm{lin}} &= \tfrac{1}{2}\left(\epsilon\,\mathrm{Grad}_S\mathbf{u}_S + \epsilon\,\mathrm{Grad}^T_S\mathbf{u}_S + \epsilon^2\,\mathrm{Grad}^T_S\mathbf{u}_S\,\mathrm{Grad}_S\mathbf{u}_S\right) \approx\\ &\approx \tfrac{1}{2}\left(\mathrm{Grad}_S\mathbf{u}_S + \mathrm{Grad}^T_S\mathbf{u}_S\right),\end{aligned} \tag{3.150}$$

which likewise holds for the elastic and inelastic deformation measures. Thus, in a geometrical linear framework, the current as well as the intermediate configurations are close to the reference configuration, so that a distinction between configurations is no longer necessary. Thus, one commonly defines

$$\boldsymbol{\varepsilon}_S := (\mathbf{E}_S)_{\mathrm{lin}} \approx [(\widehat{\boldsymbol{\Gamma}}_S)_n]_{\mathrm{lin}} \approx (\mathbf{A}_S)_{\mathrm{lin}}\,, \quad \boldsymbol{\sigma}^S_E := (\mathbf{S}^S_E)_{\mathrm{lin}} \approx [(\widehat{\boldsymbol{\tau}}^S_E)_n]_{\mathrm{lin}} \approx (\boldsymbol{\tau}^S_E)_{\mathrm{lin}}\,, \tag{3.151}$$

which transferred to the equilibrium and non-equilibrium contributions and inserted into the linearized expressions $(3.144)_1$ and (3.148) precisely recovers the linear viscoelasticity formulation of the small strain regime given in box (3.39). □

3.3 Viscous Pore-fluid Constituent

Now, focusing on the description of the pore-fluid constituent, the flow-dependent dissipative effects resulting from the nonlinear percolation process through the deformable solid skeleton are discussed. At first, a constitutive law for the description of compressible pore gases is provided. Then, a 3-d non-*Darcy* filter law is derived and the theoretical treatment of deformation-dependent as well as anisotropic permeability properties is presented in regard to the conceivable finite deformation processes.

3.3.1 Compressible Fluid Behavior

In the case of compressible fluid behavior, a further constitutive law is necessary, which uniquely assigns the effective fluid density to the present pressure state or *vice versa*. Proceeding from isothermal conditions $\Theta^\alpha \equiv \Theta = \text{const.}$, according to equation (3.32), the free energy $\psi^F = \psi^F(\rho^{FR})$ must be specified in order to find functions $p = p(\rho^{FR})$ or $\rho^{FR} = \rho^{FR}(p)$ describing *barotropic*[26] fluid behavior. For the purpose of this work, the compressible pore gas air is of particular interest. Thus, excluding extremal values of p and Θ, it is convenient to proceed from the ideal gas law (*Boyle-Mariotte*'s law)

$$\psi^F(\rho^{FR}, \Theta) = \frac{R\,\Theta}{M_m^F} \ln \rho^{FR} + g(\Theta) \quad \longrightarrow \quad p(\rho^{FR}) = (\rho^{FR})^2 \frac{\partial \psi^F}{\partial \rho^{FR}} = \frac{R\,\Theta}{M_m^F}\,\rho^{FR}\,, \quad (3.152)$$

where R is the universal gas constant, M_m^F is the molar mass of the considered gas, and $g(\Theta)$ is a temperature-dependent function. In general, the ideal gas law may be replaced by a more sophisticated state equation, such as the law of Muskat [130], the *Van-der-Waals* equation (van der Waals [187]), or by introduction of an imaginary *mixture phase*, which describes the compressible fluid as an inseparable mixture of an incompressible liquid enclosing a trapped ideal gas (Mahnkopf [118]). A qualitative comparison of different state equations for the description of a compressible pore fluid can be found in Diebels [43]. In this context, recall that for the case of an incompressible pore liquid, no constitutive equation is necessary, as p simply acts as a *Lagrange*an multiplier, which has to be determined from the boundary conditions of the considered problem.

3.3.2 *Darcy* and Non-*Darcy* Filter Laws

The simplest model for the description of 1-d incompressible pore-fluid flow through a homogeneous, saturated porous medium goes back to Darcy (1856) [41]. Investigating the flow of water through vertical sand filters for water purification, *Darcy* found a linear proportionality of the volumetric flow rate per cross-sectional area to the pressure drop over the length of the flow path yielding a simple linear transport equation commonly referred to as *Darcy's law*[27]. However, further empirical evidence revealed that the linearity between superficial velocity and hydraulic gradient breaks down for large enough flow speeds (Forchheimer [69]), which restricts the applicability of *Darcy*'s law to lingering flows governed by small permeabilities or driven by slight pressure gradients. In other words, *Darcy flows* proceed from a regular, smooth pore-fluid motion (laminar flow) in the limit of a vanishingly small *Reynolds* number associated with negligible intertia forces[28].

From a physical perspective, the percolation process is mainly governed by the solid-fluid interaction mechanisms taking place at the walls of the pore channels (wall friction). These dissipative mechanisms depend on the properties of the permeating fluid as well as the morphology (structure and connectivity) of the pore space. The general capability

[26] A compressible fluid is said to be barotropic, if its density only changes with pressure.

[27] Note that *Darcy*'s law obeys a similar form as the constitutive laws named after *Fick*, *Fourier*, or *Ohm* for the description of diffusion, heat conduction, or electrical current flux, respectively.

[28] See remark on page 85.

of a porous material to transmit fluid is known as permeability, whereas the ease of the pore-fluid flow is usually subsumed by the term tortuosity, which can be thought of as a measure of the irregularity of the pore-channels cross-sections. Particularly the expansion and contraction losses during the flow through microscopically disordered porous media strongly depend on the flow speed and are assumed to be responsible for the deviations from the narrow range where linear conditions are valid. The loss of linearity is also brought into connection with the onset of turbulence in the seepage flow, which is believed to be enhanced by the tortuosity of the pore structure.

Here, proceeding from the macroscopic TPM approach, singlephasic pore-fluid flow is governed by the local interaction force per unit volume of fluid $\widehat{\mathbf{p}}_E^F$, which must constitutively account for the relevant mechanisms of momentum transfer between the deforming skeleton and the permeating fluid. Following this, according to the sufficient condition $(3.35)_3$, it is convenient to proceed from the ansatz

$$\widehat{\mathbf{p}}_E^F \propto -\mathbf{w}_{FR} \quad \longrightarrow \quad \widehat{\mathbf{p}}_E^F = -(n^F)^2\,(\mathbf{K}^F)^{-1}\,\mathbf{w}_{FR} = -n^F\,(\mathbf{K}^F)^{-1}\,\mathbf{w}_F \tag{3.153}$$

with $(\mathbf{K}^F)^{-1}$ representing a positive definite hydraulic resistivity or inverse permeability tensor, which apparently depends on the deformable pore structure, the fluid properties, and also on the filter velocity $\mathbf{w}_F = n^F\,\mathbf{w}_{FR}$ consistent with the principle of equipresence. To continue, the quasi-static fluid momentum balance $(3.4)_2$ is rewritten by means of the extra quantities $(3.15)_{2,3}$ yielding

$$\mathbf{0} = \operatorname{div}\mathbf{T}_E^F + \widehat{\mathbf{p}}_E^F - n^F\operatorname{grad} p + \rho^F\,\mathbf{b}\,, \tag{3.154}$$

where, on the basis of magnitude arguments, an admissible estimate of the volume-specific fluid friction force $\mathbf{t}_E^F := \operatorname{div}\mathbf{T}_E^F$ is $|\mathbf{t}_E^F| \ll |\widehat{\mathbf{p}}_E^F|$, thus assuming that dissipation only occurs in the wall boundary layers of the pore channels, whereas the fluid behaves more or less inviscid in the flow, i. e., $\mathbf{T}_E^F \approx \mathbf{0}$ (see also remark on page 85). Finally, by inserting the constitutive ansatz (3.153), one obtains a generalized 3-d filter law:

$$\mathbf{0} = -n^F\,(\mathbf{K}^F)^{-1}\,\mathbf{w}_F - n^F\operatorname{grad} p + \rho^F\,\mathbf{b} \quad \longrightarrow \quad \mathbf{w}_F = -\mathbf{K}^F\,(\operatorname{grad} p - \rho^{FR}\,\mathbf{b})\,. \tag{3.155}$$

For the following considerations, the presentation is restricted to deformation-independent and isotropic permeability properties, so that the permeability tensor simplifies to

$$\mathbf{K}^F = K^F\,\mathbf{I} = \frac{k^F}{\gamma^{FR}}\,\mathbf{I} = \frac{K^S}{\mu^{FR}}\,\mathbf{I}\,. \tag{3.156}$$

Herein, K^F, k^F, and K^S represent the commonly used scalar-valued permeability parameters (see box (3.158)), which, for the moment, depend only on the filter velocity $\mathbf{w}_F$. Moreover, $\gamma^{FR}(p) = g\,\rho^{FR}(p) > 0$ is the effective fluid weight with $g = |\mathbf{b}|$ as the scalar gravitational acceleration and $\mu^{FR} > 0$ is the effective fluid viscosity, which for the purpose of this work is regarded as constant[29]. Thus, using the conventional permeability

[29] The influence of pressure on the viscosity is usually neglected for moderate levels of pressure. Generally, an increase in pressure will increase the effective viscosity of a fluid.

parameter k^F, one can rewrite the filter law $(3.155)_2$ in the well-known form

$$\mathbf{w}_F = k^F\,\mathbf{i} \qquad \text{with} \qquad \mathbf{i} = -\frac{1}{\gamma^{FR}}\,(\operatorname{grad} p - \rho^{FR}\,\mathbf{b}) \tag{3.157}$$

representing the dimensionless hydraulic gradient.

Summary of permeability measures

hydraulic conductivity, Darcy flow coefficient:	$k^F := \gamma^{FR}\,K^F = \dfrac{\gamma^{FR}}{\mu^{FR}}\,K^S$	$\left[\dfrac{\mathrm{m}}{\mathrm{s}}\right]$
"specific permeability":	$K^F := \dfrac{k^F}{\gamma^{FR}} = \dfrac{K^S}{\mu^{FR}}$	$\left[\dfrac{\mathrm{m}^4}{\mathrm{N\,s}}\right]$
intrinsic permeability:	$K^S := \mu^{FR}\,K^F = \dfrac{\mu^{FR}}{\gamma^{FR}}\,k^F$	$[\mathrm{m}^2]$
non-Darcy flow coefficient:	$b^S := g\,B^S = \dfrac{g}{\beta^S}$	$\left[\dfrac{\mathrm{m}^2}{\mathrm{s}^2}\right]$
tortuosity parameter, passability factor:	$B^S := \dfrac{b^S}{g} = \dfrac{1}{\beta^S}$	$[\mathrm{m}]$
inertial resistance:	$\beta^S := \dfrac{g}{b^S} = \dfrac{1}{B^S}$	$[\mathrm{m}^{-1}]$

(3.158)

Remark: In geomechanics and hydrology, one usually neglects the fluid extra (friction) stress, i. e., the fluid viscosity is not considered explicitly but only implicitly via the viscous drag described by the extra momentum production $\widehat{\mathbf{p}}_E^F$. In order to validate this *a priori* assumption within the thermodynamically consistent framework of the TPM, one proceeds from the sufficient condition $(3.35)_2$. Following this, neglecting the bulk viscosity of the pore fluid based on *Stokes*' assumption (Prandtl [146], Schlichting [157]), one explicitly considers an isochoric fluid friction stress via

$$\mathbf{T}_E^F \propto \mathbf{D}_F \quad \longrightarrow \quad \mathbf{T}_E^F = 2\,\mu^F\,\mathbf{D}_F^D = \mu^F\left[\operatorname{grad}\mathbf{v}_F + \operatorname{grad}^T\mathbf{v}_F - \tfrac{2}{3}\,(\operatorname{div}\mathbf{v}_F)\,\mathbf{I}\right], \tag{3.159}$$

such that the fluid friction force becomes

$$\mathbf{t}_E^F = \operatorname{div}\mathbf{T}_E^F = \mu^F\left[\Delta\mathbf{v}_F + \tfrac{1}{3}\operatorname{grad}\operatorname{div}\mathbf{v}_F\right]. \tag{3.160}$$

Therein, $\mu^F = n^F\,\mu^{FR} > 0$ is the partial shear viscosity (dynamic viscosity) of the pore fluid and $\Delta(\,\cdot\,) = \operatorname{div}\operatorname{grad}(\,\cdot\,)$ is the *Laplace* operator. Insertion into the fluid momentum balance of box (2.131) yields the *Navier-Stokes* equation extended to porous media applications

$$\rho^F\,(\mathbf{v}_F)'_F = \mathbf{t}_E^F + \widehat{\mathbf{p}}_E^F - n^F\operatorname{grad} p + \rho^F\,\mathbf{b}\,. \tag{3.161}$$

Next, by applying the procedure of a dimensional analysis, it is possible to establish physical relationships among the variables by discussion of the corresponding dimensionless

quantities (Hutter & Jöhnk [98], ch. 8). Following this, introducing the characteristic values L, V, P, and $g = |\mathbf{b}|$ of length, velocity, pressure, and gravitation and assuming $|\mathbf{w}_F| \approx |\mathbf{v}_F|$, one obtains a dimensionless form of the extended *Navier-Stokes* equation

$$\frac{\rho^{FR}\,\mathrm{V}^2}{\mathrm{L}}\,[(\mathbf{v}_F)'_F]^* = \frac{\mu^{FR}\,\mathrm{V}}{\mathrm{L}^2}\,[\mathbf{t}_E^F]^* + \frac{\mathrm{V}}{K^F}\,[\widehat{\mathbf{p}}_E^F]^* - \frac{\mathrm{P}}{\mathrm{L}}\,[\mathrm{grad}\,p]^* + \rho^{FR}\,g\,[\mathbf{b}]^*\,, \tag{3.162}$$

where $[\,\cdot\,]^*$ indicates the dimensionless physical variables. Then, a dimensionless number is introduced relating the factor of the dimensionless friction force to the one of the dimensionless interaction force yielding

$$\Pi = \frac{\textit{friction force}}{\textit{interaction force}} = \frac{\mu^{FR}\,K^F}{\mathrm{L}^2} = \frac{K^S}{\mathrm{L}^2}\,. \tag{3.163}$$

In the framework of a macroscopic continuum theory, it is an obvious fact that the characteristic length of the macroscopic process L, e. g., the size of the specimen, is considerably larger than the internal length $\sqrt{K^S}$ characterizing the microstructure of the porous material, such as the average pore diameter. Accordingly, on the basis of this scale difference, it is directly concluded that

$$\mathrm{L} \gg \sqrt{K^S} \quad \longrightarrow \quad \Pi \ll 1 \quad \longrightarrow \quad |\mathbf{t}_E^F| \ll |\widehat{\mathbf{p}}_E^F|\,, \tag{3.164}$$

which implies that in the macroscopic Theory of Porous Media the interaction force dominates the nonlinear percolation process, whereas the fluid friction force is *a priori* negligible (Ehlers *et al.* [58]).

Note that from equation (3.162), one also recovers the conventional *Reynolds* number

$$Re = \frac{\textit{inertia force}}{\textit{friction force}} = \frac{\rho^{FR}\,\mathrm{V}\,\mathrm{L}}{\mu^{FR}} = \frac{\mathrm{V}\,\mathrm{L}}{\nu^{FR}}\,, \tag{3.165}$$

where $\nu^{FR} = \mu^{FR}/\rho^{FR}$ denotes the effective kinematic viscosity of φ^F. Thus, Re provides an estimate of the relative importance of the non-viscous inertia and viscous friction forces acting on a unit volume of fluid. For more details, see any text on fluid mechanics. ■

To continue, in order to constitutively describe the nonlinear influence on the flow speed, it is convenient for most applications to proceed from the classical 1-d *Forchheimer* equation (Forchheimer [69])

$$-\frac{\partial p}{\partial x} = \frac{\mu^{FR}}{K^S}\,w_F + \frac{\rho^{FR}}{B^S}\,w_F^2\,, \tag{3.166}$$

where the increasing importance of inertia effects at larger filter velocities w_F is described proportional to the kinetic energy $\frac{1}{2}\,\rho^{FR}\,w_F^2$ per unit fluid volume. Therein, the nonlinear velocity dependence is controlled by the tortuosity parameter B^S, which describes the inherent irregularity of the pore channels. Note that the usage of the intrinsic measures K^S and B^S is preferred as they are independent of the properties of the permeating fluid (cf. Rusch [153]). Transferred to 3-D, the quadratic form is retained by use of the norm

of the filter velocity yielding

$$-\operatorname{grad} p = \Big(\frac{\mu^{FR}}{K^S} + \frac{\rho^{FR}}{B^S}\,|\mathbf{w}_F|\Big)\,\mathbf{w}_F \quad \Leftrightarrow \quad -\frac{1}{\gamma^{FR}}\operatorname{grad} p = \Big(\frac{1}{k^F} + \frac{1}{b^S}\,|\mathbf{w}_F|\Big)\,\mathbf{w}_F\,. \tag{3.167}$$

Following this, the included nonlinearity can be totally assigned to a velocity-dependent permeability parameter as desired, viz.,

$$\mathbf{w}_F = -K_F^F \operatorname{grad} p \quad \text{with} \quad K_F^F(\mathbf{w}_F) := K^F \Big(1 + \frac{\rho^{FR}\,K^S}{\mu^{FR}\,B^S}\,|\mathbf{w}_F|\Big)^{-1}. \tag{3.168}$$

Herein, the rational expression $|\mathbf{w}_F|\,K^S/(\nu^{FR}\,B^S)$ represents a *Reynolds*-type dimensionless number (cf. relation (3.165)), which governs the relative importance of the tortuosity-induced inertia forces. However, for the further treatment, it is expedient to substitute the dependency on the filter velocity in equation $(3.168)_2$ with a pressure-gradient dependence by eliminating $|\mathbf{w}_F|$. This can be accomplished by taking the norm on both sides of equation $(3.167)_1$ and by solving the resulting quadratic equation for $|\mathbf{w}_F|$ yielding

$$|\mathbf{w}_F| = \tfrac{1}{2}\left(-\frac{\mu^{FR}\,B^S}{\rho^{FR}\,K^S} \underset{(-)}{+} \sqrt{\Big(\frac{\mu^{FR}\,B^S}{\rho^{FR}\,K^S}\Big)^2 + 4\,\frac{B^S}{\rho^{FR}}\,|\operatorname{grad} p|}\right), \tag{3.169}$$

where only the positive root is of interest as it satisfies the natural condition $|\mathbf{w}_F| = 0$ whenever $|\operatorname{grad} p| = 0$. Then, by inserting $|\mathbf{w}_F|$ into equation $(3.168)_2$, one finally obtains

$$K_F^F(\operatorname{grad} p) := K^F \left(\tfrac{1}{2} + \sqrt{\tfrac{1}{4} + \frac{\rho^{FR}}{B^S}\Big(\frac{K^S}{\mu^{FR}}\Big)^2 |\operatorname{grad} p|}\right)^{-1}. \tag{3.170}$$

It is seen that the permeability changes with $|\operatorname{grad} p|^{-1/2}$ as expected and it is apparent that the nonlinear effect is negligible when

$$|\operatorname{grad} p| \ll \frac{B^S}{\rho^{FR}}\Big(\frac{\mu^{FR}}{K^S}\Big)^2. \tag{3.171}$$

Note that the parameter K^F in equations (3.168) and (3.170) can be equivalently replaced by other permeability measures according to box (3.158), in order to define permeability functions $k_F^F(\mathbf{w}_F)$ and $k_F^F(\operatorname{grad} p)$ or $K_F^S(\mathbf{w}_F)$ and $K_F^S(\operatorname{grad} p)$, respectively. Moreover, it should be pointed out that the presented approach based on the quadratic *Forchheimer* formulation (3.166), as it is also described by Knupp & Lage [102], cannot recover all nonlinear effects, particularly when studying extremely high flow velocities. However, there is enough constitutive freedom to improve the nonlinear factor in expression (3.170), for instance, by incorporating an additional power $\delta > 0$ to explicitly control the nonlinear dependence on the pressure gradient, viz.:

$$K_F^F := K^F \left(\tfrac{1}{2} + \sqrt{\tfrac{1}{4} + \Big[\frac{\rho^{FR}}{B^S}\Big(\frac{K^S}{\mu^{FR}}\Big)^2 |\operatorname{grad} p|\Big]^{\delta}}\right)^{-1}. \tag{3.172}$$

Nevertheless, the present work adheres to the classical quadratic formulation associated with $\delta = 1$ because the second order inertia correction is not purely empirical as it can be derived from an appropriate averaging procedure of the *Navier-Stokes* equation for the flow of a *Newton*ian fluid in a rigid porous medium (Chen *et al.* [29]). For a more general discussion of nonlinear percolation processes, it is moreover referred to the books of Dullien [48] and Bear [7] and the quotations therein.

3.3.3 Deformation-dependent Permeability Properties

The sensitivity of the permeability to the current size of the interconnected pore volume (effective porosity) is apparent. Thus, proceeding from a finite deformation theory, it is inevitable to consider the flow controlling parameters as functions of the deformation state. For obvious reasons, the deformation dependency is best described if permeability changes are directly linked to porosity changes, which becomes clear by investigating the corresponding extremal values. On the one hand, the permeability decreases to zero (impermeable state) whenever the volumetric compression increases until all pores are closed (compaction point). On the other hand, a finite dilatation of the pore space is associated with rather perfectly permeable conditions, i. e., an infinitely increasing permeability. Thus, proceeding from the initial values k^F_{0S}, K^F_{0S}, K^S_{0S}, b^S_{0S}, B^S_{0S}, and β^S_{0S} of the flow controlling parameters in the undeformed state, the following limits must be met:

$$\{k^F, K^F, K^S, b^S, B^S, \beta^S\} \rightarrow \left\{ \begin{array}{c} 0 \\ \infty \end{array} \right\} \text{ if } \left\{ \begin{array}{l} n^F \rightarrow 0 \;\Leftrightarrow\; n^S \rightarrow 1 \;\Leftrightarrow\; J_S \rightarrow n^S_{0S}\,, \\ n^F \rightarrow 1 \;\Leftrightarrow\; n^S \rightarrow 0 \;\Leftrightarrow\; J_S \rightarrow \infty\,. \end{array} \right. \tag{3.173}$$

In this regard, Eipper [64] proposed a porosity-dependent hydraulic conductivity in the form of a power function

$$k^F(n^F) = k^F_{0S} \left(\frac{n^F}{n^F_{0S}} \right)^{\kappa} = k^F_{0S} \left(\frac{1 - n^S_{0S}\, J_S^{-1}}{1 - n^S_{0S}} \right)^{\kappa}, \tag{3.174}$$

where the exponent $\kappa \geq 0$ denotes an additional material parameter to govern the deformation dependency. An alternative approach, which is often used in the field of soft tissue biomechanics, is based on an exponential ansatz (Lai & Mow [105])

$$K^F(\mathrm{e}_{VS}) = K^F_{0S}\, e^{\kappa\, \mathrm{e}_{VS}} = K^F_{0S}\, e^{\kappa\,(J_S - 1)}\,, \tag{3.175}$$

where e_{VS} is the volumetric strain as defined in equation (2.15) and $\kappa \geq 0$ is a control parameter as before. However, applied to highly porous materials, such as soft polymeric foams, which allow absolutely finite compression and dilatation, both functions are unable to completely describe the nonlinear development of the permeability in the whole deformation range. In particular, for moderate values of κ, the power function does not increase rapidly enough in the extension region as it cannot describe the limiting case of an infinitely increasing permeability, whereas the exponential function violates the lower permeability limit in the finite compression region, which leads to circumstantial improvements of the exponential formulation (Holmes & Mow [91]). Therefore, a new

deformation-dependent permeability function is proposed, which similar to formulation (3.174) proceeds from a power ansatz but includes a hyperbolic expression of the porosity. Following this, a deformation-dependent intrinsic permeability is defined via

$$K^S(n^F) = K^S_{0S}\left(\frac{n^F}{1-n^F}\,\frac{1-n^F_{0S}}{n^F_{0S}}\right)^{\kappa} = K^S_{0S}\left(\frac{n^F}{n^F_{0S}}\,\frac{n^S_{0S}}{n^S}\right)^{\kappa} = K^S_{0S}\left(\frac{J_S - n^S_{0S}}{1-n^S_{0S}}\right)^{\kappa}, \qquad (3.176)$$

which considers both physical limits consistent with (3.173). The advantage of this formulation becomes clear by a direct comparison with the other presented functions. As can be seen in figure 3.2, the hyperbolic power law combines a sufficient increase in the extension region and a suitable decrease towards the fully compacted impermeable state. Note that for $\kappa = 0$ all formulations describe constant permeability properties depending on the initial value.

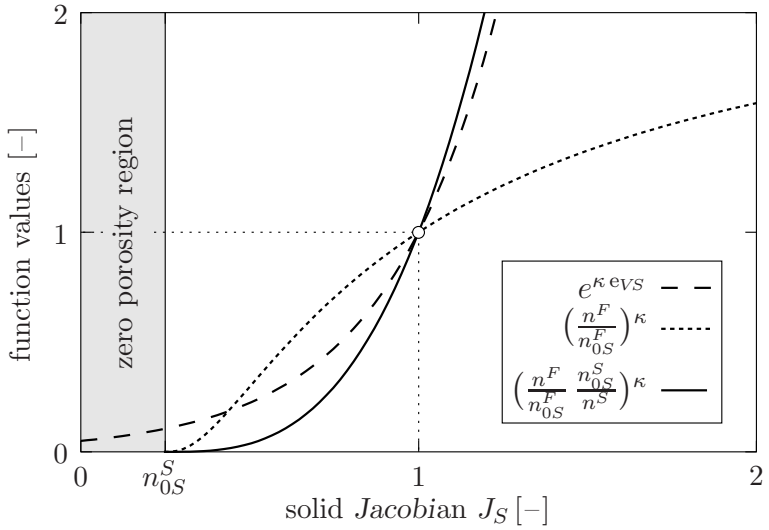

Figure 3.2: *Comparison of different deformation-dependent permeability functions with chosen values* $n^S_{0S} = 0.25$ *and* $\kappa = 3.0$

Analogously, one proceeds from a porosity-dependent tortuosity parameter

$$B^S(n^F) = B^S_{0S}\left(\frac{n^F}{1-n^F}\,\frac{1-n^F_{0S}}{n^F_{0S}}\right)^{\beta} = B^S_{0S}\left(\frac{n^F}{n^F_{0S}}\,\frac{n^S_{0S}}{n^S}\right)^{\beta} \qquad (3.177)$$

with the power $\beta \geq 0$ controlling the nonlinearity. As will be shown in section 5.2.2, the proposed formulations (3.176) and (3.177) can successfully be correlated with experimental data obtained from permeability studies on a high-porosity polyurethane foam.

3.3.4 Anisotropic Permeability

Hitherto, the presentation was restricted to isotropic permeability properties. However, real materials, such as layered soils, often show distinct orientation-dependent seepage flows, i. e., their interconnected pore space possesses preferred flow directions. Besides

this natural hydraulic anisotropy, moreover preferred flow paths may develop during finite distortions of the solid skeleton. Following this, it is expedient to proceed from a permeability tensor of the form

$$\mathbf{K}^F := K^F \, \boldsymbol{\mathcal{H}}^S \qquad \text{with} \qquad \boldsymbol{\mathcal{H}}^S := \boldsymbol{\mathcal{H}}^S_{0S} \, \boldsymbol{\mathcal{K}}^S \tag{3.178}$$

representing a dimensionless, symmetric, and positive definite hydraulic structural tensor, which is composed of a constant part $\boldsymbol{\mathcal{H}}^S_{0S}$ and a deformation-dependent part $\boldsymbol{\mathcal{K}}^S = \boldsymbol{\mathcal{K}}^S(\mathbf{F}_S)$. In particular, $\boldsymbol{\mathcal{H}}^S_{0S}$ describes the natural hydraulic anisotropy of φ^S (cf. figure 3.3(a)) and can be associated with a *hydraulic symmetry group* $\mathcal{HG}_3$ describing the inherent type of anisotropic permeability comparable to the material symmetry group introduced in the paragraph on page 63. Following this, the six independent components of $\boldsymbol{\mathcal{H}}^S_{0S} = (\boldsymbol{\mathcal{H}}^S_{0S})^T$ must be determined from permeability experiments on undeformed but variously rotated samples of the considered porous material. Therefore, in order that $\boldsymbol{\mathcal{H}}^S_{0S}$ is dimensionless, the experimentally determined permeability tensor, say $\mathbf{K}^{\text{exp}}_{0S}$, must be normalized, for instance with respect to its mean value or the average value of its coefficients. Then, by interpreting the normalizing constant as the initial, scalar-valued permeability parameter, e. g., $K^F_{0S} = \frac{1}{3} \operatorname{tr} \mathbf{K}^{\text{exp}}_{0S}$ or $K^F_{0S} = \frac{1}{9} \sum K^{\text{exp}}_{0S(kl)}$, one finally obtains $\boldsymbol{\mathcal{H}}^S_{0S} = \mathbf{K}^{\text{exp}}_{0S} / K^F_{0S}$. Following this, in the case of isotropic permeability properties associated with $\mathbf{K}^{\text{exp}}_{0S} = K^F_{0S} \, \mathbf{I}$, it is easily concluded that $\boldsymbol{\mathcal{H}}^S_{0S} \equiv \mathbf{I}$ (cf. figure 3.3(b)).

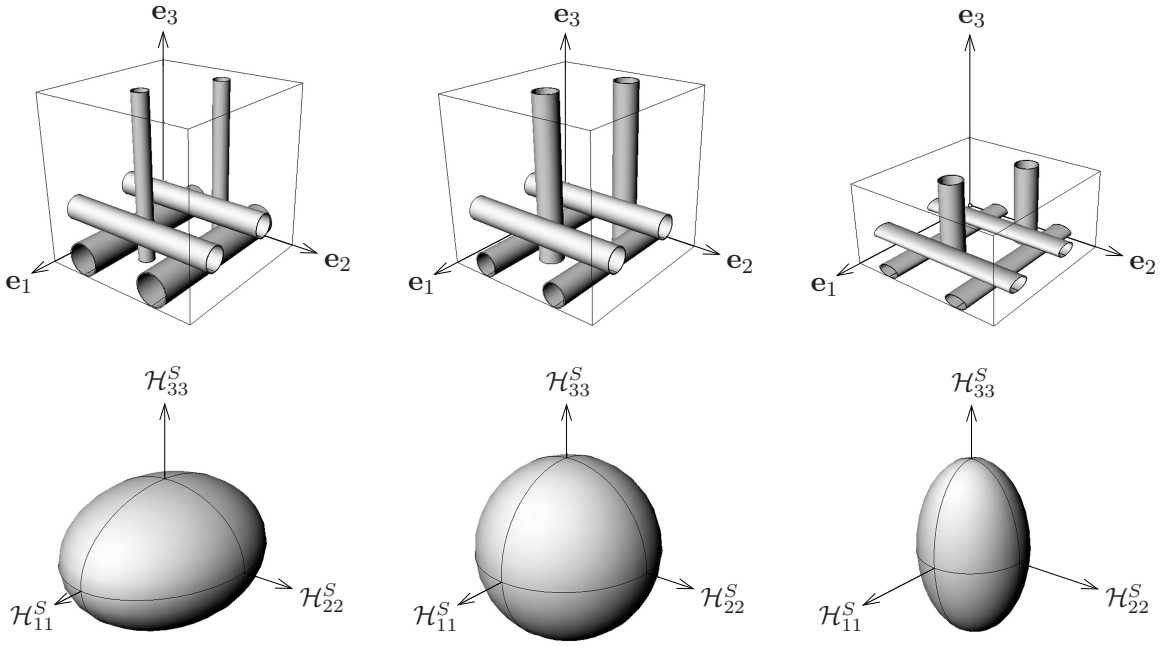

(a) undeformed initial state, anisotropic permeability, $\boldsymbol{\mathcal{H}}^S = \boldsymbol{\mathcal{H}}^S_{0S} \neq \mathbf{I}$, $\boldsymbol{\mathcal{K}}^S_{0S} = \mathbf{I}$

(b) undeformed initial state, isotropic permeability, $\boldsymbol{\mathcal{H}}^S = \boldsymbol{\mathcal{H}}^S_{0S} = \mathbf{I}$, $\boldsymbol{\mathcal{K}}^S_{0S} = \mathbf{I}$

(c) deformed configuration, anisotropic permeability, $\boldsymbol{\mathcal{H}}^S = \boldsymbol{\mathcal{K}}^S \neq \mathbf{I}$, $\boldsymbol{\mathcal{H}}^S_{0S} = \mathbf{I}$

Figure 3.3: *Simple capillary tube model of a porous solid illustrating initial and deformation-induced anisotropic permeability properties and visualization of the corresponding hydraulic structural tensor*

To continue, the deformation-dependent part of the hydraulic structural tensor $\boldsymbol{\mathcal{K}}^S$ must be specified in order to describe the deformation-induced permeability changes with respect to an undeformed reference state where $\boldsymbol{\mathcal{K}}^S_{0S} = \boldsymbol{\mathcal{K}}^S(\mathbf{F}_S = \mathbf{I}) \equiv \mathbf{I}$. As described by Eipper [64], the derivation of $\boldsymbol{\mathcal{K}}^S$ can be motivated with the help of capillary tube models, which proceed from an idealization of the real pore channels by a bundle of parallel tubes embedded in a solid material (cf. Bear [7], sec. 5.10.1). Assuming the tubes to be oriented along the orthogonal axes of a cube, confined uniaxial compression in the direction of one of the axes causes a decrease in the permeable cross-sections perpendicular to the loading direction, whereas the flow through the pipes in the loading direction is assumed to remain unchanged (see figure 3.3(c)). Note that this must not be regarded as a rigorous assumption as the general deformation dependency of the seepage flow is independently governed by the porosity-dependent parameters $K^S(n^F)$ and $B^S(n^F)$ given in equations (3.176) and (3.177) of the previous section.

Now, expressing the deformation dependency of $\boldsymbol{\mathcal{K}}^S$ by means of the eigenvalues of the deformation tensors, it is apparent from the situation depicted in figure 3.3(c) that the diagonal elements take the form $\mathcal{K}^S_{kk} = \mathcal{K}^S_{kk}(\lambda_{S(l)})\ \dot{\sum} k\ \forall\ l \neq k$, so that

$$\boldsymbol{\mathcal{K}}^S(\lambda_{S(k)}) = \begin{bmatrix} \mathcal{K}^S_{11}(\lambda_{S(2)}\,\lambda_{S(3)}) & 0 & 0 \\ 0 & \mathcal{K}^S_{22}(\lambda_{S(3)}\,\lambda_{S(1)}) & 0 \\ 0 & 0 & \mathcal{K}^S_{33}(\lambda_{S(1)}\,\lambda_{S(2)}) \end{bmatrix} \mathbf{e}_k \otimes \mathbf{e}_l\,. \tag{3.179}$$

Following this, proceeding from $\boldsymbol{\mathcal{K}}^S$ as an isotropic tensor function of the current configuration, which in contrast to $\boldsymbol{\mathcal{H}}^S_{0S}$ is invariant to changes of the reference configuration, formal generalization yields the following spectral representation (recall section 2.2.4):

$$\boldsymbol{\mathcal{K}}^S(\lambda_{S(k)}) = \tfrac{1}{2} \sum_{\substack{k=1 \\ j\neq l\neq k\neq j}}^{3} (\lambda_{S(j)}\,\lambda_{S(l)})^{\vartheta}\, \mathbf{N}_{S(k)} \equiv (\operatorname{cof} \mathbf{B}_S)^{\vartheta}\,. \tag{3.180}$$

Herein, the real-valued power $\vartheta \geq 0$ is introduced to control the nonlinearity of the deformation-induced anisotropy, where the deformation dependency is turned off if $\vartheta = 0$, i. e., $\boldsymbol{\mathcal{K}}^S \equiv \mathbf{I}$ (Eipper [64]). Moreover, since $\lambda_{S(j)}\,\lambda_{S(l)}$ $(j \neq l)$ represent the eigenvalues of the cofactors of the deformation tensors, the deformation-dependent hydraulic anisotropy tensor essentially represents a real-valued power of the cofactor of $\mathbf{B}_S$. Consequently, from a computational perspective, the calculation of $\boldsymbol{\mathcal{K}}_S$ does not cause additional expenses as the eigenvalues and eigentensors of $\mathbf{B}_S$ are also required for the equilibrium-stress computation based on the *Ogden*-type formulation presented in section 3.2.3.

Finally, to conclude this section, the constitutive filter law is summarized in box (3.181), where the advantage of the proposed formulation is directly seen. Although all relevant nonlinearities are included, it still has the simple form of a *Darcy*-type equation as the nonlinear dependencies are completely considered by the permeability tensor $\mathbf{K}^F$. Thus, the anisotropic, non-*Darcy* filter law is easy to implement and the idea of a velocity and deformation-dependent permeability can at least be adopted to extend existing linear formulations.

Complete nonlinear filter law

$$
\begin{aligned}
&\textit{basic filter law:} && \mathbf{w}_F = n^F\,\mathbf{w}_{FR} = -\mathbf{K}^F\,(\operatorname{grad} p - \rho^{FR}\,\mathbf{b}) \\
&\textit{permeability tensor:} && \mathbf{K}^F = K_F^F\,\boldsymbol{\mathcal{H}}^S = K_F^F\,\boldsymbol{\mathcal{H}}_{0S}^S\,(\operatorname{cof}\mathbf{B}_S)^{\vartheta}\,, \quad \vartheta \geq 0 \\
&\textit{nonlinear permeability:} && K_F^F = \frac{K^S}{\mu^{FR}}\left(\tfrac{1}{2} + \sqrt{\tfrac{1}{4} + \frac{\rho^{FR}}{B^S}\left(\frac{K^S}{\mu^{FR}}\right)^2 |\operatorname{grad} p|}\,\right)^{-1} \\
&\textit{intrinsic permeability:} && K^S = K_{0S}^S\left(\frac{n^F}{n_{0S}^F}\,\frac{n_{0S}^S}{n^S}\right)^{\kappa}\,, \quad \kappa \geq 0 \\
&\textit{tortuosity parameter:} && B^S = B_{0S}^S\left(\frac{n^F}{n_{0S}^F}\,\frac{n_{0S}^S}{n^S}\right)^{\beta}\,, \quad \beta \geq 0
\end{aligned}
\tag{3.181}
$$

4 Numerical Treatment

This chapter is concerned with the numerical treatment of the biphasic solid-fluid model discussed in the preceding chapter. For this purpose, the finite element method (FEM) has been proven to provide a suitable formalism for generating a discrete algorithm to approximate the solution of the descriptive set of coupled partial differential equations. In this regard, the required weak formulations of the governing balance relations and their linearizations are presented, followed by appropriate techniques for the discretization of the arising mixed formulation in the space and the time domain including the local treatment of the inelastic evolution equations. Finally, the algorithm for the nonlinear viscoelastic solid stress computation is discussed, followed by a paragraph on the eigenvalue and eigentensor calculation.

4.1 Weak Formulation

The quasi-static biphasic model under consideration incorporates three independent fields, namely the solid displacement $\mathbf{u}_S$, the seepage velocity $\mathbf{w}_{FR}$, and the effective pore-fluid pressure p, which basically demands three corresponding equations for the solution[1]. However, proceeding from quasi-static conditions, the seepage velocity can be substituted by the constitutive filter law (3.181), which is actually a function of $\mathbf{u}_S$ and p. Consequently, $\mathbf{w}_{FR}$ looses the nature of an independent field variable and thus, can be calculated in a post processing step, so that the number of unknowns of the process as well as the number of required conditional equations reduces to two. In particular, the governing partial differential equations are the fluid mass balance (3.3) with $\mathbf{w}_{FR}$ eliminated by use of the filter law (3.181) and the time derivatives rewritten with respect to the solid motion

$$n^F (\rho^{FR})'_S + \rho^{FR} \operatorname{div} (\mathbf{u}_S)'_S - \operatorname{div} \left[\rho^{FR} \mathbf{K}^F \left(\operatorname{grad} p - \rho^{FR} \mathbf{b} \right) \right] = 0 \,, \tag{4.1}$$

and the momentum balance of the mixture obtained as the sum of the partial momentum balances (3.4) by taking into account that $\widehat{\mathbf{p}}^S + \widehat{\mathbf{p}}^F = \mathbf{0}$ yielding

$$\operatorname{div} (\mathbf{T}^S_E - p \, \mathbf{I}) + (n^S \rho^{SR} + n^F \rho^{FR}) \, \mathbf{b} = \mathbf{0} \,. \tag{4.2}$$

Now, following the idea of the FEM, the above field equations must be transferred to weak formulations. Therefore, the balance relations are weighted by independent test functions and integrated over the spatial domain Ω occupied by the mixture body $\mathcal{B}$. As usual, the surface $\Gamma = \partial \Omega$ is split into a *Dirichlet* (essential) and a *Neumann* (natural)

[1] Actually, the solution of the viscoelastic solid model, which is based on the internal variable concept, additionally requires the corresponding evolution equations. As usual in computational inelasticity, the internal (history) variables will be computed in the sense of a collocation method at the integration points of the discretized spatial domain. Following this, the internal variables are only indirectly included in the weak formulation via the solid extra stress tensor and will therefore be described later.

boundary yielding $\Gamma = \Gamma_p \cup \Gamma_q$ for the fluid mass balance and $\Gamma = \Gamma_{\mathbf{u}_s} \cup \Gamma_{\mathbf{t}}$ for the mixture momentum balance. Then, applying the product rule and the *Gaußian* integral theorem, one obtains the weak formulation of the fluid balance of mass as

$$\begin{aligned} \mathcal{G}_p(\delta p, \mathbf{u}_S, p) \equiv \int_\Omega \delta p \left[n^F (\rho^{FR})'_S + \rho^{FR} \operatorname{div} (\mathbf{u}_S)'_S \right] \mathrm{d}v + \\ + \int_\Omega \operatorname{grad} \delta p \cdot \left[\rho^{FR} \mathbf{K}^F \left(\operatorname{grad} p - \rho^{FR} \mathbf{b} \right) \right] \mathrm{d}v + \int_{\Gamma_q} \delta p \, \overline{q} \, \mathrm{d}a = 0 \,, \end{aligned} \tag{4.3}$$

and the weak formulation of the mixture momentum balance becomes

$$\begin{aligned} \mathcal{G}_{\mathbf{u}_S}(\delta \mathbf{u}_S, \mathbf{u}_S, p) \equiv \int_\Omega \operatorname{grad} \delta \mathbf{u}_S \cdot (\mathbf{T}^S_E - p \, \mathbf{I}) \, \mathrm{d}v - \\ - \int_\Omega \delta \mathbf{u}_S \cdot (n^S \rho^{SR} + n^F \rho^{FR}) \, \mathbf{b} \, \mathrm{d}v - \int_{\Gamma_{\mathbf{t}}} \delta \mathbf{u}_S \cdot \overline{\mathbf{t}} \, \mathrm{d}a = 0 \,. \end{aligned} \tag{4.4}$$

Herein, $\delta \mathbf{u}_S$ and δp are the test functions, which can be interpreted as virtual fields corresponding to the solid displacement $\mathbf{u}_S$ and the pore-fluid pressure p. In this context, note that $\mathbf{u}_S = \overline{\mathbf{u}}_S$ on $\Gamma_{\mathbf{u}_S}$ and $p = \overline{p}$ on Γ_p exactly fulfill the *Dirichlet* boundary conditions, whereas the test functions $\delta \mathbf{u}_S$ and δp identically vanish on *Dirichlet* boundaries. Moreover, $\overline{\mathbf{t}} = (\mathbf{T}^S_E - p \, \mathbf{I}) \, \mathbf{n}$ is the external load vector acting on the *Neumann* boundary $\Gamma_{\mathbf{t}}$ with the outward oriented unit surface normal $\mathbf{n}$ and $\overline{q} = n^F \rho^{FR} \, \mathbf{w}_{FR} \cdot \mathbf{n}$ denotes the filter mass flow rate of the fluid draining through the *Neumann* boundary Γ_q. Note that the surface traction $\overline{\mathbf{t}} = \overline{\mathbf{t}}^S + \overline{\mathbf{t}}^F$ acts on both the solid and the fluid phase. This is essential for the formulation of boundary-value problems as no separation of the boundary conditions into actions on the different phases is needed and thus, physically meaningful boundary conditions can be applied.

For the special case of a materially incompressible pore liquid ($\rho^{FR} = \text{const.}$), the weak form of the fluid mass balance (4.3) naturally reduces to a volume balance

$$\begin{aligned} \mathcal{G}_p(\delta p, \mathbf{u}_S, p) \equiv \int_\Omega \delta p \operatorname{div} (\mathbf{u}_S)'_S \, \mathrm{d}v + \\ + \int_\Omega \operatorname{grad} \delta p \cdot \left[\mathbf{K}^F \left(\operatorname{grad} p - \rho^{FR} \mathbf{b} \right) \right] \mathrm{d}v + \int_{\Gamma_q} \delta p \, \overline{v} \, \mathrm{d}a = 0 \end{aligned} \tag{4.5}$$

with $\overline{v} = n^F \, \mathbf{w}_{FR} \cdot \mathbf{n}$ denoting the volume efflux of φ^F through the boundary Γ_q. However, both weak formulations (4.3) and (4.5) essentially determine p such that the saturation condition is preserved, which becomes clear from the fact that both relations can be attributed to the constraint $(n^S + n^F)'_S = 0$ (cf. equations (3.12) and (3.13)). For a more detailed discussion of the weak formulations within the TPM approach including extensions to dynamic porous media problems, the reader is encouraged to refer to Diebels & Ehlers [44], Ehlers & Ellsiepen [57], and Ellsiepen [65].

4.2 Linearization

The two-field variational formulation given by equations (4.3) and (4.4) possesses geometrical as well as material nonlinearities. Therefore, in preparation for an efficient numerical treatment by an iterative solution technique, such as the *Newton-Raphson* method, the linearization of the weak forms is required. In this context, a so-called *consistent* linearization must be carried out, which proceeds from a complete (consistent) equal-order linearization with respect to all occurring unknowns of the process, namely the solid displacement $\mathbf{u}_S$ and the effective pore-fluid pressure p. The keystone of the linearization procedure is the directional or *Gâteaux* derivative (Hughes & Pister [97], Wriggers [194])

$$\mathcal{D}_{\Delta \boldsymbol{u}} \mathcal{F}(\boldsymbol{u}) := \lim_{\epsilon \to 0} \frac{\mathcal{F}(\boldsymbol{u} + \epsilon\, \Delta \boldsymbol{u}) - \mathcal{F}(\boldsymbol{u})}{\epsilon} = \frac{\mathrm{d}}{\mathrm{d}\epsilon} \mathcal{F}(\boldsymbol{u} + \epsilon\, \Delta \boldsymbol{u}) \Big|_{\epsilon=0} \tag{4.6}$$

assuming that a linear *Gâteaux* differential (weak differential) $\mathcal{D}_{\Delta \boldsymbol{u}} \mathcal{F}(\boldsymbol{u})$ exists, which describes the change of the function $\mathcal{F}$ at $\boldsymbol{u}$ in the direction of $\Delta \boldsymbol{u}$. Thus, the linearization of a nonlinear function $\mathcal{F}$ about $\widetilde{\boldsymbol{u}}$ results from a first-order *Taylor* series expansion

$$\mathcal{F}(\boldsymbol{u}) = \mathcal{F}(\widetilde{\boldsymbol{u}}) + \mathcal{D}_{\Delta \boldsymbol{u}} \mathcal{F}(\widetilde{\boldsymbol{u}}) + \mathcal{R}(\Delta \boldsymbol{u}) \quad \longrightarrow \quad \mathcal{F}_{\mathrm{lin}}(\boldsymbol{u}) = \mathcal{F}(\widetilde{\boldsymbol{u}}) + \mathcal{D}_{\Delta \boldsymbol{u}} \mathcal{F}(\widetilde{\boldsymbol{u}}) \tag{4.7}$$

under the assumption that the remainder term $\mathcal{R}(\Delta \boldsymbol{u})$ is negligibly small.

To begin with, for the sake of a clear and compact representation, the weak forms $\mathcal{G}_{\mathbf{u}_S}$ and $\mathcal{G}_p$ are collected in a function vector $\boldsymbol{\mathcal{G}}_{\boldsymbol{u}}$ and the primary unknown field variables $\mathbf{u}_S$ and p are summarized in a vector of unknowns $\boldsymbol{u}$:

$$\boldsymbol{\mathcal{G}}_{\boldsymbol{u}} = \begin{bmatrix} \mathcal{G}_{\mathbf{u}_S} \\ \mathcal{G}_p \end{bmatrix}, \quad \boldsymbol{u} = \begin{bmatrix} \mathbf{u}_S \\ p \end{bmatrix}, \quad \delta \boldsymbol{u} = \begin{bmatrix} \delta \mathbf{u}_S \\ \delta p \end{bmatrix}, \quad (\boldsymbol{u})'_S = \begin{bmatrix} (\mathbf{u}_S)'_S \\ (p)'_S \end{bmatrix}, \quad \Delta \boldsymbol{u} = \begin{bmatrix} \Delta \mathbf{u}_S \\ \Delta p \end{bmatrix}. \tag{4.8}$$

In this connection, one additionally introduces the corresponding vector of test functions $\delta \boldsymbol{u}$, the solid time derivative of the vector of unknowns $(\boldsymbol{u})'_S$, which will be discretized by an appropriate time integration scheme[2], and the incremental vector $\Delta \boldsymbol{u}$, which can be viewed as the increment of an iterative solution procedure at a fixed time. Following this, the linearization of the two-field variational formulation, which is still continuous in the space and the time domain, takes the form

$$(\boldsymbol{\mathcal{G}}_{\boldsymbol{u}})_{\mathrm{lin}}[\delta \boldsymbol{u}, \boldsymbol{u}, (\boldsymbol{u})'_S] = \widetilde{\boldsymbol{\mathcal{G}}}_{\boldsymbol{u}} + \mathcal{D}_{\Delta \boldsymbol{u}} \widetilde{\boldsymbol{\mathcal{G}}}_{\boldsymbol{u}} + \mathcal{D}_{\Delta (\boldsymbol{u})'_S} \widetilde{\boldsymbol{\mathcal{G}}}_{\boldsymbol{u}} \quad \text{with} \quad \widetilde{\boldsymbol{\mathcal{G}}}_{\boldsymbol{u}} = \boldsymbol{\mathcal{G}}_{\boldsymbol{u}}[\delta \boldsymbol{u}, \widetilde{\boldsymbol{u}}, (\widetilde{\boldsymbol{u}})'_S], \tag{4.9}$$

where $\widetilde{\boldsymbol{u}}$ indicates the expansion point of the current configuration. In this representation, the *Gâteaux* differentials can be expressed in concise matrix form, viz.

$$\mathcal{D}_{\Delta \boldsymbol{u}} \widetilde{\boldsymbol{\mathcal{G}}}_{\boldsymbol{u}} = \left[\begin{array}{c|c} \mathcal{D}_{\Delta \mathbf{u}_S} \widetilde{\mathcal{G}}_{\mathbf{u}_S} & \mathcal{D}_{\Delta p} \widetilde{\mathcal{G}}_{\mathbf{u}_S} \\ \hline \mathcal{D}_{\Delta \mathbf{u}_S} \widetilde{\mathcal{G}}_p & \mathcal{D}_{\Delta p} \widetilde{\mathcal{G}}_p \end{array}\right], \quad \mathcal{D}_{\Delta (\boldsymbol{u})'_S} \widetilde{\boldsymbol{\mathcal{G}}}_{\boldsymbol{u}} = \left[\begin{array}{c|c} \mathcal{D}_{\Delta (\mathbf{u}_S)'_S} \widetilde{\mathcal{G}}_{\mathbf{u}_S} & \mathcal{D}_{\Delta (p)'_S} \widetilde{\mathcal{G}}_{\mathbf{u}_S} \\ \hline \mathcal{D}_{\Delta (\mathbf{u}_S)'_S} \widetilde{\mathcal{G}}_p & \mathcal{D}_{\Delta (p)'_S} \widetilde{\mathcal{G}}_p \end{array}\right]. \tag{4.10}$$

[2] Note that $(\mathbf{u}_S)'_S$ and $(p)'_S$ are not additional degrees of freedom (DOF) in the sense of a weak formulation. They merely serve to transform the global set of equations into a system of first-order differential equations in time (cf. Ellsiepen [65]).

Since the directional derivative (4.6) represents a linear operator, the common rules of differential calculus can be applied. Following this, together with the transport properties of the gradient operator (2.41), the required basic linearizations can be straightforwardly computed (cf. Eipper [64]) and are summarized in box (4.11). For convenience, in the

Collection of basic linearizations

$$
\begin{aligned}
\mathcal{D}_{\Delta\mathbf{u}_S}\mathbf{F}_S &= \frac{\mathrm{d}}{\mathrm{d}\epsilon}\,\mathrm{Grad}_S(\mathbf{x}+\epsilon\,\Delta\mathbf{u}_S)\Big|_{\epsilon=0} = \mathrm{Grad}_S\Delta\mathbf{u}_S \\
\mathcal{D}_{\Delta\mathbf{u}_S}\mathbf{F}_S^{-1} &= -\mathbf{F}_S^{-1}\,(\mathcal{D}_{\Delta\mathbf{u}_S}\mathbf{F}_S)\,\mathbf{F}_S^{-1} = -\mathbf{F}_S^{-1}\,\mathrm{grad}\,\Delta\mathbf{u}_S \\
\mathcal{D}_{\Delta\mathbf{u}_S}\,\mathrm{grad}\,\boldsymbol{\Psi} &= (\mathrm{Grad}_S\,\boldsymbol{\Psi})\,\mathcal{D}_{\Delta\mathbf{u}_S}\mathbf{F}_S^{-1} = -(\mathrm{grad}\,\boldsymbol{\Psi})\,\mathrm{grad}\,\Delta\mathbf{u}_S \\
\mathcal{D}_{\Delta\mathbf{u}_S}\,\mathrm{grad}\,\Psi &= (\mathcal{D}_{\Delta\mathbf{u}_S}\mathbf{F}_S^{T-1})\,\mathrm{Grad}_S\,\Psi = -(\mathrm{grad}^T\Delta\mathbf{u}_S)\,\mathrm{grad}\,\Psi \\
\mathcal{D}_{\Delta\mathbf{u}_S}J_S &= \frac{\partial J_S}{\partial\mathbf{F}_S}\cdot\mathcal{D}_{\Delta\mathbf{u}_S}\mathbf{F}_S = J_S\,\mathbf{F}_S^{T-1}\cdot\mathrm{Grad}_S\Delta\mathbf{u}_S = J_S\,\mathrm{div}\Delta\mathbf{u}_S \\
\mathcal{D}_{\Delta\mathbf{u}_S}\Big[\int_{\Omega}(\,\bullet\,)\,\mathrm{d}v\Big] &= \int_{\Omega_0}\mathcal{D}_{\Delta\mathbf{u}_S}\big[(\,\bullet\,)\,J_S\big]\,\mathrm{d}V_S = \int_{\Omega}\big[\mathcal{D}_{\Delta\mathbf{u}_S}(\,\bullet\,) + (\,\bullet\,)\,\mathrm{div}\Delta\mathbf{u}_S\big]\,\mathrm{d}v \\
\mathcal{D}_{\Delta(\mathbf{u}_S)'_S}\,\mathrm{div}\,(\mathbf{u}_S)'_S &= \frac{\mathrm{d}}{\mathrm{d}\epsilon}\,\mathrm{div}\,[(\mathbf{u}_S)'_S + \epsilon\,\Delta(\mathbf{u}_S)'_S]\Big|_{\epsilon=0} = \mathrm{div}\Delta(\mathbf{u}_S)'_S \\
\mathcal{D}_{\Delta p}\,\mathrm{grad}\,p &= \frac{\mathrm{d}}{\mathrm{d}\epsilon}\,\mathrm{grad}\,(p+\epsilon\,\Delta p)\Big|_{\epsilon=0} = \mathrm{grad}\,\Delta p
\end{aligned}
\tag{4.11}
$$

following considerations, the boundary terms $\overline{\mathbf{t}}$ and $\overline{q}$ and thus, the surface integrals are assumed to be independent of the deformation, i. e., they do not contribute to the linearization. Moreover, the uniform mass-specific external body force $\mathbf{b}$ is identified with the gravitational acceleration and regarded as constant. Therefore, for the determination of the individual elements of $\mathcal{D}_{\Delta\boldsymbol{u}}\widetilde{\boldsymbol{\mathcal{G}}}_{\boldsymbol{u}}$ and $\mathcal{D}_{\Delta(\boldsymbol{u})'_S}\widetilde{\boldsymbol{\mathcal{G}}}_{\boldsymbol{u}}$, besides the basic linearizations in box (4.11), it remains to take into account the functional dependencies of the solid extra stress tensor, the effective fluid density, and the permeability tensor on the set of primary unknowns $\boldsymbol{u}$ according to the underlying constitutive equations. In particular, with the inelastic deformation tensors summarized in a vector of internal (history) variables $\boldsymbol{q} = [(\mathbf{C}_{Si})_1, ..., (\mathbf{C}_{Si})_N]^T$, it holds[3]

$$
\begin{aligned}
&\mathbf{T}_E^S = J_S^{-1}\,\mathbf{F}_S\,\mathbf{S}_E^S\,\mathbf{F}_S^T \qquad \text{with} \qquad \mathbf{S}_E^S = \mathbf{S}_E^S[\mathbf{u}_S, \boldsymbol{q}(\mathbf{u}_S)]\,, \\
&\rho^{FR} = \rho^{FR}(p) \quad \longrightarrow \quad (\rho^{FR})'_S = \frac{\partial\rho^{FR}}{\partial p}\,(p)'_S\,, \qquad \mathbf{K}^F = \mathbf{K}^F(\mathbf{u}_S, p)\,.
\end{aligned}
\tag{4.12}
$$

Beginning with the weak formulation of the mixture momentum balance (4.4), lineariza-

[3] For more details on the indirect dependency of $\mathbf{S}_E^S$ on the displacement field through the internal variables $(\mathbf{C}_{Si})_n$, see the paragraph on page 97.

tion of the individual terms yields the following partial results:

$$\mathcal{D}_{\Delta\mathbf{u}_S}\big[\int_\Omega \operatorname{grad}\delta\mathbf{u}_S\cdot\mathbf{T}^S_E\,\mathrm{d}v\big] = \\ = \int_\Omega \operatorname{grad}\delta\mathbf{u}_S\cdot\big[J_S^{-1}\,\mathbf{F}_S\,(\mathcal{D}_{\Delta\mathbf{u}_S}\mathbf{S}^S_E)\,\mathbf{F}_S^T + (\operatorname{grad}\Delta\mathbf{u}_S)\,\mathbf{T}^S_E\big]\,\mathrm{d}v\,, \tag{4.13}$$

$$\mathcal{D}_{\Delta\mathbf{u}_S}\big[\int_\Omega -\operatorname{grad}\delta\mathbf{u}_S\cdot p\,\mathbf{I}\,\mathrm{d}v\big] = \int_\Omega \operatorname{grad}\delta\mathbf{u}_S\cdot p\,\big[\operatorname{grad}^T\Delta\mathbf{u}_S - (\operatorname{div}\Delta\mathbf{u}_S)\,\mathbf{I}\big]\,\mathrm{d}v\,, \tag{4.14}$$

$$\mathcal{D}_{\Delta\mathbf{u}_S}\big[\int_\Omega \delta\mathbf{u}_S\cdot(n^S\rho^{SR}+n^F\rho^{FR})\,\mathbf{b}\,\mathrm{d}v\big] = \int_\Omega \delta\mathbf{u}_S\cdot(\operatorname{div}\Delta\mathbf{u}_S)\,\rho^{FR}\,\mathbf{b}\,\mathrm{d}v\,, \tag{4.15}$$

$$\mathcal{D}_{\Delta p}\big[\int_\Omega -\operatorname{grad}\delta\mathbf{u}_S\cdot p\,\mathbf{I}\,\mathrm{d}v\big] = \int_\Omega -\operatorname{grad}\delta\mathbf{u}_S\cdot\Delta p\,\mathbf{I}\,\mathrm{d}v\,, \tag{4.16}$$

$$\mathcal{D}_{\Delta p}\big[\int_\Omega \delta\mathbf{u}_S\cdot(n^S\rho^{SR}+n^F\rho^{FR})\,\mathbf{b}\,\mathrm{d}v\big] = \int_\Omega -\delta\mathbf{u}_S\cdot n^F\,\frac{\partial\rho^{FR}}{\partial p}\,\Delta p\,\mathbf{b}\,\mathrm{d}v\,. \tag{4.17}$$

Therein, in equation (4.13), the covariant push-forward of the directional derivative of the referential solid extra stress tensor is obtained as

$$\begin{aligned}\mathbf{F}_S\,(\mathcal{D}_{\Delta\mathbf{u}_S}\mathbf{S}^S_E)\,\mathbf{F}_S^T &= \mathbf{F}_S\Big(\frac{\mathrm{d}\mathbf{S}^S_E}{\mathrm{d}\mathbf{E}_S}\,\mathcal{D}_{\Delta\mathbf{u}_S}\mathbf{E}_S\Big)\mathbf{F}_S^T = (\mathbf{F}_S\otimes\mathbf{F}_S)^{\overset{23}{T}}\,\frac{\mathrm{d}\mathbf{S}^S_E}{\mathrm{d}\mathbf{E}_S}\,\mathcal{D}_{\Delta\mathbf{u}_S}\mathbf{E}_S \\ &= (\mathbf{F}_S\otimes\mathbf{F}_S)^{\overset{23}{T}}\,\overset{4}{\boldsymbol{\mathcal{B}}}{}^S\,\tfrac{1}{2}\,\big[\mathbf{F}_S^T\operatorname{Grad}_S\Delta\mathbf{u}_S + (\operatorname{Grad}_S^T\Delta\mathbf{u}_S)\,\mathbf{F}_S\big] \\ &= (\mathbf{F}_S\otimes\mathbf{F}_S)^{\overset{23}{T}}\,\overset{4}{\boldsymbol{\mathcal{B}}}{}^S\,(\mathbf{F}_S^T\otimes\mathbf{F}_S^T)^{\overset{23}{T}}\,\tfrac{1}{2}\,\big[\operatorname{grad}\Delta\mathbf{u}_S + \operatorname{grad}^T\Delta\mathbf{u}_S\big] \\ &= \overset{4}{\boldsymbol{\mathcal{C}}}{}^S\,\tfrac{1}{2}\,\big[\operatorname{grad}\Delta\mathbf{u}_S + \operatorname{grad}^T\Delta\mathbf{u}_S\big]\,,\end{aligned} \tag{4.18}$$

where

$$\overset{4}{\boldsymbol{\mathcal{B}}}{}^S := \frac{\mathrm{d}\mathbf{S}^S_E}{\mathrm{d}\mathbf{E}_S} \qquad \text{and} \qquad \overset{4}{\boldsymbol{\mathcal{C}}}{}^S := (\mathbf{F}_S\otimes\mathbf{F}_S)^{\overset{23}{T}}\,\overset{4}{\boldsymbol{\mathcal{B}}}{}^S\,(\mathbf{F}_S^T\otimes\mathbf{F}_S^T)^{\overset{23}{T}} \tag{4.19}$$

represent the consistent tangent moduli of the finite solid viscoelasticity formulation related to the reference and the actual configuration.

Consistent viscoelastic tangent operator: In the course of the subsequent discretization procedure, the viscoelastic solid stress tangent $(\boldsymbol{\mathcal{C}}^S)^{\underline{4}}$ must be replaced with its discrete counterpart. In order to improve the convergence characteristic of the global iterative solution algorithm in expectation of a quadratic rate of asymptotic convergence of the overall nonlinear biphasic problem, the consistency of the inelastic stiffness tensor is essential (see Simo & Taylor [166] among others). Particularly, the included transient non-equilibrium stiffness contributions associated with the *Maxwell* elements must be carefully handled taking into account the algorithmic treatment of the viscous evolution equations. This becomes clear by looking closer at the *algorithmically consistent* tangent operator of the

reference configuration. In analogy to the continuum tangent, the consistent tangent can be split into an equilibrium and a non-equilibrium part:

$$\overset{4}{\boldsymbol{\mathcal{B}}}{}^{S} = \frac{\mathrm{d}\mathbf{S}_E^S}{\mathrm{d}\mathbf{E}_S} = \overset{4}{\boldsymbol{\mathcal{B}}}{}^{S}_{EQ} + \overset{4}{\boldsymbol{\mathcal{B}}}{}^{S}_{NEQ}\,, \quad \text{where} \quad \begin{cases} \overset{4}{\boldsymbol{\mathcal{B}}}{}^{S}_{EQ} = \dfrac{\mathrm{d}\mathbf{S}_{EQ}^S}{\mathrm{d}\mathbf{E}_S} \equiv \overset{4}{\mathbf{B}}{}^{S}_{EQ}\,, \\ \overset{4}{\boldsymbol{\mathcal{B}}}{}^{S}_{NEQ} = \dfrac{\mathrm{d}\mathbf{S}_{NEQ}^S}{\mathrm{d}\mathbf{E}_S} \neq \overset{4}{\mathbf{B}}{}^{S}_{NEQ}\,. \end{cases} \tag{4.20}$$

It is apparent that the non-equilibrium parts of the consistent and the continuum tangents are different, which calls for a detailed examination. In anticipation of the numerical solution strategy, the consistent non-equilibrium tangent is derived as follows:

$$\overset{4}{\boldsymbol{\mathcal{B}}}{}^{S}_{NEQ} = \frac{\mathrm{d}\mathbf{S}_{NEQ}^S}{\mathrm{d}\mathbf{E}_S} = \underbrace{\overbrace{\sum_{n=1}^{N} \frac{\partial \mathbf{S}_n^S}{\partial (\mathbf{E}_{Se})_n} \frac{\mathrm{d}(\mathbf{E}_{Se})_n}{\mathrm{d}\mathbf{E}_S}}^{(\mathbf{F}_{Si})_n = \text{const.}}}_{\overset{4}{\mathbf{B}}{}^{S}_{NEQ}} + \underbrace{\overbrace{\sum_{n=1}^{N} \frac{\partial \mathbf{S}_n^S}{\partial (\mathbf{E}_{Si})_n} \frac{\mathrm{d}(\mathbf{E}_{Si})_n}{\mathrm{d}\mathbf{E}_S}}^{\mathbf{F}_S = \text{const.}}}_{\overset{4}{\mathbf{B}}{}^{S}_{\boldsymbol{q}}}} . \tag{4.21}$$

Herein, besides the non-equilibrium continuum tangent known from equations (3.129 – 3.131), a new 4th-order tensor $(\mathbf{B}_{\boldsymbol{q}}^S)^{\underline{4}}$ can be identified, which involves contributions related to the internal inelastic strain variables. Thus, as a matter of fact, the consistent non-equilibrium tangent depends on the implemented solution algorithm. Here, following the common practice in computational plasticity (cf. Simo & Hughes [165]), a two-stage iterative solution strategy is applied. First, the internal variables $\boldsymbol{q}$ are determined locally at the integration points of the numerical quadrature for fixed global variables $\boldsymbol{u}$, i. e., the actual configuration is regarded as fixed implying $\mathbf{F}_S(\mathbf{u}_S) = \text{const.}$ for the iterative solution of the time discrete viscous evolution equations. Thereafter, in the global iteration step, the inelastic deformation tensors $(\mathbf{C}_{Si})_n$ are regarded as constant given history variables associated with fixed intermediate configurations $(\mathbf{F}_{Si})_n = \text{const}$. However, the internal variables are iterated depending on the current values of the external variables and thus, indirectly contribute as an explicit function of $\mathbf{u}_S$ to the *Jacobi*an matrix of the discrete nonlinear global system. For further particulars on the solution algorithm, see section 4.3.2. A general description of the solution strategy based on a more abstract mathematical representation is given by Ehlers & Ellsiepen [57], ch. 5.

For the sake of completeness, supposing $\mathbf{F}_S = \text{const.}$, the first term of $(\mathbf{B}_{\boldsymbol{q}}^S)^{\underline{4}}$ is given as

$$\frac{\partial \mathbf{S}_n^S}{\partial (\mathbf{E}_{Si})_n} = 2\,\frac{\partial \mathbf{S}_n^S}{\partial (\mathbf{C}_{Si})_n} = 2\,(\mathbf{F}_S^{-1} \otimes \mathbf{F}_S^{-1})^{\frac{23}{T}} \frac{\partial \boldsymbol{\mathcal{T}}_n^S}{\partial (\mathbf{B}_{Se})_n} \frac{\partial (\mathbf{B}_{Se})_n}{\partial (\mathbf{C}_{Si})_n} \tag{4.22}$$

with the derivative of the solid *Kirchhoff* overstress tensor

$$\frac{\partial \boldsymbol{\mathcal{T}}_n^S}{\partial (\mathbf{B}_{Se})_n} = \sum_{k=1}^{3} \Big(\underbrace{\frac{\partial \boldsymbol{\mathcal{T}}_n^S}{\partial (\lambda_{Se(k)})_n}}_{\text{(a)}} \otimes \underbrace{(\mathbf{N}_{Se(k)})_n}_{(2.103)_1} + \underbrace{\frac{\partial \boldsymbol{\mathcal{T}}_n^S}{\partial (\mathbf{N}_{Se(k)})_n}}_{\text{(b)}} \underbrace{(\overset{4}{\mathbf{N}}{}_{Se(k)})_n}_{(2.103)_3} \Big)\,, \tag{4.23}$$

where in detail[4]

$$\begin{aligned}(\mathrm{a}) &= 2\sum_{l=1}^{3}\Big(\frac{\partial^2 \mathcal{W}^S_{NEQ}}{\partial(\lambda_{Se(k)})_n\,\partial(\lambda_{Se(l)})_n}\,(\lambda_{Se(l)})_n\,(\mathbf{N}_{Se(l)})_n\Big) + 2\,\frac{\partial \mathcal{W}^S_{NEQ}}{\partial(\lambda_{Se(k)})_n}\,(\mathbf{N}_{Se(k)})_n\,,\\ (\mathrm{b}) &= 2\,\frac{\partial \mathcal{W}^S_{NEQ}}{\partial(\lambda_{Se(k)})_n}\,(\lambda_{Se(k)})_n\,\overset{4}{\mathbf{I}}\,.\end{aligned} \tag{4.24}$$

Moreover, the second partial derivative in (4.22) takes the form

$$\frac{\partial(\mathbf{B}_{Se})_n}{\partial(\mathbf{C}_{Si})_n} = (\mathbf{F}_S \otimes \mathbf{F}_S)^{\overset{23}{T}}\,\frac{\partial(\mathbf{C}^{-1}_{Si})_n}{\partial(\mathbf{C}_{Si})_n} = -\big[\mathbf{F}_S\,(\mathbf{C}^{-1}_{Si})_n \otimes \mathbf{F}_S\,(\mathbf{C}^{-1}_{Si})_n\big]^{\overset{23}{T}}. \tag{4.25}$$

Note that the determination of the total derivative $\mathrm{d}(\mathbf{E}_{Si})_n/\mathrm{d}\mathbf{E}_S = \mathrm{d}(\mathbf{C}_{Si})_n/\mathrm{d}\mathbf{C}_S$ in $(\mathbf{B}^S_{\boldsymbol{q}})^{\underline{4}}$ depends on the time discretization method used for the evolution equations and is therefore discussed later in section 4.4. □

To continue, linearization of the weak form of the fluid mass balance equation yields:

$$\mathcal{D}_{\Delta\mathbf{u}_S}\big[\int_{\Omega}\delta p\,n^F\,\frac{\partial \rho^{FR}}{\partial p}\,(p)'_S\,\mathrm{d}v\big] = \int_{\Omega}\delta p\,(\mathrm{div}\Delta\mathbf{u}_S)\,\frac{\partial \rho^{FR}}{\partial p}\,(p)'_S\,\mathrm{d}v\,, \tag{4.26}$$

$$\begin{aligned}\mathcal{D}_{\Delta\mathbf{u}_S}\big[\int_{\Omega}\delta p\,\rho^{FR}\,\mathrm{div}(\mathbf{u}_S)'_S\,\mathrm{d}v\big] &=\\ = \int_{\Omega}\delta p\,\rho^{FR}\,\big[\mathrm{div}(\mathbf{u}_S)'_S\,\mathrm{div}\Delta\mathbf{u}_S - \mathrm{grad}\,(\mathbf{u}_S)'_S\cdot\mathrm{grad}^T\Delta\mathbf{u}_S\big]\,\mathrm{d}v\,,\end{aligned} \tag{4.27}$$

$$\begin{aligned}\mathcal{D}_{\Delta\mathbf{u}_S}\big[\int_{\Omega}\mathrm{grad}\,\delta p\cdot\rho^{FR}\,\mathbf{K}^F\,(\mathrm{grad}\,p-\rho^{FR}\,\mathbf{b})\,\mathrm{d}v\big] &=\\ = \int_{\Omega}\mathrm{grad}\,\delta p\cdot\rho^{FR}\Big\{\big[(\mathrm{div}\Delta\mathbf{u}_S)\,\mathbf{K}^F + \mathcal{D}_{\Delta\mathbf{u}_S}\mathbf{K}^F - (\mathrm{grad}\,\Delta\mathbf{u}_S)\,\mathbf{K}^F\big]&\\ (\mathrm{grad}\,p-\rho^{FR}\,\mathbf{b}) - \mathbf{K}^F\,(\mathrm{grad}^T\Delta\mathbf{u}_S)\,\mathrm{grad}\,p\Big\}\,\mathrm{d}v\,,&\end{aligned} \tag{4.28}$$

$$\mathcal{D}_{\Delta p}\big[\int_{\Omega}\delta p\,\rho^{FR}\,\mathrm{div}(\mathbf{u}_S)'_S\,\mathrm{d}v\big] = \int_{\Omega}\delta p\,\frac{\partial \rho^{FR}}{\partial p}\,\Delta p\,\mathrm{div}(\mathbf{u}_S)'_S\,\mathrm{d}v\,, \tag{4.29}$$

$$\begin{aligned}\mathcal{D}_{\Delta p}\big[\int_{\Omega}\mathrm{grad}\,\delta p\cdot\rho^{FR}\,\mathbf{K}^F\,(\mathrm{grad}\,p-\rho^{FR}\,\mathbf{b})\,\mathrm{d}v\big] &=\\ = \int_{\Omega}\mathrm{grad}\,\delta p\cdot\Big[\Big(\frac{\partial \rho^{FR}}{\partial p}\,\Delta p\,\mathbf{K}^F + \rho^{FR}\,\mathcal{D}_{\Delta p}\mathbf{K}^F\Big)\,(\mathrm{grad}\,p-\rho^{FR}\,\mathbf{b}) +&\\ + \rho^{FR}\,\mathbf{K}^F\,\Big(\mathrm{grad}\,\Delta p - \frac{\partial \rho^{FR}}{\partial p}\,\Delta p\,\mathbf{b}\Big)\Big]\,\mathrm{d}v\,,&\end{aligned} \tag{4.30}$$

[4] Note that $(J_{Se})_n$ and $(n^S_{Si})_n$ in the non-equilibrium strain-energy function $\mathcal{W}^S_{NEQ}$ are rewritten in terms of the eigenvalues of $(\mathbf{B}_{Se})_n$ as $(J_{Se})_n = \prod_k \sqrt{(\lambda_{Se(k)})_n}$ and $(n^S_{Si})_n = n^S\,(J_{Se})_n$.

$$\mathcal{D}_{\Delta p}\Big[\int_{\Omega} \delta p\, n^F\, \frac{\partial \rho^{FR}}{\partial p}\,(p)'_S\,\mathrm{d}v\Big] = \int_{\Omega} \delta p\, n^F\, \frac{\partial^2 \rho^{FR}}{\partial p^2}\,\Delta p\,(p)'_S\,\mathrm{d}v\,, \tag{4.31}$$

$$\mathcal{D}_{\Delta(\mathbf{u}_S)'_S}\Big[\int_{\Omega} \delta p\, \rho^{FR}\,\mathrm{div}\,(\mathbf{u}_S)'_S\,\mathrm{d}v\Big] = \int_{\Omega} \delta p\, \rho^{FR}\,\mathrm{div}\Delta(\mathbf{u}_S)'_S\,\mathrm{d}v\,, \tag{4.32}$$

$$\mathcal{D}_{\Delta(p)'_S}\Big[\int_{\Omega} \delta p\, n^F\, \frac{\partial \rho^{FR}}{\partial p}\,(p)'_S\,\mathrm{d}v\Big] = \int_{\Omega} \delta p\, n^F\, \frac{\partial \rho^{FR}}{\partial p}\,\Delta(p)'_S\,\mathrm{d}v\,. \tag{4.33}$$

Herein, in equations (4.28) and (4.30), the corresponding *Gâteaux* differentials of the permeability tensor are obtained by use of the chain rule, viz.

$$\begin{aligned}\mathcal{D}_{\Delta\mathbf{u}_S}\mathbf{K}^F = \frac{\partial \mathbf{K}^F}{\partial K_F^F}\Big(\frac{\partial K_F^F}{\partial J_S}\,J_S\,\mathrm{div}\Delta\mathbf{u}_S + \frac{\partial K_F^F}{\partial|\mathrm{grad}\,p|}\,|(\mathrm{grad}^T\Delta\mathbf{u}_S)\,\mathrm{grad}\,p|\Big)+\\ + \frac{\partial \mathbf{K}^F}{\partial \mathrm{cof}\,\mathbf{B}_S}\,\frac{\partial \mathrm{cof}\,\mathbf{B}_S}{\partial \mathbf{B}_S}\left[(\mathrm{grad}\,\Delta\mathbf{u}_S)\,\mathbf{B}_S + \mathbf{B}_S\,\mathrm{grad}^T\Delta\mathbf{u}_S\right],\end{aligned} \tag{4.34}$$

$$\mathcal{D}_{\Delta p}\mathbf{K}^F = \frac{\partial \mathbf{K}^F}{\partial K_F^F}\,\frac{\partial K_F^F}{\partial|\mathrm{grad}\,p|}\,|\mathrm{grad}\,\Delta p|\,.$$

Thus, with the above linearizations, the *Gâteaux* differentials (4.10) are assembled as

$$\begin{aligned}\mathcal{D}_{\Delta\boldsymbol{u}}\widetilde{\boldsymbol{\mathcal{G}}}_{\boldsymbol{u}} &= \left[\begin{array}{c:c} (4.13)+(4.14)+(4.15) & (4.16)+(4.17) \\ \hdashline (4.26)+(4.27)+(4.28) & (4.29)+(4.30)+(4.31) \end{array}\right],\\ \mathcal{D}_{\Delta(\boldsymbol{u})'_S}\widetilde{\boldsymbol{\mathcal{G}}}_{\boldsymbol{u}} &= \left[\begin{array}{c:c} 0 & 0 \\ \hdashline (4.32) & (4.33) \end{array}\right].\end{aligned} \tag{4.35}$$

Note that the linearized expression (4.31) actually yields zero as this work proceeds from the ideal gas law (3.152) for the description of a compressible pore gas, such that the second derivative of the fluid density with respect to the effective pore-fluid pressure vanishes identically, i. e., $\partial^2\rho^{FR}/\partial p^2 \equiv 0$. Moreover, it should be noted that in the special case of a materially incompressible pore liquid, relation (4.33) also becomes zero as no evolution equation for $\rho^{FR}(p)$ or $p(\rho^{FR})$, respectively, exists and p degenerates to an unspecified *Lagrange*an multiplier, which must be determined from the boundary conditions as already mentioned.

4.3 Discretization

4.3.1 Spatial Semi-discretization

Proceeding from the weak formulations (4.3) and (4.4) together with the introduced abbreviations, the two-field variational problem can be rewritten in abstract form as follows (Ehlers & Ellsiepen [57]):

$$\boxed{\text{Find} \quad \boldsymbol{u} \in \mathcal{S}_{\boldsymbol{u}}(t) \quad \text{such that} \quad \boldsymbol{\mathcal{G}}_{\boldsymbol{u}}(\delta\boldsymbol{u}, \boldsymbol{u}; \boldsymbol{q}) = \boldsymbol{0} \quad \forall\, \delta\boldsymbol{u} \in \mathcal{T}_{\boldsymbol{u}},\ t \in [t_0, T]\,.} \tag{4.36}$$

Herein, $\mathcal{S}_{\boldsymbol{u}}(t)$ is the trial space for the external variables $\boldsymbol{u}$, $\mathcal{T}_{\boldsymbol{u}}$ is the test space for the corresponding test functions $\delta\boldsymbol{u}$, and $[t_0, T]$ is the considered time interval. Without going into mathematical details, the function spaces $\mathcal{S}_{\boldsymbol{u}}$ and $\mathcal{T}_{\boldsymbol{u}}$ must be chosen in such a way that the integrals involved in the definition of $\boldsymbol{\mathcal{G}}_{\boldsymbol{u}}$ "make sense". Moreover, the dependence on the internal variables $\boldsymbol{q}$ is noted after a semicolon as they enter the weak form only indirectly via the solid extra stress tensor. Now, for the solution of the variational problem (4.36), the finite element method (FEM) is applied. Therefore, the spatial domain occupied by the mixture body $\mathcal{B}$ is subdivided into N_e finite elements yielding an approximation of the continuous domain Ω by the discrete domain Ω^h. This spatial semi-discretization yields a finite element mesh with $N_{\mathbf{x}}$ nodes for the geometry approximation, on which the following discrete trial and test functions are defined:

$$\begin{aligned} \boldsymbol{u}^h(\mathbf{x}, t) &= \overline{\boldsymbol{u}}^h(\mathbf{x}, t) + \sum_{i=1}^{N_{\boldsymbol{u}}} \boldsymbol{N}_{\boldsymbol{u}(i)}(\mathbf{x})\, \boldsymbol{u}_{(i)}(t) \in \mathcal{S}^h_{\boldsymbol{u}}(t)\,, \\ \delta\boldsymbol{u}^h(\mathbf{x}) &= \sum_{i=1}^{M_{\boldsymbol{u}}} \boldsymbol{M}_{\boldsymbol{u}(i)}(\mathbf{x})\, \delta\boldsymbol{u}_{(i)} \in \mathcal{T}^h_{\boldsymbol{u}}\,. \end{aligned} \tag{4.37}$$

Therein, $\overline{\boldsymbol{u}}^h = [\,\overline{\mathbf{u}}^h_S,\, \overline{p}^h\,]^T$ represents the approximated *Dirichlet* boundary conditions of the considered problem, $N_{\boldsymbol{u}}$ denotes the number of FE nodes used for the approximation of $\mathbf{u}_S$ and p, respectively, and $\boldsymbol{N}_{\boldsymbol{u}(i)}$ represents the global basis functions at node i, which depend only on the spatial position $\mathbf{x}$, while the degrees of freedom (DOF) $\boldsymbol{u}_{(i)}$ are the time-dependent nodal coefficients. Moreover, $M_{\boldsymbol{u}}$ is the number of FE nodes used for the test functions $\delta\mathbf{u}_S$ and δp, respectively, $\boldsymbol{M}_{\boldsymbol{u}(i)}$ denotes the global basis functions, and $\delta\boldsymbol{u}_{(i)}$ represents the corresponding nodal values of the test functions. Furthermore, $\mathcal{S}^h_{\boldsymbol{u}}(t)$ and $\mathcal{T}^h_{\boldsymbol{u}}$ are the discrete, finite-dimensional trial and test spaces.

Remark: Without entering into particulars of the FE implementation, note that the shape functions are defined on the element level using local coordinates $\boldsymbol{\xi}$. The corresponding global basis functions $\boldsymbol{N}_{\boldsymbol{u}(i)}$ and $\boldsymbol{M}_{\boldsymbol{u}(i)}$ are then obtained from a transformation to global coordinates $\mathbf{x}$. In this context, the present work proceeds from an isoparametric representation of finite elements, where geometry and displacements are described by the same set of shape functions involving all nodes of the FE mesh, i. e., $N_{\mathbf{u}_S} \equiv N_{\mathbf{x}}$. Moreover, the *Bubnov-Galerkin* procedure is applied using the same basis functions $\boldsymbol{N}_{\boldsymbol{u}(i)} \equiv \boldsymbol{M}_{\boldsymbol{u}(i)}$ for the approximation of $\boldsymbol{u}$ and $\delta\boldsymbol{u}$, which implies that the trial and test spaces coincide

except for the shift through the *Dirichlet* boundary conditions $\mathcal{S}_{\boldsymbol{u}}^h(t) = \overline{\boldsymbol{u}}^h + \mathcal{T}_{\boldsymbol{u}}^h$. However, the individual approximation spaces of $\mathbf{u}_S$ and p usually differ in the sense of a *mixed method* meaning that $N_{\mathbf{u}_S}$ and $\boldsymbol{N}_{\mathbf{u}_S(i)}$ in general do not coincide with N_p and $\boldsymbol{N}_{p(i)}$, respectively. For more details, it is referred to the paragraph on mixed element formulations below. ■

Next, in the course of the FE discretization, one additionally introduces a space-discrete set of internal variables $\boldsymbol{q}^h = \boldsymbol{q}^h(\mathbf{x}_j, t) =: \boldsymbol{q}_{(j)}(t)$ at the $j = 1, ..., N_{\boldsymbol{q}}$ integration points of the FE mesh with global coordinates $\mathbf{x}_j$. Following this, the semi-discrete FE-*Galerkin* formulation of the variational problem (4.36) reads:

$$\boxed{\text{Find} \quad \boldsymbol{u}^h \in \mathcal{S}_{\boldsymbol{u}}^h(t) \quad \text{such that} \quad \boldsymbol{\mathcal{G}}_{\boldsymbol{u}}^h(\delta\boldsymbol{u}^h, \boldsymbol{u}^h; \boldsymbol{q}^h) = \boldsymbol{0} \quad \forall\, \delta\boldsymbol{u}^h \in \mathcal{T}_{\boldsymbol{u}}^h,\ t \in [t_0, T]\,.} \tag{4.38}$$

To complete the spatial discretization procedure, the discrete trial and test functions must be specified by choosing an appropriate mixed finite element formulation. A pragmatic way of finding potential interpolation functions is to look at the form in which the basis functions enter the variational problem. For instance, regarding the fluid mass balance (4.3), the gradient of the pressure field and thus, the derivatives of $\boldsymbol{N}_{p(i)}$ are required, which at least demands for a linear interpolation of p. Furthermore, in the mixture momentum balance (4.4), the pressure enters the stress term directly, whereas the gradient of $\mathbf{u}_S$ and thus, the derivatives of the basis functions $\boldsymbol{N}_{\mathbf{u}_S(i)}$ come into play indirectly via the extra stress tensor. Thus, in regard to an equal-order representation of the total stress, it suggests itself to choose the displacement interpolation one order higher than the pressure interpolation yielding a quadratic ansatz for $\mathbf{u}_S$. This, at a first glance, fairly natural choice of a quadratic displacement-linear pressure mixed finite element formulation was already proposed by Sandhu & Wilson [156] in 1969. However, the suitable choice of mixed element formulations in regard to accuracy, stability, and computational costs is by no means natural and is therefore the subject of the next paragraph.

Mixed element formulations: Since the considered solid-fluid problem belongs to the class of *strongly coupled*[5] systems (Zienkiewicz & Taylor [199]), the simultaneous approximation of the primary unknowns $\mathbf{u}_S$ and p is required. Accordingly, this entails the usage of the mixed finite element method with discrete approximation spaces for $\mathbf{u}_S$ and p, which is known to exhibit a great robustness with respect to the roughness of the coefficients of the equations. However, in analogy to the *Stokes* problem of viscous incompressible fluid flow, the considered two-field variational principle yields a saddle-point problem rather than an extremal problem, i. e., the solution corresponds simultaneously to a minimum with respect to the displacement $\mathbf{u}_S$ and a maximum with respect to the pressure p. In general, minimization of an energy functional subject to a side condition, such as the continuity condition in the *Stokes* problem or the saturation constraint in the porous media problem, results in a saddle-point problem, i. e., the discrete system is indefinite so that a number of standard solution methods cannot be applied directly. Moreover, the problem occurs that not all choices of finite element spaces will lead to convergent ap-

[5] Note that a coupling is called strong if the solution depends significantly on the accuracy of the coupling term calculation (cf. Lewis & Schrefler [109]).

proximations, i. e., the stability of mixed methods is by no means automatic (Arnold [2]). Therefore, in mixed formulations, the *inf-sup condition* (*Ladyszenskaya-Babuška-Brezzi* (LBB) condition) is a crucial criterion for the stability of the numerical solution (Brezzi & Fortin [27]). Without going into mathematical details, the inf-sup condition compares the size of the approximation spaces, e. g., here of $\mathcal{S}^h_{\mathbf{u}_S}$ and $\mathcal{S}^h_p$, and essentially serves as a compatibility condition in the sense that it keeps the balance between consistency error and approximation quality (see Gresho & Sani [77] for references).

One possible choice of a stable discretization, which fulfills the discrete version of the LBB condition, is to use quadratic shape functions for the solid displacement $\mathbf{u}_S$ and linear shape functions for the pressure p as proposed by Sandhu & Wilson, which is known as the *Taylor-Hood* element. However, using this element formulation the major disadvantage of the simultaneous approximation of $\mathbf{u}_S$ and p emerges as the discrete system will typically involve many more degrees of freedom. In particular, in the three-dimensional case, the quadratic approximation of the displacements leads to an enormous number of mid nodes in finer meshes, which increases the computational costs rapidly. In order to overcome this problem, one has to reduce the order of the displacement interpolation, which leads to an equal-interpolation element with a linear approximation for both the solid displacement $\mathbf{u}_S$ and the pore pressure p. In general, this mixed element can be used for the computation of coupled problems but users have to be aware that their results are strongly mesh dependent. More precisely, the element formulation is unstable in the sense of giving non-physical oscillations in the pore pressure caused by a very strange instability of the pressure approximation due to so-called *spurious pressure modes* (Brezzi & Fortin [27]). This unpredictable behavior of equal-order interpolation methods led to the introduction of the more sophisticated *Taylor-Hood* elements as mentioned above.

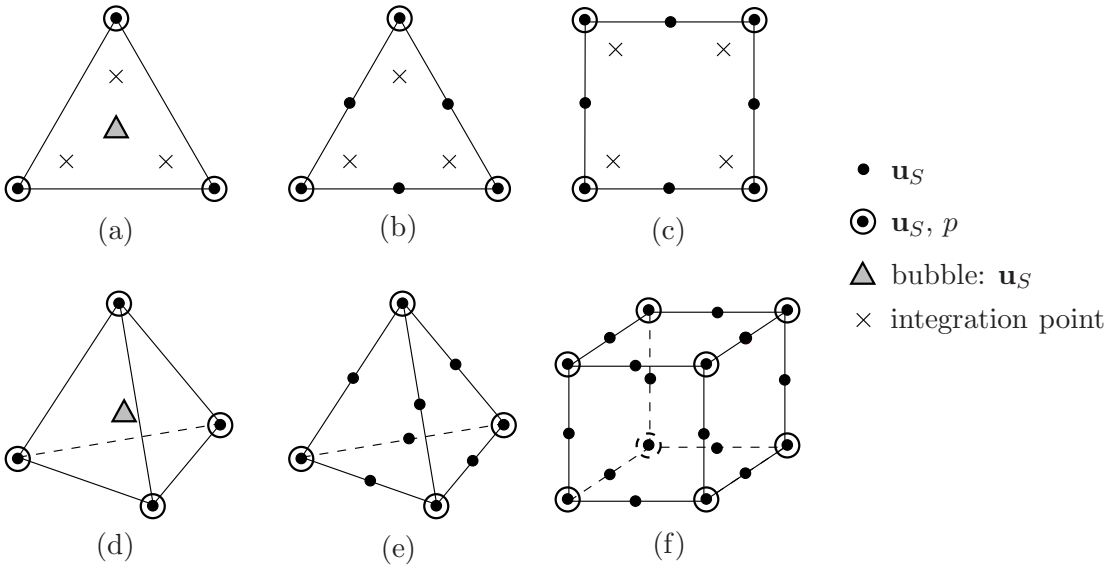

Figure 4.1: Stable mixed finite elements: (a) 2-d MINI element (T3P3B), (b) triangular *Taylor-Hood* element (T6P3), (c) quadrilateral *Taylor-Hood* element (Q8P4), (d) 3-d MINI element (T4P4B), (e) tetrahedral *Taylor-Hood* element (T10P4), (f) hexahedral *Taylor-Hood* element (H20P8)

However, to get a stable pressure-continuous element while keeping the linear approximation for $\mathbf{u}_S$, one has to add bubble functions to the displacement field. This results in the so-called MINI element of Arnold *et al.* [3], where the additional bubbles enrich the trial space for the displacements $\mathcal{S}^h_{\mathbf{u}_S}$, which guarantees stability (see also Braess [24]). Since the bubble functions are restricted to a single finite element, the barycentric bubble nodes can be removed via static condensation. A further strategy of enrichment is to use a finer mesh for the displacement approximation than for the pressure. However, this involves at least as many DOFs as the *Taylor-Hood* element but has a lower accuracy, as the quadratic interpolation of the *Taylor-Hood* element is replaced by a piecewise linear approximation and therefore, the method is deemed inefficient for general porous media applications. Thus, for the numerical treatment of large coupled solid-fluid problems in the sense of the TPM approach, besides the established *Taylor-Hood* element, the MINI element is a compromise concerning accuracy and computational costs in the framework of the mixed finite element method. Particularly for porous media problems with complex 3-d geometries, which require a detailed spatial discretization, the tetrahedral MINI element may have tangible advantages. For illustration, the reasonable and employed 2-d and 3-d mixed element formulations are depicted in figure 4.1. □

To continue, in preparation for the time discretization, the contravariant viscoelastic evolution equations[6] (3.135) are collected in a local residuum vector

$$\boldsymbol{\mathcal{L}_q} \equiv \begin{bmatrix} [(\mathbf{C}_{Si})_1]'_S - \frac{1}{\eta_1^S}\,(\mathbf{C}_{Si})_1\,\mathbf{S}_1^S\,(\mathbf{C}_{Si})_1 + \frac{\zeta_1^S}{\eta_1^S\,(2\,\eta_1^S + 3\,\zeta_1^S)}\,\big[\mathbf{S}_1^S \cdot (\mathbf{C}_{Si})_1\big]\,(\mathbf{C}_{Si})_1 \\ \cdots \qquad\qquad \cdots \qquad\qquad \cdots \\ [(\mathbf{C}_{Si})_N]'_S - \frac{1}{\eta_N^S}\,(\mathbf{C}_{Si})_N\,\mathbf{S}_N^S\,(\mathbf{C}_{Si})_N + \frac{\zeta_N^S}{\eta_N^S\,(2\,\eta_N^S + 3\,\zeta_N^S)}\,\big[\mathbf{S}_N^S \cdot (\mathbf{C}_{Si})_N\big]\,(\mathbf{C}_{Si})_N \end{bmatrix} = \boldsymbol{0}\,. \tag{4.39}$$

After the finite element discretization, its semi-discrete counterpart $\boldsymbol{\mathcal{L}}^h_{\boldsymbol{q}}$ contains the set of space-discrete evolution equations of all $N_{\boldsymbol{q}}$ integration points of the FE mesh for the computation of the inelastic solid deformation tensors in the sense of a collocation method.

4.3.2 Time Discretization

For the time discretization, let $\boldsymbol{u}$ represent all nodal degrees of freedom $\boldsymbol{u}_{(i)}(t)$ of the FE mesh and $\boldsymbol{q}$ all the internal variables $\boldsymbol{q}_{(j)}(t)$ at the integration points. Then, introducing an entire vector of unknowns $\boldsymbol{y} := [\boldsymbol{u}, \boldsymbol{q}]^T \in \mathbb{R}^m$ with $m = \dim(\boldsymbol{u}) + \dim(\boldsymbol{q})$ and taking all semi-discrete equations together, one obtains an initial-value problem of differential-algebraic equations (DAE) in time

$$\boldsymbol{F}\big[\,t, \boldsymbol{y}, (\boldsymbol{y})'_S\,\big] \equiv \begin{bmatrix} \boldsymbol{\mathcal{G}}^h_{\boldsymbol{u}}\big[t, \boldsymbol{u}, (\boldsymbol{u})'_S; \boldsymbol{q}\big] \\ \boldsymbol{\mathcal{L}}^h_{\boldsymbol{q}}\big[t, \boldsymbol{q}, (\boldsymbol{q})'_S; \boldsymbol{u}\big] \end{bmatrix} \equiv \begin{bmatrix} \boldsymbol{M}\,(\boldsymbol{u})'_S + \boldsymbol{k}\big[\boldsymbol{u}; \boldsymbol{q}\big] - \boldsymbol{f} \\ \boldsymbol{A}\,(\boldsymbol{q})'_S - \boldsymbol{l}\big[\boldsymbol{q}; \boldsymbol{u}\big] \end{bmatrix} \stackrel{!}{=} \boldsymbol{0} \tag{4.40}$$

with $\boldsymbol{y}(t_0) = \boldsymbol{y}_0$ and $t \in [t_0, T]$ (Ehlers & Ellsiepen [56]). Therein, the upper equation is an abstract representation of the semi-discrete balance equations at all FE nodes, where

[6] Alternatively, the covariant representation of the evolution equations (3.136) can be used implying the choice of covariant strain-equivalent internal variables, i. e., $\boldsymbol{q} = [(\mathbf{C}_{Si})_1^{-1}, ..., (\mathbf{C}_{Si})_N^{-1}]^T$.

$\boldsymbol{M}$ denotes a generalized mass matrix, $\boldsymbol{k}$ is a generalized stiffness vector, and $\boldsymbol{f}$ is a generalized external force vector. The lower equation represents the space-discrete evolution equations of all integration points of the FE mesh, which essentially are ordinary differential equations (ODE) with $\boldsymbol{A}$ being simply the identity matrix and the vector $\boldsymbol{l}$ containing the semi-discrete right-hand sides of the original evolution equations (3.135). In the case of a quasi-static and/or a materially incompressible description, the generalized mass matrix does not possess the full rank. In particular, the quasi-static formulation of the mixture balance of momentum (4.4) delivers no contribution to the generalized mass matrix that is related to $(\mathbf{u}_S)'_S$. Furthermore, concerning the materially incompressible model, no evolution equation for p exists and, as a consequence, $\boldsymbol{M}$ has no entry corresponding to $(p)'_S$. Thus, (4.40) becomes an index 1 system of differential-algebraic equations (DAE) of first order in time (Ellsiepen [65]), which must be handled by a suitable time integration method. In this context, note that if the evaluation of the inelastic evolution equations is additionally subject to algebraic constraints, such as the yield condition in plasticity, $\boldsymbol{\mathcal{L}}^h_{\boldsymbol{q}} = \boldsymbol{0}$ also becomes a DAE system with singular matrix $\boldsymbol{A}$.

In order to integrate large DAE systems of index 1, one-step s-stage diagonally-implicit *Runge-Kutta* (DIRK) methods provide a suitable means at moderate storage and computational costs, as they allow the solution of the stage equations in a decoupled fashion (Diebels *et al.* [46], Ellsiepen [65]). In this connection, with regard to a proper treatment of the included algebraic equations, stiffly accurate methods are appropriate. Moreover, certain stability requirements must be fulfilled in order to enable large time steps and to guarantee the accurate time integration of the overall dissipative physical problem. Following this, for the solution of the time-continuous initial-value problem

$$\boxed{\text{Find} \quad \boldsymbol{y}(t) \in \mathbb{R}^m \quad \text{such that} \quad \boldsymbol{F}\big[t, \boldsymbol{y}, (\boldsymbol{y})'_S\big] = \boldsymbol{0}\,, \quad \boldsymbol{y}(t_0) = \boldsymbol{y}_0 \quad \forall\, t \in [t_0, T]} \tag{4.41}$$

by use of a stiffly accurate s-stage DIRK, the considered time interval is divided into a finite number of subintervals $[t_n, t_{n+1}]$ with time step size $\Delta t_n = t_{n+1} - t_n$, on which (4.41) is successively solved according to the time step algorithm given in box (4.44).

Remark: Regarding the time step algorithm of box (4.44) for a current time step n, it should be noted that instead of the stage solutions $\boldsymbol{Y}_{ni}$, the stage increments $\Delta\boldsymbol{Y}_{ni} := \boldsymbol{Y}_{ni} - \boldsymbol{y}_n$ are used as unknowns in order to reduce round-off errors during the solution of the time-discrete nonlinear system in step 1(b) (Hairer & Wanner [79], IV.8). In this context, the accumulated stage derivatives $\overline{\boldsymbol{Y}}_{ni}$ depend only on previously computed quantities and thus, are constant for the current *Runge-Kutta* stage i.

For the special choice of coefficients $s = 1$ and $c_1 = a_{11} = 1$, one obtains the well-known implicit or backward *Euler* method and the nonlinear system simplifies to

$$\boldsymbol{R}_n(\Delta\boldsymbol{Y}_n) \equiv \boldsymbol{F}\big(\underbrace{t_n + \Delta t_n}_{t_{n+1}}, \underbrace{\boldsymbol{y}_n + \Delta\boldsymbol{Y}_n}_{\boldsymbol{y}_{n+1}}, \underbrace{\Delta\boldsymbol{Y}_n/\Delta t_n}_{\boldsymbol{y}'_{n+1}}\big) = \boldsymbol{0}\,. \tag{4.42}$$

Note that the implicit *Euler* scheme is in fact a one-stage singly diagonal-implicit *Runge-Kutta* (SDIRK) method. For *mildly* nonlinear systems, SDIRK methods are advantageous

as they allow the reusability of previously factorized matrices, such as in the simplified *Newton* method, which may drastically reduce the required solution time.

Moreover, it is worth mentioning that so-called *embedded Runge-Kutta* methods allow for an efficient estimation of the time error. In particular, these methods compute, besides the approximate solution $\boldsymbol{y}_{n+1}$ of order r, an additional approximate solution $\hat{\boldsymbol{y}}_{n+1}$ of lower order $\hat{r} < r$. As a result, an embedded error estimation is given by the difference of these solutions through

$$ERR \approx \|\boldsymbol{y}_{n+1} - \hat{\boldsymbol{y}}_{n+1}\| \,. \tag{4.43}$$

Accordingly, as pointed out by Diebels *et al.* [46], this type of an error estimation is *cheap* as it does not require the additional solution of nonlinear systems but only a weighted sum of already computed quantities. Following this, *Runge-Kutta* methods with embedded error estimators are well suited for large nonlinear systems of equations. ■

Time step algorithm of a stiffly accurate *s*-stage DIRK method

Given: coefficients c_i, a_{ij} of a stiffly accurate s-stage DIRK method, approximate solution $\boldsymbol{y}_n \approx \boldsymbol{y}(t_n)$ at time t_n, time step size Δt_n

Find: approximate solution $\boldsymbol{y}_{n+1} \approx \boldsymbol{y}(t_{n+1})$ at time t_{n+1}

Step 1: for each *Runge-Kutta* stage $i = 1, ..., s$

(a) set stage time $T_{ni} := t_n + c_i\,\Delta t_n$ and accumulated stage derivative $\overline{\boldsymbol{Y}}_{ni} := \Delta t_n \sum_{j=1}^{i-1} a_{ij} \boldsymbol{Y}'_{nj}$

(b) solve nonlinear system for stage increments $\Delta \boldsymbol{Y}_{ni}$

$$\boldsymbol{R}_{ni}(\Delta \boldsymbol{Y}_{ni}) \equiv \boldsymbol{F}\Big(T_{ni},\, \boldsymbol{y}_n + \Delta \boldsymbol{Y}_{ni},\, \frac{1}{\Delta t_n\, a_{ii}} \left[\Delta \boldsymbol{Y}_{ni} - \overline{\boldsymbol{Y}}_{ni}\right]\Big) = \boldsymbol{0}$$

(c) set stage derivative $\boldsymbol{Y}'_{ni} := \dfrac{1}{\Delta t_n\, a_{ii}} \left[\Delta \boldsymbol{Y}_{ni} - \overline{\boldsymbol{Y}}_{ni}\right]$

Step 2: set $\boldsymbol{y}_{n+1} := \boldsymbol{Y}_{ns} = \boldsymbol{y}_n + \Delta \boldsymbol{Y}_{ns}$ and $t_{n+1} := T_{ns}$ (4.44)

The main computational effort in solving the initial-value problem (4.41) using a DIRK method is in the solution of the nonlinear system given in step 1(b) of the algorithm in box (4.44). For its efficient solution with the *Newton-Raphson* method, the derivative of the nonlinear vector function $\boldsymbol{R}_{ni}(\Delta \boldsymbol{Y}_{ni})$ with respect to the stage increments $\Delta \boldsymbol{Y}_{ni}$ is required. The *Jacobi*an matrix of the whole nonlinear system takes the form

$$\boldsymbol{J}_{ni} := \frac{\mathrm{d}\boldsymbol{R}_{ni}}{\mathrm{d}\Delta \boldsymbol{Y}_{ni}} = \left.\frac{\partial \boldsymbol{F}}{\partial \boldsymbol{y}}\right|_{\boldsymbol{z}} + \frac{1}{\Delta t_n\, a_{ii}} \left.\frac{\partial \boldsymbol{F}}{\partial (\boldsymbol{y})'_S}\right|_{\boldsymbol{z}} , \tag{4.45}$$

where $\boldsymbol{z} = \{T_{ni}, \boldsymbol{Y}_{ni}, \boldsymbol{Y}'_{ni}\}$ denotes the current set of arguments of $\boldsymbol{F}$ in $\boldsymbol{R}_{ni}$. However, it would be disastrous to solve the linear system directly with $\boldsymbol{J}_{ni}$, as the usual sparse structure of the linearized global FEM equations is completely destroyed by the included linearizations of the time-discrete system of local evolution equations (Ehlers & Ellsiepen

[57]). Therefore, it is better to take advantage of the special structure of the DAE system (4.40) and apply a suitable blockwise solution strategy, which retains the sparse structure of the FEM system and treats the integration point equations in a decoupled fashion. Following this, proceeding from a consistent time integration by use of the same time-discretization method for both the global FEM system as well as the local viscoelastic rate equations, the discrete nonlinear system $\boldsymbol{R}_{ni}(\Delta\boldsymbol{Y}_{ni})$ reads

$$\begin{bmatrix} \boldsymbol{G}_{ni}(\Delta\boldsymbol{U}_{ni};\Delta\boldsymbol{Q}_{ni}) \\ \boldsymbol{L}_{ni}(\Delta\boldsymbol{Q}_{ni};\Delta\boldsymbol{U}_{ni}) \end{bmatrix} \equiv \begin{bmatrix} \frac{1}{\Delta t_n\, a_{ii}}\, \boldsymbol{M}\,[\Delta\boldsymbol{U}_{ni} - \overline{\boldsymbol{U}}_{ni}] + \boldsymbol{k}(\boldsymbol{u}_n + \Delta\boldsymbol{U}_{ni};\boldsymbol{q}_n + \Delta\boldsymbol{Q}_{ni}) - \boldsymbol{f} \\ \frac{1}{\Delta t_n\, a_{ii}}\, \boldsymbol{A}\,[\Delta\boldsymbol{Q}_{ni} - \overline{\boldsymbol{Q}}_{ni}] - \boldsymbol{l}(\boldsymbol{q}_n + \Delta\boldsymbol{Q}_{ni};\boldsymbol{u}_n + \Delta\boldsymbol{U}_{ni}) \end{bmatrix} = \boldsymbol{0}\,. \tag{4.46}$$

Herein, $\Delta\boldsymbol{U}_{ni}$, $\Delta\boldsymbol{Q}_{ni}$ are the unknown stage increments and $\overline{\boldsymbol{U}}_{ni}$, $\overline{\boldsymbol{Q}}_{ni}$ are the accumulated stage derivatives of the global FEM variables $\boldsymbol{u}$ and the local history variables $\boldsymbol{q}$, respectively. Then, exploiting the inherent dependence of the global equations $\boldsymbol{G}$ on the local equations $\boldsymbol{L}$, the nonlinear DAE system (4.46) is efficiently iterated by a generalized Block *Gauß Seidel Newton* (BGSN) method, in the sense of a two-stage *Newton* procedure. In particular, at first the evolution equations of the viscoelasticity model are solved by a local *Newton* iteration with fixed increments $\Delta\boldsymbol{U}_{ni}$ of the global variables resulting in local increments $\Delta\boldsymbol{Q}_{ni}(\Delta\boldsymbol{U}_{ni})$ depending on the fixed global increments. This actually corresponds to a local evaluation of the constitutive equations in each finite element. The second step of the procedure is the solution of the global sparse linear FEM system by taking into account the local algorithm during the linearization (*algorithmically consistent linearization*, cf. Simo & Taylor [166]). In summary, for each global *Newton* step k of the current *Runge-Kutta* stage i of the current time step n, the nonlinear system (4.46) is solved according to the algorithm given in box (4.47). The procedure is repeated until a suitable convergence criterion, such as $\|\boldsymbol{G}_{ni}^k\| < TOL_{\boldsymbol{G}}$ or $\|\Delta\boldsymbol{u}_{ni}^k\| < TOL_{\boldsymbol{u}}$, is met. For a more comprehensive discussion of solution strategies based on *Runge-Kutta* methods including time and space adaptivity for nonlinear DAEs arising from inelastic TPM problems, it is referred to the monograph of Ellsiepen [65] and the quotations therein.

2-stage solution algorithm for the nonlinear *G*-*L* system

Stage 1: solve nonlinear local integration point system with fixed $\Delta\boldsymbol{U}_{ni}^k$

$$\boldsymbol{L}_{ni}^k(\Delta\boldsymbol{Q}_{ni}^k;\Delta\boldsymbol{U}_{ni}^k) = \boldsymbol{0} \quad \longrightarrow \quad \Delta\boldsymbol{Q}_{ni}^k = \Delta\boldsymbol{Q}_{ni}^k(\Delta\boldsymbol{U}_{ni}^k)$$

Stage 2: solve nonlinear global FEM system

(a) compute consistent global *Jacobi*an matrix

$$(\boldsymbol{J}_{\boldsymbol{u}})_{ni}^k = \frac{\mathrm{d}\boldsymbol{G}_{ni}^k}{\mathrm{d}\Delta\boldsymbol{U}_{ni}^k} = \frac{\partial\boldsymbol{G}_{ni}^k}{\partial\Delta\boldsymbol{U}_{ni}^k} + \frac{\partial\boldsymbol{G}_{ni}^k}{\partial\Delta\boldsymbol{Q}_{ni}^k}\,\frac{\mathrm{d}\Delta\boldsymbol{Q}_{ni}^k}{\mathrm{d}\Delta\boldsymbol{U}_{ni}^k}$$

(b) solve global sparse linear FEM system

$$(\boldsymbol{J}_{\boldsymbol{u}})_{ni}^k\,\Delta\boldsymbol{u}_{ni}^k = -\boldsymbol{G}_{ni}^k \quad \longrightarrow \quad \Delta\boldsymbol{u}_{ni}^k$$

(c) update vector of global variables (nodal DOFs)

$$\boldsymbol{u}_{ni}^{k+1} := \boldsymbol{u}_{ni}^k + \Delta\boldsymbol{u}_{ni}^k$$

(4.47)

4.4 Solid Stress Computation

The principle of the overall solution algorithm has been described in the previous section. However, in a finite element code, a stress computation algorithm is required that returns the solid stress tensor $\mathbf{T}_E^S$ as well as the consistent tangent operator $(\boldsymbol{\mathcal{C}}^S)^{\underline{4}}$. This algorithm is applied for every integration point of the numerical quadrature and thus, includes the solution of the local system (4.39) as well as the computation of the contribution to the global *Jacobi*an matrix from the current integration point.

For the considered viscoelastic model, according to the additive split of the solid extra stress into an equilibrium and a non-equilibrium part,

$$\mathbf{T}_E^S = \mathbf{T}_{EQ}^S + \mathbf{T}_{NEQ}^S = J_S^{-1} \left(\boldsymbol{\tau}_{EQ}^S + \boldsymbol{\tau}_{NEQ}^S \right), \tag{4.48}$$

the stress computation is carried out in two steps. First, the purely elastic part $\boldsymbol{\tau}_{EQ}^S$ is computed using relation (3.111), which requires the preceding determination of the eigenvalues and tensors of the solid deformation tensor $\mathbf{B}_S$ (see paragraph on page 109). In a second step, the total overstress $\boldsymbol{\tau}_{NEQ}^S = \sum_{n=1}^{N} \boldsymbol{\tau}_n^S$ is obtained by sequentially computing the individual non-equilibrium stresses $\boldsymbol{\tau}_n^S$ together with the time-discrete evolution of the internal variables $(\mathbf{C}_{Si})_n$ associated with the $n = 1, ..., N$ *Maxwell* elements. The procedure is basically similar to the one known from elastoplasticity except for the fact that there is no yield criterion to be checked. Following this, for each *Maxwell* branch an independent elastic trial state is computed via

$$(\mathbf{B}_{Se})_n^{\text{trial}} = (\mathbf{F}_S)^{\text{act}} \, (\mathbf{C}_{Si}^{-1})_n^{\text{last}} \, (\mathbf{F}_S^T)^{\text{act}} \tag{4.49}$$

with the actual solid deformation gradient $(\mathbf{F}_S)^{\text{act}}$ but with the history variables $(\mathbf{C}_{Si})_n^{\text{last}}$ taken from the last time step or *Runge-Kutta* stage. Then, the corresponding elastic eigenvalues and tensors are calculated as described in the paragraph on page 109 followed by the computation of the individual trial stress $(\boldsymbol{\tau}_n^S)^{\text{trial}}$ using equation (3.115). Next, for the treatment of the viscoelastic evolution equations, the resulting stress is pulled back to the reference configuration, $(\mathbf{S}_n^S)^{\text{trial}} = (\mathbf{F}_S^{-1})^{\text{act}} \, (\boldsymbol{\tau}_n^S)^{\text{trial}} \, (\mathbf{F}_S^{T-1})^{\text{act}}$. Then, the time-discrete viscoelastic ODE system corresponding to the nth *Maxwell* element of the considered integration point, which is included in the local equation vector $\boldsymbol{L}$, is solved by *Newton*'s method. After the iteration, the final $\boldsymbol{\tau}_n^S$ is accumulated in $\boldsymbol{\tau}_{NEQ}^S$ and the history variable is updated.

If, in addition, the global *Jacobi*an $\boldsymbol{J_u}$ is to be computed in stage 2(a) of the solution algorithm given in box (4.47), the consistent solid stress tangent of the actual configuration is required. From equations (4.19) and (4.20), it is apparent that

$$\overset{4}{\boldsymbol{\mathcal{C}}}{}^S = \overset{4}{\boldsymbol{\mathcal{C}}}{}_{EQ}^S + \overset{4}{\boldsymbol{\mathcal{C}}}{}_{NEQ}^S = \overset{4}{\mathbf{C}}{}_{EQ}^S + (\mathbf{F}_S \otimes \mathbf{F}_S)^{\overset{23}{T}} \, \overset{4}{\boldsymbol{\mathcal{B}}}{}_{NEQ}^S \, (\mathbf{F}_S^T \otimes \mathbf{F}_S^T)^{\overset{23}{T}}. \tag{4.50}$$

Therein, the purely elastic part $(\mathbf{C}_{EQ}^S)^{\underline{4}}$ is directly computed from equation (3.122), whereas the non-equilibrium tangent, as a matter of fact, depends on the solution of the local system. In particular, according to equation (4.21), the consistent tangent modulus

of the reference configuration is determined from

$$\overset{4}{\boldsymbol{\mathcal{B}}}{}^{S}_{NEQ} = \sum_{n=1}^{N} \left(\overset{4}{\mathbf{B}}{}^{S}_{n} + 2\, \frac{\partial \mathbf{S}^{S}_{n}}{\partial (\mathbf{C}_{Si})_n}\, \frac{\mathrm{d}(\mathbf{C}_{Si})_n}{\mathrm{d}\mathbf{C}_S} \right), \tag{4.51}$$

where, after the iteration of the viscoelastic evolution equations, only the total derivative on the right is still unknown. However, assuming the local system to be solved exactly for the increment $\Delta(\mathbf{C}_{Si})_n$ for any given $\Delta\mathbf{C}_S$ on each *Runge-Kutta* stage,

$$\boldsymbol{L}[\Delta(\mathbf{C}_{Si})_n; \Delta\mathbf{C}_S] = \boldsymbol{0} \quad \longrightarrow \quad \Delta(\mathbf{C}_{Si})_n = \Delta(\mathbf{C}_{Si})_n[\Delta\mathbf{C}_S]\,, \tag{4.52}$$

the total derivative of $\boldsymbol{L}$ with respect to $\Delta\mathbf{C}_S$ also vanishes identically. Thus, the unknown derivative is obtained as follows (Ehlers & Ellsiepen [57], Ellsiepen [65]):

$$\begin{aligned} \frac{\mathrm{d}\boldsymbol{L}}{\mathrm{d}\Delta\mathbf{C}_S} &= \frac{\partial \boldsymbol{L}}{\partial \Delta\mathbf{C}_S} + \frac{\partial \boldsymbol{L}}{\partial \Delta(\mathbf{C}_{Si})_n}\, \frac{\mathrm{d}\Delta(\mathbf{C}_{Si})_n}{\mathrm{d}\Delta\mathbf{C}_S} = \boldsymbol{0} \\ \longrightarrow \quad \frac{\mathrm{d}\Delta(\mathbf{C}_{Si})_n}{\mathrm{d}\Delta\mathbf{C}_S} &= -\left[\frac{\partial \boldsymbol{L}}{\partial \Delta(\mathbf{C}_{Si})_n} \right]^{-1} \frac{\partial \boldsymbol{L}}{\partial \Delta\mathbf{C}_S}\,. \end{aligned} \tag{4.53}$$

Finally, the global *Jacobi*an matrix $\boldsymbol{J_u}$ is obtained by the usual summation over all integration points together with the FE assembly of all element contributions.

Eigenvalue computation: The determination of eigenvalues, vectors, and tensors of symmetric positive definite 2nd-order tensors or 3×3 matrices, respectively, is a common issue of computational mechanics. At first sight, this does not seem to be difficult as the eigenvalue problem can be boiled down to the calculation of the real roots of the cubic characteristic polynomial for which analytical solutions exist, such as the explicit formulæ of *Cardano*[7] or *Viète*[8]. However, from a computational perspective, this apparent simplification completely destroys the originally well-conditioned problem, especially, in the case of almost identical roots. In particular, previous errors in the last significant digits of the coefficients of the polynomial may lead to a completely different shape and hence, a completely different set of roots, which becomes disastrous, if eigenvectors or eigentensors have to be computed in a subsequent step as their precision essentially depends on the accuracy of the eigenvalue computation (see, e. g., Hartmann [81]). Therefore, focusing on volumetrically deformable porous materials, which typically involve deformation tensors with multiple eigenvalues, the more sophisticated solution of the eigenvalue problem by iterative methods is required.

A powerful class of iterative eigenvalue solvers are the so-called transformation methods, named after *Jacobi*, *Givens*, and *Householder*. These methods basically diagonalize a matrix by a sequence of orthogonal similarity transformations, which preserve eigenvalues and vectors, thereby gradually eliminating off-diagonal elements until the matrix is

[7] *Girolamo Cardano* (1501–1576) published one of the first Latin treatise on algebra, *Ars Magna De Regulis Algebraicis*, in 1545 including explicit solutions of cubic and quartic equations.

[8] *François Viète*'s (1540–1603) work *De Aquationum Recognotione Et Emendatione* was published posthumously in 1615 including closed-form solutions for 2nd-, 3rd-, and 4th-order polynomials.

diagonal (Wilkinson [191]). One of the most efficient techniques for finding eigenvalues and vectors of real symmetric matrices is the combination of the *Householder* reduction followed by the QL decomposition. In particular, $m-2$ orthogonal *Householder* transformations $\boldsymbol{Q}_H$ are carried out to reduce a symmetric matrix $\boldsymbol{A} \in \mathbb{R}^{m\times m}$ to a tridiagonal matrix $\boldsymbol{T} := \mathrm{tridiag}(\boldsymbol{A}) = \boldsymbol{Q}_H^T \boldsymbol{A}\, \boldsymbol{Q}_H$, which is still symmetric. Thereafter, the QL algorithm iteratively computes the eigenvalues and vectors of the resulting tridiagonal matrix by factoring $\boldsymbol{T} = \boldsymbol{Q}\, \boldsymbol{L}$, where $\boldsymbol{Q}$ is orthogonal and $\boldsymbol{L}$ is lower triangular. This can be accomplished algorithmically by applying a sequence of (at least $m-1$) *Givens* rotations from the left to annihilate the upper right off-diagonal elements of $\boldsymbol{T}$ (Törnig & Spellucci [176]). Finally, the diagonal elements of $\boldsymbol{L}$ represent the eigenvalues of $\boldsymbol{T}$ and also of $\boldsymbol{A}$, and the columns of the accumulated *Givens* rotations and *Householder* transformations from the previous tridiagonalization are the eigenvectors of $\boldsymbol{A}$. The related eigentensors are then simply computed from dyadic products as described in section 2.2.4.

For the purpose of this work, the *Householder*-QL algorithm is only applied to 3×3 matrices, namely the coefficient matrices of $\mathbf{B}_S$ and $(\mathbf{B}_{Se})_n$, respectively. Following this, the *Householder* reduction for the tridiagonalization is carried out symbolically, which yields a speed up compared to standard codes designed for large dimension matrices. Proceeding from a real symmetric matrix $\boldsymbol{A} \in \mathbb{R}^{3\times 3}$ with its entries labeled

$$\boldsymbol{A} = \begin{bmatrix} a & b & c \\ b & d & e \\ c & e & f \end{bmatrix}, \tag{4.54}$$

the tridiagonalization is easily computed. To begin, if $c = 0$, the matrix is already tridiagonal, i. e., $\boldsymbol{T} \equiv \boldsymbol{A}$ and the *Householder* transformation is just the identity matrix, $\boldsymbol{Q}_H \equiv \boldsymbol{I}$. Otherwise, if $c \neq 0$, it is apparent that the tridiagonalization only requires a single *Householder* transformation as only c must be zeroed. Thus, with $\boldsymbol{Q}_H$ describing a plane rotation and reflection, one concludes

$$\boldsymbol{Q}_H = \begin{bmatrix} 1 & 0 & 0 \\ 0 & u & v \\ 0 & v & -u \end{bmatrix} \quad \longrightarrow \quad \boldsymbol{T} = \begin{bmatrix} a & l & 0 \\ l & d+v\,w & e-u\,w \\ 0 & e-u\,w & f-v\,w \end{bmatrix} \tag{4.55}$$

with the respective coefficients computed as

$$l = \sqrt{b^2+c^2}\,, \quad u = b/l\,, \quad v = c/l\,, \quad w = 2\,e\,u + (f-d)\,v\,. \tag{4.56}$$

For convenience, the routine of the QL algorithm is directly adopted from Press *et al.* [147], sec. 11.3, which additionally uses implicit shifting to accelerate the convergence and avoids the loss of precision of the eigenvalues. □

5 Application to Polymeric Foams

In order to demonstrate the practical applicability of the proposed viscoelastic porous media model, the model is adapted for the description of soft open-cell polyurethane (PUR) foams. The challenge of describing such highly hysteretic polymer foams lies in the fact that all nonlinearities included in the macroscopic formulation are simultaneously addressed. For a better understanding, at first, the principle mechanical behavior of light-weight polymer foams is briefly explained, where the characteristic microscopic deformation mechanisms are illustrated using the results of discrete simulations on an idealized cellular microstructure. Next, the viscoelastic TPM model is brought into correlation with experimental observations of a specific PUR foam by identifying the constitutively introduced material parameters. In particular, the parameters governing the porous characteristics, the basic solid elasticity, and the intrinsic solid viscoelasticity are successively determined with the help of a derivative-free optimization algorithm. Finally, two numerical simulations are carried out to reveal the efficiency of the numerical implementation, the considerable influence of the pore fluid on the transient material response, and the overall applicability of the presented model to real engineering problems.

5.1 Mechanical Behavior of Polymeric Foams

Viscoelastic polymer foams and synthetic sponges are exploited in a wide range of engineering applications. The cellular microstructure, as a result of the foaming process, gives these porous materials their outstanding mechanical characteristics. Particularly the recovery and energy absorbing capabilities of soft polymer foams under large compressive deformations or during impacts predestines their usage for bumper systems, packaging, or cushioning. Basically, low-density polymer foams consist of a biphasic microstructure built by an interconnected network of air-filled polyhedral cells with slender strut edges (cf. figure 1.1), where the cell faces can be open, partly closed, or closed depending on the chemical constitution of the ground substance. Under external loads, this cellular microstructure undergoes complex deformation mechanisms resulting in the characteristic highly nonlinear stress-strain behavior of the macroscopic foam.

For the purpose of this work, the focus is on soft polyurethane foams, which exhibit a permeable cellular structure with open cell faces. During a complete uniaxial loading and unloading cycle, soft PUR foams are capable of absorbing a large amount of energy due to their highly hysteretic nature. This strain-rate-dependent behavior is due to the intrinsic viscoelasticity of the polymer matrix and the deformation-dependent viscous fluid flow through the open-celled structure. In principle, the typical stress-strain curve from a cyclic uniaxial experiment can be separated into four distinct regions, which are governed by the deformation mechanisms on the cell level (see figure 5.1). In particular, small macroscopic deformations are associated with bending of the beam-like cell edges resulting in a linearly increasing stress response. Moderate to large compressions of the foam are governed by

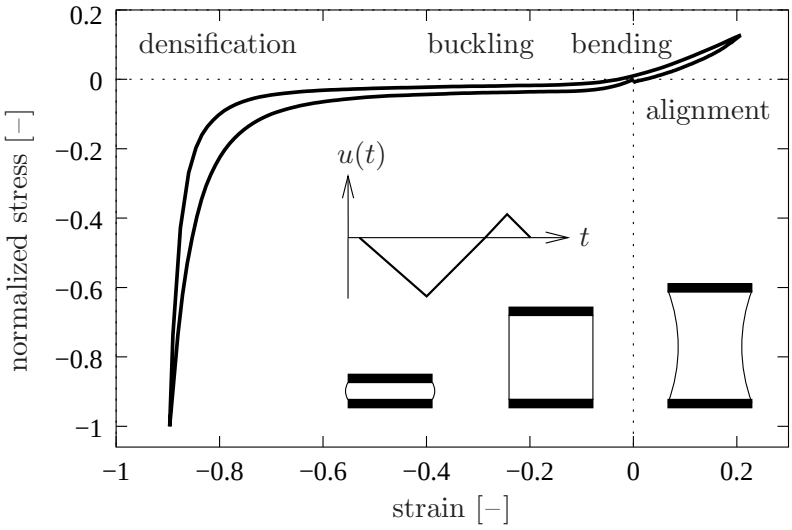

Figure 5.1: Typical uniaxial stress-strain response of an open-celled polyurethane foam. Here, results of a displacement-driven uniaxial hysteresis experiment performed in our laboratory on a cubic PUR foam specimen are given (size $70 \times 70 \times 70\,\mathrm{mm}^3$, bulk density $48\,\mathrm{kg/m}^3$, deformation rate $7.7\,\mathrm{mm/s}$, 90 % compression and 20 % tension)

buckling of the slender struts, which macroscopically results in a low-level stress plateau. Under very large compressions, where the cells are almost collapsed and the cell edges are folded on each other, a stiffening of the foam can be observed due to the densification of the polymeric skeleton. It is worth mentioning that high-porosity foams show almost no lateral deformation or bulging under finite uniaxial compression. Conversely, large tension causes the cell edges to rotate towards the loading direction accompanied by a contraction of the foam perpendicular to the tensile axis. This alignment of the struts results in a stiffening of the structure with the stress response reflecting the tensile properties of solid polyurethane. In this context, it should be noted that soft PUR foams on the one hand are non-crushable under compression, i. e., they recover (sometimes with low recovery rate) from complete compression without showing remarkable permanent deformations, but, on the other hand, they only sustain moderate tensile strains before certain struts begin to rupture. However, the tensile properties are important as they also dominate the shear response and allow the development of high gas pressures inside the foam, which is essential for the pneumatic damping behavior during impacts.

Next, in order to illustrate the above mentioned properties of open-cell foams, discrete simulations are carried out on an idealized beam structure using LS-DYNA[1]. For convenience, proceeding from a 3-d periodic cellular network, a cubic lattice composed of volume-filling dodecahedral cells is generated. Each cell edge is discretized using eight beam elements, where the initial orientation of the beam cross sections are randomly chosen. The principal axes of inertia are set based on the assumption of ellipsoidal cross sections and the ratio of strut thickness to cell radius is reasonably chosen as 1/20. Additionally, in order to avoid unwanted symmetry effects, the vertex coordinates of the

[1] LS-DYNA is a general purpose transient dynamic FE program of the Livermore Software Technology Corporation (`http://www.lstc.com`).

initially regular lattice are randomly perturbed and an imperfection is included on each cell edge. For computational efficiency, the *Belytschko-Schwer* resultant beam formulation (`ELFORM = 2`) with a 2×2 *Gauß* quadratic integration is used. Since at this point only the deformation mechanism is of interest, the matrix material is modeled as linear elastic (`*MAT_ELASTIC`) using the density and the *Young*'s modulus of flexible solid polyurethane according to Gibson & Ashby [72], tab. 3.1.

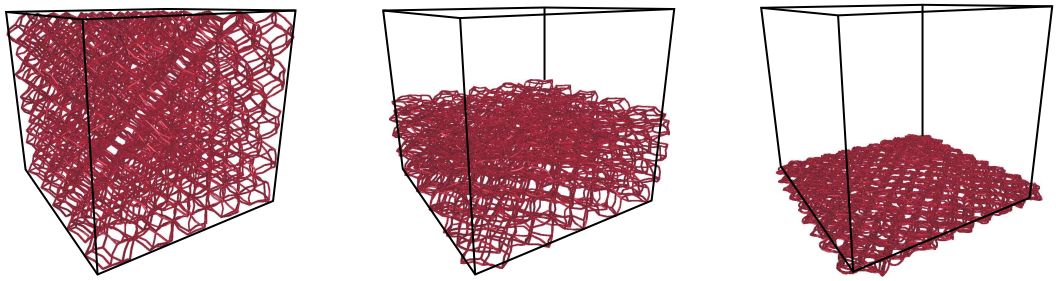

(a) Displacement-driven compression (moving rigid wall): Initial and deformed configurations showing 50 % and total ($\approx$ 98 %) compression

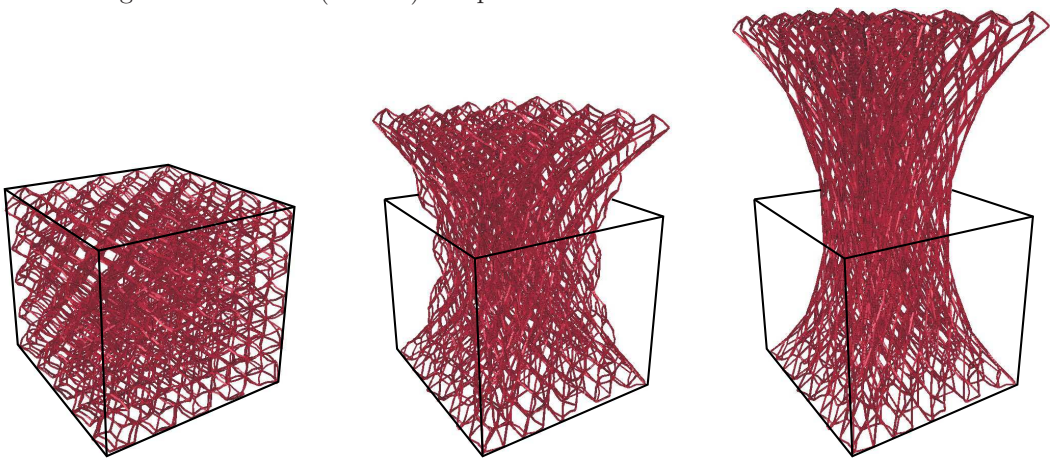

(b) Displacement-driven tension (prescribed nodal motion): Initial and deformed configurations showing 40 % and 80 % tension

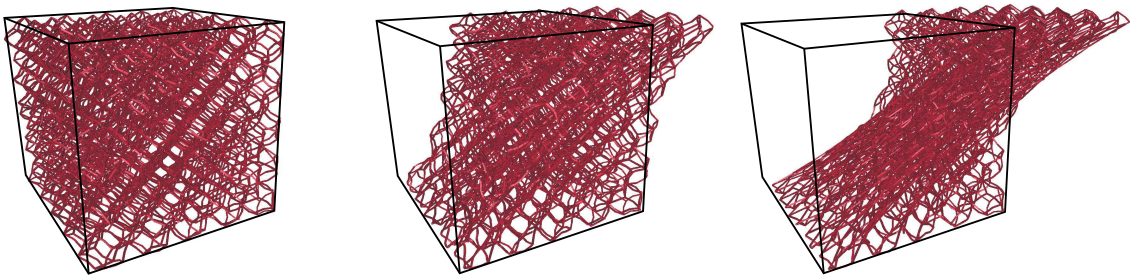

(c) Displacement-driven shear (prescribed nodal motion): Initial and deformed configurations showing 40 % and 80 % shear

Figure 5.2: *Three-point perspective views of deformed configurations of simulated compression (a), tension (b), and shear (c) with an idealized cubic cellular structure (365 dodecahedrons, 31 168 beam elements) using* LS-DYNA

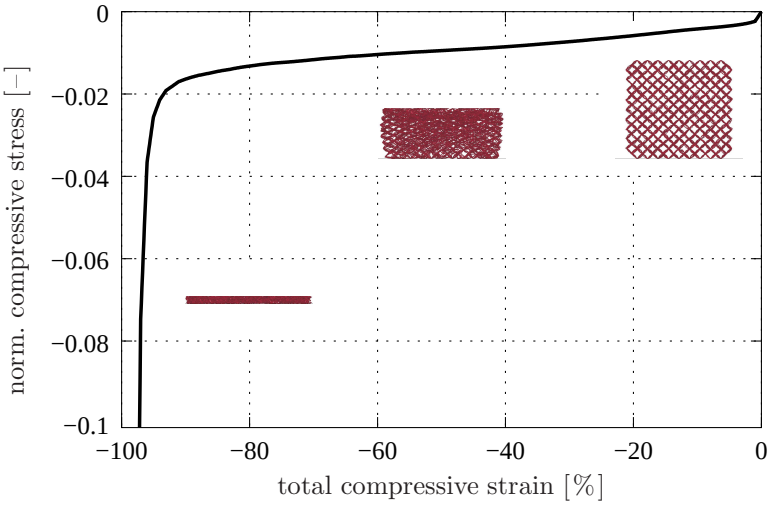

(a) Simulated compression

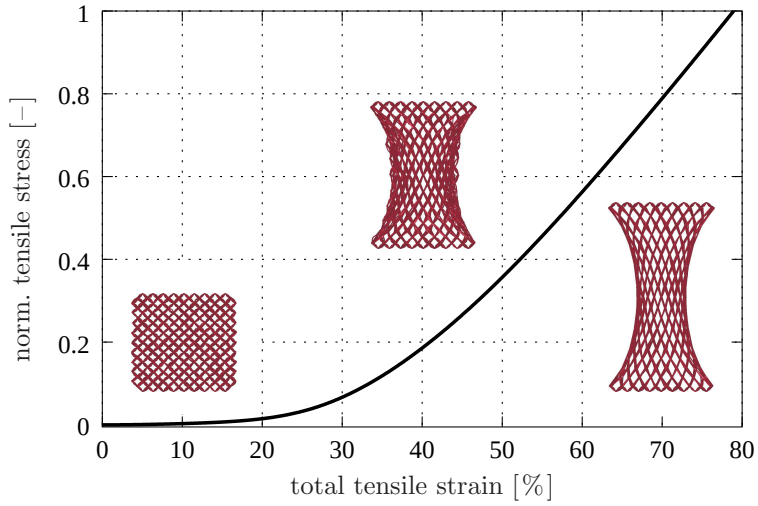

(b) Simulated tension

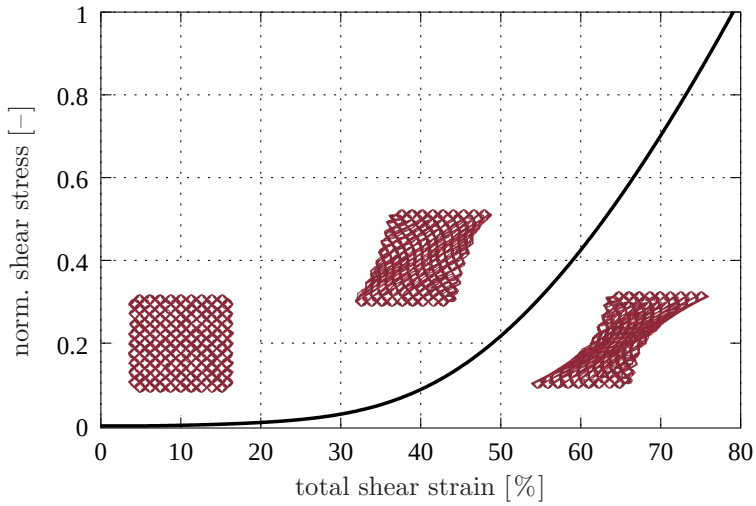

(c) Simulated shear

Figure 5.3: *Resultant stress-strain curves from discrete simulations*

The contact is modeled setting the keyword option `*CONTACT_AUTOMATIC_SINGLE_SURFACE` (cf. LS-DYNA keyword manual). Following this, a cubic geometry containing 365 dodecahedral cells discretized by a total of 31 168 beam elements is generated to simulate uniaxial compression, tension, and shear. In particular, for the compression simulation, the geometry is placed between a fixed and a moving rigid wall, whereas for the tension and shear simulations an adhesive bonding is modeled by defining single point constraints on the lower boundary and by prescribing an uniform displacement on the nodes of the upper boundary. The resulting deformed configurations are depicted in figure 5.2. It is directly seen that the compression of the discrete beam structure almost shows no lateral deformation or bulging, whereas tension is accompanied by a distinct contraction. Moreover, regarding the shear simulation, the cell edge alignment along the diagonal tension field reveals the tension dominated response. This becomes clearer by looking at the computed stress-strain curves in figure 5.3, which show that the result from the tensile simulation is almost identical to the computed shear response.

For further particulars on discrete lattice models of open-cell foams, see, e. g., Laroussi *et al.* [107] and the quotations therein. Moreover, for more details on the behavior of cellular solids in general and foamed plastics in particular, the reader is referred to the book by Gibson & Ashby [72] and the books edited by Hilyard [89] as well as Hilyard & Cunningham [90].

5.2 Model Adaption

To set an example, the biphasic viscoelastic model is adapted for the description of a highly porous soft polyurethane (PUR) foam with a bulk density of 48 kg/m^3, which finds its main application as cushioning material in seating systems. Therefore, the material-specific and unknown parameters, which are theoretically introduced in the constitutive equations (3.106), (3.113), and (3.181), must be identified. In this regard, some basics of the general identification procedure, which is commonly subsumed under the title *parameter optimization*, are discussed before the actual adjustment of the material model is presented.

5.2.1 Parameter Optimization

The adaption to real material behavior essentially proceeds from well-defined experiments, which are suitable to determine all relevant physical properties of the considered material. The identification is then carried out by comparing the experimental observations with the results of numerical simulations based on the chosen material model. A common procedure for this purpose is to strategically vary the searched material parameters until the numerical simulation is satisfactorily correlated with the experimental data. Usually, this strategy leads to a nonlinear optimization problem, which implies the minimization of a least-squares functional representing the deviation between simulation and experiment (see box (5.1)). More precisely, the least-squares functional $F = F(\boldsymbol{\kappa})$ (*objective func-*

Definition of the optimization problem

Objective: Minimize deviation between simulation and experiment

General procedure:

- compare simulation and experiment at a set of N_{opt} discrete points

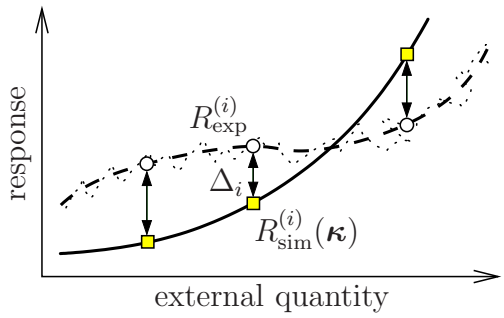

simulation results:

$$R^{(i)}_{\text{sim}} = R^{(i)}_{\text{sim}}(\boldsymbol{\kappa})\,,\ i = 1, ..., N_{\text{opt}}$$

material parameters:

$$\boldsymbol{\kappa} = \{\kappa_j\}\,,\ j = 1, ..., N_{\text{mat}}$$

$$\longrightarrow \left\{ \begin{array}{l} \text{variables of the} \\ \text{adaption process} \end{array} \right. \tag{5.1}$$

- compile least-squares functional by summation of the squared offsets

$$F(\boldsymbol{\kappa}) = \sum_{i=1}^{N_{\text{opt}}} w_i\, \Delta_i^2 = \sum_{i=1}^{N_{\text{opt}}} w_i \big[R^{(i)}_{\text{exp}} - R^{(i)}_{\text{sim}}(\boldsymbol{\kappa})\big]^2, \quad w_i \geq 0 : \text{weighting factor}$$

- solve the general constrained nonlinear optimization (CNLO) problem

$$\text{Minimize} \quad F(\boldsymbol{\kappa})\,,\ \boldsymbol{\kappa} \in \mathbb{R}^{N_{\text{mat}}} \quad \text{subject to} \quad \left\{ \begin{array}{l} h_k(\boldsymbol{\kappa}) = 0\,,\ k = 1, ..., N_{\text{eq}} \\ g_l(\boldsymbol{\kappa}) \geq 0\,,\ l = 1, ..., N_{\text{inq}} \end{array} \right.$$

tion) has to be minimized[2] in consideration of certain equality and inequality constraints $h_k(\boldsymbol{\kappa})$ and $g_l(\boldsymbol{\kappa})$, respectively, which represent the restrictions on the unknown set of material parameters collected in $\boldsymbol{\kappa}$, such as the stability and compatibility conditions (3.95), (3.98), and (3.99). In principle, the constraints simply restrict the search space for the parameters to some feasible set $\mathcal{K}$ yielding a constrained optimization problem seeking for the minimizing feasible vector $\boldsymbol{\kappa}^*$ in $\mathcal{K} \subseteq \mathbb{R}^{N_{\text{mat}}}$. The major task is now the solution of the constrained nonlinear optimization (CNLO) problem given in the last item of box (5.1) by use of an appropriate numerical optimization strategy. Following the statement by Brent [26] that "*the question of which is the best strategy is itself a kind of optimization problem*", for convenience, we focus on direct search or derivative-free methods.

Direct search or derivative-free methods: The main advantage of direct search or derivative-free methods is that they only require function values but no derivatives with respect to the unknown parameters. Thus, they can be applied without any modifications to the existing FE implementation of the considered material model. This makes them particularly interesting for problems, where the objective function $F(\boldsymbol{\kappa})$ is calculated using the simulation results from *black box* computations, where no direct access to the material routine is available, e. g., when commercial FE programs are used (Hartmann *et al.* [82]).

[2] In general, the *objective function* F is the function to be maximized or minimized. Here, optimization is associated with the minimization of F, however, it is apparent that $\min(F) = \max(-F)$.

In general, most of the derivative-free methods are applicable to non-smooth and noisy objective functions, where the comprehensible and self-contained algorithms usually allow the straightforward application of available codes and libraries (see Press *et al.* [147]). However, due to the lack of gradient and curvature information, derivative-free methods unfortunately require a larger number of function evaluations compared to gradient-based methods, which makes them only expedient for problems whose computational burden is small. At first glance, this sounds like an exclusion criterion for optimization problems that involve time-consuming FE simulations. To ease this disadvantage, the adaption process can be carried out in a hierarchical fashion. Therefore, the optimization process is started using a coarse FE approximation for the simulation in order to find a trend in the parameters and to create a good initial parameter set. Then, the parameter vector is improved by the successive restart of the optimization procedure using refined FE meshes for the simulations with the previously found parameters as starting values. This essentially guarantees the cheap computation of the objective function $F(\boldsymbol{\kappa})$ at the beginning of the optimization process, where the parameters are worse and many function evaluations are required. In the course of approaching the minimizing feasible vector $\boldsymbol{\kappa}^*$, the accuracy of the FE approximation and thus, the computing time is stepwise increased, whereas, conversely, the number of function evaluations decreases. A further possibility to overcome the costly calculations of the objective function is to take advantage of multi-processor systems by recourse to parallel implementations of direct search algorithms (Dennis & Torczon [42]). In general, depending on the underlying search strategy, the following basic group of direct search or derivative-free optimization methods can be distinguished (cf. Brent [26], Fletcher [68], Nocedal & Wright [132] among others):

- amoeba or simplex methods,
- trust region methods,
- response surface methods,
- evolution strategies,
- pattern search or discrete grid methods,
- line search or direction set methods,
- linear and quadratic approximation methods,
- simulated annealing and genetic algorithms.

For the purpose of this work, Powell's [143] *constraint optimization by linear approximation* (COBYLA) algorithm is the method of choice. COBYLA is a sequential trust region method for constrained nonlinear optimization (CNLO), which iteratively makes use of linear programming (LP) problems in the sense of a sequential linear programming (SLP) algorithm. There are no smoothness assumptions to the objective function, but only inequality constraints are considered, which, however, does not affect the applicability of COBYLA for the parameter optimization. Thus, proceeding from the CNLO problem

$$\text{Minimize} \quad F(\boldsymbol{\kappa})\,,\ \boldsymbol{\kappa} \in \mathbb{R}^{N_{\text{mat}}} \quad \text{subject to} \quad g_k(\boldsymbol{\kappa}) \geq 0\,,\ k = 1, ..., N_{\text{inq}}\,, \tag{5.2}$$

analogously to the well-known *Nelder-Mead* method (Nelder & Mead [131]), a new variable vector is generated from function values at the $j = 1, ..., N_{\text{mat}}$ vertices of a non-degenerated simplex. Therefore, F and g_k are interpolated by linear functions $\widehat{F}$ and $\widehat{g}_k$ at the vertices of the simplex, i. e., the CNLO problem (5.2) is approximated by the linear programming

problem

$$\boxed{\text{Minimize} \quad \widehat{F}(\boldsymbol{\kappa})\,,\ \boldsymbol{\kappa} \in \mathbb{R}^{N_{\mathrm{mat}}} \quad \text{subject to} \quad \widehat{g}_k(\boldsymbol{\kappa}) \geq 0\,,\ k = 1, ..., N_{\mathrm{inq}}\,.} \tag{5.3}$$

The solution of the LP problem (5.3) then guides the changes to the variables restricted by a spherical trust region bound of a monotone decreasing radius. The main advantage of COBYLA lies in the individual treatment of the inequality constraints during the iterative optimization procedure instead of lumping all constraints into a single penalty function. In particular, this is accomplished by a merit function, which compares the quality of different variable vectors giving attention to the greatest constraint violation. Moreover, the optimization process is accompanied by *acceptability iterations* to improve the shape of the simplex, if necessary, in order to yield acceptable linear approximations of the objective and constraint functions. However, it should be noted that linear approximations can be highly inefficient, so that the number of variables should be kept small. For further particulars on the COBYLA algorithm, it is referred to the related articles by Powell [143–145]. □

Following the above, in order to get interpretable and sound solutions, the possibility of reducing the number of variables is decisive for the convergence property and the efficiency of the numerical optimization process. In general, the material parameters of the viscoelastic porous media model can be divided into three classes, viz., the parameters that govern (i) the porous characteristics and fluid properties, (ii) the basic solid elasticity, and (iii) the intrinsic solid viscoelasticity. However, to realize this separation, experiments are needed that allow the unique assignment of the material response either to the flow-dependent mechanisms or to the equilibrium and non-equilibrium properties of the solid skeleton, respectively. Here, applying the viscoelastic TPM model to a high-porosity PUR foam, one can take advantage of the highly permeable microstructure of cellular polyurethane, which allows the successive determination of the three parameter classes. Therefore, at first, the porous and flow-dependent properties are obtained from appropriate permeability experiments. Then, displacement-driven uniaxial compression-tension tests with incorporated relaxation periods are performed for the identification of the macroscopic equilibrium response of the skeleton. Finally, after the adjustment of the basic elasticity model, the parameters of the rate-dependent solid overstress formulation are determined from respective hysteresis experiments.

5.2.2 Porous Characteristics and Fluid Properties

Following the previous paragraph, the first class of parameters to be determined governs the porous and flow-dependent properties of the viscoelastic TPM model. In this parameter set, the cellular polyurethane structure, its permeability properties, and the percolating pore fluid (here: pore gas air) are characterized. To begin, at first, the initial solidity is determined from the definition of the mixture density $(2.5)_3$. Accordingly,

proceeding from a homogeneous foam material, it is easily concluded that

$$\rho_0 = \sum_\alpha n_{0S}^\alpha \, \rho_{0S}^{\alpha R} \quad \longrightarrow \quad n_{0S}^S = \frac{\rho_0 - \rho_{0S}^{FR}}{\rho_{0S}^{SR} - \rho_{0S}^{FR}} \approx \frac{\rho_0}{\rho_{0S}^{SR}} \,, \tag{5.4}$$

where the ground-state bulk density of the considered PUR foam is about $\rho_0 = 48\,\mathrm{kg/m^3}$ and the effective density of flexible solid polyurethane is $\rho_{0S}^{SR} = 1200\,\mathrm{kg/m^3}$ (Gibson & Ashby [72], tab. 3.1), which is regarded as constant assuming a materially incompressible skeleton. Since the effective density of air at standard conditions is comparatively low, viz., $\rho_{0S}^{FR} = 1.2\,\mathrm{kg/m^3}$ at 20 °C at an ambient pressure of $p_0 = 1.013 \cdot 10^5\,\mathrm{N/m^2}$, the initial solid volume fraction can be approximately determined assuming an empty solid skeleton. Following this, the initial solidity of the PUR foam is about $n_{0S}^S = 0.04$.

Next, to obtain information about the deformation-dependent permeability properties of the foam, respective percolation experiments must be performed. For this purpose, we constructed two experimental devices (figure 5.4), which allow permeability measurements on cylindrical foam specimens at different deformation states. In particular, for low filter velocities, the testing device depicted on the left-hand side in figure 5.4 is used with degassed water as the permeating fluid, where the ingoing pressure is measured for varying prescribed fluid volume fluxes and a constant outgoing pressure. In order to ensure a complete water saturation, the foam samples are initially flooded with carbon dioxide (CO_2) to displace the air inside the pores, as CO_2 dissolves better in water. However, the problem occurs that high flow velocities enlarge the apertures between the ribs outlining the individual cells, which causes an overestimation of the permeability. Therefore, for higher filter velocities, the second testing device (figure 5.4 right) is used with compressed

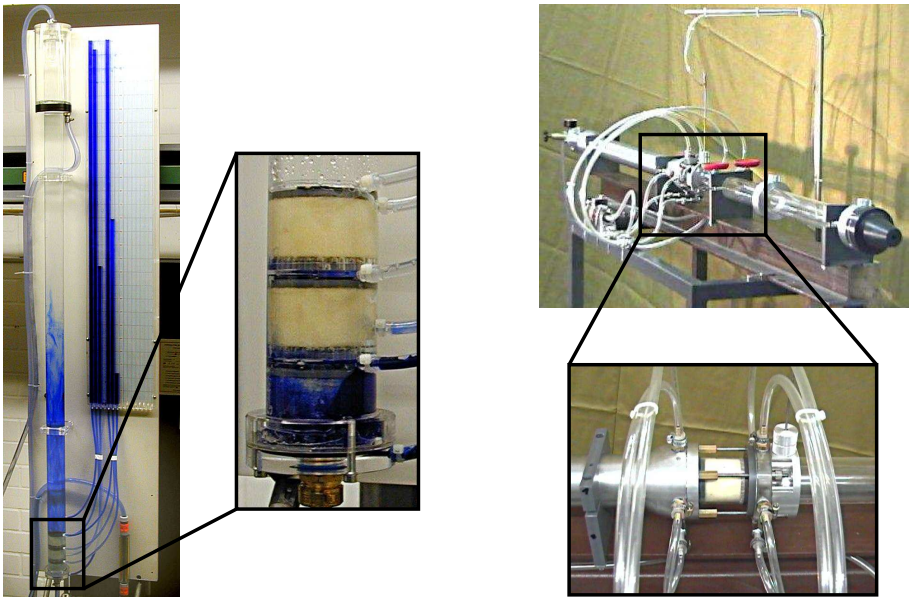

Figure 5.4: *Testing devices for percolation experiments with degassed water (left) and compressed air (right). The zoomed details show the assembled cylindrical PUR foam specimens, where the design of the devices allows variable specimen dimensions*

air as the permeating fluid, where, for varying ingoing pressures, the pressure drop and the velocity profile are measured with a pressure transducer and a *Prandtl* tube. For both experimental devices, cylindrical foam specimens are prepared (initial height $h_0 = 70\,\mathrm{mm}$, radius $r = 27\,\mathrm{mm}$), which are compressed along the cylinder axis and pasted into acrylic glass tubes of different length to verify the deformation dependency of the permeability (cf. figure 5.5). Then, the tubes are integrated into the testing devices and the specimens are streamed parallel to their compression direction. Moreover, in order to prove whether the considered PUR foam exhibits anisotropic permeability properties, additional percolation experiments are carried out, where in contrast to the previously mentioned setup, rectangular specimens are tested, which are deformed perpendicular to the flow direction. However, neither initial nor deformation-induced anisotropic permeability properties are observed, so that, for the following considerations, it is convenient to proceed from an isotropic permeability associated with $\boldsymbol{\mathcal{H}}^S \equiv \mathbf{I}$ (cf. section 3.3.4)[3].

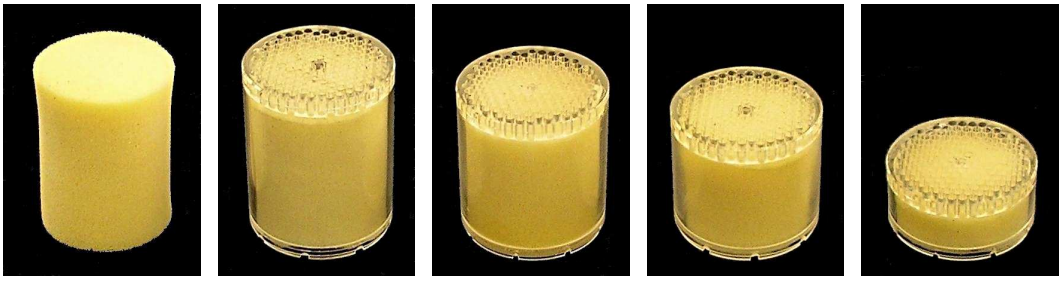

D0	**D1**	**D2**	**D3**	**D4**
$h_0 = 70.0\,\mathrm{mm}$	$h = 56.0\,\mathrm{mm}$	$h = 46.0\,\mathrm{mm}$	$h = 36.0\,\mathrm{mm}$	$h = 11.5\,\mathrm{mm}$
$\varepsilon = 0.0\,\%$	$\varepsilon = -20.0\,\%$	$\varepsilon = -34.3\,\%$	$\varepsilon = -48.6\,\%$	$\varepsilon = -83.6\,\%$

Figure 5.5: *Cylindrical PUR foam specimens for the permeability experiments (initial height* $h_0 = 70\,\mathrm{mm}$*, radius* $r = 27\,\mathrm{mm}$*) pasted into acrylic glass tubes of different length*

Following this, based on the data obtained from the 1-d percolation experiments, the constitutive filter law (3.181) has to be adapted. Therefore, the basic flow equation in the form of the 1-d *Forchheimer* law (3.166) is correlated with the experimental data by optimizing the intrinsic permeability K^S and the tortuosity parameter B^S independently for each of the compression states D1 – D4. Since in addition to incompressible water compressible air is also used as a permeating fluid, the variability of the fluid density along the flow path must be conveniently taken into account. This can be accomplished by a suitable redefinition of the dependent and independent variables in the *Forchheimer* equation through multiplication by the factor $\rho^{FR}/(\mu^{FR})^2$ yielding (cf. Muskat [130])

$$\underbrace{-\frac{\rho^{FR}}{(\mu^{FR})^2}\frac{\partial p}{\partial x}}_{\partial\widetilde{p}/\partial x} = \frac{1}{K^S}\underbrace{\left(\frac{\rho^{FR}}{\mu^{FR}}w_F\right)}_{\widetilde{q}} + \frac{1}{B^S}\underbrace{\left(\frac{\rho^{FR}}{\mu^{FR}}w_F\right)^2}_{\widetilde{q}^{\,2}} \quad\longrightarrow\quad -\frac{\partial\widetilde{p}}{\partial x} = \frac{1}{K^S}\,\widetilde{q} + \frac{1}{B^S}\,\widetilde{q}^{\,2}. \tag{5.5}$$

[3] It should be noted that some low-density polymer foams exhibit a distinct inherent anisotropy due to the manufacturing process, where the cells are elongated in the foam rise direction (see, e. g., Zhu *et al.* [195]).

Therein,

$$\frac{\partial \widetilde{p}}{\partial x} := \frac{\rho^{FR}(p)}{(\mu^{FR})^2}\,\frac{\partial p}{\partial x} = \frac{M_m^F}{R\,\Theta\,(\mu^{FR})^2}\,\frac{\partial p^2}{\partial x} \qquad \text{and} \qquad \widetilde{q} := \frac{\rho^{FR}(p)}{\mu^{FR}}\,w_F = \frac{1}{\mu^{FR}}\,q \tag{5.6}$$

define the new dependent and independent variables, where the ideal gas law (3.152) and the specific filter mass flux $q := \rho^{FR}\,w_F$ have been used. The results of the permeability experiments and the corresponding curves of the fitted flow equation (5.5) are depicted in figure 5.6. Particularly the double-logarithmic representation in subfigure 5.6(b) shows

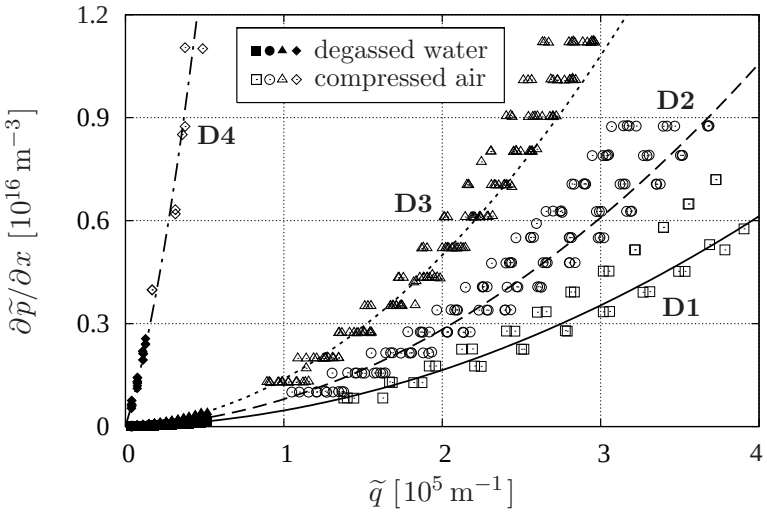

(a) Data and curves plotted using a linear scale

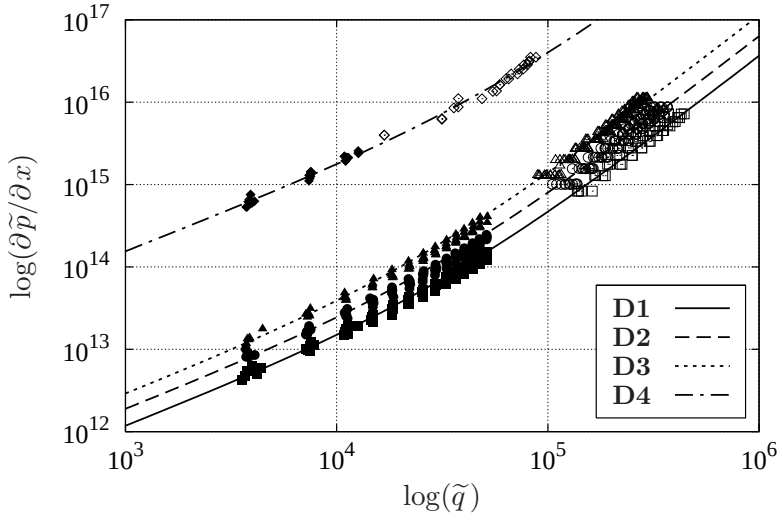

(b) Data and curves plotted using a double-logarithmic scale

Figure 5.6: *Experimental data of percolation experiments and curves of the fitted Forchheimer equation (5.5) plotted using a (a) linear and (b) double-logarithmic scale*

the very good accordance of the quadratic *Forchheimer* ansatz for all compression states within the considered range of the flow velocity. Subsequently, the previously found

parameter pairs $\{K^S_{\mathrm{D1}}, B^S_{\mathrm{D1}}\}, ..., \{K^S_{\mathrm{D4}}, B^S_{\mathrm{D4}}\}$ are used as optimization points for the fit of the porosity-dependent permeability and tortuosity functions (3.176) and (3.177). For comparison, the power law of Eipper (3.174) and the exponential ansatz of Lai & Mow (3.175) are also adapted. The optimized parameters yielding the best approximation based on a least-squares fit of the respective functions are given in table (5.7) and the corresponding graphs are depicted in figure 5.7. It is directly seen that only the new power law can be brought into satisfactory accordance with the four discrete values of K^S and B^S associated with the deformation states D1 – D4. Finally, the whole set of parameters governing the porous characteristics and the fluid properties is listed in box (5.8).

constitutive function	$K^S_{0S}\,[10^{-10}\,\mathrm{m}^2]$	$\kappa\,[-]$	$B^S_{0S}\,[10^{-5}\,\mathrm{m}]$	$\beta\,[-]$
Eipper (3.174)	9.351176	22.493503	2.608980	18.418420
Lai & Mow (3.175)	41.665746	7.169968	11.310917	6.416593
new function (3.176)	16.945190	2.649075	4.767115	2.342505

(5.7)

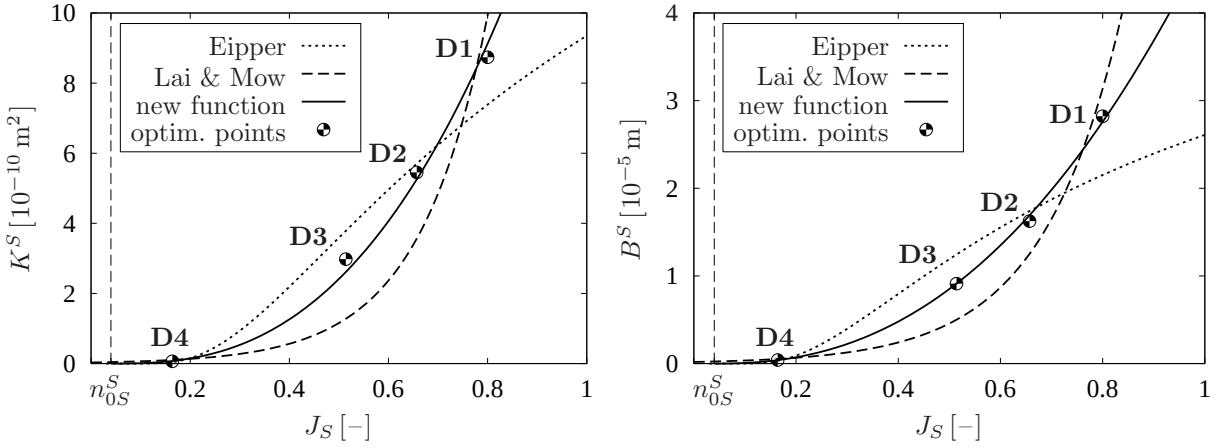

(a) Deformation-dependent intrinsic permeability (b) Deformation-dependent tortuosity parameter

Figure 5.7: *Comparison of the best approximations by least-squares fits of different functions for the description of the deformation-dependent flow properties*

5.2.3 Basic Solid Elasticity

After the definition of the porous characteristics and the fluid properties, the basic solid elasticity model (3.106) has to be adjusted. Therefore, proceeding from viscoelastic skeleton properties, the equilibrium response of the cellular polyurethane matrix must be separated from the rate-dependent contributions. As usual, this is accomplished by displacement-driven experiments with incorporated holding times, which allow the relaxation of the non-equilibrium stresses at distinct deformation states finally yielding a set of discrete optimization points representing the purely elastic response. In particular, unconfined uniaxial compression-tension experiments on cubic PUR foam specimens of size $70 \times 70 \times 70\,\mathrm{mm}^3$ (figure 5.8) are performed in our laboratory and at the Institute

Porous characteristics and fluid properties

$n^S_{0S} = 0.04$	$[-]$	: initial solidity ($\rightarrow\ n^F_{0S} = 0.96$)
$\rho^{SR} = 1200.0$	$[\mathrm{kg/m^3}]$	: effective density of flexible PUR
$K^S_{0S} = 1.6945 \cdot 10^{-9}$	$[\mathrm{m^2}]$	: initial intrinsic permeability
$\kappa = 2.6491$	$[-]$	: exponent def.-dep. permeability
$B^S_{0S} = 4.7671 \cdot 10^{-5}$	$[\mathrm{m}]$	: initial tortuosity parameter
$\beta = 2.3425$	$[-]$	: exponent def.-dep. tortuosity
$g = 9.81$	$[\mathrm{m/s^2}]$	: scalar gravitational acceleration
$p_0 = 1.013 \cdot 10^5$	$[\mathrm{N/m^2}]$	: average atmospheric pressure
$R = 8.3144$	$[\mathrm{J/(K\,mol)}]$	: universal gas constant
$\Theta = 293.15$	$[\mathrm{K}]$	: ambient temperature (20 °C)
$M^F_m = 2.897 \cdot 10^{-2}$	$[\mathrm{kg/mol}]$	: molecular mass of dry air
$\mu^{FR} = 1.82 \cdot 10^{-5}$	$[\mathrm{N\,s/m^2}]$	: effective viscosity of air at 20 °C

(5.8)

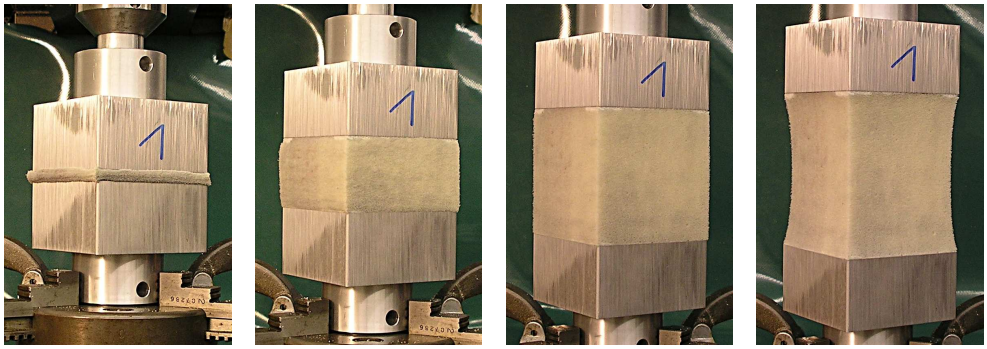

90 % compression | 45 % compression | undeformed | 20 % tension

Figure 5.8: *Deformed PUR foam specimen during a compression-tension experiment*

for Polymer Testing and Polymer Science (IKP) of the University of Stuttgart. During the experiments, the specimens are subjected to complete deformation cycles at a constant deformation rate of 0.077 mm/s, which are interspersed with several holding times of 60 minutes, while the responding force is continuously recorded. Therefore, the foam specimens are bonded to aluminum platens at two opposite sides using a quick-setting adhesive, where, during the tests, one platen is used to prescribe the deformation, whereas the other one is fixed. In particular, a maximal compression of 90 % and a maximal tension of 20 % of the initial edge length is imposed, where the prescribed tensile deformation is kept comparatively small in order to limit damage effects and to avoid the rupture of the adhesive bonds. The obtained experimental results are depicted in the stress-strain diagram in figure 5.9. Since the overstresses are not completely relaxed, it is apparent that the chosen holding times of 60 minutes are too short. However, assuming the PUR matrix to behave purely viscoelastic, thereby excluding a plastic equilibrium hysteresis, the midpoints between the relaxed stress tips of the two branches of the stress-strain loops can be taken as input values for the numerical optimization procedure. In fact, for the

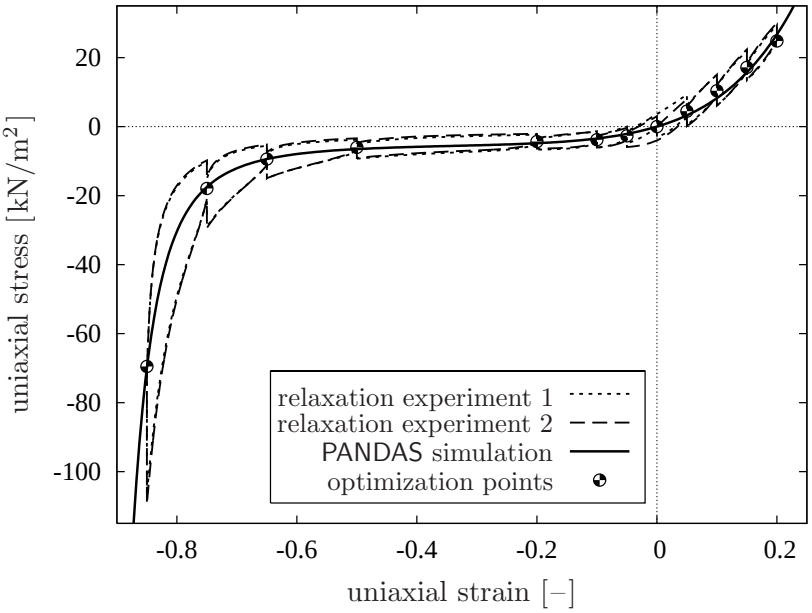

Figure 5.9: *Stress-strain diagram of uniaxial holding-time experiments and the basic elasticity response computed with* PANDAS[4] *using the optimized parameters of box (5.11)*

considered PUR foam this is not an arbitrary assumption, as the complete stress relaxation onto a non-hysteretic equilibrium curve can be verified by long term experiments with holding times above 20 hours (Klar & Ehlers [100]). Thus, proceeding from the midpoints as optimization points, the actual adaption of the extended *Ogden* formulation (3.106) is carried out numerically using the previously described COBYLA algorithm of Powell [143] for the parameter optimization. In this regard, following the arguments of section 3.2.3, the involved material parameters are subject to the inequality constraints

$$\mu_0^S > 0\,, \quad \Lambda_0^S \geq 0\,, \quad \gamma_0^S \geq 1\,, \quad \sum_{m=1}^{M_0} \mu_{0(m)}^* \geq 0\,, \quad \mu_{0(m)}^* \left(\alpha_{0(m)} - 1\right) \geq 0\,. \tag{5.9}$$

Moreover, the compatibility condition (3.98) as an equality constraint is considered by expressing one of the unknown *Ogden* parameters dependent on the others, viz.,

$$\sum_{m=1}^{M_0} \mu_{0(m)}^* \, \alpha_{0(m)} = 2 \quad \longrightarrow \quad \mu_{0(1)}^* = \frac{1}{\alpha_{0(1)}} \left(2 - \sum_{m=2}^{M_0} \mu_{0(m)}^* \, \alpha_{0(m)}\right), \tag{5.10}$$

thereby reducing the number of variables of the optimization process. According to the general procedure given in box (5.1), the evaluation of the least-squares functional furthermore demands appropriate FE simulations of the uniaxial compression-tension experiments, where, at first, only the computed elastic response is considered. Therefore, proceeding from the numerical treatment described in chapter 4, the presented material model is implemented in the FE package PANDAS[4] and respective boundary-value prob-

[4] PANDAS (**P**orous media **A**daptive **N**onlinear finite element solver based on **D**ifferential **A**lgebraic **S**ystems) is an adaptive finite element tool designed for multi-phase problems (`www.get-pandas.com`).

lems describing the displacement-driven uniaxial experiments are defined. In this context, it should be noted that all simulations required for the optimization are carried out fully three-dimensional, since the displacement-boundary constraints representing the adhesive bonds and the possibility of a developing pore pressure may generally lead to inhomogeneous stress states. Following this, pursuing a hierarchical adaption strategy, the successive restart of the optimization procedure using refined FE meshes for the simulations with the previously found parameters as starting values, already yields an acceptable fit of the basic elasticity model to the experimental data for $M_0 = 2$ *Ogden* terms (see figure 5.9). The final set of material parameters resulting from the optimization procedure with COBYLA is given in box (5.11). For illustration, the admissibility of the found parameters in regard to material stability can be graphically verified by a *convexity plot* of the equilibrium solid strain-energy function (3.106). For instance, plotting $\mathcal{W}^S_{EQ}$ for variable values of $\lambda_{S(1)}$ and $\lambda_{S(2)}$ but a constant value of $\lambda_{S(3)} = 1$ as depicted in figure 5.10, the contours of the energy surface in the plane of the principal stretches are clearly convex, which implies the stability of the material formulation for the found set of parameters.

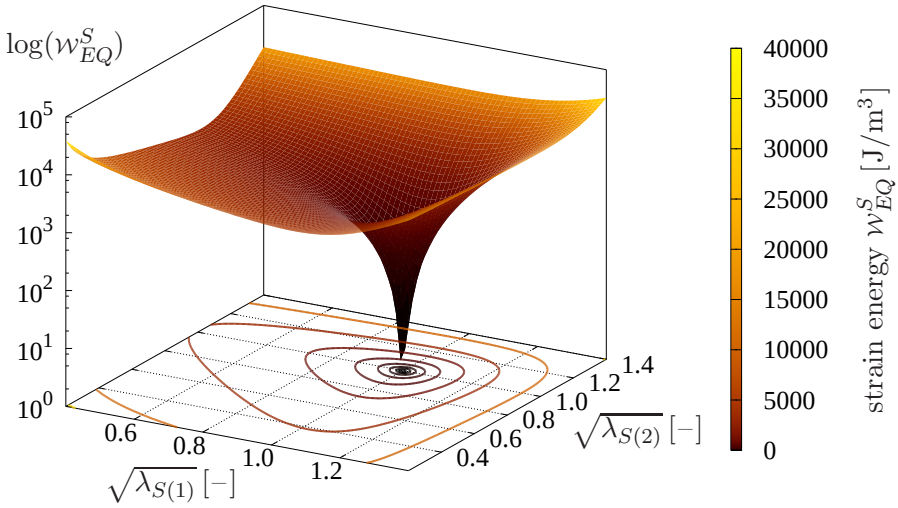

Figure 5.10: *"Convexity plot" of the equilibrium solid strain-energy function for a constant value of $\lambda_{S(3)} = 1$ using the optimized material parameters of box (5.11)*

Basic solid elasticity (equilibrium part)

$\mu^S_0 = 2.5743 \cdot 10^4$	[N/m^2]	: 1st *Lamé* constant (shear modulus)
$\Lambda^S_0 = 6.879 \cdot 10^2$	[N/m^2]	: 2nd *Lamé* constant
$\gamma^S_0 = 1.836$	[–]	: volumetric control parameter
$M_0 = 2$	[–]	: number of *Ogden* terms
$\mu^*_{0(1)} = 2.0098 \cdot 10^{-1}$	[–]	: *Ogden* parameter
$\alpha_{0(1)} = 1.0951 \cdot 10^1$	[–]	: *Ogden* parameter
$\mu^*_{0(2)} = -2.0098 \cdot 10^{-1}$	[–]	: *Ogden* parameter
$\alpha_{0(2)} = 1.0$	[–]	: *Ogden* parameter

(5.11)

5.2.4 Intrinsic Solid Viscoelasticity

After the adjustment of the basic elasticity model, the parameters of the non-equilibrium material formulation (3.113) and the viscous evolution equations (3.135) must be identified. Therefore, proceeding from the previously described experimental setups, additional displacement-driven hysteresis tests without holding times are performed at varying deformation velocities to capture the rate-dependent properties of the skeleton. In particular, cyclic compression-tension experiments are carried out at deformation rates of 7.7, 0.77, 0.077, and 0.0077 mm/s, where the maximum speed is limited by the available spindle-driven testing device. The obtained stress-strain curves are plotted in figure 5.11, where it can be seen that the hysteresis loops exhibit a distinct sensitivity to the strain rate within the considered four decades of the velocity range. In this context, the necessity of the preceding identification of the permeability properties emerges, since otherwise the intrinsic dissipative contributions of the PUR skeleton to the transient response of the foam could not be separated from the flow-dependent ones. In other words, due to the overlay of the dissipative solid and fluid properties, the rate-dependent behavior could be neither clearly assigned to the viscoelastic polymer matrix nor to the viscous percolation process, which would make an unique parameter identification almost impossible.

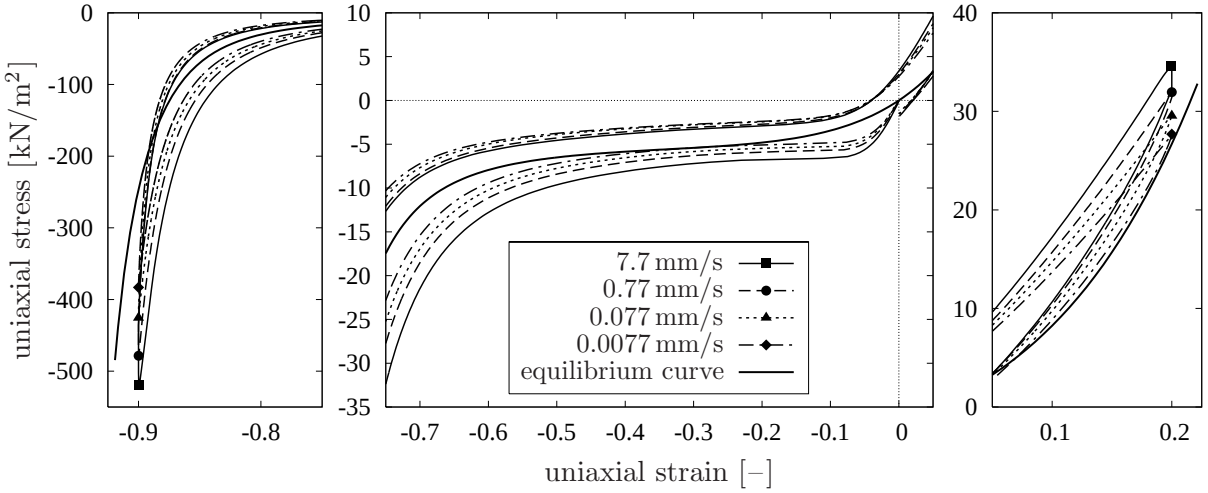

Figure 5.11: *Stress-strain diagram of uniaxial hysteresis experiments in comparison with computed elastic response using the optimized parameter set of box (5.11)*

To continue, based on the above hysteresis data and the relaxation data from the previously described holding-time experiments, the parameter optimization is again carried out numerically using the COBYLA method, where the required FE computations are performed with PANDAS. Therefore, in analogy to the material parameter constraints (5.9) and (5.10) of the basic elasticity model, respective conditions must also be taken into account for each *Maxwell* element during the adaption of the non-equilibrium elasticity formulation (3.113). Moreover, according to relations (3.134), the viscosity parameters associated with the rheological dashpot elements must satisfy $\eta_n^S > 0$ and $\frac{2}{3}\,\eta_n^S + \zeta_n^S > 0$. In this connection, a shortcoming of the discrete spectrum algorithm becomes apparent, as the satisfactory description of the nonlinear relaxation behavior of the PUR skeleton

requires the consideration of an adequate number of *Maxwell* elements. Accompanied with each additional *Maxwell* element is a total of $4+2M_n$ unknown material parameters depending on the individual number M_n of *Ogden* terms, where compatibility conditions analogous to (5.10) are already taken into account. Therefore, in order to keep the optimization effort under an acceptable limit, besides a hierarchical adaption strategy, we proceed from the simplifying assumption that the individual deviatoric and volumetric relaxation times coincide (cf. page 81):

$$\tau_n^S := (\tau_{\mathrm{dev}}^S)_n = (\tau_{\mathrm{vol}}^S)_n \quad \longrightarrow \quad \frac{\eta_n^S}{\mu_n^S} = \frac{\frac{2}{3}\,\eta_n^S + \zeta_n^S}{\frac{2}{3}\,\mu_n^S + \Lambda_n^S} \quad \longrightarrow \quad \zeta_n^S = \frac{\eta_n^S\,\Lambda_n^S}{\mu_n^S}\,. \tag{5.12}$$

Hence, the second viscosity parameters ζ_n^S can be removed from the list of unknowns. Moreover, the maximum number of *Maxwell* elements is restricted to $N=3$, where the individual non-equilibrium elasticity laws are *a priori* equipped with $M_n=2$ *Ogden* terms. Following this, for the adaption of the rate-dependent part of the solid model, one seeks for an optimal feasible set of $N_{\mathrm{mat}}=21$ material parameters in comparison to $N_{\mathrm{mat}}=6$ independent parameters required for the basic elasticity model (cf. section 5.2.3). Accordingly, it is even more important to start the optimization with a good initial guess of the parameters in the right order of magnitude, as the COBYLA algorithm of Powell may become very inefficient due to the sometimes fast decrease of the trust region radius resulting in only small changes to the variables. Actually, this gives rise to future improvements of the COBYLA code by also allowing a controlled increase of the trust region during the optimization.

In the present contribution, the model adaption is additionally aggravated by the fact that the optimization is only based on uniaxial experimental data. In general, it would be necessary to gain more information about the material behavior by further experimental investigations, as for instance volumetric compression or shear tests, which particularly address specific subsets of the parameters and thus, allow for a stepwise fitting procedure with a reduced number of variables. Furthermore, it seems promising to additionally incorporate information about the local material response into the least-squares functional of box (5.1), e. g., by applying optical methods in combination with point tracking algorithms, which are able to capture local deformations on the skin of the test specimens. Nevertheless, as is shown in figure 5.12, the restricted model can already be brought into good accordance with the available hysteresis data yielding the optimized set of material parameters listed in table (5.13). The result gets blurred a little when comparing the simulation with the data of the relaxation experiments. Apparently, the stress-time diagram in figure 5.13 reveals the rough approximation of the stress-relaxation response by using only three *Maxwell* elements, which is obviously not sufficient to precisely recover the fading memory property of the considered PUR foam. However, the general adaptability of the proposed solid viscoelasticity formulation for the description of real material behavior could be shown. Although, it is beyond question that further efforts are necessary in both experimental techniques as well as optimization strategies to facilitate the adaption process and further establish such complex macroscopic material models in the engineering praxis.

Intrinsic solid viscoelasticity (non-equilibrium part)

$N = 3$	[–]	: number of *Maxwell* elements
····· *1st Maxwell element* ·····		
$\mu_1^S = 2.0025 \cdot 10^4$	[N/m^2]	: 1st *Lamé* constant (shear modulus)
$\lambda_1^S = 2.5969 \cdot 10^{-2}$	[N/m^2]	: 2nd *Lamé* constant
$\eta_1^S = 1.603 \cdot 10^6$	[N s/m^2]	: 1st viscosity parameter (shear viscosity)
$\zeta_1^S = 2.0788 \cdot 10^5$	[N s/m^2]	: 2nd viscosity parameter
$\tau_1^S = 8.005 \cdot 10^1$	[s]	: unique relaxation time constant
$\gamma_1^S = 1.0307$	[–]	: volumetric control parameter
$M_1 = 2$	[–]	: number of *Ogden* terms
$\mu^*_{1(1)} = 4.2065 \cdot 10^{-1}$	[–]	: *Ogden* parameter
$\alpha_{1(1)} = 5.7545$	[–]	: *Ogden* parameter
$\mu^*_{1(2)} = -4.2065 \cdot 10^{-1}$	[–]	: *Ogden* parameter
$\alpha_{1(2)} = 1.0$	[–]	: *Ogden* parameter
····· *2nd Maxwell element* ·····		
$\mu_2^S = 3.7342 \cdot 10^4$	[N/m^2]	: 1st *Lamé* constant (shear modulus)
$\lambda_2^S = 1.1117 \cdot 10^2$	[N/m^2]	: 2nd *Lamé* constant
$\eta_2^S = 3.3296 \cdot 10^3$	[N s/m^2]	: 1st viscosity parameter (shear viscosity)
$\zeta_2^S = 9.9121$	[N s/m^2]	: 2nd viscosity parameter
$\tau_2^S = 8.9165 \cdot 10^{-2}$	[s]	: unique relaxation time constant
$\gamma_2^S = 7.7397$	[–]	: volumetric control parameter
$M_2 = 2$	[–]	: number of *Ogden* terms
$\mu^*_{2(1)} = 3.0835$	[–]	: *Ogden* parameter
$\alpha_{2(1)} = 1.0951$	[–]	: *Ogden* parameter
$\mu^*_{2(2)} = -1.3918$	[–]	: *Ogden* parameter
$\alpha_{2(2)} = 9.8913 \cdot 10^{-1}$	[–]	: *Ogden* parameter
····· *3rd Maxwell element* ·····		
$\mu_3^S = 9.8088 \cdot 10^1$	[N/m^2]	: 1st *Lamé* constant (shear modulus)
$\lambda_3^S = 4.1837 \cdot 10^1$	[N/m^2]	: 2nd *Lamé* constant
$\eta_3^S = 1.5259 \cdot 10^7$	[N s/m^2]	: 1st viscosity parameter (shear viscosity)
$\zeta_3^S = 6.5085 \cdot 10^6$	[N s/m^2]	: 2nd viscosity parameter
$\tau_3^S = 1.5556 \cdot 10^5$	[s]	: unique relaxation time constant
$\gamma_3^S = 2.9212$	[–]	: volumetric control parameter
$M_3 = 2$	[–]	: number of *Ogden* terms
$\mu^*_{3(1)} = 4.924 \cdot 10^{-1}$	[–]	: *Ogden* parameter
$\alpha_{3(1)} = 4.061$	[–]	: *Ogden* parameter
$\mu^*_{3(2)} = -2.018 \cdot 10^{-2}$	[–]	: *Ogden* parameter
$\alpha_{3(2)} = -1.8122 \cdot 10^{-2}$	[–]	: *Ogden* parameter

(5.13)

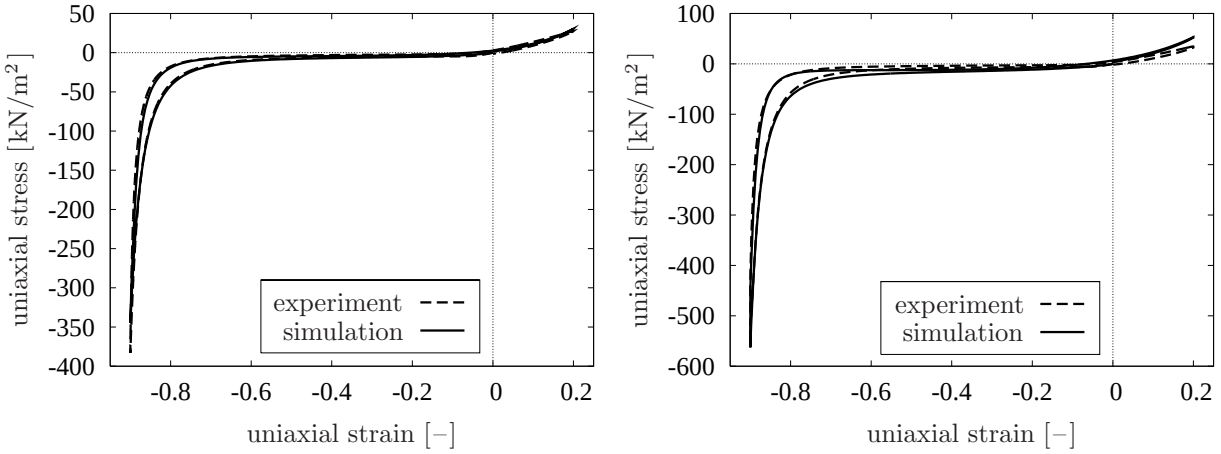

(a) Slowest deformation rate ($v = 0.0077\,\mathrm{mm/s}$) (b) Fastest deformation rate ($v = 7.7\,\mathrm{mm/s}$)

Figure 5.12: *Stress-strain diagrams of uniaxial hysteresis experiments in comparison with the* PANDAS *simulations using the optimized parameter set of box (5.13)*

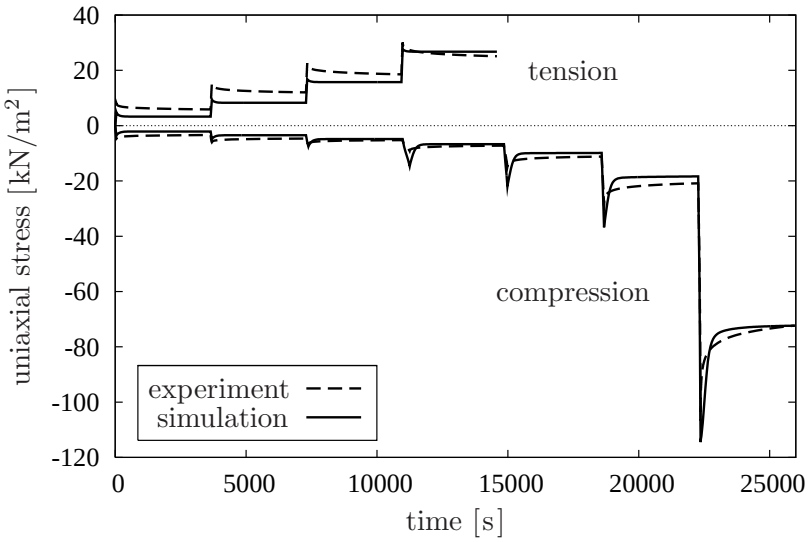

Figure 5.13: *Stress-time diagram of uniaxial relaxation experiments in comparison with the* PANDAS *simulations using the optimized parameter set of box (5.13)*

5.3 Numerical Examples

5.3.1 Impact of a Foam Cushion

As previously mentioned, the considered PUR foam is primarily used as cushioning material for automotive seating systems. In regard to the increasing requirements for passenger safety during crash situations, the further development of seating systems is an important issue. The proper design demands a detailed understanding of the mechanical behavior of

the cushioning material under impact loading. Therefore, by order of the German Association for Research in Automotive Technology FAT, working party AK 27, subgroup *Foam in Crash Simulation*, the Fraunhofer Institute for High-Speed Dynamics, Ernst Mach Institute (EMI) in Freiburg investigated the influence of the cushion size on the transient compressive response of soft PUR foam during impact experiments. In particular, PUR foam cushions with an original size of $400 \times 400 \times 100\,\mathrm{mm}^3$ were impacted by a pneumatically driven impactor with a mass of 150 kg at an impact velocity of about 5 m/s and the responding force and the resulting deformation were recorded. For these experiments, some of the original foam cushions were cut into equal-sized pieces, e. g., four pieces of size $200 \times 200 \times 100\,\mathrm{mm}^3$, and tested together with a small space in between the pieces to allow their unconfined deformation. A photo of the impact testing device and a plot of the experimentally obtained stress-strain curves for a whole cushion, a quartered cushion, and a cushion divided into sixteen pieces are given in figure 5.14. It is easily recognized that an increasing fragmentation of the cushion is accompanied by a decrease in the transient stiffness that can only be explained by the outstreaming pore air through the permeable cut surfaces. More precisely, by increasing the fragmentation, the drained surface is enlarged, thereby concurrently reducing the flow path length of the air to that surface. Therefore, the consolidation process is much faster causing a lower pore-pressure development and, as a consequence, results in a softer material response.

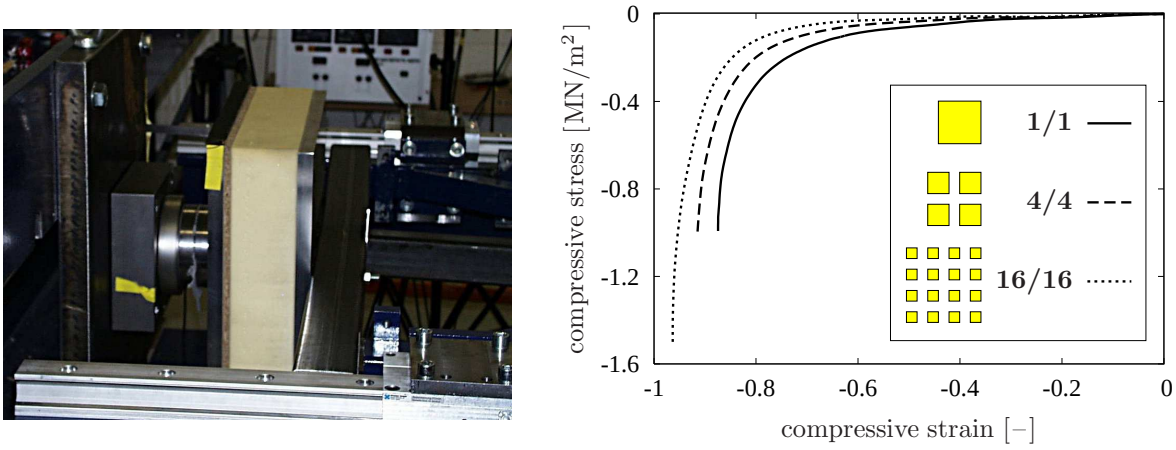

(a) Component crash device (FhG EMI)

(b) Recorded stress-strain curves

Figure 5.14: *Impact testing device and experimental results of impact experiments showing the softening of fragmented PUR foam cushions (courtesy of the FAT working party AK 27, subgroup "Foam in Crash Simulation")*

Now, this flow-dependent size effect is simulated with PANDAS using the previously adapted biphasic viscoelastic material model. For convenience, the impact of the different PUR foam cushions is simulated by a displacement-driven computation at a constant deformation rate of 5 m/s, which is equal to the average impact velocity of the crash experiments. Note in passing that the prescription of a high but constant deformation velocity in combination with a low fluid density is consistent with the quasi-static model, as we have $\rho^S \overset{''}{\mathbf{x}}_S = \mathbf{0}$ and $\rho\,\ddot{\mathbf{x}} \approx \mathbf{0}$. Concerning the drainage conditions, the original PUR foam cushions have a closed skin due to the manufacturing process, which is regarded as

impermeable for the computations, whereas the cut surfaces are modeled as fully drained boundaries. As can be seen from the simulation results depicted in figure 5.15, the phenomenon that under high-speed compression an undivided cushion of the considered foam is much stiffer than a fragmented cushion of the same size is perfectly described. The slightly stiffer response of the simulations in comparison with the experimental curves of figure 5.14(b) can be explained by the inaccurate definition of the boundary conditions by prescription of a linearly increasing displacement rather than an impact load by solving a contact problem. Moreover, the non-equilibrium part of the model is not adapted to really high deformation rates and the foam material used for the parameter optimization does not come from the same production batch as the cushions used for the impact experiments.

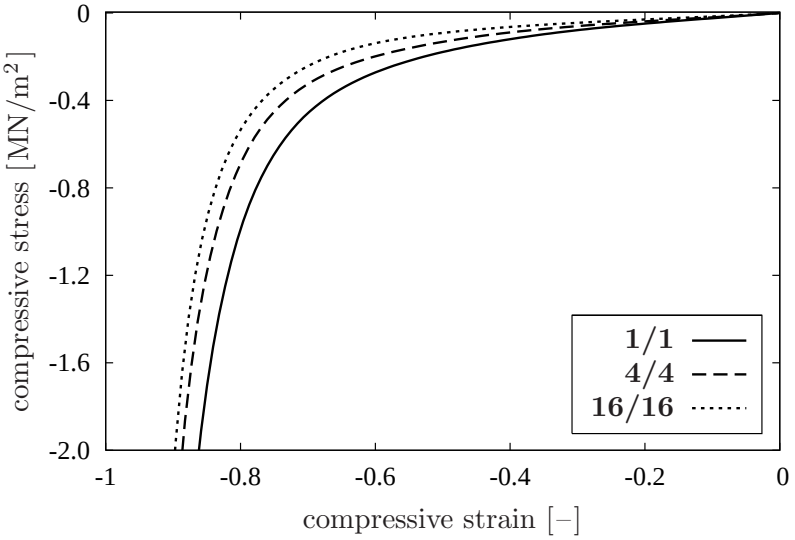

Figure 5.15: *Computed stress-strain curves of the simulated impact experiments of variously fragmented PUR foam cushions using the adapted model*

Next, in order to gain insight into the development of the pore-fluid pressure, the pressure distribution at different deformation states for a non-fragmented cushion is given in figure 5.16. It can be observed that the pressure develops significantly primarily beyond 60 % compression due to the large compressibility of the pore air as well as the deformation-dependent permeability and tortuosity properties of the PUR skeleton. The dynamic compression is accompanied by an immense bulging of the cushion, as the air cannot escape through the assumed impermeable skin. Moreover, it is remarkable that at 85 % compression, the developed internal gas pressure contributes to more than one third of the computed macroscopic stress response. In this context, it should be mentioned that in some of the impact experiments, the occurrence of high pore pressures actually caused the non-fragmented foam cushions to burst. Particularly the above described pneumatic damping behavior gives open-celled polymer foams their outstanding mechanical characteristics under dynamical loading and makes these types of materials favorable for cushioning or packaging applications. Consequently, only a multiphasic model that accounts for the nonlinear and deformation-dependent percolation process as well as the complex deformation habits of the cellular polymer skeleton is appropriate for the realistic description.

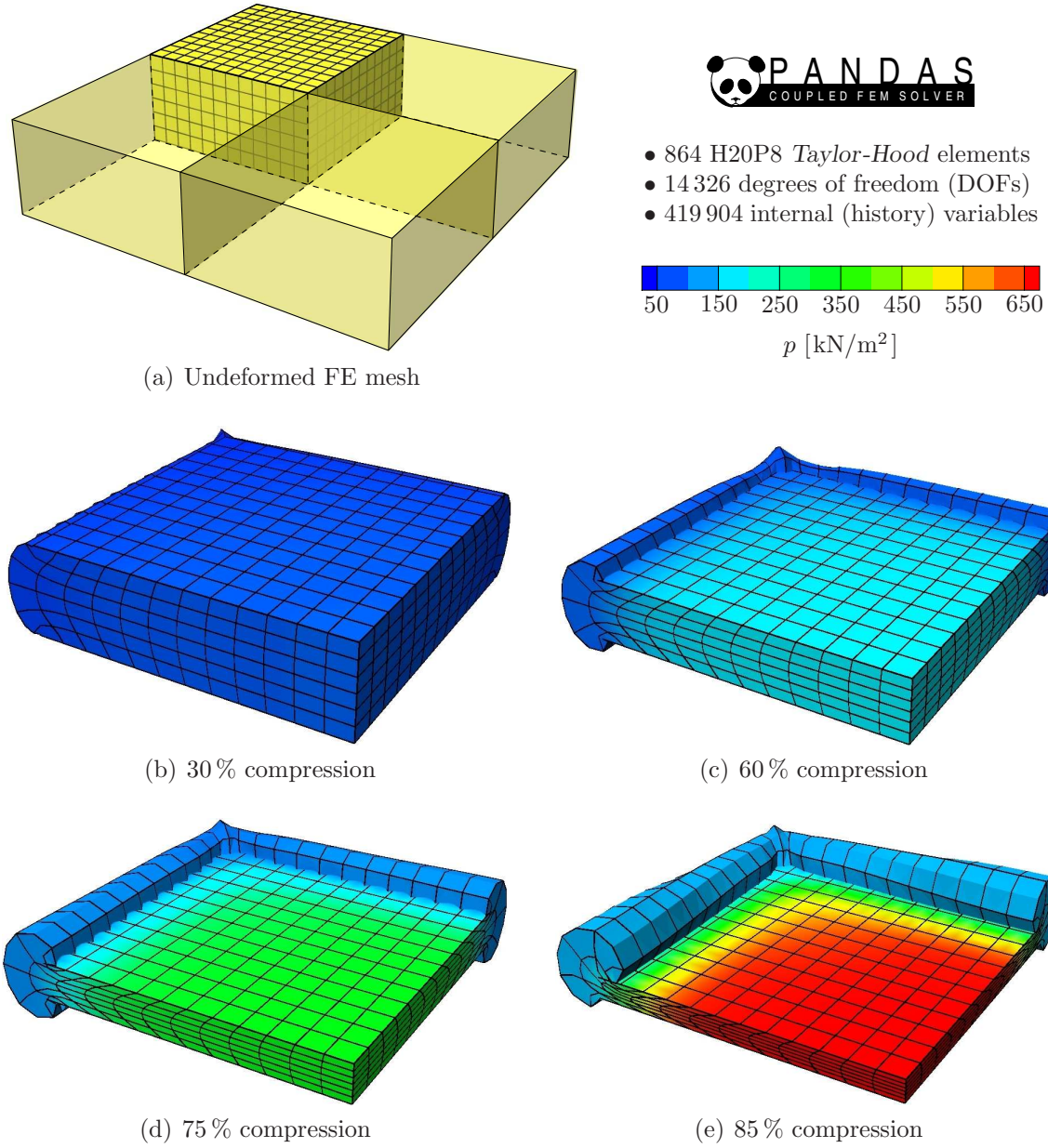

(a) Undeformed FE mesh

(b) 30 % compression

(c) 60 % compression

(d) 75 % compression

(e) 85 % compression

Figure 5.16: *Undeformed FE mesh and computed pore-pressure distributions during the dynamic compression of a non-fragmented PUR foam cushion. Note that due to double symmetry only a quarter of the cushion is computed*

5.3.2 Simulation of a Real Car Seat Cushion

In order to demonstrate the overall applicability of the presented model and the efficiency of its numerical implementation within the mixed finite element method, the dynamic loading of the cushioning of a real car seat is simulated. Therefore, the geometry of an AUDI A6 limousine seat cushion is reconstructed in a slightly simplified form using the Rhinocerus NURBS (non-uniform rational B-splines) modeling software[5]. The recon-

[5] Rhinocerus NURBS modeling for Windows (`http://www.rhino3d.com`)

structed geometry model of the cushioning is then spatially discretized by the different 3-d mixed finite elements shown in figure 4.1, where several meshes with variable degrees of refinement are generated using the CUBIT mesh generation toolkit[6]. A photo of the original car seat, the reconstructed geometry model of the cushion, and a selection of the generated FE meshes are depicted in figure 5.17. As an illustrative example, an initial boundary-value problem is defined, which qualitatively simulates an impact of the seat cushion, e. g., by a passenger or a crash-test dummy. For convenience, the abrupt loading is idealized by a distributed force on the mid parts of the cushion (see figure 5.17(a) right), which is applied within 0.2 s, where the magnitude is reasonably chosen in order to yield realistic deformations. Against the background of the low density of the considered foam and the moderate acceleration during loading, it is assumed that inertial effects are negligibly small in comparison to the occurring rate-dependent phenomena, such that the quasi-static approximation is still valid. For the computations, the bottom of the seat and the rear of the back are regarded as spatially fixed (cf. figure 5.18). Moreover, the dense textile cover of the cushioning is assumed to be impermeable under transient conditions and therefore, all surfaces are modeled as undrained boundaries. Note that due to the symmetry properties only half of the seat cushion must be computed taking into account appropriate symmetry boundary conditions.

For comparison of the different element types and discretizations, all computations are carried out with the sequential 64 bit version of PANDAS[7] on the Beowulf Linux Cluster in our institute, which is based on dual and quad AMD Opteron compute nodes equipped with 2.2 GHz CPUs and a maximum of 6 GB memory available for single processor jobs. Due to the large sparse linear systems of equations that arise from the finer FE discretizations, the application of *Krylov*-subspace iterative solvers (see, e. g., Barrett *et al.* [6]) is expedient. Following this, based on a compact sparse row (CSR) storage format, the generalized minimal residual (GMRES) method (Saad & Schultz [155]) is used in conjunction with an ILUK[8] preconditioner, which in sequential computations yields a good performance and a stable convergence for the considered class of problems and fairly holds the balance between computational effort and required storage. For the global as well as the local time discretization, the implicit *Euler* scheme is used, where the time step size is adaptively controlled depending on the number of required *Newton* iterations as an objective indicator of the actual convergence behavior. The numerical quadrature proceeds from 27 integration points in the case of the hexahedral H20P8 *Taylor-Hood* elements and 15 *Gauß* points for both types of the mixed tetrahedral elements T10P4 and T4P4B, respectively. Following this, proceeding from the adapted solid viscoelasticity model with $N = 3$ *Maxwell* elements, a total number of $3 \times 6 = 18$ internal (history) variables must be treated and stored at each integration point of the FE mesh (recall equation (4.39)). Moreover, concerning the implementation of the T4P4B MINI element, it should be noted that for the present investigations, the barycentric bubble nodes are not condensed on the element level, i. e., the associated three solid displacements per element enter the global equation system as additional unknowns.

[6] CUBIT FE Mesh Generation Toolkit, Sandia National Laboratories (`http://cubit.sandia.gov`)

[7] For MPI-based, parallel solution strategies with PANDAS, see the articles by Wieners *et al.* [189, 190].

[8] Incomplete LU (ILU) factorization type preconditioner with a prescribed number of non-zero elements per row in the preconditioned matrix (cf. Saad [154] among others).

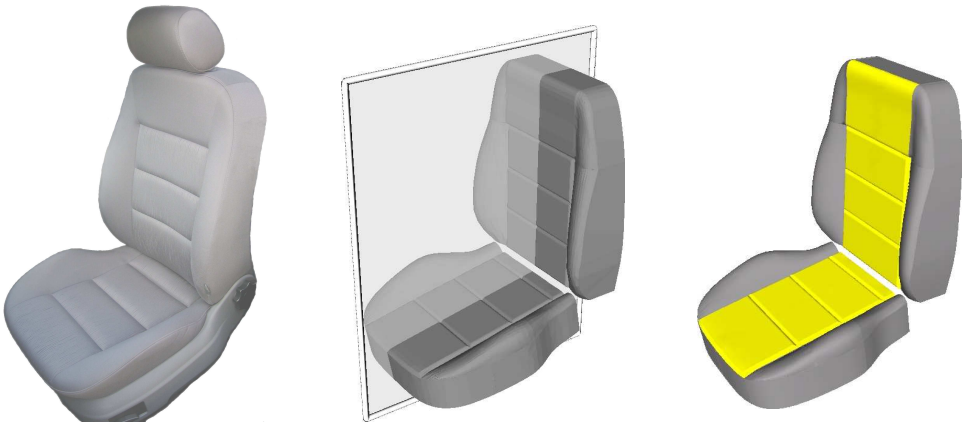

(a) Original car seat, reconstructed cushion geometry model with symmetry plane, and geometry with highlighted loaded mid parts

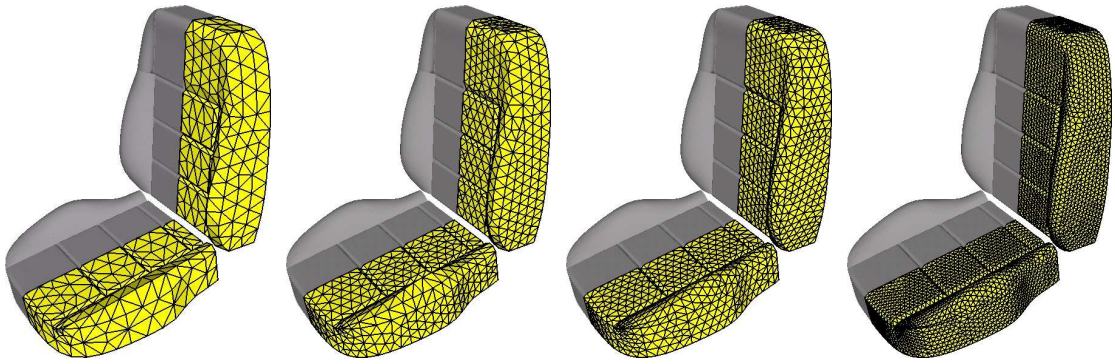

2 030 elements 9 113 elements 16 637 elements 75 792 elements

(b) Tetrahedral FE discretizations (T10P4, T4P4B)

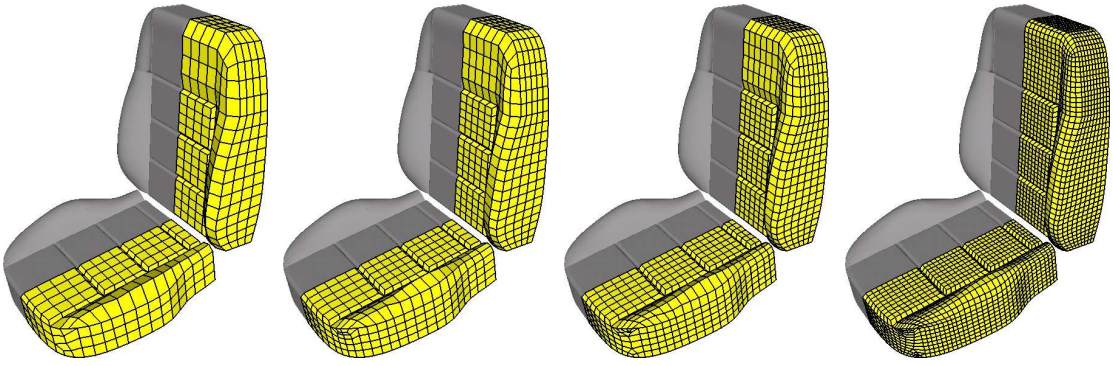

817 elements 1 722 elements 2 906 elements 10 502 elements

(c) Hexahedral FE discretizations (H20P8)

Figure 5.17: *A photo of the original car seat, the reconstructed geometry model of the seat cushion, and a selection of tetra- and hexahedral FE discretizations*

Following the above, altogether 19 computations have been carried out of which 18 converged successfully comprising six different refinement levels of the spatial discretization for all three types of the considered mixed finite elements. The corresponding statistical information of the generated FE meshes including the total numbers of elements, de-

grees of freedom (DOFs), and internal variables, as well as the required storage (RAM in MB) and computing times (CPU time in hh:mm:ss) with the number of accepted versus rejected time steps and whether the end time is reached is provided in the following table:

	# elems.	# DOFs	# int. vars.	RAM	CPU time (steps)	end
H20P8 (1)	344	7 061	167 184		00:07:14 (9/2)	yes
(2)	817	15 051	397 062		00:30:51 (11/4)	yes
(3)	1 722	29 227	836 892		01:00:31 (10/2)	yes
(4)	2 906	47 587	1 412 316		02:13:33 (11/2)	yes
(5)	5 030	80 793	2 444 580	1 582	07:30:43 (15/5)	yes
(6)	7 120	109 948	3 460 320	2 343	17:30:06 (20/10)	yes
(7)	10 502	159 707	5 103 972	4 360	57:31:28 (27/30)	no
T10P4 (1)	673	4 576	181 710		00:04:20 (7/0)	yes
(2)	2 030	11 817	548 100		00:17:23 (8/1)	yes
(3)	9 113	45 779	2 460 510		02:14:04 (11/2)	yes
(4)	16 637	81 029	4 491 990	878	05:31:16 (14/3)	yes
(5)	33 340	157 047	9 001 800	1 505	16:55:01 (14/4)	yes
(6)	47 256	219 447	12 759 120	4 880	53:14:06 (24/17)	yes
T4P4B (1)	673	3 079	181 710		00:06:10 (7/0)	yes
(MINI) (2)	2 030	8 562	548 100		00:17:36 (7/0)	yes
(3)	9 113	35 915	2 460 510		01:29:34 (7/0)	yes
(4)	16 637	64 703	4 491 990	439	02:42:56 (7/0)	yes
(5)	33 340	127 908	9 001 800	1 259	10:36:35 (14/0)	yes
(6)	75 792	287 400	20 463 840	2 204	39:26:37 (22/1)	yes

(5.14)

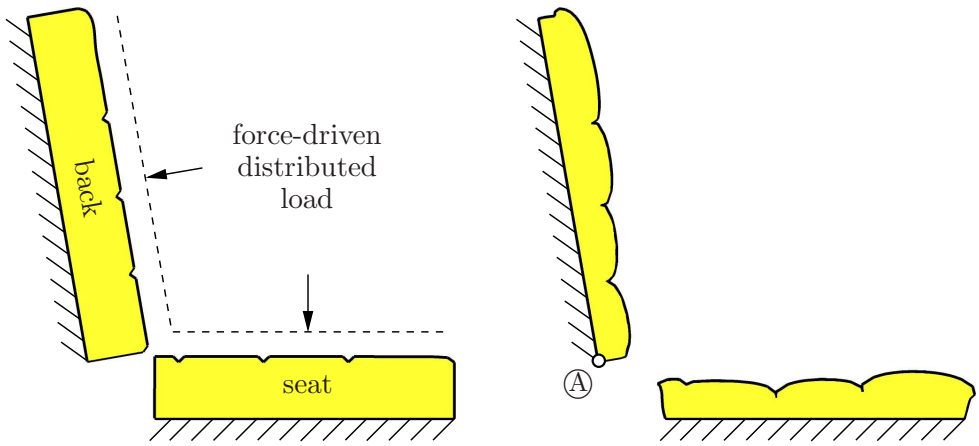

Figure 5.18: *Undeformed and deformed geometry in the symmetry plane of the seat cushion*

Now, based on the obtained simulation results, the comparison is carried out in two ways. At first, the computed deformations of the seat surface in the symmetry plane (cf. figure 5.18) are compared by plotting the final vertical displacements of the surface relative to its undeformed reference position for all discretizations (see figure 5.19).

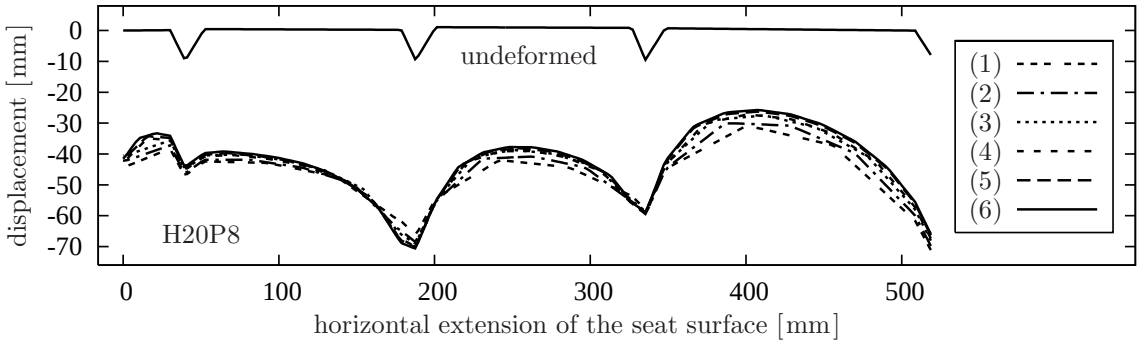

(a) Hexahedral discretizations with H20P8 *Taylor-Hood* elements

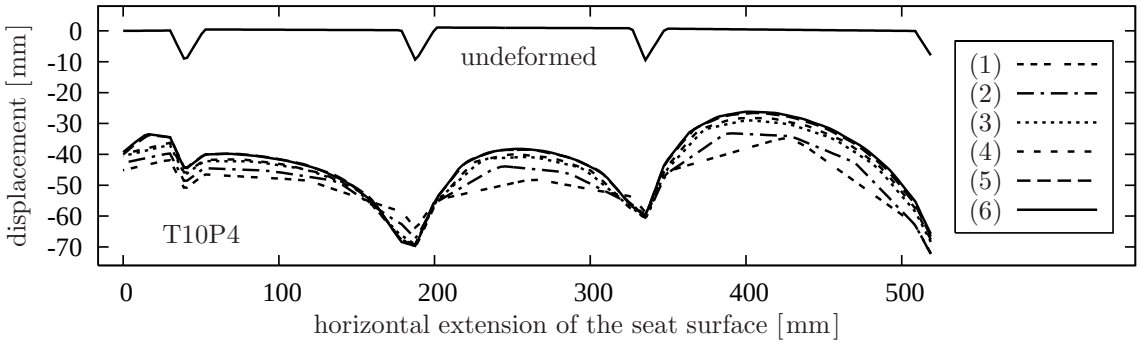

(b) Tetrahedral discretizations with T10P4 *Taylor-Hood* elements

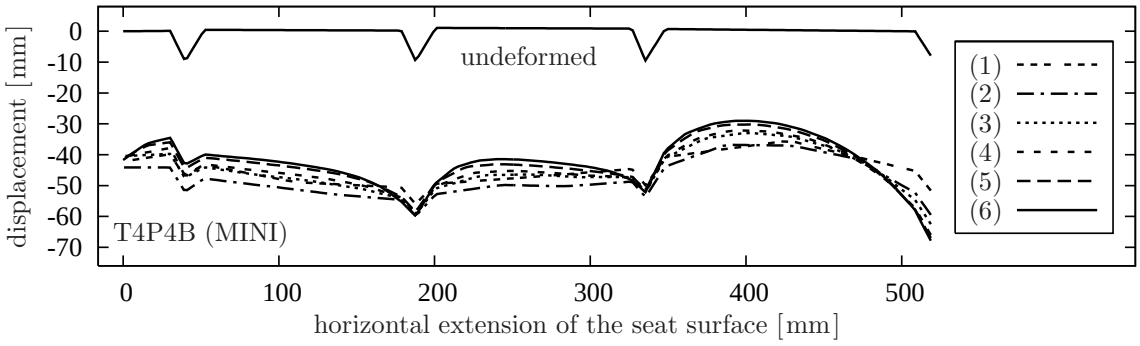

(c) Tetrahedral discretizations with T4P4B (MINI) elements

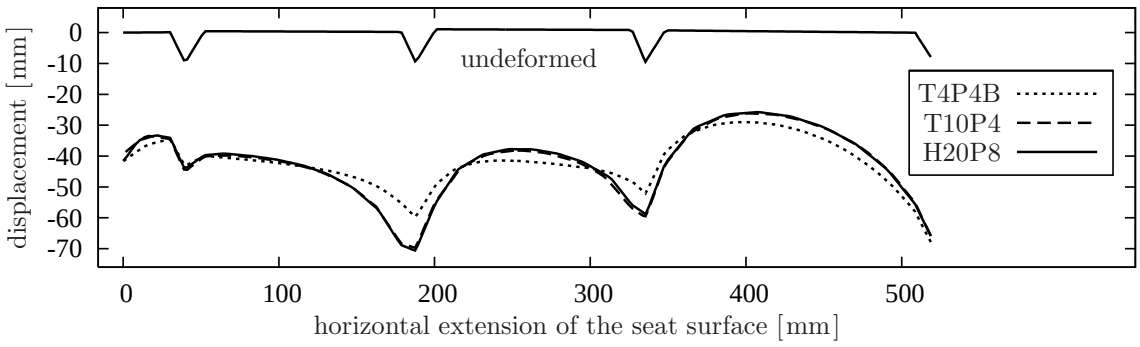

(d) Comparison of the finest (refinement level (6)) mixed FE discretizations

Figure 5.19: *Comparison of the computed vertical displacements of the seat surface in the symmetry plane for the different mixed FE discretizations listed in table (5.14)*

As can be observed in subfigures 5.19(a)-(c), by increasing the refinement of the spatial discretization the convergence property of the FEM is clearly verified for each element formulation. In this regard, coarse discretizations usually yield stiffer solutions than finer meshes, which, following the basic idea of the finite element method, are closer to the real solution. However, comparison of the finest discretizations of all element types in subfigure 5.19(d) reveals the inferior approximation of the seat surface deformation by the MINI elements as expected. It is a well-known fact that 1st-order tetrahedral elements are stiffer than 2nd-order tetrahedrons, which is also the major drawback of the T4P4B element followed by its undoubtful lower accuracy, which may falsify the results especially in areas around stress concentrations. Nevertheless, the disadvantages of the MINI element can be put into perspective by looking at the computational effort and the required storage in comparison to the H20P8 or T10P4 *Taylor-Hood* elements, respectively. Due to the additional mid nodes needed for the quadratic interpolation of $\mathbf{u}_S$, which, in contrast to the barycentric bubble nodes, are shared with adjacent elements, besides the larger number of unknowns also the bandwidth of the global system matrix is generally larger causing a higher memory load and an increase of the total solution time. Moreover, for the problem under study, where all simulations proceed from the same settings (tolerances, stopping criteria, etc.), the computations with the *Taylor-Hood* elements show a more cumbersome convergence behavior. It is apparent from table (5.14) that the number of rejected time steps, i. e., the computed time steps where finally no convergence is found in the global *Newton* iteration, is considerably larger for the discretizations based on the *Taylor-Hood* elements than on the MINI element. For the finest hexahedral mesh H20P8 (7), the force-driven analysis is interrupted when 95.8 % of the final load is applied, as the chosen minimal time step size of 10^{-10} s is reached and still no convergence is found. This might be explained by the general observation that in large deformation problems the finer discretizations by 20-noded brick elements are more vulnerable to critical aspect ratios and interior angles than tetrahedral meshes.

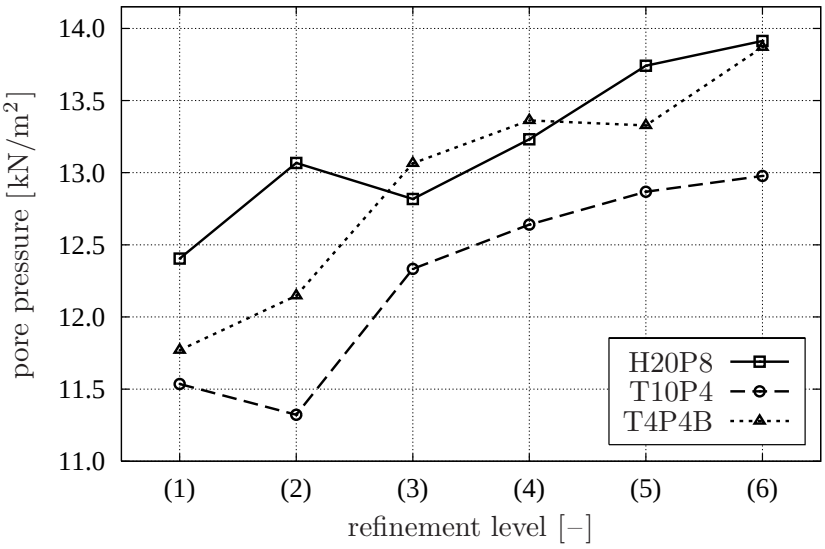

Figure 5.20: *Computed maximal pore-gas pressures in the back of the seat cushion (point Ⓐ) depending on the element type and the refinement level according to table (5.14)*

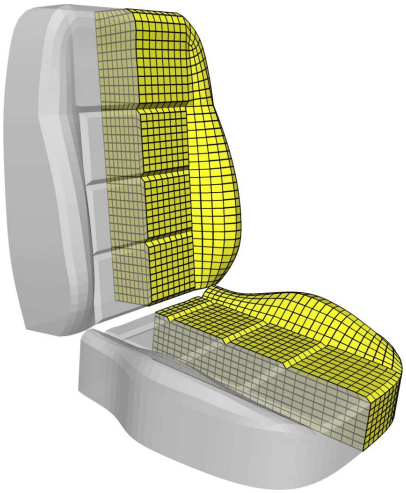

(a) Undeformed FE mesh

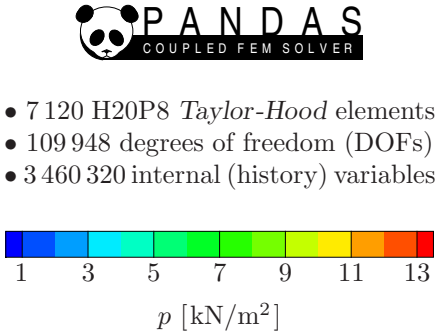

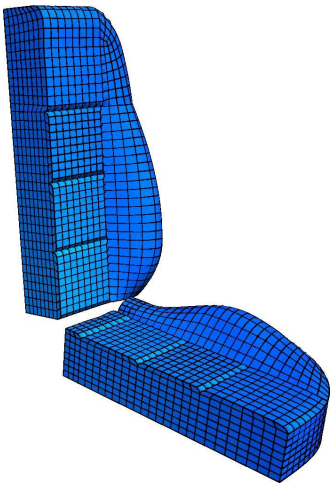

(b) 15 % loading

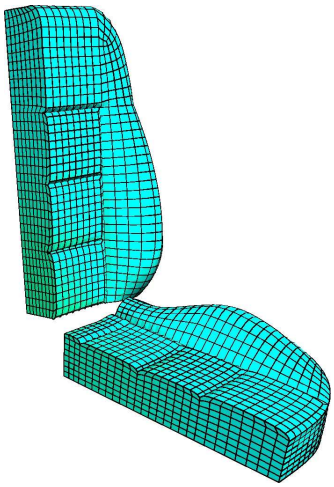

(c) 40 % loading

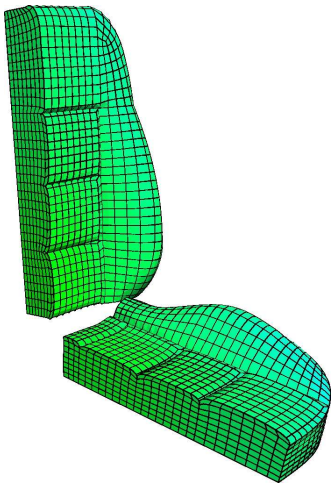

(d) 50 % loading

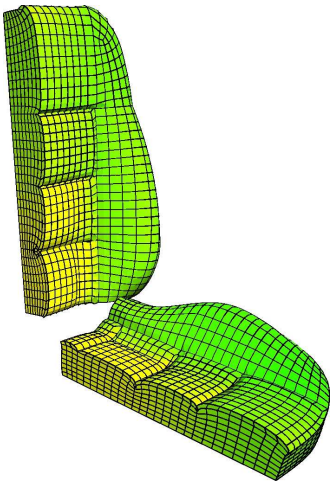

(e) 75 % loading

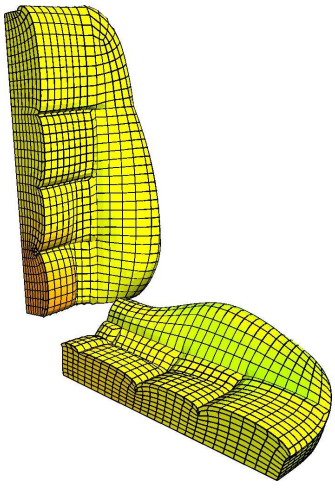

(f) 87.5 % loading

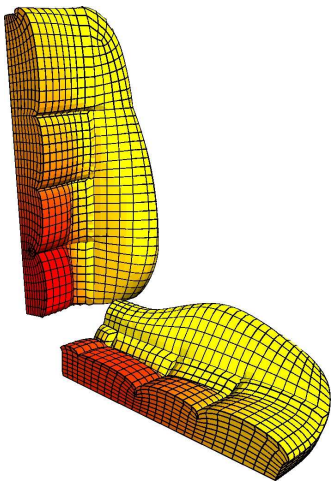

(g) 100 % loading

Figure 5.21: *Computed deformations and pore-pressure distributions during the force-driven simulation of an impaction of a car seat cushion using the H20P8 (6) discretization*

As a next step, the quality of the pore-pressure approximations is compared. Therefore, the computed maximum pore-gas pressure occurring in the lower part of the back of the seat cushion in the symmetry plane at point Ⓐ marked in figure 5.18 is plotted for all element types over the six refinement levels of the respective discretization (see figure 5.20). Surprisingly, despite the underestimated solid displacements, the pressure approximations based on the MINI element are close to those of the H20P8 brick elements, which are known to yield good interpolations of the pressure field, whereas the tetrahedral *Taylor-Hood* elements underestimate the maximal pressure of about 6 %. Finally, in order to get an impression of the overall development of the pore-gas pressure and the 3-d deformation behavior of the seat cushion, a sequence of deformed configurations at different loading states with the pore-pressure distribution displayed as isosurfaces is depicted in figure 5.21.

In conclusion, the above example convincingly shows that the presented biphasic viscoelastic model together with its numerical treatment by the mixed finite element method is well suited for application to real engineering problems. Concerning the choice of the mixed element type, one has to balance between computational costs and accuracy. On the one hand, for 3-d porous media problems with moderate solid stresses and small skeleton deformations or generally lower accuracy requirements, such as for testing purposes or qualitative simulations, the T4P4B element seems to be the economic choice. Another potential application of the MINI element might be its use in commercial FE packages, where sophisticated TPM models can be incorporated via the user material interface, as higher-order mixed element formulations are usually not or only partly available. On the other hand, whenever high accuracy is required, the H20P8 or T10P4 *Taylor-Hood* elements are the convenient choice. However, if the complexity of the geometry or the used material model demands a fine-resolution mesh, the large equation system that arises can only be efficiently handled by recourse to domain decomposition methods, which enable a distributed parallel treatment of the strongly coupled problem.

6 Conclusions

6.1 Summary

The goal of this contribution was to present a consistent viscoelastic porous media model that accounts for the essential nonlinearities and the rate-dependent solid and fluid properties within the realm of a finite deformation theory. Therefore, on the basis of the established Theory of Porous Media (TPM), a general biphasic solid-fluid model was modularly extended by incorporating a sophisticated solid viscoelasticity formulation and a 3-d deformation-dependent non-*Darcy* filter law. The efficient numerical treatment of the strongly coupled inelastic problem was carried out by the mixed finite element method (FEM), where the overall solution procedure and the algorithmic implementation were described. In order to show its practical applicability, the proposed model was adapted to real experimental data of a soft open-celled polyurethane (PUR) foam by use of a numerical optimization strategy. Finally, two illustrative boundary-value problems were computed to show the capabilities of the macroscopic formulation and its numerical implementation, and the overall applicability of the model to real engineering problems.

6.2 Conclusion and Discussion

Proceeding from a comprehensible introduction of finite deformation measures by means of natural curvilinear coordinates, it could be shown that the multiplicative geometric concept associated with stress-free intermediate configurations represents a convenient constitutive basis in finite solid inelasticity. For the considered case of a viscoelastic solid skeleton, from a modeling as well as a computational perspective, the rheological structure of the generalized *Maxwell* model turned out to be well suited to serve as a constitutive phenomenological framework. In particular, the differential representation of viscoelasticity with a discrete relaxation spectrum in combination with strain-equivalent internal variables, such as the inelastic deformation tensors, allows the application of an efficient iterative solution algorithm based on a two-stage *Newton* procedure. In conjunction with sophisticated *Runge-Kutta* time integration schemes this enables the economic computation of large coupled viscoelastic DAE systems.

The proposed isotropic strain-energy function for the description of the macroscopically compressible viscoelastic skeleton could be very well correlated with the highly nonlinear stress-strain data of a low-density polyurethane foam. This was only possible through the polynomial structure of the strain energy, which basically proceeds from *Ogden*-type formulations for the equilibrium and non-equilibrium parts extended by appropriate volumetric response functions. In this context, the developing non-equilibrium contributions are governed by adequate rate equations formulated on the intermediate configurations, such that the model remains its validity even for finite viscoelastic processes, which are far away from thermodynamic equilibrium.

Concerning the description of the nonlinear percolation process, it could be shown that the proposed non-*Darcy* filter law is very successful in describing real liquid and gas flows through variously compressed samples of the considered PUR foam. Since for this foam no distinct anisotropic effects were observed in the pore-fluid flow, it remains to be shown that the presented ansatz of a deformation-induced anisotropic permeability can be experimentally verified for other permeable porous materials.

The general adjustment of the biphasic viscoelastic model for the description of an open-celled polyurethane foam was successfully carried out by use of a gradient-free, sequential, trust region optimization algorithm. In this regard, the used hierarchical simulation strategy kept the computational overhead under an acceptable limit and somehow weakens the conventional wisdom by which function-value only methods should be avoided unless there is no other choice. However, in order to fit the constitutive model more accurately and possibly expose its weak points, further experimental evidence is necessary to precisely capture the properties of the considered foam material under general loading conditions. This will additionally guide further improvements of the biphasic model.

The two final numerical examples convincingly showed that the presented biphasic viscoelastic model together with its numerical treatment by the mixed FEM is well suited for practical applications. From the impact simulations, it became apparent that only a multiphasic model that accounts for the essential nonlinearities and rate-dependent solid and fluid properties is appropriate for the realistic description of soft polymeric foams. Concerning the choice of the mixed element type, a convergence study showed that all discussed element formulations yield a stable solution and an increasing accuracy in finer meshes. However, in comparison to the computationally more expensive H20P8 and T10P4 *Taylor-Hood* elements, one has to be aware of the generally stiffer solution and lower accuracy, if the T4P4B MINI element is used for the spatial discretization.

In conclusion, the present work delivers several new aspects to porous media theories concerning consistent modeling, efficient numerical treatment, and model adaption, where the overall combination defines the new state of the art in porous media viscoelasticity.

6.3 Future Work

Due to the manifold further improvements of the presented viscoelastic porous media model, only a selective choice of conceivable extensions is presented. Two obvious improvements could be the generalization to overall anisotropic skeleton properties and the consideration of damage and aging effects. In this connection, quite a lot of work exists in the related literature of singlephasic materials, where the basic concepts can be straightforwardly adopted and integrated into the existing model. Further interesting possibilities are provided by an extension of the biphasic model with an additional fluid constituent and the consideration of individual constituent temperatures, which allows the description of partially saturated conditions and heat transfer processes. Moreover, the presented approach offers future potentials when applied in the aspiring field of biomechanics, e. g., for the description of soft biological tissues, such as articular cartilage. Particularly hydrated biological tissues are believed to exhibit intrinsic rate-dependent properties besides

the dissipative interstitial flow and diffusion phenomena, which may be explained by their proteinic microstructure that is somehow comparable to a viscoelastic network of polymer chains. Furthermore, as the modular structure of the constitutive equations is not only restricted to binary solid-fluid mixtures, they may be exploited in all kinds of multiphasic TPM models and thus, can find their application in various engineering disciplines.

References

[1] Antman, S. S.: Existence of solutions of the equilibrium equations for nonlinearly elastic rings and arches. *Indiana University Mathematics Journal* **20** (1970), 281–302.

[2] Arnold, D. N.: Mixed finite element methods for elliptic problems. *Computer Methods in Applied Mechanics and Engineering* **82** (1990), 281–300.

[3] Arnold, D. N., Brezzi, F. & Fortin, M.: A stable finite element for the Stokes equations. *Calcolo* **21** (1984), 337–344.

[4] Baker, M. & Ericksen, J. L.: Inequalities restricting the form of the stress deformation relations for isotropic elastic solids and Reiner-Rivlin fluids. *Journal of the Washington Academy of Sciences* **44** (1954), 33–35.

[5] Ball, J. M.: Convexity conditions and existence theorems in non-linear elasticity. *Archives for Rational Mechanics and Analysis* **63** (1977), 337–403.

[6] Barrett, R., Berry, M., Chan, T., Demmel, J., Donato, J., Dongarra, J., Eijkhout, V., Pozo, R., Romine, C. & van der Vorst, H.: *Templates for the Solution of Linear Systems: Building Blocks for Iterative Methods*. Society for Industrial and Applied Mathematics (SIAM), Philadalphia 1994, 2nd edn.

[7] Bear, J.: *Dynamics of Fluids in Porous Media*. Dover Publications, Mineola 1988, reprint of American Elsevier Publishing Company, New York, 1972.

[8] Bertram, A.: An alternative approach to finite plasticity based on material isomorphisms. *International Journal of Plasticity* **15** (1999), 353–374.

[9] Bertram, A. & Böhlke, T.: Simulation of texture induced elastic anisotropy of polycrystalline copper. *Computational Materials Science* **16** (1999), 2–9.

[10] Biot, M. A.: General theory of three-dimensional consolidation. *Journal of Applied Physics* **12** (1941), 155–164.

[11] Biot, M. A.: Theory of deformation of a porous viscoelastic anisotropic solid. *Journal of Applied Physics* **5** (1956), 459–467.

[12] Bischoff, J. R., Catsiff, E. & Tobolsky, A. V.: Elastoviscous properties of amorphous polymers in the transition region – I. *Journal of the American Chemical Society* **74** (1952), 3378–3381.

[13] Bishop, A. W.: The effective stress principle. *Teknisk Ukeblad* **39** (1959), 859–863.

[14] Blatz, P. J. & Ko, W. L.: Application of finite elasticity theory to the deformation of rubbery materials. *Transactions of the Society of Rheology* **6** (1962), 223–251.

[15] Bluhm, J.: *Ein Modell zur Berechnung geometrisch nichtlinearer Probleme der Elastoplastizität mit Anwendung auf ebene Stabtragwerke*. Dissertation, Fortschritt-Berichte VDI, Reihe 18, Nr. 94, VDI-Verlag, Düsseldorf 1991.

[16] Boehler, J. P.: Introduction of the invariant formulation of anisotropic constitutive equations. In *Applications of Tensor Functions in Solid Mechanics*, Boehler, J. P., ed., Springer-Verlag, Wien 1987, CISM Courses and Lectures No. 292, pp. 13–30.

[17] de Boer, R.: *Vektor- und Tensorrechnung für Ingenieure*. Springer-Verlag, Berlin 1982.

[18] de Boer, R.: Highlights in the historical development of porous media theory: Toward a consistent macroscopic theory. *Applied Mechanics Reviews* **49** (1996), 201–262.

[19] de Boer, R.: *Theory of Porous Media*. Springer-Verlag, Berlin 2000.

[20] de Boer, R. & Ehlers, W.: The development of the concept of effective stresses. *Acta Mechanica* **83** (1990), 77–92.

[21] Bowen, R. M.: Theory of mixtures. In *Continuum Physics*, Eringen, A. C., ed., Academic Press, New York 1976, vol. III, pp. 1–127.

[22] Bowen, R. M.: Incompressible porous media models by use of the theory of mixtures. *International Journal of Engineering Sciences* **18** (1980), 1129–1148.

[23] Bowen, R. M.: Compressible porous media models by use of the theory of mixtures. *International Journal of Engineering Sciences* **20** (1982), 697–735.

[24] Braess, D.: *Finite Elemente*. Springer-Verlag, Berlin 1997.

[25] Brenan, K. E., Campbell, S. L. & Petzold, L. R.: *Numerical Solution of Initial-Value Problems in Differential-Algebraic Equations*. North-Holland, New York 1989.

[26] Brent, R. P.: *Algorithms for Minimization Without Derivatives*. Prentice-Hall, Englewood Cliffs, New Jersey 1973.

[27] Brezzi, F. & Fortin, M.: *Mixed and Hybrid Finite Element Methods*. Springer-Verlag, New York 1991.

[28] Carter, J. P., Small, J. C. & Booker, J. R.: A theory of finite elastic consolidation. *International Journal of Solids and Structures* **13** (1977), 467–478.

[29] Chen, Z., Lyons, S. L. & Qin, G.: Derivation of the Forchheimer law via homogenization. *Transport in Porous Media* **44** (2001), 325–335.

[30] Christensen, R. M.: *Theory of Viscoelasticity: An Introduction*. Academic Press, New York 1971.

[31] Christian, J. T. & Boehmer, J. W.: Plane strain consolidation by finite elements. *ASCE Journal of the Soil Mechanics and Foundations Division* **96** (1970), 1435–1457.

[32] Ciarlet, P. G.: *Mathematical Elasticity: Three Dimensional Elasticity*, vol. 1. North-Holland, Amsterdam 1988.

[33] Coleman, B. D.: Thermodynamics of materials with memory. *Archives for Rational Mechanics and Analysis* **17** (1964), 1–46.

[34] Coleman, B. D. & Gurtin, M. E.: Thermodynamics with internal state variables. *Journal of Chemical Physics* **47** (1967), 597–613.

[35] Coleman, B. D. & Noll, W.: An approximation theorem for functionals, with applications in continuum mechanics. *Archives for Rational Mechanics and Analysis* **6** (1960), 356–370.

[36] Coleman, B. D. & Noll, W.: The thermodynamics of elastic materials with heat conduction and viscosity. *Archives for Rational Mechanics and Analysis* **13** (1963), 167–178.

[37] Cosserat, E. & Cosserat, F.: *Théorie des corps déformables*. A. Hermann et fils, Paris 1909, (Theory of Deformable Bodies, NASA TT F-11 561, 1968).

[38] Coussy, O.: *Mechanics of Porous Continua*. John Wiley & Sons, Chichester 1995, 2nd edn.

[39] Crochet, M. J. & Naghdi, P. M.: On constitutive equations for flow of fluid through an elastic solid. *International Journal of Engineering Sciences* **4** (1966), 383–401.

[40] Dacorogna, B.: *Direct Methods in the Calculus of Variations*. Springer-Verlag, Berlin 1989.

[41] Darcy, H.: *Les fontaines publiques de la ville de Dijon*. Dalmont, Paris 1856.

[42] Dennis, J. E. & Torczon, V.: Direct search methods on parallel machines. *SIAM Journal on Optimization* **1** (1991), 448–474.

[43] Diebels, S.: *Mikropolare Zweiphasenmodelle: Formulierung auf der Basis der Theorie Poröser Medien*. Habilitation, Bericht Nr. II-4 aus dem Institut für Mechanik (Bauwesen), Universität Stuttgart 2000.

[44] Diebels, S. & Ehlers, W.: Dynamic analysis of a fully saturated porous medium accounting for geometrical and material non-linearities. *International Journal of Numerical Methods in Engineering* **39** (1996), 81–97.

[45] Diebels, S. & Ehlers, W.: On fundamental concepts of multiphase micropolar materials. *Technische Mechanik* **16** (1996), 77–88.

[46] Diebels, S., Ellsiepen, P. & Ehlers, W.: Error-controlled Runge-Kutta time integration of a viscoplastic hybrid two-phase model. *Technische Mechanik* **19** (1999), 19–27.

[47] Droste, A.: *Beschreibung und Anwendung eines elastisch-plastischen Materialmodells mit Schädigung für hochporöse Metallschäume*. Dissertation, Bericht Nr. II-9 aus dem Institut für Mechanik (Bauwesen), Universität Stuttgart 2002.

[48] Dullien, F. A. L.: *Porous Media – Fluid Transport and Pore Structure*. Academic Press, New York 1979.

[49] Ehlers, W.: *Poröse Medien – ein kontinuumsmechanisches Modell auf der Basis der Mischungstheorie*. Habilitation, Forschungsberichte aus dem Fachbereich Bauwesen, Heft 47, Universität-GH-Essen 1989.

[50] Ehlers, W.: Constitutive equations for granular materials in geomechanical context. In *Continuum Mechanics in Environmental Sciences and Geophysics*, Hutter, K., ed., Springer-Verlag, Wien 1993, CISM Courses and Lectures No. 337, pp. 313–402.

[51] Ehlers, W.: A single-surface yield function for geomaterials. *Archive of Applied Mechanics* **65** (1995), 246–259.

[52] Ehlers, W.: *Vector and Tensor Calculus: An Introduction*. Lecture Notes, Institute of Applied Mechanics (CE), University of Stuttgart 1995–2005, URL `http://www.mechbau.uni-stuttgart.de/ls2`.

[53] Ehlers, W.: Grundlegende Konzepte in der Theorie Poröser Medien. *Technische Mechanik* **16** (1996), 63–76.

[54] Ehlers, W.: Foundations of multiphasic and porous materials. In *Porous Media: Theory, Experiments and Numerical Applications*, Ehlers, W. & Bluhm, J., eds., Springer-Verlag, Berlin 2002, pp. 3–86.

[55] Ehlers, W. & Eipper, G.: Finite elastic deformations in liquid-saturated and empty porous solids. *Transport in Porous Media* **34** (1999), 179–191.

[56] Ehlers, W. & Ellsiepen, P.: Zeitschrittgesteuerte Verfahren bei stark gekoppelten Festkörper-Fluid-Problemen. *Zeitschrift für Angewandte Mathematik und Mechanik* **77** (1997), S81–S82.

[57] Ehlers, W. & Ellsiepen, P.: Theoretical and numerical methods in environmental continuum mechanics based on the theory of porous media. In *Environmental Geomechanics*, Schrefler, B. A., ed., Springer-Verlag, Wien 2001, CISM Courses and Lectures No. 417, pp. 1–81.

[58] Ehlers, W., Ellsiepen, P., Blome, P., Mahnkopf, D. & Markert, B.: *Theoretische und numerische Studien zur Lösung von Rand- und Anfangswertproblemen in der Theorie Poröser Medien, Abschlußbericht zum DFG-Forschungsvorhaben Eh 107/6-2*. Bericht aus dem Institut für Mechanik (Bauwesen), Nr. 99-II-1, Universität Stuttgart 1999.

[59] Ehlers, W. & Markert, B.: On the viscoelastic behaviour of fluid-saturated materials. *Granular Matter* **2** (2000), 153–161.

[60] Ehlers, W. & Markert, B.: A linear viscoelastic biphasic model for soft tissues based on the Theory of Porous Media. *ASME Journal of Biomechanical Engineering* **123** (2001), 418–424.

[61] Ehlers, W., Markert, B. & Acartürk, A.: Large strain analysis of 3-d viscoelastic swelling of charged tissues and gels. In *IUTAM Symposium on the Mechanics of Physiochemical and Electromechanical Interactions in Porous Media*, Huyghe, J., ed., Kluwer, Dordrecht 2004, in press.

[62] Ehlers, W. & Müllerschön, H.: Stress-strain behaviour of cohesionless soils: Experiments, theory and numerical computations. In *Application of Numerical Methods to Geotechnical Problems*, Cividini, A., ed., Springer-Verlag, Wien 1998, CISM Courses and Lectures No. 397, pp. 675–684.

[63] Ehlers, W. & Volk, W.: On theoretical and numerical methods in the theory of porous media based on polar and non-polar elasto-plastic solid materials. *International Journal of Solids and Structures* **35** (1998), 4597–4617.

[64] Eipper, G.: *Theorie und Numerik finiter elastischer Deformationen in fluidgesättigten porösen Medien*. Dissertation, Bericht Nr. II-1 aus dem Institut für Mechanik (Bauwesen), Universität Stuttgart 1998.

[65] Ellsiepen, P.: *Zeit- und ortsadaptive Verfahren angewandt auf Mehrphasenprobleme poröser Medien*. Dissertation, Bericht Nr. II-3 aus dem Institut für Mechanik (Bauwesen), Universität Stuttgart 1999.

[66] Ericksen, J. L.: Tensor fields. In *Handbuch der Physik*, Flügge, S., ed., Springer-Verlag, Berlin 1960, vol. III/1, pp. 794–858.

[67] Findley, W. N., Lai, J. S. & Onaran, K.: *Creep and Relaxation of Nonlinear Viscoelastic Materials: With an Introduction to Linear Viscoelasticity*. North-Holland, Amsterdam 1976.

[68] Fletcher, R.: *Practical Methods of Optimization*. John Wiley & Sons, Chichester 1987.

[69] Forchheimer, P.: Wasserbewegung durch Boden. *Zeitschrift des Vereins Deutscher Ingenieure* **50** (1901), 1781–1788.

[70] Fung, Y. C.: Stress-strain-history relations of soft tissues in simple elongation. In *Biomechanics: Its Foundations and Objectives*, Fung, Y. C., Perrone, N. & Anliker, M., eds., Prentice-Hall, Englewood Cliffs, New Jersey 1972, pp. 181–208.

[71] Fung, Y. C.: Bio-viscoelastic solids. In *Biomechanics: Mechanical Properties of Living Tissues*, Fung, Y. C., ed., Springer-Verlag, New York 1981, pp. 106–260.

[72] Gibson, L. J. & Ashby, F.: *Cellular Solids: Structure and Properties*. Cambridge University Press 1997, 2nd edn.

[73] Gibson, R. E., England, G. L. & Hussey, M. J. L.: The theory of one-dimensional consolidation of saturated clays. *Géotechnique* **17** (1967), 261–273.

[74] Green, A. E. & Naghdi, P. M.: Some remarks on elastic-plastic deformation at finite strain. *International Journal of Engineering Sciences* **9** (1971), 1219–1229.

[75] Green, A. E. & Zerna, W.: *Theoretical Elasticity*. Oxford University Press 1968, 2nd edn.

[76] Green, M. S. & Tobolsky, A. V.: A new approach to the theory of relaxing polymeric media. *Journal of Chemical Physics* **14** (1946), 80–92.

[77] Gresho, P. M. & Sani, R. L.: *Incompressible Flow and the Finite Element Method, Volume Two*. John Wiley & Sons, Chichester 2000, second corrected reprint of 1998.

[78] Gurtin, M. E. & Sternberg, E.: On the linear theory of viscoelasticity. *Archives for Rational Mechanics and Analysis* **11** (1962), 291–356.

[79] Hairer, E. & Wanner, G.: *Solving Ordinary Differential Equations, Vol. 2: Stiff and Differential-Algebraic Problems*. Springer-Verlag, Berlin 1991.

[80] Hartmann, S.: Computation in finite strain viscoelasticity: Finite elements based on the interpretation as differential-algebraic equations. *Computer Methods in Applied Mechanics and Engineering* **191** (2002), 1439–1470.

[81] Hartmann, S.: Computational aspects of the symmetric eigenvalue problem of second order tensors. *Technische Mechanik* **23** (2003), 283–294.

[82] Hartmann, S., Haupt, P. & Tschöpe, T.: Parameter identification with a direct search method using finite elements. In *Constitutive Models for Rubber II*, Besdo, D., Schuster, R. H. & Ihlemann, J., eds., Balkema, Lisse 2001, pp. 249–256.

[83] Hartmann, S. & Neff, P.: Polyconvexity of generalized polynomial-type hyperelastic strain energy functions for near-incompressibility. *International Journal of Solids and Structures* **40** (2003), 2767–2791.

[84] Hassanizadeh, S. M. & Gray, W. G.: General conservation equations for multiphase-systems: 2. mass, momenta, energy and entropy equations. *Advances in Water Resources* **2** (1979), 191–203.

[85] Haupt, P.: On the concept of an intermediate configuration and its application to a representation of viscoelastic-plastic material behavior. *International Journal of Plasticity* **1** (1985), 303–316.

[86] Haupt, P.: Foundation of continuum mechanics. In *Continuum Mechanics in Environmental Sciences and Geophysics*, Hutter, K., ed., Springer-Verlag, Wien 1993, CISM Courses and Lectures No. 337, pp. 1–77.

[87] Haupt, P.: *Continuum Mechanics and Theory of Materials*. Springer-Verlag, Berlin 2000.

[88] Haupt, P. & Tsakmakis, Ch.: On the application of dual variables in continuum mechanics. *Journal of Continuum Mechanics and Thermodynamics* **1** (1985), 165–196.

[89] Hilyard, N. C. (ed.): *Mechanics of Cellular Plastics*. Macmillan Publishing Co., New York 1982.

[90] Hilyard, N. C. & Cunningham, A. (eds.): *Low Density Cellular Plastics: Physical Basis of Behaviour*. Chapman & Hall, London 1994.

[91] Holmes, M. H. & Mow, V. C.: The nonlinear characteristics of soft gels and hydrated connective tissues in ultrafiltration. *Journal of Biomechanics* **23** (1990), 1145–1156.

[92] Holzapfel, G. A.: On large strain viscoelasticity: Continuum formulation and finite element applications to elastomeric structures. *International Journal of Numerical Methods in Engineering* **39** (1996), 3903–3926.

[93] Holzapfel, G. A.: *Nonlinear Solid Mechanics: A Continuum Approach for Engineering*. John Wiley & Sons, Chichester 2000.

[94] Holzapfel, G. A. & Simo, J. C.: A new viscoelastic constitutive model for continuous media at finite thermomechanical changes. *International Journal of Solids and Structures* **33** (1996), 3019–3034.

[95] Huber, N. & Tsakmakis, Ch.: Finite deformation viscoelasticity laws. *Mechanics of Materials* **32** (2000), 1–18.

[96] Hughes, T. J. R.: *The Finite Element Method*. Prentice-Hall, London 1987.

[97] Hughes, T. J. R. & Pister, K. S.: Consistent linearization in mechanics of solids and structures. *Computers and Structures* **8** (1978), 391–397.

[98] Hutter, K. & Jöhnk, K.: *Continuum Methods of Physical Modeling*. Springer-Verlag, Berlin 2004.

[99] Kaliske, M. & Rothert, H.: Formulation and implementation of three-dimensional viscoelasticity at small and finite strains. *Computational Mechanics* **19** (1997), 228–239.

[100] Klar, O. & Ehlers, W.: Experimental investigations on polymeric foams. *Proceedings in Applied Mathematics and Mechanics* **4** (2005), 402–403.

[101] Kleiber, M.: Kinematics of deformation processes in materials subjected to finite elastic-plastic strains. *International Journal of Engineering Sciences* **13** (1975), 513–525.

[102] Knupp, P. M. & Lage, J. L.: Generalization of the Forchheimer-extended Darcy flow model to the tensor permeability case via a variational principle. *Journal of Fluid Mechanics* **299** (1995), 97–104.

[103] Kocks, U. F., Thomé, C. N. & Wenk, H. R.: *Texture and Anisotropy. Preferred Orientations in Polycrystals and their Effect on Materials Properties*. Cambridge University Press 1998.

[104] Kröner, E.: Allgemeine Kontinuumstheorie der Versetzungen und Eigenspannungen. *Archives for Rational Mechanics and Analysis* **4** (1960), 273–334.

[105] Lai, W. M. & Mow, V. C.: Drag-induced compression of articular cartilage during a permeation experiment. *Biorheology* **17** (1980), 111–123.

[106] Lambrecht, M.: *Theorie und Numerik von Materialinstabilitäten elastoplastischer Festkörper auf der Grundlage inkrementeller Variationsformulierungen*. Dissertation, Bericht Nr. I-8 aus dem Institut für Mechanik (Bauwesen), Universität Stuttgart 2002.

[107] Laroussi, M., Sab, K. & Alaoui, A.: Foam mechanics: Nonlinear response of an elastic 3d-periodic microstructure. *International Journal of Solids and Structures* **39** (2002), 3599–3623.

[108] Lee, E. H.: Elastic-plastic deformation at finite strains. *Journal of Applied Mechanics* **36** (1969), 1–6.

[109] Lewis, R. W. & Schrefler, B. A.: *The Finite Element Method in the Static and Dynamic Deformation and Consolidation of Porous Media*. John Wiley & Sons, Chichester 1998, 2nd edn.

[110] Li, X., Zienkiewicz, O. C. & Xie, Y. M.: A numerical model for immiscible two-phase fluid flow in a porous medium and its time domain solution. *International Journal of Numerical Methods in Engineering* **30** (1990), 1195–1212.

[111] Lion, A.: A physically based method to represent the thermomechanical behaviour of elastomers. *Acta Mechanica* **123** (1997), 1–25.

[112] Lion, A.: Thixotropic behaviour of rubber under dynamic loading histories: Experiments and theory. *Journal of the Mechanics and Physics of Solids* **46** (1998), 895–930.

[113] Liu, I.-S.: Method of Lagrange multipliers for exploitation of the entropy principle. *Archives for Rational Mechanics and Analysis* **46** (1972), 131–148.

[114] Liu, I.-S. & Müller, I.: Thermodynamics of mixtures of fluids. In *Rational Thermodynamics*, Truesdell, C., ed., Springer-Verlag, New York 1984, 2nd edn., pp. 264–285.

[115] Lubliner, J.: On the structure of the rate equations of materials with internal variables. *Acta Mechanica* **17** (1973), 109–119.

[116] Lubliner, J.: A model of rubber viscoelasticity. *Mechanics Research Communications* **12** (1985), 93–99.

[117] Luenberger, D. G.: *Linear and Nonlinear Programming*. Addison-Wesley, Massachusetts 1984.

[118] Mahnkopf, D.: *Lokalisierung fluidgesättigter poröser Festkörper bei finiten elastoplastischen Deformationen*. Dissertation, Bericht Nr. II-5 aus dem Institut für Mechanik (Bauwesen), Universität Stuttgart 2000.

[119] Mak, A. F.: The apparent viscoelastic behaviour of articular cartilage – the contributions from the intrinsic matrix viscoelasticity and interstitial fluid flows. *ASME Journal of Biomechanical Engineering* **108** (1986), 123–130.

[120] Marsden, J. E. & Hughes, T. J. R.: *Mathematical Foundations of Elasticity*. Dover Publications 1994, reprint of Prentice-Hall, 1983.

[121] Miehe, C.: Aspects of the formulation and finite element implementation of large strain isotropic elasticity. *International Journal of Numerical Methods in Engineering* **37** (1994), 1981–2004.

[122] Miehe, C.: A constitutive frame of elastoplasticity at large strains based on the notion of a plastic metric. *International Journal of Solids and Structures* **35** (1998), 3859–3897.

[123] Miehe, C.: A formulation of finite elastoplasticity based on dual co- and contravariant eigenvector triads normalized with respect to a plastic metric. *Computer Methods in Applied Mechanics and Engineering* **159** (1998), 223–260.

[124] Miehe, C. & Keck, J.: Superimposed finite elastic-viscoelastic-plastoelastic stress response with damage in filled rubbery polymers. Experiments, modelling and algorithmic implementation. *Journal of the Mechanics and Physics of Solids* **48** (2000), 323–365.

[125] Mooney, M.: A theory of large elastic deformation. *Journal of Applied Physics* **11** (1940), 582–592.

[126] Morman, K. N.: The generalized strain measure with application to nonhomogeneous deformations in rubber-like solids. *Journal of Applied Mechanics* **53** (1986), 726–728.

[127] Morrey, C. B.: Quasi-convexity and the lower semicontinuity of multiple integrals. *Pacific Journal of Mathematics* **2** (1952), 25–53.

[128] Mow, V. C., Lai, W. M. & Holmes, M. H.: Advanced theoretical and experimental techniques in cartilage research. In *Biomechanics: Principles and Applications*, Huiskes, R., Campen, D. V. & Wijn, J. D., eds., Martinus Nijhoff Publishers, The Hague 1982, pp. 47–74.

[129] Mullins, L.: Effect of stretching on the properties of rubber. *Journal of Rubber Research* **16** (1947), 275–289.

[130] Muskat, M.: *The flow of homogeneous fluids through porous media*. McGraw-Hill, New York 1937.

[131] Nelder, J. A. & Mead, R.: A simplex method for function minimization. *The Computer Journal* **7** (1965), 308–313.

[132] Nocedal, J. & Wright, S. J.: *Numerical Optimization*. Springer-Verlag, Wien 1999.

[133] Noll, W.: On the continuity of the solid and fluid states. *Journal of Rational Mechanics and Analysis* **4** (1955), 3–81.

[134] Noll, W.: A mathematical theory of the mechanical behavior of continuous media. *Archives for Rational Mechanics and Analysis* **2** (1958), 197–226.

[135] Ogden, R. W.: Large deformation isotropic elasticity – On the correlation of theory and experiment for compressible rubberlike solids. In *Proceedings of the Royal Society of London Series A*, 1972, vol. 328, pp. 323–338.

[136] Ogden, R. W.: Large deformation isotropic elasticity – On the correlation of theory and experiment for incompressible rubberlike solids. In *Proceedings of the Royal Society of London Series A*, 1972, vol. 326, pp. 565–584.

[137] Ogden, R. W.: Inequalities associated with the inversion of elastic stress-deformation relations and their implications. *Mathematical Proceedings of the Cambridge Philosophical Society* **81** (1977), 313–324.

[138] Ogden, R. W.: Elastic deformations of rubberlike solids. In *Mechanics of Solids*, Hopkins, H. G. & Sewell, M. J., eds., Pergamon Press 1982, pp. 499–537, the Rodney Hill 60th Anniversary Volume.

[139] Ogden, R. W.: *Nonlinear elastic deformations*. Ellis Harwood Ltd., Chichester 1984.

[140] Oldroyd, J. G.: On the formulation of rheological equations of state. In *Proceedings of the Royal Society of London Series A*, 1950, vol. 200, pp. 523–541.

[141] Papastavridis, J. G.: *Tensor calculus and analytical dynamics*. CRC Press LLC, Boca Raton 1999.

[142] Pastor, M., Li, T., Liu, X., Zienkiewicz, O. C. & Quecedo, M.: A fractional step algorithm allowing equal order of interpolation for coupled analysis of saturated soil problems. *Mechanics of Cohesive-Frictional Materials* **5** (2000), 511–534.

[143] Powell, M. J. D.: A direct search optimization method that models the objective and constraint functions by linear interpolation. In *Advances in Optimization and Numerical Analysis*, Gomez, S. & Hennart, J. P., eds., Kluwer Academic Publishers, Dordrecht 1994, pp. 51–67.

[144] Powell, M. J. D.: Direct search algorithms for optimization calculations. *Acta Numerica* **7** (1998), 287–336.

[145] Powell, M. J. D.: On trust region methods for unconstrained minimization without derivatives. *Mathematical Programming* **97** (2003), 605–623.

[146] Prandtl, L.: *Strömungslehre*. Friedrich Vieweg & Sohn, Braunschweig 1965.

[147] Press, W. H., Teukolsky, S. A., Vetterling, W. T. & Flannery, B. P.: *Numerical Recipes in C*. Cambridge University Press 1999, 2nd edn., corrected reprint of 1992.

[148] Prevost, J. H.: Consolidation of anelastic porous media. *ASCE Journal of the Engineering Mechanics Division* **107** (1981), 169–186.

[149] Reese, S.: *Thermomechanische Modellierung gummiartiger Polymerstrukturen*. Habilitation, Bericht Nr. F01/4 aus dem Institut für Baumechanik und Numerische Mechanik, Universität Hannover 2001.

[150] Reese, S. & Govindjee, S.: Theoretical and numerical aspects in the thermo-viscoelastic material behaviour of rubber-like polymers. *Mechanics of Time-dependent Materials* **1** (1998), 357–396.

[151] Reese, S. & Govindjee, S.: A theory of finite viscoelasticity and numerical aspects. *International Journal of Solids and Structures* **35** (1998), 3455–3482.

[152] Rivlin, R. S.: Large elastic deformations of isotropic materials. *Proceedings of the Royal Society of London Series A* **241** (1948), 379–397.

[153] Rusch, K. C.: *Dynamic Behaviour of Flexible Open-cell Foams*. Ph. D. Thesis, Engineering, general, University of Akron 1965.

[154] Saad, Y.: *Iterative Methods for Sparse Linear Systems*. SIAM Society for Industrial and Applied Mathematics, Philadelphia 2003, 2nd edn.

[155] Saad, Y. & Schultz, M.: Gmres: A generalized minimal residual algorithm for solving nonsymmetric linear systems. *SIAM Journal on Scientific and Statistical Computing* **7** (1986), 856–869.

[156] Sandhu, R. S. & Wilson, E. L.: Finite-element analysis of seepage in elastic media. *ASCE Journal of the Engineering Mechanics Division* **95** (1969), 641–652.

[157] Schlichting, H.: *Grenzschicht-Theorie*. G. Braun GmbH, Karlsruhe 1965, 5th edn.

[158] Schröder, J.: *Homogenisierungsmethoden der nichtlinearen Kontinuumsmechanik unter Beachtung von Stabilitätsproblemen*. Habilitation, Bericht Nr. I-7 aus dem Institut für Mechanik (Bauwesen), Universität Stuttgart 2000.

[159] Schröder, J. & Neff, P.: Invariant formulation of hyperelastic transverse isotropy based on polyconvex free energy functions. *International Journal of Solids and Structures* **40** (2003), 401–445.

[160] Setton, L. A., Zhu, W. & Mow, V. C.: The biphasic poroviscoelastic behavior of articular cartilage: Role of the surface zone in governing the compressive behavior. *Journal of Biomechanics* **26** (1993), 581–592.

[161] Sidoroff, F.: The geometrical concept of intermediate configuration and elastic-plastic finite strain. *Archives of Mechanics* **25** (1973), 299–308.

[162] Sidoroff, F.: Un modèle viscoélastique non linéaire avec configuration intermédiaire. *Journal de Mécanique* **13** (1974), 679–713.

[163] Šilhavý, M.: *The Mechanics and Thermodynamics of Continuous Media*. Springer-Verlag, Berlin 1997.

[164] Simo, J. C.: On a fully three-dimensional finite-strain viscoelastic damage model: Formulation and computational aspects. *Computer Methods in Applied Mechanics and Engineering* **99** (1987), 153–173.

[165] Simo, J. C. & Hughes, T. J. R.: *Computational Inelasticity*. Springer-Verlag, New York 1998.

[166] Simo, J. C. & Taylor, R. L.: Consistent tangent operators for rate-independent elastoplasticity. *Computer Methods in Applied Mechanics and Engineering* **48** (1985), 101–118.

[167] Skempton, A. W.: Significance of Terzaghi's concept of effective stress (Terzaghi's discovery of effective stress). In *From Theory to Practice in Soil Mechanics*, Bjerrum, L., Casagrande, A., Peck, R. B. & Skempton, A. W., eds., John Wiley & Sons, New York 1960, pp. 42–53.

[168] Spellucci, P.: *Numerische Verfahren der nichlinearen Optimierung*. Birkhäuser, Basel 1993.

[169] Spencer, A. J. M.: Theory of invariants. In *Continuum Physics*, Eringen, A. C., ed., Academic Press, New York 1971, vol. I, pp. 239–353.

[170] Spencer, A. J. M.: The formulation of constitutive equations for anisotropic solids. In *Mechanical Behavior of Anisotropic Solids*, Boehler, J. P., ed., Martinus Nijhoff Publishers, The Haque 1982, pp. 2–26.

[171] Suh, J.-K. & Bai, S.: Finite element formulation of biphasic poroviscoelastic model of articular cartilage. *ASME Journal of Biomechanical Engineering* **120** (1998), 195–201.

[172] Svendsen, B.: A thermodynamic formulation of finite-deformation elastoplasticity with hardening based on the concept of material isomorphism. *International Journal of Plasticity* **14** (1998), 473–488.

[173] le Tallec, P., Rahier, C. & Kaiss, A.: Three-dimensional incompressible viscoelasticity in large strains: Formulation and numerical approximation. *Computer Methods in Applied Mechanics and Engineering* **109** (1993), 133–258.

[174] Taylor, R. L., Pister, K. S. & Goudreau, G. L.: Thermomechanical analysis of viscoelastic solids. *International Journal of Numerical Methods in Engineering* **2** (1970), 45–59.

[175] Terzaghi, K. & Jelinek, R.: *Theoretische Bodenmechanik*. Springer-Verlag, Berlin 1954.

[176] Törnig, W. & Spellucci, P.: *Numerische Mathematik für Ingenieure und Physiker, Band 1*. Springer-Verlag, Berlin 1988, 2nd edn.

[177] Treloar, L. R. G.: *The Physics of Rubber Elasticity*. Clarendon Press, Oxford 1975, 3rd edn.

[178] Truesdell, C.: *A new definition of a fluid, II. The Maxwellian fluid*. US Naval Research Laboratory, Report No. P-3553, § 19 1949.

[179] Truesdell, C.: Thermodynamics of diffusion. In *Rational Thermodynamics*, Truesdell, C., ed., Springer-Verlag, New York 1984, 2nd edn., pp. 219–236.

[180] Truesdell, C. & Noll, W.: In *The Non-linear Field Theories of Mechanics*, Antman, S. S., ed., Springer, Berlin 2004, 3rd edn.

[181] Truesdell, C. & Toupin, R. A.: The classical field theories. In *Handbuch der Physik*, Flügge, S., ed., Springer-Verlag, Berlin 1960, vol. III/1, pp. 226–902.

[182] Tsakmakis, Ch.: *Über inkrementelle Materialgleichungen zur Beschreibung großer inelastischer Deformationen*. Fortschritt-Berichte VDI, Reihe 18, Nr. 36, VDI-Verlag, Düsseldorf 1987.

[183] Tschoegl, N. W.: *The Phenomenological Theory of Linear Viscoelastic Behavior: An Introduction*. Springer-Verlag, New York 1989.

[184] Valanis, K. C.: Internal variable theory. In *Irreversible Thermodynamics of Continous Media*, Valanis, K. C., ed., Springer-Verlag, Wien 1971, CISM Courses and Lectures No. 77.

[185] Valanis, K. C. & Landel, R. F.: The strain-energy function of a hyperelastic material in terms of the extension ratios. *Journal of Applied Physics* **38** (1967), 2997–3002.

[186] Varga, O. H.: *Stress-Strain Behavior of Elastic Materials*. Interscience, New York 1966.

[187] van der Waals, J. D.: *Over de Continuiteit van den Gas – en Vloeistoftoestand*. Leiden 1873, doctoral Dissertation.

[188] Weber, G. & Anand, L.: Finite deformation constitutive equations and a time integration procedure for isotropic, hyperelastic-viscoplastic solids. *Computer Methods in Applied Mechanics and Engineering* (1990), 173–202.

[189] Wieners, C., Ammann, M., Diebels, S. & Ehlers, W.: Parallel 3-d simulations for porous media models in soil mechanics. *Computational Mechanics* **29** (2002), 75–87.

[190] Wieners, C., Ammann, M., Ehlers, W. & Graf, T.: Parallel Krylov methods and the application to 3-d simulations of a triphasic porous media model in soil mechanics. *Computational Mechanics* **36** (2005), 409–420.

[191] Wilkinson, J. H.: *The Algebraic Eigenvalue Problem*. Oxford University Press 1965.

[192] Williams, G. & Watts, D. C.: Non-symmetrical dielectric relaxation behavior arising from a simple empirical decay function. *Transactions of the Faraday Society* **66** (1970), 80–85.

[193] Wineman, A. S. & Rajagopal, K. R.: *Mechanical Response of Polymers: An Introduction*. Cambridge University Press 2000.

[194] Wriggers, P.: *Konsistente Linearisierung in der Kontinuumsmechanik und ihre Anwendung auf die Finite-Elemente-Methode*. Technischer Bericht Nr. F88/4, Forschungs- und Seminarberichte aus dem Bereich der Mechanik der Universität Hannover 1988.

[195] Zhu, H. X., Mills, N. J. & Knott, J. F.: Analysis of high strain compression of open-cell foams having tetrakaidecahedral cells. *Journal of the Mechanics and Physics of Solids* **45** (1997), 1875–1904.

[196] Zienkiewicz, O. C., Chan, A. H. C., Pastor, M., Schrefler, B. A. & Shiomi, T.: *Computational geomechanics with special reference to earthquake engineering*. John Wiley & Sons, Chichester 1999.

[197] Zienkiewicz, O. C. & Codina, R.: A general algorithm for compressible and incompressible flow – Part I. The split, characteristic-based scheme. *International Journal for Numerical Methods in Fluids* **20** (1995), 869–885.

[198] Zienkiewicz, O. C., Rojek, J., Taylor, R. L. & Pastor, M.: Triangles and tetrahedra in explicit dynamic codes for solids. *International Journal of Numerical Methods in Engineering* **43** (1998), 565–583.

[199] Zienkiewicz, O. C. & Taylor, R. L.: *The Finite Element Method. The Basis*, vol. 1. Butterworth Heinemann, Oxford 2000, 5th edn.

[200] Zienkiewicz, O. C. & Taylor, R. L.: *The Finite Element Method. Solid Mechanics*, vol. 2. Butterworth Heinemann, Oxford 2000, 5th edn.

[201] Zienkiewicz, O. C. & Taylor, R. L.: *The Finite Element Method. Fluid Dynamics*, vol. 3. Butterworth Heinemann, Oxford 2000, 5th edn.

A Tensor Calculus

This appendix provides a collection of certain useful rules that allow the concise and easy treatment of tensor operations within the sometimes abstract and lengthy formalisms of tensor calculus. However, for a more comprehensive discussion, the interested reader is encouraged to refer to the textbook of de Boer [17] and the tensor script of our institute, which is available online (Ehlers [52]).

A.1 Tensor Algebra

For the following considerations let $\{\alpha, \beta\} \in \mathbb{R}$ be arbitrary scalars, $\{\mathbf{a}, \mathbf{b}, \mathbf{c}, \mathbf{d}\} \in \mathcal{V}^3$ be arbitrary 3-d vectors and $\{\mathbf{A}, \mathbf{B}, \mathbf{C}, \mathbf{D}\} \in \mathcal{V}^3 \otimes \mathcal{V}^3$ be arbitrary 2nd-order tensors.

A.1.1 Collected Rules

The scalar product of tensors (inner product):

$$\begin{aligned}
\mathbf{A} \cdot \mathbf{B} &= \mathbf{B} \cdot \mathbf{A} && : \text{commutative law} \\
\mathbf{A} \cdot (\mathbf{B} + \mathbf{C}) &= \mathbf{A} \cdot \mathbf{B} + \mathbf{A} \cdot \mathbf{C} && : \text{distributive law} \\
(\alpha\, \mathbf{A}) \cdot \mathbf{B} &= \mathbf{A} \cdot (\alpha\, \mathbf{B}) = \alpha\, (\mathbf{A} \cdot \mathbf{B}) && : \text{associative law} \\
\mathbf{A} \cdot \mathbf{B} &= 0 \quad \forall\, \mathbf{A} \text{ if } \mathbf{B} \equiv \mathbf{0} \\
\mathbf{A} \cdot \mathbf{A} &> 0 \quad \forall\, \mathbf{A} \neq \mathbf{0} \\
\mathbf{A} \cdot (\mathbf{a} \otimes \mathbf{b}) &= \mathbf{a} \cdot \mathbf{A}\, \mathbf{b}
\end{aligned} \tag{A.1}$$

The tensor product of tensors:

$$\begin{aligned}
\mathbf{A}\, \mathbf{B} &\neq \mathbf{B}\, \mathbf{A} \\
(\mathbf{A}\, \mathbf{B})\, \mathbf{C} &= \mathbf{A}\, (\mathbf{B}\, \mathbf{C}) && : \text{associative law} \\
\mathbf{A}\, (\mathbf{B} + \mathbf{C}) &= \mathbf{A}\, \mathbf{B} + \mathbf{A}\, \mathbf{C} && : \text{distributive law} \\
(\mathbf{A} + \mathbf{B})\, \mathbf{C} &= \mathbf{A}\, \mathbf{C} + \mathbf{B}\, \mathbf{C} && : \text{distributive law} \\
\alpha\, (\mathbf{A}\, \mathbf{B}) &= (\alpha\, \mathbf{A})\, \mathbf{B} = \mathbf{A}\, (\alpha\, \mathbf{B}) && : \text{associative law} \\
(\mathbf{A}\, \mathbf{B})\, \mathbf{v} &= \mathbf{A}\, (\mathbf{B}\, \mathbf{v}) \\
\mathbf{I}\, \mathbf{T} &= \mathbf{T}\, \mathbf{I} = \mathbf{T} && : \mathbf{I} \ : \text{identity element} \\
\mathbf{0}\, \mathbf{T} &= \mathbf{T}\, \mathbf{0} = \mathbf{0} && : \mathbf{0} \ : \text{zero element} \\
(\mathbf{a} \otimes \mathbf{b})\, (\mathbf{c} \otimes \mathbf{d}) &= (\mathbf{b} \cdot \mathbf{c})\, \mathbf{a} \otimes \mathbf{d}
\end{aligned} \tag{A.2}$$

The transposed tensor:

$$\begin{aligned}
\mathbf{w}\cdot(\mathbf{A}\,\mathbf{u}) &= (\mathbf{A}^T\,\mathbf{w})\cdot\mathbf{u}\\
(\mathbf{A}+\mathbf{B})^T &= \mathbf{A}^T+\mathbf{B}^T\\
(\alpha\,\mathbf{A})^T &= \alpha\,\mathbf{A}^T\\
(\mathbf{A}\,\mathbf{B})^T &= \mathbf{B}^T\,\mathbf{A}^T\\
(\mathbf{a}\otimes\mathbf{b})^T &= \mathbf{b}\otimes\mathbf{a}
\end{aligned} \tag{A.3}$$

The outer tensor product of tensors (double cross product):

$$\begin{aligned}
\mathbf{A}\circledast\mathbf{B} &= \mathbf{B}\circledast\mathbf{A} \quad \in \mathcal{V}^3\otimes\mathcal{V}^3\\
(\mathbf{A}\circledast\mathbf{B})^T &= \mathbf{A}^T\circledast\mathbf{B}^T\\
(\mathbf{A}\circledast\mathbf{B})\,(\mathbf{C}\circledast\mathbf{D}) &= (\mathbf{A}\,\mathbf{C}\circledast\mathbf{B}\,\mathbf{D})+(\mathbf{A}\,\mathbf{D}\circledast\mathbf{B}\,\mathbf{C})\\
(\mathbf{I}\circledast\mathbf{I}) &= 2\,\mathbf{I}\\
(\mathbf{A}\circledast\mathbf{B})\cdot\mathbf{C} &= (\mathbf{B}\circledast\mathbf{C})\cdot\mathbf{A} = (\mathbf{C}\circledast\mathbf{A})\cdot\mathbf{B}\\
(\mathbf{a}\otimes\mathbf{b})\circledast(\mathbf{c}\otimes\mathbf{d}) &= (\mathbf{a}\times\mathbf{c})\otimes(\mathbf{b}\times\mathbf{d})
\end{aligned} \tag{A.4}$$

The inverse tensor:

$$\begin{aligned}
&\mathbf{A}^{-1}\text{ exists if }\det\mathbf{A}\neq 0\\
&\mathbf{A}^{-1} = (\det\mathbf{A})^{-1}\operatorname{adj}\mathbf{A} \qquad :\operatorname{adj}\mathbf{A}\ :\text{adjoint}\\
&\mathbf{A}^{-1} = (\det\mathbf{A})^{-1}\operatorname{cof}\mathbf{A}^T \qquad :\operatorname{cof}\mathbf{A}\ :\text{cofactor}\\
&\mathbf{A}\,\mathbf{A}^{-1} = \mathbf{A}^{-1}\,\mathbf{A} = \mathbf{I}\\
&(\mathbf{A}^{-1})^T = (\mathbf{A}^T)^{-1} =: \mathbf{A}^{T-1}\\
&(\mathbf{A}\,\mathbf{B})^{-1} = \mathbf{B}^{-1}\,\mathbf{A}^{-1}
\end{aligned} \tag{A.5}$$

Rules for the adjoint tensor, the cofactor tensor, the determinant, and the inverse tensor:

$$\begin{aligned}
\operatorname{adj}\mathbf{A} &:= \operatorname{cof}\mathbf{A}^T\\
(\operatorname{cof}\mathbf{A})^T &= \operatorname{cof}(\mathbf{A}^T)\\
(\operatorname{adj}\mathbf{A})^T &= \operatorname{adj}(\mathbf{A}^T)\\
\operatorname{adj}\mathbf{A} &= (\det\mathbf{A})\,\mathbf{A}^{-1}\\
\operatorname{cof}\mathbf{A} &= (\det\mathbf{A})\,\mathbf{A}^{T-1}\\
\operatorname{adj}(\mathbf{A}\,\mathbf{B}) &= \operatorname{adj}\mathbf{A}\,\operatorname{adj}\mathbf{B}\\
\det(\mathbf{A}\,\mathbf{B}) &= \det\mathbf{A}\,\det\mathbf{B}\\
\det(\alpha\,\mathbf{A}) &= \alpha^3\det\mathbf{A}\\
\det\mathbf{I} &= 1\\
\det\mathbf{A}^T &= \det\mathbf{A}\\
\det(\operatorname{adj}\mathbf{A}) &= \det(\operatorname{cof}\mathbf{A}) = (\det\mathbf{A})^2\\
\det\mathbf{A}^{-1} &= (\det\mathbf{A})^{-1}\\
\det(\mathbf{A}+\mathbf{B}) &= \det\mathbf{A}+\operatorname{cof}\mathbf{A}\cdot\mathbf{B}+\mathbf{A}\cdot\operatorname{cof}\mathbf{B}+\det\mathbf{B}
\end{aligned} \tag{A.6}$$

The trace operator:

$$\begin{aligned}
\operatorname{tr}\mathbf{A} &:= \mathbf{A}\cdot\mathbf{I}\\
\operatorname{tr}(\alpha\,\mathbf{A}) &= \alpha\operatorname{tr}\mathbf{A}\\
\operatorname{tr}(\mathbf{a}\otimes\mathbf{b}) &= \mathbf{a}\cdot\mathbf{b}\\
\operatorname{tr}\mathbf{A}^T &= \operatorname{tr}\mathbf{A}\\
\operatorname{tr}(\mathbf{A}\,\mathbf{B}) &= \operatorname{tr}(\mathbf{B}\,\mathbf{A})\\
(\mathbf{A}\,\mathbf{B})\cdot\mathbf{I} &= \mathbf{A}^T\cdot\mathbf{B} = \mathbf{A}\cdot\mathbf{B}^T\\
\operatorname{tr}(\mathbf{A}\,\mathbf{B}\,\mathbf{C}) &= \operatorname{tr}(\mathbf{B}\,\mathbf{C}\,\mathbf{A}) = \operatorname{tr}(\mathbf{C}\,\mathbf{A}\,\mathbf{B})
\end{aligned} \tag{A.7}$$

A.1.2 Higher-order Tensor Operations

The 4th-order fundamental tensors:

$$\begin{aligned}
\overset{4}{\mathbf{I}} &:= (\mathbf{I}\otimes\mathbf{I})^{\overset{23}{T}} && : \text{identical map}\\
\overset{4}{\mathbf{I}}_T &:= (\mathbf{I}\otimes\mathbf{I})^{\overset{24}{T}} && : \text{transposing map}\\
\overset{4}{\mathbf{I}}_{\mathrm{tr}} &:= \mathbf{I}\otimes\mathbf{I} && : \text{tracing map}
\end{aligned} \tag{A.8}$$

Properties of simple 4th-order tensors:

$$\begin{aligned}
\overset{4}{\mathbf{A}} &:= (\mathbf{A}\otimes\mathbf{B})^{\overset{23}{T}} = (\mathbf{B}^T\otimes\mathbf{A}^T)^{\overset{14}{T}}\\
\overset{4}{\mathbf{A}}^T &= [(\mathbf{A}\otimes\mathbf{B})^{\overset{23}{T}}]^T = (\mathbf{A}^T\otimes\mathbf{B}^T)^{\overset{23}{T}}\\
\overset{4}{\mathbf{A}}^{-1} &= [(\mathbf{A}\otimes\mathbf{B})^{\overset{23}{T}}]^{-1} = (\mathbf{A}^{-1}\otimes\mathbf{B}^{-1})^{\overset{23}{T}}\\
\overset{4}{\mathbf{B}} &:= (\mathbf{A}\otimes\mathbf{B})^{\overset{24}{T}} = [(\mathbf{A}\otimes\mathbf{B})^{\overset{13}{T}}]^T\\
\overset{4}{\mathbf{B}}^T &= [(\mathbf{A}\otimes\mathbf{B})^{\overset{24}{T}}]^T = (\mathbf{B}\otimes\mathbf{A})^{\overset{24}{T}}\\
\overset{4}{\mathbf{B}}^{-1} &= [(\mathbf{A}\otimes\mathbf{B})^{\overset{24}{T}}]^{-1} = (\mathbf{B}^{T-1}\otimes\mathbf{A}^{T-1})^{\overset{24}{T}}
\end{aligned} \tag{A.9}$$

A selection of related rules:

$$\begin{aligned}
(\overset{4}{\bullet})^T &:= [(\overset{4}{\bullet})^{\overset{13}{T}}]^{\overset{24}{T}}\\
(\mathbf{A}\otimes\mathbf{B})^{\overset{23}{T}}(\mathbf{C}\otimes\mathbf{D})^{\overset{23}{T}} &= (\mathbf{A}\,\mathbf{C}\otimes\mathbf{B}\,\mathbf{D})^{\overset{23}{T}}\\
(\mathbf{A}\otimes\mathbf{B})^{\overset{23}{T}}(\mathbf{C}\otimes\mathbf{D}) &= (\mathbf{A}\,\mathbf{C}\,\mathbf{B}^T\otimes\mathbf{D})\\
(\mathbf{A}\otimes\mathbf{B})\,(\mathbf{C}\otimes\mathbf{D})^{\overset{23}{T}} &= (\mathbf{A}\otimes\mathbf{C}^T\mathbf{B}\,\mathbf{D})\\
(\mathbf{A}\otimes\mathbf{B})^{\overset{23}{T}}\mathbf{C} &= \mathbf{A}\,\mathbf{C}\,\mathbf{B}^T\\
(\mathbf{A}\otimes\mathbf{B})^{\overset{23}{T}}\mathbf{c} &= [\mathbf{A}\otimes(\mathbf{B}\,\mathbf{c})]^{\overset{23}{T}}
\end{aligned} \tag{A.10}$$

$$
\begin{aligned}
(\mathbf{A}\otimes\mathbf{B})^{\overset{24}{T}}(\mathbf{C}\otimes\mathbf{D})^{\overset{24}{T}} &= (\mathbf{A}\,\mathbf{D}^T\otimes\mathbf{B}^T\mathbf{C})^{\overset{23}{T}}\\
(\mathbf{A}\otimes\mathbf{B})^{\overset{23}{T}}(\mathbf{C}\otimes\mathbf{D})^{\overset{24}{T}} &= (\mathbf{A}\,\mathbf{C}\otimes\mathbf{D}\,\mathbf{B}^T)^{\overset{24}{T}}\\
(\mathbf{A}\otimes\mathbf{B})^{\overset{24}{T}}(\mathbf{C}\otimes\mathbf{D})^{\overset{23}{T}} &= (\mathbf{A}\,\mathbf{D}\otimes\mathbf{C}^T\mathbf{B})^{\overset{24}{T}}\\
(\mathbf{A}\otimes\mathbf{B})^{\overset{24}{T}}(\mathbf{C}\otimes\mathbf{D}) &= (\mathbf{A}\,\mathbf{C}^T\mathbf{B}\otimes\mathbf{D})\\
(\mathbf{A}\otimes\mathbf{B})\,(\mathbf{C}\otimes\mathbf{D})^{\overset{24}{T}} &= (\mathbf{A}\otimes\mathbf{D}\,\mathbf{B}^T\mathbf{C})\\
(\mathbf{A}\otimes\mathbf{B})^{\overset{24}{T}}\mathbf{C} &= \mathbf{A}\,\mathbf{C}^T\mathbf{B}
\end{aligned}
\tag{A.11}
$$

A.2 Tensor Analysis

Derivative of products of functions (product rule):

$$
\begin{aligned}
(\mathbf{a}\otimes\mathbf{b})' &= \mathbf{a}'\otimes\mathbf{b}+\mathbf{a}\otimes\mathbf{b}'\\
(\mathbf{A}\,\mathbf{B})' &= \mathbf{A}'\,\mathbf{B}+\mathbf{A}\,\mathbf{B}'\\
(\mathbf{A}^{-1})' &= -\mathbf{A}^{-1}\,\mathbf{A}'\,\mathbf{A}^{-1}
\end{aligned}
\tag{A.12}
$$

A selection of useful derivatives:

$$
\begin{aligned}
\frac{\partial\mathbf{A}}{\partial\mathbf{A}} &= (\mathbf{I}\otimes\mathbf{I})^{\overset{23}{T}} = \overset{4}{\mathbf{I}}\\
\frac{\partial\mathbf{A}^T}{\partial\mathbf{A}} &= (\mathbf{I}\otimes\mathbf{I})^{\overset{24}{T}} = \overset{4}{\mathbf{I}}_T\\
\frac{\partial\mathbf{A}^{-1}}{\partial\mathbf{A}} &= -(\mathbf{A}^{-1}\otimes\mathbf{A}^{T-1})^{\overset{23}{T}}\\
\frac{\partial I_{\mathbf{A}}}{\partial\mathbf{A}} &= \frac{\partial\operatorname{tr}\mathbf{A}}{\partial\mathbf{A}} = \mathbf{I}\\
\frac{\partial II_{\mathbf{A}}}{\partial\mathbf{A}} &= \frac{\partial\operatorname{tr}(\operatorname{cof}\mathbf{A})}{\partial\mathbf{A}} = \mathbf{A}\,\overline{\times}\,\mathbf{I}\\
\frac{\partial III_{\mathbf{A}}}{\partial\mathbf{A}} &= \frac{\partial\det\mathbf{A}}{\partial\mathbf{A}} = \operatorname{cof}\mathbf{A}\\
\frac{\partial(\mathbf{A}\cdot\mathbf{I})\,\mathbf{I}}{\partial\mathbf{A}} &= \mathbf{I}\otimes\mathbf{I} = \overset{4}{\mathbf{I}}_{\mathrm{tr}}\\
\frac{\partial\operatorname{cof}\mathbf{A}}{\partial\mathbf{A}} &= \det\mathbf{A}\,[(\mathbf{A}^{T-1}\otimes\mathbf{A}^{T-1})-(\mathbf{A}^{T-1}\otimes\mathbf{A}^{T-1})^{\overset{24}{T}}]\\
\frac{\partial\overset{\mathrm{A}}{\mathbf{t}}(\mathbf{A})}{\partial\mathbf{A}} &= -\tfrac{1}{2}\overset{3}{\mathbf{E}}
\end{aligned}
\tag{A.13}
$$

$$
\begin{aligned}
\frac{\partial(\mathbf{A}\,\mathbf{B})}{\partial\mathbf{B}} &= (\mathbf{A}\otimes\mathbf{I})^{\overset{23}{T}}\\
\frac{\partial(\mathbf{A}\,\mathbf{B})}{\partial\mathbf{A}} &= (\mathbf{I}\otimes\mathbf{B}^T)^{\overset{23}{T}}\\
\frac{\partial(\mathbf{A}\,\mathbf{A})}{\partial\mathbf{A}} &= (\mathbf{A}\otimes\mathbf{I})^{\overset{23}{T}} + (\mathbf{I}\otimes\mathbf{A}^T)^{\overset{23}{T}}\\
\frac{\partial(\mathbf{A}^T\mathbf{A})}{\partial\mathbf{A}} &= (\mathbf{A}^T\otimes\mathbf{I})^{\overset{23}{T}} + (\mathbf{I}\otimes\mathbf{A})^{\overset{24}{T}}\\
\frac{\partial(\mathbf{A}\,\mathbf{A}^T)}{\partial\mathbf{A}} &= (\mathbf{A}\otimes\mathbf{I})^{\overset{24}{T}} + (\mathbf{I}\otimes\mathbf{A})^{\overset{23}{T}}\\
\frac{\partial(\mathbf{A}\,\mathbf{B}\,\mathbf{C})}{\partial\mathbf{B}} &= (\mathbf{A}\otimes\mathbf{C}^T)^{\overset{23}{T}}
\end{aligned}
\tag{A.14}
$$

Derivatives with $\alpha, \beta, \mathbf{a}, \mathbf{b}, \mathbf{A}, \mathbf{B}$ as tensor functions of $\mathbf{C}$:

$$
\begin{aligned}
\frac{\partial(\alpha\,\beta)}{\partial\mathbf{C}} &= \alpha\,\frac{\partial\beta}{\partial\mathbf{C}} + \beta\,\frac{\partial\alpha}{\partial\mathbf{C}}\\
\frac{\partial(\alpha\,\mathbf{b})}{\partial\mathbf{C}} &= \mathbf{b}\otimes\frac{\partial\alpha}{\partial\mathbf{C}} + \alpha\,\frac{\partial\mathbf{b}}{\partial\mathbf{C}}\\
\frac{\partial(\alpha\,\mathbf{A})}{\partial\mathbf{C}} &= \mathbf{A}\otimes\frac{\partial\alpha}{\partial\mathbf{C}} + \alpha\,\frac{\partial\mathbf{A}}{\partial\mathbf{C}}\\
\frac{\partial(\mathbf{A}\,\mathbf{b})}{\partial\mathbf{C}} &= \left[\left(\frac{\partial\mathbf{A}}{\partial\mathbf{C}}\right)^{\overset{24}{T}}\right]^{\overset{23}{T}}\mathbf{b} + \left[\mathbf{A}\,\frac{\partial\mathbf{b}}{\partial\mathbf{C}}\right]^{\underline{3}}\\
\frac{\partial(\mathbf{a}\cdot\mathbf{b})}{\partial\mathbf{C}} &= \left[\left(\frac{\partial\mathbf{a}}{\partial\mathbf{C}}\right)^{\overset{13}{T}}\mathbf{b}\right]^T + \left[\left(\frac{\partial\mathbf{b}}{\partial\mathbf{C}}\right)^{\overset{13}{T}}\mathbf{a}\right]^T\\
\frac{\partial(\mathbf{A}\cdot\mathbf{B})}{\partial\mathbf{C}} &= \left(\frac{\partial\mathbf{A}}{\partial\mathbf{C}}\right)^T\mathbf{B} + \left(\frac{\partial\mathbf{B}}{\partial\mathbf{C}}\right)^T\mathbf{A}\\
\frac{\partial(\mathbf{A}\,\mathbf{B})}{\partial\mathbf{C}} &= \left(\left[\left(\frac{\partial\mathbf{A}}{\partial\mathbf{C}}\right)^{\overset{24}{T}}\mathbf{B}\right]^{\underline{4}}\right)^{\overset{24}{T}} + \left(\left[\left(\frac{\partial\mathbf{B}}{\partial\mathbf{C}}\right)^{\overset{14}{T}}\mathbf{A}^T\right]^{\underline{4}}\right)^{\overset{14}{T}}
\end{aligned}
\tag{A.15}
$$

B Kinematical Relations

B.1 Transport properties of strain tensors

Transport properties of contravariant solid strain tensors $(N = 1)$

reference configuration

$$\mathbf{E}_S = \tfrac{1}{2}\left(\mathbf{C}_S - \mathbf{I}\right) = \tfrac{1}{2}\left(a_{kl} - h_{kl}\right)\mathbf{h}^k \otimes \mathbf{h}^l$$
$$\mathbf{E}_{Se} = \tfrac{1}{2}\left(\mathbf{C}_S - \mathbf{C}_{Si}\right) = \tfrac{1}{2}\left(a_{kl} - \widehat{z}_{kl}\right)\mathbf{h}^k \otimes \mathbf{h}^l$$
$$\mathbf{E}_{Si} = \tfrac{1}{2}\left(\mathbf{C}_{Si} - \mathbf{I}\right) = \tfrac{1}{2}\left(\widehat{z}_{kl} - h_{kl}\right)\mathbf{h}^k \otimes \mathbf{h}^l$$

$$\mathbf{E}_S = \mathbf{E}_{Se} + \mathbf{E}_{Si}$$

$\mathbf{F}_{Si}^{T\,-1}(\,\cdot\,)\,\mathbf{F}_{Si}^{-1}$ / $\mathbf{F}_{Si}^{T}(\,\cdot\,)\,\mathbf{F}_{Si}$

$\mathbf{F}_{S}^{T\,-1}(\,\cdot\,)\,\mathbf{F}_{S}^{-1}$ / $\mathbf{F}_{S}^{T}(\,\cdot\,)\,\mathbf{F}_{S}$

intermediate configuration

$$\widehat{\mathbf{\Gamma}}_S = \tfrac{1}{2}\left(\widehat{\mathbf{C}}_{Se} - \widehat{\mathbf{B}}_{Si}^{-1}\right) = \tfrac{1}{2}\left(a_{kl} - h_{kl}\right)\widehat{\mathbf{z}}^k \otimes \widehat{\mathbf{z}}^l$$
$$\widehat{\mathbf{\Gamma}}_{Se} = \tfrac{1}{2}\left(\widehat{\mathbf{C}}_{Se} - \mathbf{I}\right) = \tfrac{1}{2}\left(a_{kl} - \widehat{z}_{kl}\right)\widehat{\mathbf{z}}^k \otimes \widehat{\mathbf{z}}^l$$
$$\widehat{\mathbf{\Gamma}}_{Si} = \tfrac{1}{2}\left(\mathbf{I} - \widehat{\mathbf{B}}_{Si}^{-1}\right) = \tfrac{1}{2}\left(\widehat{z}_{kl} - h_{kl}\right)\widehat{\mathbf{z}}^k \otimes \widehat{\mathbf{z}}^l$$

$$\widehat{\mathbf{\Gamma}}_S = \widehat{\mathbf{\Gamma}}_{Se} + \widehat{\mathbf{\Gamma}}_{Si}$$

(B.1)

current configuration

$$\mathbf{A}_S = \tfrac{1}{2}\left(\mathbf{I} - \mathbf{B}_S^{-1}\right) = \tfrac{1}{2}\left(a_{kl} - h_{kl}\right)\mathbf{a}^k \otimes \mathbf{a}^l$$
$$\mathbf{A}_{Se} = \tfrac{1}{2}\left(\mathbf{I} - \mathbf{B}_{Se}^{-1}\right) = \tfrac{1}{2}\left(a_{kl} - \widehat{z}_{kl}\right)\mathbf{a}^k \otimes \mathbf{a}^l$$
$$\mathbf{A}_{Si} = \tfrac{1}{2}\left(\mathbf{B}_{Se}^{-1} - \mathbf{B}_S^{-1}\right) = \tfrac{1}{2}\left(\widehat{z}_{kl} - h_{kl}\right)\mathbf{a}^k \otimes \mathbf{a}^l$$

$$\mathbf{A}_S = \mathbf{A}_{Se} + \mathbf{A}_{Si}$$

$\mathbf{F}_{Se}^{T\,-1}(\,\cdot\,)\,\mathbf{F}_{Se}^{-1}$ / $\mathbf{F}_{Se}^{T}(\,\cdot\,)\,\mathbf{F}_{Se}$

Transport properties of covariant solid strain tensors $(N = 1)$

reference configuration

$$\overset{\mathrm{R}}{\mathbf{K}}_S = \tfrac{1}{2}\left(\mathbf{I} - \mathbf{C}_S^{-1}\right) = \tfrac{1}{2}\left(h^{kl} - a^{kl}\right)\mathbf{h}_k \otimes \mathbf{h}_l$$
$$\overset{\mathrm{R}}{\mathbf{K}}_{Se} = \tfrac{1}{2}\left(\mathbf{C}_{Si}^{-1} - \mathbf{C}_S^{-1}\right) = \tfrac{1}{2}\left(\widehat{z}^{kl} - a^{kl}\right)\mathbf{h}_k \otimes \mathbf{h}_l$$
$$\overset{\mathrm{R}}{\mathbf{K}}_{Si} = \tfrac{1}{2}\left(\mathbf{I} - \mathbf{C}_{Si}^{-1}\right) = \tfrac{1}{2}\left(h^{kl} - \widehat{z}^{kl}\right)\mathbf{h}_k \otimes \mathbf{h}_l$$

$$\overset{\mathrm{R}}{\mathbf{K}}_S = \overset{\mathrm{R}}{\mathbf{K}}_{Se} + \overset{\mathrm{R}}{\mathbf{K}}_{Si}$$

$\mathbf{F}_{Si}(\,\cdot\,)\,\mathbf{F}_{Si}^T$ / $\mathbf{F}_{Si}^{-1}(\,\cdot\,)\,\mathbf{F}_{Si}^{T\,-1}$

$\mathbf{F}_S(\,\cdot\,)\,\mathbf{F}_S^T$ / $\mathbf{F}_S^{-1}(\,\cdot\,)\,\mathbf{F}_S^{T\,-1}$

intermediate configuration

$$\widehat{\mathbf{K}}_S = \tfrac{1}{2}\left(\widehat{\mathbf{B}}_{Si} - \widehat{\mathbf{C}}_{Se}^{-1}\right) = \tfrac{1}{2}\left(h^{kl} - a^{kl}\right)\widehat{\mathbf{z}}_k \otimes \widehat{\mathbf{z}}_l$$
$$\widehat{\mathbf{K}}_{Se} = \tfrac{1}{2}\left(\mathbf{I} - \widehat{\mathbf{C}}_{Se}^{-1}\right) = \tfrac{1}{2}\left(\widehat{z}^{kl} - a^{kl}\right)\widehat{\mathbf{z}}_k \otimes \widehat{\mathbf{z}}_l$$
$$\widehat{\mathbf{K}}_{Si} = \tfrac{1}{2}\left(\widehat{\mathbf{B}}_{Si} - \mathbf{I}\right) = \tfrac{1}{2}\left(h^{kl} - \widehat{z}^{kl}\right)\widehat{\mathbf{z}}_k \otimes \widehat{\mathbf{z}}_l$$

$$\widehat{\mathbf{K}}_S = \widehat{\mathbf{K}}_{Se} + \widehat{\mathbf{K}}_{Si}$$

(B.2)

current configuration

$$\mathbf{K}_S = \tfrac{1}{2}\left(\mathbf{B}_S - \mathbf{I}\right) = \tfrac{1}{2}\left(h^{kl} - a^{kl}\right)\mathbf{a}_k \otimes \mathbf{a}_l$$
$$\mathbf{K}_{Se} = \tfrac{1}{2}\left(\mathbf{B}_{Se} - \mathbf{I}\right) = \tfrac{1}{2}\left(\widehat{z}^{kl} - a^{kl}\right)\mathbf{a}_k \otimes \mathbf{a}_l$$
$$\mathbf{K}_{Si} = \tfrac{1}{2}\left(\mathbf{B}_S - \mathbf{B}_{Se}\right) = \tfrac{1}{2}\left(h^{kl} - \widehat{z}^{kl}\right)\mathbf{a}_k \otimes \mathbf{a}_l$$

$$\mathbf{K}_S = \mathbf{K}_{Se} + \mathbf{K}_{Si}$$

$\mathbf{F}_{Se}(\,\cdot\,)\,\mathbf{F}_{Se}^T$ / $\mathbf{F}_{Se}^{-1}(\,\cdot\,)\,\mathbf{F}_{Se}^{T\,-1}$

B.2 Transport properties of strain rate tensors

Transport properties of contravariant solid strain rates $(N = 1)$

reference configuration

$$(\mathbf{E}_S)'_S = \tfrac{1}{2}\,(\mathbf{C}_S)'_S = \tfrac{1}{2}\,(a_{kl})'_S\,\mathbf{h}^k \otimes \mathbf{h}^l$$
$$(\mathbf{E}_{Se})'_S = \tfrac{1}{2}\,(\mathbf{C}_S - \mathbf{C}_{Si})'_S = \tfrac{1}{2}\,(a_{kl} - \widehat{z}_{kl})'_S\,\mathbf{h}^k \otimes \mathbf{h}^l$$
$$(\mathbf{E}_{Si})'_S = \tfrac{1}{2}\,(\mathbf{C}_{Si})'_S = \tfrac{1}{2}\,(\widehat{z}_{kl})'_S\,\mathbf{h}^k \otimes \mathbf{h}^l$$
$$(\mathbf{E}_S)'_S = (\mathbf{E}_{Se})'_S + (\mathbf{E}_{Si})'_S$$

$\mathbf{F}_{Si}^{T-1}(\,\cdot\,)\,\mathbf{F}_{Si}^{-1}$ / $\mathbf{F}_{Si}^{T}(\,\cdot\,)\,\mathbf{F}_{Si}$

$\mathbf{F}_S^{T-1}(\,\cdot\,)\,\mathbf{F}_S^{-1}$ / $\mathbf{F}_S^{T}(\,\cdot\,)\,\mathbf{F}_S$

intermediate configuration

$$(\widehat{\mathbf{\Gamma}}_S)^{\triangle}_{Si} = \tfrac{1}{2}\,(\widehat{\mathbf{C}}_{Se})^{\triangle}_{Si} = \tfrac{1}{2}\,(a_{kl})'_S\,\widehat{\mathbf{z}}^k \otimes \widehat{\mathbf{z}}^l$$
$$(\widehat{\mathbf{\Gamma}}_{Se})^{\triangle}_{Si} = \tfrac{1}{2}\,(\widehat{\mathbf{C}}_{Se} - \mathbf{I})^{\triangle}_{Si} = \tfrac{1}{2}\,(a_{kl} - \widehat{z}_{kl})'_S\,\widehat{\mathbf{z}}^k \otimes \widehat{\mathbf{z}}^l$$
$$(\widehat{\mathbf{\Gamma}}_{Si})^{\triangle}_{Si} = \widehat{\mathbf{D}}_{Si} = \tfrac{1}{2}\,(\widehat{z}_{kl})'_S\,\widehat{\mathbf{z}}^k \otimes \widehat{\mathbf{z}}^l$$
$$(\widehat{\mathbf{\Gamma}}_S)^{\triangle}_{Si} = (\widehat{\mathbf{\Gamma}}_{Se})^{\triangle}_{Si} + (\widehat{\mathbf{\Gamma}}_{Si})^{\triangle}_{Si}$$

$\mathbf{F}_{Se}^{T-1}(\,\cdot\,)\,\mathbf{F}_{Se}^{-1}$ / $\mathbf{F}_{Se}^{T}(\,\cdot\,)\,\mathbf{F}_{Se}$

current configuration

$$(\mathbf{A}_S)^{\triangle}_S = \mathbf{D}_S = \tfrac{1}{2}\,(a_{kl})'_S\,\mathbf{a}^k \otimes \mathbf{a}^l$$
$$(\mathbf{A}_{Se})^{\triangle}_S = \tfrac{1}{2}\,(\mathbf{I} - \mathbf{B}_{Se}^{-1})^{\triangle}_S = \tfrac{1}{2}\,(a_{kl} - \widehat{z}_{kl})'_S\,\mathbf{a}^k \otimes \mathbf{a}^l$$
$$(\mathbf{A}_{Si})^{\triangle}_S = \tfrac{1}{2}\,(\mathbf{B}_{Se}^{-1})^{\triangle}_S = \tfrac{1}{2}\,(\widehat{z}_{kl})'_S\,\mathbf{a}^k \otimes \mathbf{a}^l$$
$$(\mathbf{A}_S)^{\triangle}_S = (\mathbf{A}_{Se})^{\triangle}_S + (\mathbf{A}_{Si})^{\triangle}_S$$

(B.3)

with the lower (contravariant) *Lie* or *Oldroyd* derivatives of φ^S

$$(\,\cdot\,)^{\triangle}_S := (\,\cdot\,)'_S + \mathbf{L}_S^T\,(\,\cdot\,) + (\,\cdot\,)\,\mathbf{L}_S\,,$$
$$(\,\widehat{\cdot}\,)^{\triangle}_{Si} := (\,\widehat{\cdot}\,)'_S + \widehat{\mathbf{L}}_{Si}^T\,(\,\widehat{\cdot}\,) + (\,\widehat{\cdot}\,)\,\widehat{\mathbf{L}}_{Si}$$

and the contravariant identities

$$\mathbf{D}_S = \tfrac{1}{2}\,(\mathbf{L}_S + \mathbf{L}_S^T) = (\mathbf{A}_S)^{\triangle}_S\,,\quad \widehat{\mathbf{D}}_{Si} = \tfrac{1}{2}\,(\widehat{\mathbf{L}}_{Si} + \widehat{\mathbf{L}}_{Si}^T) = (\widehat{\mathbf{\Gamma}}_{Si})^{\triangle}_{Si}\,,$$
$$(\mathbf{B}_S^{-1})^{\triangle}_S = (h_{kl}\,\mathbf{a}^k \otimes \mathbf{a}^l)^{\triangle}_S = \mathbf{0}\,,\quad (\widehat{\mathbf{B}}_{Si}^{-1})^{\triangle}_{Si} = (h_{kl}\,\widehat{\mathbf{z}}^k \otimes \widehat{\mathbf{z}}^l)^{\triangle}_{Si} = \mathbf{0}\,.$$

Transport properties of covariant solid strain rates $(N = 1)$

reference configuration

$$
\begin{gathered}
(\overset{\mathrm{R}}{\mathbf{K}}{}_S)'_S = \tfrac{1}{2}\,(\mathbf{C}_S^{-1})'_S = \tfrac{1}{2}\,(a^{kl})'_S\,\mathbf{h}_k \otimes \mathbf{h}_l \\
(\overset{\mathrm{R}}{\mathbf{K}}{}_{Se})'_S = \tfrac{1}{2}\,(\mathbf{C}_{Si}^{-1} - \mathbf{C}_S^{-1})'_S = \tfrac{1}{2}\,(\widehat{z}^{kl} - a^{kl})'_S\,\mathbf{h}_k \otimes \mathbf{h}_l \\
(\overset{\mathrm{R}}{\mathbf{K}}{}_{Si})'_S = -\tfrac{1}{2}\,(\mathbf{C}_{Si}^{-1})'_S = -\tfrac{1}{2}\,(\widehat{z}^{kl})'_S\,\mathbf{h}_k \otimes \mathbf{h}_l \\
\hline
\overset{\mathrm{R}}{\mathbf{K}}{}_S = \overset{\mathrm{R}}{\mathbf{K}}{}_{Se} + \overset{\mathrm{R}}{\mathbf{K}}{}_{Si}
\end{gathered}
$$

$\mathbf{F}_{Si}(\,\cdot\,)\,\mathbf{F}_{Si}^T$ / $\mathbf{F}_{Si}^{-1}(\,\cdot\,)\,\mathbf{F}_{Si}^{T-1}$

$\mathbf{F}_S(\,\cdot\,)\,\mathbf{F}_S^T$ / $\mathbf{F}_S^{-1}(\,\cdot\,)\,\mathbf{F}_S^{T-1}$

intermediate configuration

$$
\begin{gathered}
(\widehat{\mathbf{K}}_S)^{\triangledown}_{Si} = -\tfrac{1}{2}\,(\widehat{\mathbf{C}}_{Se}^{-1})^{\triangledown}_{Si} = \tfrac{1}{2}\,(a^{kl})'_S\,\widehat{\mathbf{z}}_k \otimes \widehat{\mathbf{z}}_l \\
(\widehat{\mathbf{K}}_{Se})^{\triangledown}_{Si} = \tfrac{1}{2}\,(\mathbf{I} - \widehat{\mathbf{C}}_{Se}^{-1})^{\triangledown}_{Si} = \tfrac{1}{2}\,(\widehat{z}^{kl} - a^{kl})'_S\,\widehat{\mathbf{z}}_k \otimes \widehat{\mathbf{z}}_l \\
(\widehat{\mathbf{K}}_{Si})^{\triangledown}_{Si} = \widehat{\mathbf{D}}_{Si} = -\tfrac{1}{2}\,(\widehat{z}^{kl})'_S\,\widehat{\mathbf{z}}_k \otimes \widehat{\mathbf{z}}_l \\
\hline
(\widehat{\mathbf{K}}_S)^{\triangledown}_{Si} = (\widehat{\mathbf{K}}_{Se})^{\triangledown}_{Si} + (\widehat{\mathbf{K}}_{Si})^{\triangledown}_{Si}
\end{gathered}
\tag{B.4}
$$

current configuration

$$
\begin{gathered}
(\mathbf{K}_S)^{\triangledown}_S = \mathbf{D}_S = \tfrac{1}{2}\,(a^{kl})'_S\,\mathbf{a}_k \otimes \mathbf{a}_l \\
(\mathbf{K}_{Se})^{\triangledown}_S = \tfrac{1}{2}\,(\mathbf{B}_{Se} - \mathbf{I})^{\triangledown}_S = \tfrac{1}{2}\,(\widehat{z}^{kl} - a^{kl})'_S\,\mathbf{a}_k \otimes \mathbf{a}_l \\
(\mathbf{K}_{Si})^{\triangledown}_S = -\tfrac{1}{2}\,(\mathbf{B}_{Se})^{\triangledown}_S = -\tfrac{1}{2}\,(\widehat{z}^{kl})'_S\,\mathbf{a}_k \otimes \mathbf{a}_l \\
\hline
(\mathbf{K}_S)^{\triangledown}_S = (\mathbf{K}_{Se})^{\triangledown}_S + \mathbf{K}_{Si})^{\triangledown}_S
\end{gathered}
$$

$\mathbf{F}_{Se}(\,\cdot\,)\,\mathbf{F}_{Se}^T$ / $\mathbf{F}_{Se}^{-1}(\,\cdot\,)\,\mathbf{F}_{Se}^{T-1}$

with the lower (covariant) *Lie* or *Oldroyd* derivatives of φ^S

$$
\begin{aligned}
(\,\cdot\,)^{\triangledown}_S &:= (\,\cdot\,)'_S - \mathbf{L}_S\,(\,\cdot\,) - (\,\cdot\,)\,\mathbf{L}_S^T\,, \\
(\,\widehat{\cdot}\,)^{\triangledown}_{Si} &:= (\,\widehat{\cdot}\,)'_S - \widehat{\mathbf{L}}_{Si}\,(\,\widehat{\cdot}\,) - (\,\widehat{\cdot}\,)\,\widehat{\mathbf{L}}_{Si}^T
\end{aligned}
$$

and the covariant identities

$$
\begin{gathered}
\mathbf{D}_S = -\tfrac{1}{2}\,(\mathbf{L}_S^{-1} + \mathbf{L}_S^{T-1}) = (\mathbf{K}_S)^{\triangledown}_S\,, \quad \widehat{\mathbf{D}}_{Si} = -\tfrac{1}{2}\,(\widehat{\mathbf{L}}_{Si}^{-1} + \widehat{\mathbf{L}}_{Si}^{T-1}) = (\widehat{\mathbf{K}}_{Si})^{\triangledown}_{Si}\,, \\
(\mathbf{B}_S)^{\triangledown}_S = (h^{kl}\,\mathbf{a}_k \otimes \mathbf{a}_l)^{\triangledown}_S = \mathbf{0}\,, \quad (\widehat{\mathbf{B}}_{Si})^{\triangledown}_{Si} = (h^{kl}\,\widehat{\mathbf{z}}_k \otimes \widehat{\mathbf{z}}_l)^{\triangledown}_{Si} = \mathbf{0}\,.
\end{gathered}
$$

B.3 Evolution equations

Contravariant inelastic evolution equations $(N = 1)$

reference configuration

$$(\mathbf{E}_{Si})'_S = \tfrac{1}{2}\,(\mathbf{C}_{Si})'_S = (\overset{4}{\overline{\mathbf{D}}}{}^S)^{-1}\,\mathbf{S}^S_{NEQ}$$

$$(\overset{4}{\overline{\mathbf{D}}}{}^S)^{-1} = \alpha\,(\mathbf{C}_{Si}\otimes\mathbf{C}_{Si})^{\overset{23}{T}} - \beta\,(\mathbf{C}_{Si}\otimes\mathbf{C}_{Si})\ ^a$$

$$(\mathbf{E}_{Si})'_S = \alpha\,\mathbf{C}_{Si}\,\mathbf{S}^S_{NEQ}\,\mathbf{C}_{Si} - \beta\,(\mathbf{S}^S_{NEQ}\cdot\mathbf{C}_{Si})\,\mathbf{C}_{Si}$$

$\mathbf{F}^{T-1}_{Si}(\,\cdot\,)\,\mathbf{F}^{-1}_{Si}$ / $\mathbf{F}^{T}_{Si}(\,\cdot\,)\,\mathbf{F}_{Si}$

$\mathbf{F}^{T-1}_{S}(\,\cdot\,)\,\mathbf{F}^{-1}_{S}$ / $\mathbf{F}^{T}_{S}(\,\cdot\,)\,\mathbf{F}_{S}$

intermediate configuration

$$(\widehat{\mathbf{\Gamma}}_{Si})^{\triangle}_{Si} = \widehat{\mathbf{D}}_{Si} = (\overset{4}{\widehat{\mathbf{D}}}{}^S)^{-1}\,\widehat{\boldsymbol{\tau}}^S_{NEQ}$$

$$(\overset{4}{\widehat{\mathbf{D}}}{}^S)^{-1} = \alpha\,(\mathbf{I}\otimes\mathbf{I})^{\overset{23}{T}} - \beta\,(\mathbf{I}\otimes\mathbf{I})\ ^a$$

$$(\widehat{\mathbf{\Gamma}}_{Si})^{\triangle}_{Si} = \alpha\,\widehat{\boldsymbol{\tau}}^S_{NEQ} - \beta\,(\widehat{\boldsymbol{\tau}}^S_{NEQ}\cdot\mathbf{I})\,\mathbf{I}$$

(B.5)

$\mathbf{F}^{T-1}_{Se}(\,\cdot\,)\,\mathbf{F}^{-1}_{Se}$ / $\mathbf{F}^{T}_{Se}(\,\cdot\,)\,\mathbf{F}_{Se}$

current configuration

$$(\mathbf{A}_{Si})^{\triangle}_S = \tfrac{1}{2}\,(\mathbf{B}^{-1}_{Se})^{\triangle}_S = (\overset{4}{\mathbf{D}}{}^S)^{-1}\,\boldsymbol{\tau}^S_{NEQ}$$

$$(\overset{4}{\mathbf{D}}{}^S)^{-1} = \alpha\,(\mathbf{B}^{-1}_{Se}\otimes\mathbf{B}^{-1}_{Se})^{\overset{23}{T}} - \beta\,(\mathbf{B}^{-1}_{Se}\otimes\mathbf{B}^{-1}_{Se})\ ^a$$

$$(\mathbf{A}_{Si})^{\triangle}_S = \alpha\,\mathbf{B}^{-1}_{Se}\,\boldsymbol{\tau}^S_{NEQ}\,\mathbf{B}^{-1}_{Se} - \beta\,(\boldsymbol{\tau}^S_{NEQ}\cdot\mathbf{B}^{-1}_{Se})\,\mathbf{B}^{-1}_{Se}$$

with the abbreviations

$$\alpha = \frac{1}{2\,\eta^S}\,,\quad \beta = \frac{\zeta^S}{2\,\eta^S\,(2\,\eta^S + 3\,\zeta^S)}\,,\quad \text{where}\quad \begin{cases}\ \eta^S > 0\,,\\ \ \tfrac{2}{3}\,\eta^S + \zeta^S > 0\,.\end{cases}$$

[a] For the transport mechanism of 4th-order tensors, see box (2.43) on page 22.

Covariant inelastic evolution equations $(N = 1)$

reference configuration

$$
\begin{aligned}
&(\overset{\mathrm{R}}{\mathbf{K}}_{Si})'_S = -\tfrac{1}{2}\,(\mathbf{C}_{Si}^{-1})'_S = (\overset{4}{\overline{\mathbf{D}}}{}^S)^{-1}\,\mathbf{S}^S_{NEQ} \\
&(\overset{4}{\overline{\mathbf{D}}}{}^S)^{-1} = \alpha\,(\mathbf{I}\otimes\mathbf{I})^{\overset{23}{T}} - \beta\,(\mathbf{C}_{Si}^{-1}\otimes\mathbf{C}_{Si}) \quad {}^{b} \\
&(\overset{\mathrm{R}}{\mathbf{K}}_{Si})'_S = \alpha\,\mathbf{S}^S_{NEQ} - \beta\,(\mathbf{S}^S_{NEQ}\cdot\mathbf{C}_{Si})\,\mathbf{C}_{Si}^{-1}
\end{aligned}
$$

$\mathbf{F}_{Si}(\,\bullet\,)\,\mathbf{F}_{Si}^{T}$ ⇄ $\mathbf{F}_{Si}^{-1}(\,\bullet\,)\,\mathbf{F}_{Si}^{T-1}$

$\mathbf{F}_{S}(\,\bullet\,)\,\mathbf{F}_{S}^{T}$ ⇄ $\mathbf{F}_{S}^{-1}(\,\bullet\,)\,\mathbf{F}_{S}^{T-1}$

intermediate configuration

$$
\begin{aligned}
&(\widehat{\mathbf{K}}_{Si})^{\triangledown}_{Si} = \widehat{\mathbf{D}}_{Si} = (\overset{4}{\widehat{\mathbf{D}}}{}^S)^{-1}\,\widehat{\boldsymbol{\tau}}^S_{NEQ} \\
&(\overset{4}{\widehat{\mathbf{D}}}{}^S)^{-1} = \alpha\,(\mathbf{I}\otimes\mathbf{I})^{\overset{23}{T}} - \beta\,(\mathbf{I}\otimes\mathbf{I}) \quad {}^{b} \\
&(\widehat{\mathbf{K}}_{Si})^{\triangledown}_{Si} = \alpha\,\widehat{\boldsymbol{\tau}}^S_{NEQ} - \beta\,(\widehat{\boldsymbol{\tau}}^S_{NEQ}\cdot\mathbf{I})\,\mathbf{I}
\end{aligned}
$$

(B.6)

$\mathbf{F}_{Se}(\,\bullet\,)\,\mathbf{F}_{Se}^{T}$ ⇄ $\mathbf{F}_{Se}^{-1}(\,\bullet\,)\,\mathbf{F}_{Se}^{T-1}$

current configuration

$$
\begin{aligned}
&(\mathbf{K}_{Si})^{\triangledown}_{S} = -\tfrac{1}{2}\,(\mathbf{B}_{Se})^{\triangledown}_{S} = (\overset{4}{\mathbf{D}}{}^S)^{-1}\,\boldsymbol{\tau}^S_{NEQ} \\
&(\overset{4}{\mathbf{D}}{}^S)^{-1} = \alpha\,(\mathbf{I}\otimes\mathbf{I})^{\overset{23}{T}} - \beta\,(\mathbf{B}_{Se}\otimes\mathbf{B}_{Se}^{-1}) \quad {}^{b} \\
&(\mathbf{K}_{Si})^{\triangledown}_{S} = \alpha\,\boldsymbol{\tau}^S_{NEQ} - \beta\,(\boldsymbol{\tau}^S_{NEQ}\cdot\mathbf{B}_{Se}^{-1})\,\mathbf{B}_{Se}
\end{aligned}
$$

with the abbreviations

$$
\alpha = \frac{1}{2\,\eta^S}\,, \quad \beta = \frac{\zeta^S}{2\,\eta^S\,(2\,\eta^S + 3\,\zeta^S)}\,, \quad \text{where} \quad \left\{ \begin{array}{l} \eta^S > 0\,, \\ \frac{2}{3}\,\eta^S + \zeta^S > 0\,. \end{array} \right.
$$

[b] For the transport mechanism of 4th-order tensors, see box (2.43) on page 22.

Curriculum Vitæ

Personal data

Name:	Bernd Markert
Address:	Robert-Schumann-Str. 17 71 083 Herrenberg, Germany
Date and place of birth:	13.12. 1971, Mayen/Eifel, Germany
Nationality:	German
Marital status:	married

Education

Aug. 1978 - Oct. 1980	elementary school 'Grundschule Pfarrer-Bechtel Mendig'
Nov. 1980 - Jun. 1982	elementary school 'Bildungszentrum Niederstetten'
Aug. 1982 - May 1992	secondary/high school 'Gymnasium Weikersheim'
May 1992	degree: 'Allgemeine Hochschulreife' (high school diploma)

Internship and military service

Jun. 1992 - Sep. 1992	civil engineering internship with Ambros Greiner Hoch und Tiefbau GmbH & Co. KG Bad Mergentheim
Oct. 1992 - Nov. 1993	military service Herrmann-Köhl-Kaserne Niederstetten

University education

Oct. 1993 - Jan. 1998	studies in civil engineering at the University of Stuttgart major subject: 'Allgemeines Bauingenieurwesen'
Oct. 1994 - Jan. 1998	student teaching assistant at several institutes of the Faculty of Civil Engineering and Surveying
Jan. 1998	degree: 'Diplom-Ingenieur (Dipl.-Ing.) Bauingenieurwesen'

Scientific development

Feb. 1998 - Jul. 1998	Ph. D. student at the Chair II of the Institute of Applied Mechanics (CE), University of Stuttgart
Aug. 1998 - Jul. 1999	research associate on a DFG research project
Aug. 1999 - Apr. 2002	assistant lecturer
Apr. 2002	nomination as 'Akademischer Rat z. A.' (lecturer)
Nov. 2003	nomination as 'Akademischer Rat' (tenure lecturer)

Released Report Series

II-1 Gernot Eipper: *Theorie und Numerik finiter elastischer Deformationen in fluidgesättigten porösen Festkörpern*, June 1998.

II-2 Wolfram Volk: *Untersuchung des Lokalisierungsverhaltens mikropolarer poröser Medien mit Hilfe der Cosserat-Theorie*, May 1999.

II-3 Peter Ellsiepen: *Zeit- und ortsadaptive Verfahren angewandt auf Mehrphasenprobleme poröser Medien*, July 1999.

II-4 Stefan Diebels: *Mikropolare Zweiphasenmodelle: Formulierung auf der Basis der Theorie Poröser Medien*, March 2000.

II-5 Dirk Mahnkopf: *Lokalisierung fluidgesättigter poröser Festkörper bei finiten elastoplastischen Deformationen*, March 2000.

II-6 Heiner Müllerschön: *Spannungs-Verformungsverhalten granularer Materialien am Beispiel von Berliner Sand*, August 2000.

II-7 Stefan Diebels (Ed.): *Zur Beschreibung komplexen Materialverhaltens: Beiträge anläßlich des 50. Geburtstages von Herrn Prof. Dr.-Ing. Wolfgang Ehlers*, August 2001.

II-8 Jack Widjajakusuma: *Quantitative Prediction of Effective Material Parameters of Heterogeneous Materials*, June 2002.

II-9 Alexander Droste: *Beschreibung und Anwendung eines elastisch-plastischen Materialmodells mit Schädigung für hochporöse Metallschäume*, October 2002.

II-10 Peter Blome: *Ein Mehrphasen-Stoffmodell für Böden mit Übergang auf Interface-Gesetze*, October 2003.

II-11 Martin Ammann: *Parallel Finite Element Simulations of Localization Phenomena in Porous Media*, April 2005.

II-12 Bernd Markert: *Porous Media Viscoelasticity with Application to Polymeric Foams*, July 2005.

II-13 Saeed Reza Ghadiani: *A Multiphasic Continuum Mechanical Model for Design Investigations of an Effusion-Cooled Rocket Thrust Chamber*, September 2005.

II-14 Wolfgang Ehlers & Bernd Markert (Eds.): *Proceedings of the 1st GAMM Seminar on Continuum Biomechanics*, September 2005.

II-15 Bernd Scholz: *Application of a Micropolar Model to the Localization Phenomena in Granular Materials: General Model, Sensitivity Analysis and Parameter Optimization*, November 2007.

II-16 Wolfgang Ehlers & Nils Karajan (Eds.): *Proceedings of the 2nd GAMM Seminar on Continuum Biomechanics*, December 2007.

II-17 Tobias Graf: *Multiphasic Flow Processes in Deformable Porous Media under Consideration of Fluid Phase Transitions*, June 2008.

II-18 Ayhan Acartürk: *Simulation of Charged Hydrated Porous Materials*, March 2009.

II-19 Nils Karajan: *An Extended Biphasic Description of the Inhomogeneous and Anisotropic Intervertebral Disc*, March 2009.

II-20 Bernd Markert: *Weak or Strong – On Coupled Problems in Continuum Mechanics*, June 2010.

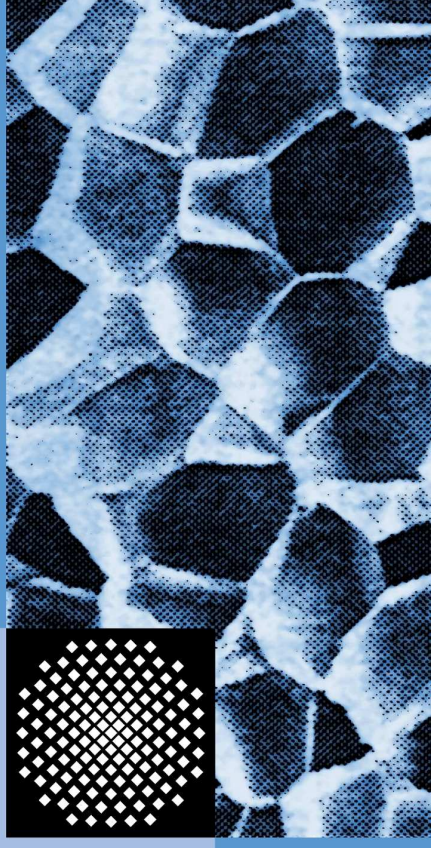

ISBN 3–937399–12–7
(D 93 – Dissertation, Universität Stuttgart)